A Study Of The Inhibition Of Second Stage Hydrocracking Catalysts By Weakly Basic Nitrogen-Containing Compounds

Carlos Mauricio Celis Cornejo

Tesis Presentada Como Requisito Para Acceder Al Título De:
Doctor En Ingeniería Química

Director
Prof. Víctor G. Baldovino-Medrano

Co-Director
Dr. David J. Pérez-Martínez

Universidad Industrial De Santander
Facultad De Ingenierías Fisicoquímicas
Escuela De Ingeniería Química
Centro De Investigaciones En Catálisis (Cicat)
Bucaramanga
2017

AGRADECIMIENTOS

Esta tesis doctoral se desarrolló gracias al convenio ECOPETROL-UIS en el marco del acta AC2-5211770 adscrita al Proyecto 8822 de la Vicerrectoría de Investigaciones de la Universidad Industrial de Santander, VIE-UIS.

A Colciencias por su apoyo económico ofrecido en las convocatorias de Doctorados Nacionales del año 2012.

A la Vicerrectoría de Investigaciones de la Universidad Industrial de Santander, por las gestiones administrativas, y el apoyo financiero para desarrollo de infraestructura destinada a la ejecución de trabajos doctorales, en el marco del proyecto 1607.

A los profesores Víctor Baldovino y Sonia A. Giraldo, y al Dr. David Pérez por sus valiosas enseñanzas, dirección y apoyo constante.

Al Staff de los grupos: Unité de Catalyse et Chimie du Solide (UCCS) - UMR 8181, de l'Université de Lille 1 y Laboratoire de Catalyse et Spectrochimie (LCS), del ENSICAEN; quienes por su valiosa ayuda durante mi estancia doctoral.

Al personal del SC3-UIS por su excelente soporte prestado en la plataforma GUANE para la realización de los cálculos computacionales de esta tesis.

Por supuesto, a los miembros del Centro de Investigaciones en Catálisis de la Universidad Industrial de Santander (CICAT-UIS) por su invaluable ayuda y amistad.

A mis padres, a mi hermano, a mi familia y a mis amigos.

Dedicatoria

"On ne voit bien qu'avec le cœur l'essentiel est invisible pour les yeux." – A.S. Exupery.

El amor finalmente es lo que hace apacible la existencia. Al hacer todo con amor, el ser, se vuelve resiliente y nunca deja de soñar. En este sentido, dedico este trabajo a todas esas personas que me recuerdan siempre que cada acción que se haga desde el amor está destinada a un buen final.

TABLE OF CONTENT

LIST OF ANNEXES

LIST OF TABLES

CHAPTER 1

CHAPTER 2

CHAPTER 3

CHAPTER 4

LIST OF FIGURES

INTRODUCTION

CHAPTER 1

CHAPTER 2

CHAPTER 3

CHAPTER 4

RESUMEN

TÍTULO: A STUDY OF THE INHIBITION OF SECOND STAGE HYDROCRACKING CATALYST BY WEAKLY BASIC NITROGEN-CONTAINING COMPOUNDS

AUTOR: CARLOS MAURICIO CELIS CORNEJO**

PALABRAS CLAVE: HIDROCRAQUEO, INHIBICIÓN, COMPUESTOS NITROGENADOS, CARBAZOL, DÉBILMENTE BÁSICOS, POLIAROMÁTICOS, PHENANTHRENE, ADSORCIÓN, ATR-IR, ESI FT-ICR-MS, DFT, MECANISMO DE ISOMERIZACIÓN.

DESCRIPCIÓN:

El procesamiento de crudos cada vez más pesados plantea un reto enorme en las refinerías modernas, respecto a la eliminación de los heterocompuestos y mejoramiento de estas cargas mediante hidroprocesos. En esta contribución, se identifican las especies químicas más refractarias al hidrotratamiento en un gasóleo de vacío Colombiano, empleando espectrometría de masas de alta resolución. Estos análisis permitieron evidenciar una alta abundancia relativa de las especies parcialmente hidrogenadas de los compuestos nitrogenados tipo pirrólicos, cuyo carácter es levemente básico. El efecto de estos compuestos débilmente básicos sobre el desempeño de un catalizador convencional de hidrocraqueo se evaluó a diferentes niveles de nitrogenados, variando no solo la cantidad, sino la fracción entre las especies seleccionadas. Los ensayos catalíticos se efectuaron siguiendo la reacción de fenantreno, a temperaturas entre 623, 638 y 653 K, velocidades espaciales entre 1.3 y 2.2 h^{-1}, y nitrógeno total entre 0, 1 y 5 ppm en la carga. El análisis estadístico de este diseño experimental permitió obtener una correlación entre las variables operacionales y establecer que el efecto de los nitrogenados es evidente en la selectividad hacia los productos tipo naftaleno y tetralina. Para dar una explicación factible a las observaciones experimentales, se llevaron a cabo simulaciones con DFT en mordenita, para modelar un sitio de Brønsted y evaluar la adsorción de distintos compuestos nitrogenados y poliaromáticos. Los nitrogenados débilmente básicos mostraron una tendencia a protonarse cuando interaccionan con los sitios ácidos, igual que los más básicos. Para validar esta predicción hecha por los cálculos, se desarrolló una metodología para seguir la adsorción de compuestos nitrogenados pirrólicos en fase líquida, sobre una zeolita protonada, mediante ATR-IR. Los resultados de este trabajo permiten concluir que los compuestos débilmente básicos pueden causar efectos inhibitorios significativos, incluso en pequeñas concentraciones (<5 ppm de N) en la carga.

---

* Tesis Doctoral.

** Facultad de Ingenierías Fisicoquímicas, Escuela de Ingeniería Química. Director: Víctor Baldovino Medrano, Profesor, Escuela de Ingeniería Química. Codirector: David Pérez Martínez, Instituto Colombiano del Petróleo.

ABSTRACT

TITLE: A STUDY OF THE INHIBITION OF SECOND STAGE HYDROCRACKING CATALYST BY WEAKLY BASIC NITROGEN-CONTAINING COMPOUNDS

AUTHOR: CARLOS MAURICIO CELIS CORNEJO**

KEYWORDS: HYDROCRACKING, INHIBITION, NITROGEN COMPOUNDS, CARBAZOLE, WEAKLY BASIC, POLYNUCLEAR AROMATIC HYDROCARBONS, PHENANTHRENE, ADSORPTION, ATR-IR, ESI FT-ICR-MS, DFT, ISOMERIZATION MECHANISM.

DESCRIPTION:

The increasing production of heavy crude oil and its process is challenging for modern refineries, regarding the elimination of hetero-compounds and the upgrading of these streams through hydroprocesses. In this contribution, the most refractory to hydrotreatment species in a Colombian vacuum gas oil were identified, using high-resolution mass spectrometry. These analyses allowed to evidence a high relative abundance of the partially hydrogenated species of nitrogenous pyrrolic compounds, whose character is slightly basic. The effect of these weakly basic compounds on the performance of a conventional hydrocracking catalyst was evaluated at different nitrogen levels, varying not only the amount but the fraction between the selected species. The catalytic tests were carried out following the phenanthrene reaction, at temperatures of 623, 638 and 653 K, space velocities between 1.3 and 2.2 h -1, and total nitrogen content of 0, 1 and 5 ppm in the feed. The statistical analysis of this experimental design allowed establishing a correlation between the operational variables and evidenced the effect of the nitrogen compounds on the selectivity towards the naphthalene and tetralin like products. To provide a feasible explanation for the experimental observations, DFT simulations were carried out in a mordenite structure, for modeling a Brønsted site and evaluate the adsorption of different nitrogen-containing and polynuclear aromatic hydrocarbons. Weakly basic nitrogen-containing compounds became protonated when interacting with acid sites, as well as the most basic species. To validate this prediction addressed by the calculations, a methodology was developed to follow the adsorption of pyrrolic compounds in the liquid phase, on a protonic zeolite, by means of ATR-IR. Summarizing our results, is possible to conclude that the weakly basic compounds can cause significant inhibitory effects, even at small concentrations (<5 ppm of N) in the feed.

---

* PhD Thesis.

** Facultad de Ingenierías Fisicoquímicas, Escuela de Ingeniería Química. Advisor: Víctor Baldovino Medrano, Professor, Escuela de Ingeniería Química. Co-advisor: David Pérez Martínez, Instituto Colombiano del Petróleo.

INTRODUCTION

Abstract

Hydrocracking is nowadays one of the most important upgrading technologies implemented in refineries for processing heavy oil fractions. These heavy oil fractions contain high specifications of heterocompounds which tend to poison or inhibit the catalytic performance of the hydrocracking stage. For such reason, it is important to study the constitution and nature of these fractions, for clarifying the possible physicochemical phenomena which occur on the active sites of the catalysts. In this chapter a complete state of the art is reviewed concerning these aforementioned affairs, aiming to direct the discussion towards the effect of the most refractory to the hydrotreating compounds, which finally are responsible for causing some inhibition of the hydrocracking desired reactions. A copious review of the analytical techniques for describing the constitution of the heavy oil fractions, as well as, kinetic and reactivity studies regarding the inhibitory effects of nitrogenated compounds is displayed hereof. The development of new methodologies based on quantum mechanics, for investigating this physicochemical issues is also showed at the end of this document. The goal of this work, which is the measurement of the impact in the hydrocracking catalyst performance of highly refractory to the hydrotreating nitrogenated compounds will be experimental, theoretical, and analytically addressed in the further chapters of this books. For enclosing, a brief description of each chapter is mentioned.

Nomenclature

APPI	Atmospheric Pressure Photoionization
CGO	Coker Gas Oil
DAO	Desasphalted Oil
DFT	Density Functional Theory
ESI	Electrospray Ionization
FCC	Fluid Catalytic Cracking
FIMS	Field Ionization Mass Spectroscopy
FT-ICR-MS	Fourier Transform Ion Cyclotron Resonance Mass Spectrometry
FT-IR	Fourier Transform Infrared Spectroscopy
GC	Gas Chromatography
HCGO	Heavy Coker Gas Oil
HCK	Hydrocracking
HDN	Hydrodenitrogenation
HDS	Hydrodesulfurization
HDT	Hydrotreatring
HCO	Heavy Cycle Oil
ISTD	Internal Standard for GC
LHSV	Liquid Hourly Space Velocity
MS	Mass Spectrometry
NMR	Nuclear Magnetic Resonance
PAH	Polynuclear Aromatic Hydrocarbon
TS	Transition State
TST	Transition State Theory
VGO	Vacuum Gas Oil

Introduction

Challenges in the upgrading of heavy oils

Hydrotreating (HDT) and hydrocracking (HCK), are catalytic hydroprocesses widely implemented in refineries [1], as solution for the increasing demand of cleaner fuels, in order to continuously enhance the quality of the fuel products. Hydrotreating goals are mainly two: first, to efficiently remove the non-desire heteroatoms, namely sulfur, nitrogen, oxygen, nickel and vanadium [1-5]; and second to hydrogenate some aromatics which could lead to the formation of particles during the fuel combustion [1, 2, 6, 7]. The problem that hydrotreating attempts to solve is to reduce the pollutants, precursors of NO_X and SO_X, and particulate matter which has become an important urban pollutant [7] and is the main responsible for premature death [8]. On the other hand, the hydrocracking is an alternative upgrading technology, whose objective is to selectively obtain the desire fuel products from heavy feedstocks and oil residues, while at the same time it performs some hydrotreating functions. The advantage of the hydrocracking over other upgrading technologies, such as thermal cracking, is the simultaneous increase in the Hydrogen/Carbon ratio of the feedstock, while a controlled cracking is carried out, thus preventing the coke formation. Nonetheless, the feedstock quality is one of the most influencing variables for the hydrocracking [5]. During the last decade in Colombia, an increase in the production of medium and heavy oils has been observed due to the nature of our available reservoirs [9]. Moreover, this is a global trend, and it will not decrease. That is to say, the heavier the feedstock, the higher the heteroatoms content, as this is depicted for sulfur in Figure 1. This behavior is the same for nitrogen, oxygen, and heavy metals within the heavy oil fractions [10]. The progressive rise of heteroatoms within the heavy oils makes more difficult to reach the desired products distribution in the hydrocracking [2].

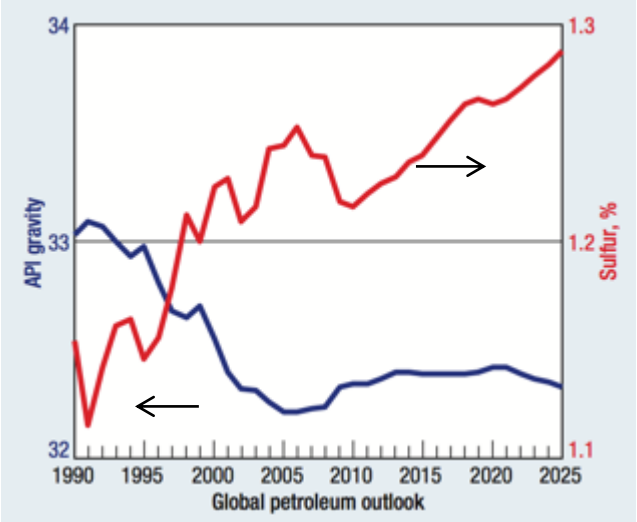

Figure 1. Global petroleum trend, the API gravity is a measure of the density of a crude oil, the higher the API gravity, the lighter the crude fraction. Taken from: [10].

Specifically, sulfur and nitrogen affect the hydrocracking catalyst performance, causing inhibition and poisoning [11-13]. For this reason, some hydrocracking configurations usually have two reactor units, one for the feedstock pretreatment, and the other one for the hydrocracking only. The first reactor unit has some hydrotreating catalyst beds, whose objective is the removal of heteroatoms (see Figure 2). The pretreatment is usually followed by a separation unit for obtaining the liquid fractions and removing the gases which contain hydrogen sulfide and ammonia, produced during the hydrotreating. It is well known that these gases induce a poisoning effect on the acidic functionalities of the hydrocracking catalyst [14]. For mild conversion, the reactor catalyst distribution is formed by some hydrotreating beds followed by some hydrocraking first stage catalyst beds [15]. The inconvenience with this type of configurations is that the hydrotreating gas products such as the ammonia, interact with the acid sites within the hydrocracking catalyst, and this negatively affects the activity and the selectivity [14, 15].

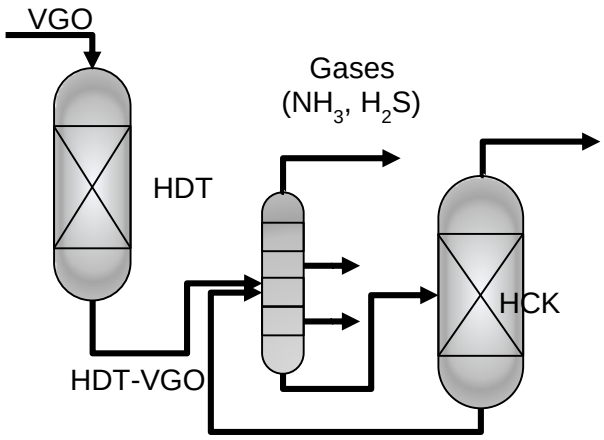

Figure 2. Two-stages HCK configuration, first reactor consists of a HDT reactor, followed by an intermediate separation unit, the final reactor is the HCK reactor. VGO: Vacuum Gas Oil.

Generalities of the hydrocracking stage

Hydrocracking has been widely studied due to its economic relevance in refineries [3, 16-21]. Its operating conditions consist of elevated temperatures and pressures, whose choice rely mainly on the feedstock properties: the heavier the feedstock, the higher the conditions. For a common feedstock, the Vacuum Gas Oil (VGO), conditions are 653 K and about 7 to 10 MPa. Table 1 shows the most common pressure conditions and the conversions reached, depending on the hydrocracking configurations and the feedstocks [1]. Cracking is an exothermic reaction, and despite high temperature do not favor the thermodynamic equilibrium, this is required to lead the catalytic reaction reaches the activation energies. However, temperature must be selected wisely, in order to avoid thermal cracking, which could lead to coke and gas formation, thus increasing the conversion, but decreasing the selectivity to the desired liquid fractions [1, 16, 22]. The slurry-phase hydrocracking is another technology used for the extra-heavy oil fractions upgrading. In this unit, low-cost oil-soluble or water-soluble catalysts are used, and they consist mainly in a molybdenum inorganic or organic compound, which enable the hydrogenation function, while the cracking takes place via thermal action [23-25]. Recent studies have included the presence of acid

solids and oil-soluble molybdenum salts for enhancing the hydrocracking activity and selectivity to the desired products when processing vacuum residua [26].

Table 1.

Hydroprocessing conditions for the HDT and HCK units depending on the type feedstock and the process configuration [1].

Process, Feedstock	**Pressure (MPa)**	**Conversion**
HDT		
Naphtha	1.8 - 3.2	0.5 - 5%
Kerosene	1.8 - 4.2	0.5 - 5%
Diesel	4.2 - 5.6	5 - 15%
VGO, DAO, CGO, HCO	5.6 - 13.8	5 - 15%
Mild Hydrocracking		
	5.6 - 8.4	20 - 40%
One-stage Hydrocracking		
VGO, DAO, CGO, HCO	10.0 - 14.0	60 - 90%
Two-stage hydrocracking		
VGO, DAO, CGO, HCO	10.0 - 14.0	80 - 99%
Ebullated bed hydrocraking		
VGO, DAO, CGO, HCO	14.0	80 - 99%
Vacuum residue	14.0 - 20.8	>50%

VGO: Vacuum Gas Oil, CGO: Coker Gas Oil, DAO: Desasphalted Oil, HCO: Heavy Cycle Oil from fluid catalytic cracking.

As mentioned above, the catalyst plays the most important role in this stage. While the pretreatment catalyst must perform hydrodemetallization, hydrodesulfurization, and hydrodenitrogenation, the hydrocracking catalyst must have a cracking and hydrogenation function simultaneously. Hydrotreating catalyst usually consists of NiMo/γ-Al_2O_3 or NiW/γ-Al_2O_3. Whilst the hydrocracking catalyst has acid properties, also, it is well known that Brønsted acidity is key in the hydrocracking, these acid sites are usually provided by zeolites which are used as supports or could be embedded into mesoporous materials [27]. Nonetheless, Lewis acidity is also present in these materials [28], and it could also promote hydrocracking. Despite hydrocracking could proceed also on Lewis acid sites, the Brønsted acidity is preferred, since some

non-desired reactions such as the coke formation could be catalyzed on Lewis sites [29]. Other materials have been studied as supports which could achieve the desired functionality, and also provides mesoporosity which allows the diffusion of bigger molecules into the pores, to reach more active sites; modified materials like the MCM-41 and SBA-15 have been tested as promising supports for hydrocracking [30-32]. For providing the hydrogenation functionality, the hydrocracking catalyst usually contains bimetallic species, commonly NiMo [27]. This hydrogenation function is very important to selectively crack the molecules [33]. Korre *et al.* [33] studied the kinetics and thermodynamics of the hydrocracking reaction for phenanthrene, a polynuclear aromatic hydrocarbon (PAH). Their findings support the fact that cracking takes place after partial or total hydrogenation of the aromatic rings. Figure 3 shows a suggested reaction scheme for the hydrocracking of phenanthrene [33]. First, phenanthrene hydrogenates, in the active centers of the bimetallic phase, then the hydrogenated molecules proceed with the isomerization into 5-membered methyl substitute compounds, followed by the ring-opening and the dealkylation steps which takes place in the acid sites of the supporting material. This scheme does not consider that also direct ring opening (skipping the isomerization step) may occur [34]. Additionally, some mechanisms have been suggested for paraffin hydrocracking, but also contemplating the interaction between the molecules and the Brønsted acid sites [35].

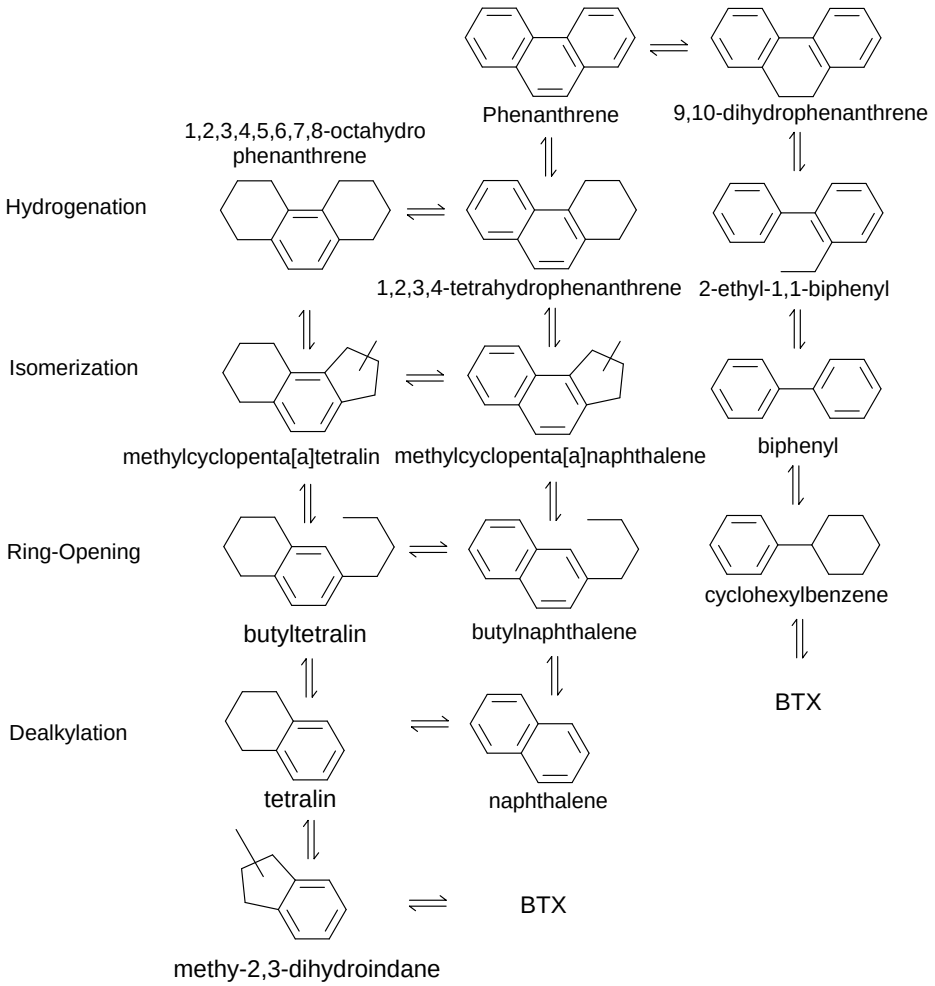

Figure 3. HCK reaction scheme for phenanthrene considering only partial hydrogenated steps, the perhydropehanthrene has not be considered in this scheme [33].

The poisoning effect of the nitrogen containing compounds over the hydrocracking

The nitrogenated compounds which are present in these heavy fractions are of two types, the organic and the inorganic molecules. The inorganic refers to the presence of ammonia, produced after the hydrodenitrogenation of the heterocycles. On the other hand, the organic nitrogenated molecules could also be classified into two groups, the one which has well defined basic character and the other with a weakly basic character [11]. These type of organic compounds are mainly: anilines which easily transform into ammonia; the 6-membered ring heterocycles, also called

pyridines, quinolines, acridines; those with a 5-membered heterocycles, namely: pyrroles, indoles and carbazoles; and in less proportion, the porphyrins [13]. One representative compound of each type is represented in Figure 4. The 6-membered ring heterocycles and the anilines often constitute the third part of the nitrogen-containing species, and they are the more basic molecules, thus being responsible for causing the acid sites poisoning. In contrast, the 5-membered ring heterocycles, more often described with a weakly basic character, have a presumably lower inhibitory effect [13].

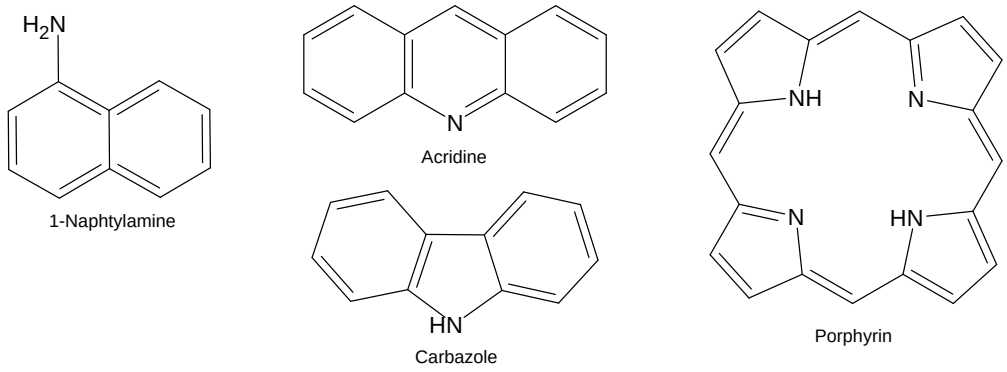

Figure 4. Some examples of nitrogen-containing species present in heavy fractions.

It is well known that ammonia and hydrogen sulfide interact with the catalyst active sites which promote the hydrogenation/dehydrogenation functionalities, also observed for some thiol and pyridine compounds [13, 36, 37]. On the other hand, the acid sites of the catalyst supporting material are considerably affected, mainly by ammonia and the organic nitrogen-containing compounds, whose basic character tend to neutralize them as depicted in Figure 5 [11, 14, 15]. It is clear then that a pretreatment unit is necessary for removing the heteroatoms that could affect the hydrocracking catalyst performance, taking into account that the catalyst deactivation has very important economic implications in the process.

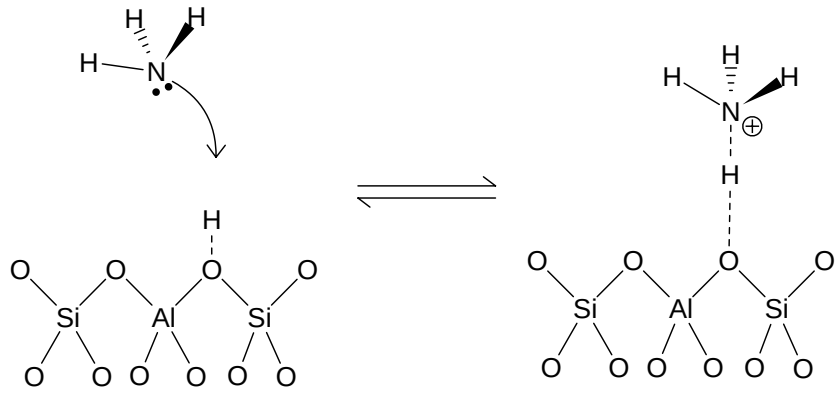

Figure 5. Ammonia adsorption on a Brønsted acid site of a silica-alumina material.

However, not all the heteroatoms are efficiently removed from the hydrocracking feedstocks, due to the presence of some molecules that are highly refractory to the hydrotreating conditions. For that reason, it is an important fact, to clearly know which species are more resistant to the hydrotreating operation, in order to understand which nitrogen-containing molecules are present during the hydrocracking.

Refractory to hydrotreating N-containing compounds in hydrocracking feedstocks

In the first characterization studies of this type, Jokuty and Murray [38] used field ionization mass spectrometry (FIMS) and nuclear magnetic resonance (NMR), to analyze a separated fraction from a previously hydrotreated Heavy Coker Gas Oil (HCGO), which contains the refractory nitrogen compounds. This Heavy Coker Gas Oil was hydrotreated with a NiMo/γ-Al_2O_3 catalyst, and the refractory nitrogen containing compounds were separated using the retention chromatography technique. They found that the most abundant species were carbazoles with alkyl substituents and partially hydrogenated benzocarbazoles. The presence of carbazole and tetrahydrocarbazole was also detected but in a lower amount. In the same way, basic compounds such as quinolines and benzoquinolines were also measured, but with a very low relative abundance. These results suggested that the basic species are easier to remove than those with a

weakly basic character. Wiwel *et al.*, based on theoretical calculations and NMR observations, suggested the existence of a very resistant to the hydrotreating carbazole-like compound, whose basic character is stronger than other carbazoles: the tetrahydrocycloheptacarbazole [39]. The authors affirm, based on their results, that this molecule has a stronger inhibitory effect than the carbazole, but they did not make any experimental test to prove it. Additionally, it is not very clear if this compound is derived from the pretreatment.

Modern mass spectrometry techniques with higher resolution power, which can resolve spectra up to 50 peaks per nominal mass, can distinguish between many families of compounds which commonly overlap with conventional mass spectrometry techniques, in these very complex fractions. The study of the constituents in these fractions is known as *petroleomics* [40, 41]. Kekäläinen *et al.* [42] implemented the Fourier Transform Ion Cyclotron Resonance Mass Spectrometry (FT-ICR-MS) coupled with Electron Spray Ionization (ESI) to determine which families of compounds were present in a hydrotreated Vacuum Gas Oil with $MoS_2/\gamma\text{-}Al_2O_3$ catalyst, at 5 MPa and temperatures between 573 and 653 K. Regarding only the nitrogen compounds, they found that the basic molecules, which are detected in the positive ESI mode, were easier to remove. The most abundant family of basic compounds after the hydrotreating is the N_1 stoichiometry, which corresponds to quinolines and benzoquinolines. Despite the N_2 stoichiometry was also very abundant before pretreating the Vacuum Gas Oil, it was almost completely removed from the products after the hydrotreating. On the other hand, the weakly basic nitrogen-containing compounds which are detected in the negative ESI mode, were mainly of stoichiometry N_1. After pretreatment a considerably amount of them remains, which leads to the conclusion that weakly basic N-containing compounds are more refractory to the hydrotreating. Furthermore, the relative abundance of benzocarbazoles decreased after treatment, but the

presence of partially hydrogenated compounds, such as the tetrahydrobenzocarbazole significantly increased. Other heavy fractions have been characterized using this high resolution mass spectrometry technique. A similar trend was found for different heavy fractions, concerning the nitrogen content [43, 44]. Al-Hajji *et al.* [45] characterized a demetallized oil (DMO) using ESI(+/-) and atmospheric pressure photoionization (APPI) with the FT-ICR-MS. Regarding the nitrogen only, they also found a high relative abundance of the N_1 and N_2 stoichiometries for basic compounds, and N_1 for the weakly basic ones. By means of the APPI they could make an estimation about the abundance of the basic and the weakly basic nitrogenates in the demetallized oil. They found that the basic compounds have a relative abundance of 13.2% in comparison with the weakly basic compounds, whose relative abundance is about 1.2%. That is to say, the basic ones are present in almost 10 times the amount of the weakly basic. All this evidences that the basic compounds are easier to remove than the weakly basic, moreover, just some of them were partially hydrogenated but not removed.

Could this highly refractory to the hydrotreating nitrogenated compounds affect the hydrocracking performance?

Basic nitrogen-containing compounds

In the mild hydrocracking and the one-stage configuration, the presence of ammonia originated during the hydrotreating tends to negatively affect the catalyst performance. An estimation for heptane hydrocracking determined that, it is necessary to increase the temperature in 100 K when is introduced 6.1 kPa of ammonia partial pressure, to level off the conversion [14]. Firstly, an increase in temperature to recover the conversion rises the operational costs; secondly, the high temperature could seriously affect the catalyst textural properties, such as: the porosity and surface area [46]. Thirdly, high temperatures could also lead to thermal cracking, thus increasing the

amount of coke and gas produced [1]; as well as, negatively limiting the hydrogenation of aromatics, in consequence, decreasing the desired properties like the cetane number [39]. The effect of basic nitrogen compounds over hydrotreating and hydrocracking have been copiously studied in the literature, because its inhibitory effect is considerably greater than the expected for the weakly basic compounds [13]. Sau *et al.* [11] studied the effect of the pyridine concentration over the hydrocracking of a real hydrotreated crude oil fraction. By doping the fraction with pyridine at 100 ppm of total nitrogen content, the conversion was reduced from 80% to 20%, and was necessary to increase the temperature in 20 K to recover the activity observed in the reaction in absence of nitrogenates. In addition, they compared the inhibition caused by doping with pyridine, against that caused by the nitrogen-containing molecules within the feedstock. In conclusion, the nitrogen-containing compounds within the feedstock inhibited more than the pyridine itself at the same total nitrogen content. That is to say, the complexity of the nitrogen compounds in the heavy fractions leads to a greater inhibition than the observed using pyridine, one of the most basic organic compounds.

Weakly basic nitrogen-containing

There is a lack of information in the literature about the influence of the weakly basic nitrogen species over the hydrocracking. Furimsky and Messoth in a review about the hydroprocessing catalyst deactivation mentioned [13], that this weakly basic nitrogen-containing compounds are presumably easier to remove, and that its contribution for poisoning is not important. This affirmation is based on the analysis of the hydrogenation heats for the nitrogenated compounds, concluding that the species with weakly basic character could get hydrogenated at greater rates, hence promoting their hydrodenitrogenation. Notwithstanding, that not correctly explains what is experimentally observed. As it was shown before, in section 1.4, several studies have found that

the basic nitrogenates are, by far, easier to remove than weakly basic during hydrotreating. Furthermore, a kinetic study on the hydrodenitrogenation of a coker gas oil, found that the hydrogenation of these weakly basic compounds were the rate determining step of the kinetic model [47]. Despite many studies have been placed their interest on the inhibitory and poisoning effect of basic nitrogen-containing compounds on hydroprocessing catalyst, more attention must be paid on the effect of weakly basics in hydrotreating and hydrocracking operations.

One key point to clarify is the nomenclature to classify these compounds. As discussed before, the weakly basic nitrogen species are mainly polynuclear aromatic 5-membered heterocycles, like pyrroles, indoles, carbazoles, benzocarbazoles, etc. We prefer to call them, weakly basic nitrogen-containing compounds, because of its basic character, which has been studied and reported [48]. Nonetheless, some authors prefer to call them non-basic compounds, and it has been used several times in literature [42, 49]. This obeys the fact that these compounds could dissociate a proton in aqueous hydroxide solution to form resonating anions [50]. Likewise, the ion fragments of these nitrogenated molecules are detected in the negative ESI mode, with the acidic species [42]. However, it has been observed via infrared spectroscopy (FT-IR) in salts of indoles, the presence of N-protonated groups, which are only possible because of their weakly basic character [51]. Interest is focus in understanding the way these compounds interact with the active sites of the hydrocracking catalyst; thus, they will be denoted as weakly basic nitrogen-containing compounds.

In one related work, Li *et al.* measured the effect of weakly basic nitrogen-containing compounds over the fluid catalytic cracking (FCC) [44]. They found that the inhibition of the observed rate in presence of these compounds is not as severe as the one observed in presence of basic compounds [44]. Nonetheless, the Fluid Catalytic Cracking catalyst, concerning its

functionalities, is simpler than the hydrocracking catalyst, which usually consists of a type of modified zeolite [44], whereas that the hydrocracking one, as already mentioned, could have a metallic content, and a more complex supporting material with meso and microporosity [27]. Kobayashi *et al.* [15] studied a hydrotreated Vacuum Gas Oil doped with carbazole, to evaluate the effect of small amount of nitrogen content on the hydrocracking, using three different catalysts consisting on NiW supported in amorphous silica. They observed a pronounced decrease in the activity even using less than 2 ppm of total nitrogen content. In this regard, there is some evidence in the literature, indicating that the weakly basic nitrogen-containing molecules could negatively affect the hydrocracking catalyst performance. However, the way these molecules interact with the catalyst active sites, and if such compounds significantly affect its activity, and in consequence, the selectivity of the reaction, remains unclear. To give a light to all these affairs, is necessary to first understand the nature and the mechanisms of the chemical reactions which proceed on the catalyst active sites.

The hydrocracking reaction mechanism

The Vacuum Gas Oil and Coker Gas Oils are common feedstocks in high conversion hydrocracking, but other distillates are used in other hydrocracking configurations, e.g. Vacuum Residue in Slurry-Phase Hydrocracking [16]. Vacuum Gas Oils usually have a high content of Saturates and Aromatics, summing both more than the 85% of the components, the rest are mainly Resins, without a significant presence of Asphaltenes [52]. In contrast, heavier fractions, such as the Vacuum Residue, have a higher content of Resins and Asphaltenes, summing both about the 40% of the content [53]. There is a special interest about the aspects concerning the mild and high conversion hydrocracking, thereby, it is necessary to focus the attention on the deasphalted

Vacuum Gas Oils. Provided that, the hydrocracking matters of the polynuclear aromatic, saturated and aliphatic hydrocarbons will be addressed.

Due to the bifunctionality of the hydrocracking catalyst, hydrogenation/dehydrogenation, and cracking functions, a series of interactions and reactions will occur on the different active sites of the catalyst. Considering the polynuclear aromatic hydrocarbons, is widely accepted that partially or total hydrogenation occurs before the catalytic cracking proceeds, as shown in Figure 3 for the scheme of the phenanthrene reaction. Some hydrocracking mechanisms have been proposed in detail for aromatic and aliphatic hydrocarbons, based on the organic chemistry knowledge [34, 35]. Figure 6 shows the hydrocracking mechanism for aliphatic hydrocarbons, also known as paraffin, described by Baltanas *et al.* [35]. In this hydrocracking mechanism hydrogenation/dehydrogenation is performed in the metallic sites of the catalyst, while the isomerization, methyl shift, hydride shift, C-C bond scission and protonation/deprotonation occurs in the acid sites of the catalyst.

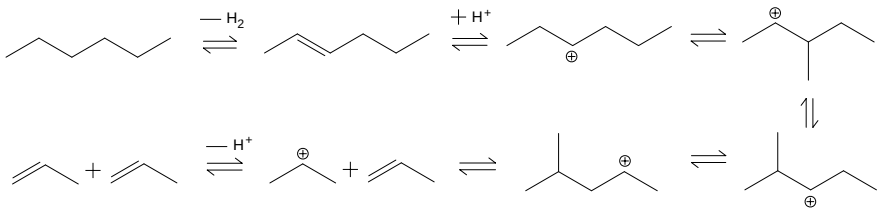

Figure 6. Hydrocracking mechanism for paraffins [35].

Lemberton *et al.* [34] proposed a similar mechanism in which dehydrogenation/protonation also take place in the metal phase, and protonation/deprotonation, hydride shifting, and isomerization takes place in the acid sites of the catalyst. Figure 7 shows the hydrocracking mechanism of a 3 rings aromatic compound, the 1,2,3,4-tetrahydrophenanthrene, leading only to one product, the 2-butylnaphthalene. Despite in appearance looks very similar to the mechanism proposed for

paraffin, as it involves almost the same chemistry, complexity in aromatics could lead, not only to different products but to different routes in which these mechanisms could occur [34]. As all these steps involve at least protonation/deprotonation, could be considered then that Brønsted acidity plays an important role during the catalytic cracking. The role of Lewis acidity has been also studied, and some mechanisms could be written for this type of acidity [29, 54]. Going back to the point, if the nitrogen containing species, in addition, interact with this acid sites, chemically or physically, then knowing the magnitude of this interaction could give an idea of what kind of inhibition (or poisoning) is undergoing; if it is strong and irreversible, or weak and some kind of competition is occurring.

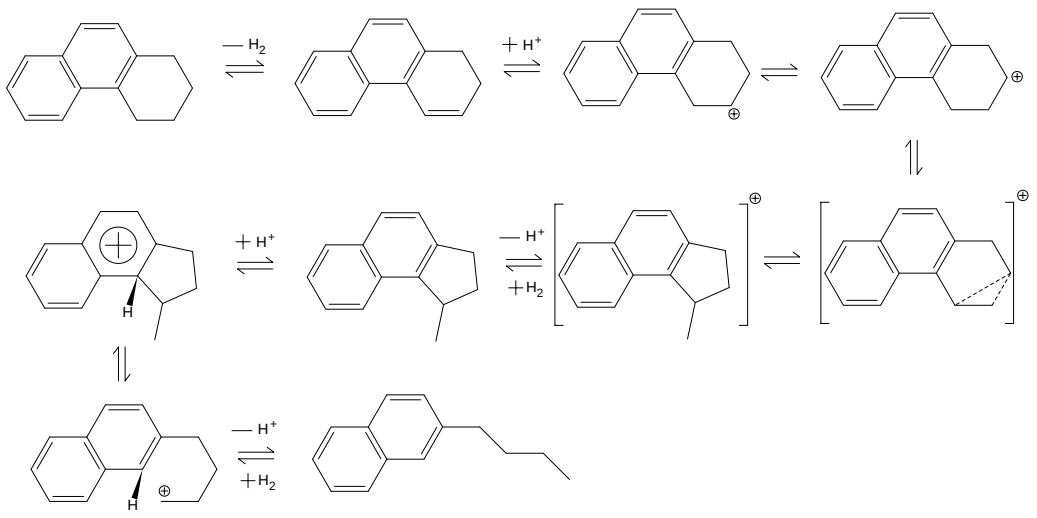

Figure 7. Hydrocracking mechanism for the 1,2,3,4-tetrahydrophenanthrene, following the external ring opening route [34].

Hydrocracking kinetics and thermochemical aspects

Having described some features about the hydrocracking mechanisms in Brønsted acid sites, a discussion about the thermochemistry and kinetics studies will provide the theoretical fundamentals for the involved catalytic phenomena. The kinetic modeling of the hydrocracking, not only explains many aspects concerning the selectivity and yields but also gives an idea of

determining steps, reaction rates, some aspects about the catalyst active sites and in fact all concerning the design of the reactor. For describing a kinetic model, it is necessary to propose some elementary steps, based on the mechanisms. But such models based on the analysis of elementary steps, are reasonable mathematical problems when the model does not involve very complex mechanism and only a few products and reactants. Nevertheless, when several components and complex mechanisms are involved, some approaches, strategies, and assumptions must be implemented.

To reduce the theoretical difficulty introduced by the complexity of the real heavy oil fractions, many studies have selected representative molecules from a chemical group, such as phenanthrene, which fairly represents the aromatic fraction within these hydrocracking feedstocks [33, 55]. Other studies have considered the use of linear paraffin, such as hexadecane, for modeling the aliphatic fraction, or to use more complex branched molecules such as the 2,6,10,15,19,23-hexametyl-tetracosane (squalene) [18]. The hydrocracking mechanism for paraffin and long aliphatic chains has been widely described in the literature [56]. Despite of this, there is not too much information available in the literature using model molecules for representing the heavy feedstocks in the kinetic modeling. Yet too many studies using real heavy crude oil fractions like vacuum gas oils [11, 14], vacuum residue [57] and even heavy and extra heavy oils [1, 16, 58]. Summarizing, many authors have drawn their attention to use real refinery feedstocks for kinetic modeling [59-62]. When a kinetic model is desired for one of these real feedstocks, then it must be considered that it involves more than 10 thousand compounds and that each reaction could lead to many products, following different routes. As the conventional heterogeneous kinetics consider non-linear equations, this becomes a huge mathematical problem. Then some solutions have been proposed to deal with this complexity.

Lumping modeling in hydrocracking

The lumped kinetic model has been extensively used in hydrocracking for describing these heavy fractions [63-67]. The methodology consists in making groups of chemical species, named lumps [60]. The complexity of the model will depend on the number of lumps considered, each lump groups chemical species with certain boiling point and they are discriminated from other lumps by a temperature range. An assumption that each lump or pseudo-component has a first-order irreversible kinetic is considered. Many of these models had contemplated that no polymerization or coke is formed. In addition, is assumed that each rate from the model is relative to the lump which represents the heavier aggrupation. The development of the kinetic model will depend on the chosen methodology, if it is discrete, or continuous [59]. These models are very accurate for reproducing the experimental values, even with real scale process [62]. Nonetheless, they are not very useful describing the mechanisms, in consequence, impractical for understanding the heterogeneous catalyst performance. In addition, this modeling strategy will be particular for the type of reactor and the composition of the feedstock, this will not be very useful for other systems, as it does not involve the reaction elementary steps [68]. Thereafter, to study inhibitory effects from a mechanistic point of view other strategies must be considered.

The Single Event approach in hydrocracking

The Single Event kinetic modeling leads to accurate predictions in hydrocracking [35]. This methodology describes the elementary steps involved; the model also includes the number of catalytic sites considered. The number of single events will depend on the symmetry number of the studied molecule. Using this methodology, the number of kinetic parameters is substantially reduced. As this approach is based on the chemistry, it will not depend on the reactor employed,

or the feedstock composition [68]. Some studies have been carried out for modeling petrochemical processes using the single event [69], in the hydrocracking of paraffin [68, 70], and also, for modeling real vacuum gas oils hydrocracking [71]. Rate parameters estimated with the Single Event approach, considering the hydrocracking elementary steps, i.e.: isomerization, hydride shifting, protonation /deprotonation, dehydrogenation /hydrogenation, methyl shifting and cracking; support the presence of the carbenium ion as a reaction intermediate of the mechanism [68, 70]. In conclusion, this strategy is suitable for studying the catalytic aspects at a kinetic level.

The Transition State Theory for modeling kinetics

A recent alternative is based on first-principles calculations, the transition state theory (TST), and the statistical thermodynamics, to estimate the thermochemical parameters of a kinetic model. This methodology is also known as the microkinetic description. Daudin *et al*. [72] studied the selectivity of the hydrogenation/hydrodesulfurization reactions of a model Fluid Catalytic Cracking. They obtained the hydrogenation and hydrodesulfurization rates, for a NiMoS catalyst, with a good agreement between the experimental results and the predicted trend. This methodology requires the structural configuration for each intermediate considered in the elementary steps and then the study of the activated complex by proposing a transition state (TS) between each intermediate. Thus, the activation energies and the reaction enthalpies are predicted by means of quantum mechanics calculations. In this order, is necessary to model the chemical structure of the catalyst active sites and how the molecule interacts with them on each elementary step. Figure 8 shows an example taken from Nurkowski *et al.* [73] for the following chemical reaction: C_2H_4 + $Si(OH)_4$ → $(OH)_3SiOCH_2$ + CH_3. In this study, the active site where the reaction occurred, is a silanol group (Si-O-H), from a $Si(OH)_4$ cluster. The authors used a fully ab-initio theory, the CASPT2 perturbational method, with a cc-pVDZ basis set. Hence, the ethylene protonation is

considered in the first elementary step, the transition state has a relative energy of -24.3 kcal·mol^{-1}, while the reactants have -75.8 kcal·mol^{-1}. In the first step, the intermediate product conformation corresponds to the protonated ethylene adsorbed on the oxygen, after transferring the proton to one carbon, this leads to a configuration with a lower energy value of -88.4 kcal·mol^{-1}. As could be appreciated, this activation energy is quite large, about 50 kcal·mol^{-1}. Firstly, because the cluster size is very small, and it does not include all the interactions which normally occur in the real catalyst (Van der Waals interactions and confinement effects), in other words, on these type of calculations, the cluster size influences strongly the predicted energies [74]. Secondly, because the acidity of silanol is not very high, compared with Brønsted acidity, in consequence it will cost more to transfer the proton from the silanol group to the carbon.

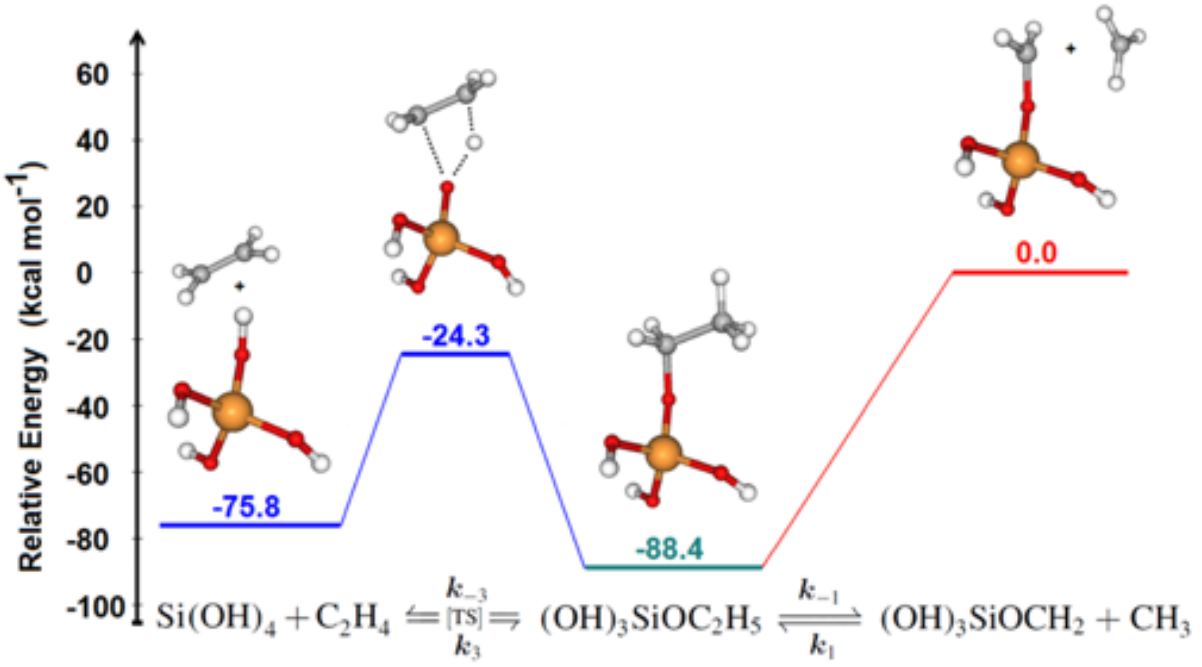

Figure 8. Transition State study in the ethylene decomposition over a $Si(OH)_4$ cluster, taken from Nurkowski *et al.* [73]

Computational chemistry as a tool for modeling hydrocracking

There are several reports in the literature about the modeling of materials for hydroprocesses using computational chemistry [75-77]. Depending on the nature of the catalyst and the characteristics of the process, some authors have focused on the metallic active phase, which often provides the hydrogenation/dehydrogenation and hydrogenolysis functionalities. Many systems have been studied using quantum mechanical calculations, in order to obtain a proper description of the different transition metal systems i.e. MoS_2 [78-80], NiMoS [81, 82], CoMoS [82], CoPd [83], and PdPt [84, 85]; commonly used in hydrotreating and hydrocracking. On the other hand, zeolites have also been studied, due to their wide application in catalysis, and in particular, in some refinery processes like Fluid Catalytic Cracking and hydrocracking [74, 86-90]. As it was mentioned before, the hydrocracking catalyst has two important functionalities, the hydrogenation/dehydrogenation and the acid one. The most common transition metal-based active phases used in hydorcracking for providing the hydrogenation/dehydrogenation function are: MoS_2 [42], NiMoS [27], FeWS [30], and NiWS. Whereas, for providing acidity to the catalyst, the most common one is the Y Zeolite [27]. There are some theories which describe the nature and reactivity of the different sulfur metallic sites of the catalyst [72, 82, 91-93]. About the structure, it is well known that the MoS_2 consists of slabs of Mo tetra and hexacoordinated with sulfur atoms with D_{3h} symmetry group, as shown in Figure 9a [78, 79, 91]. When nickel or cobalt is added, a possible conformation could be hexacoordinated in the edge, as shown for nickel in Figure 9b [81, 82].

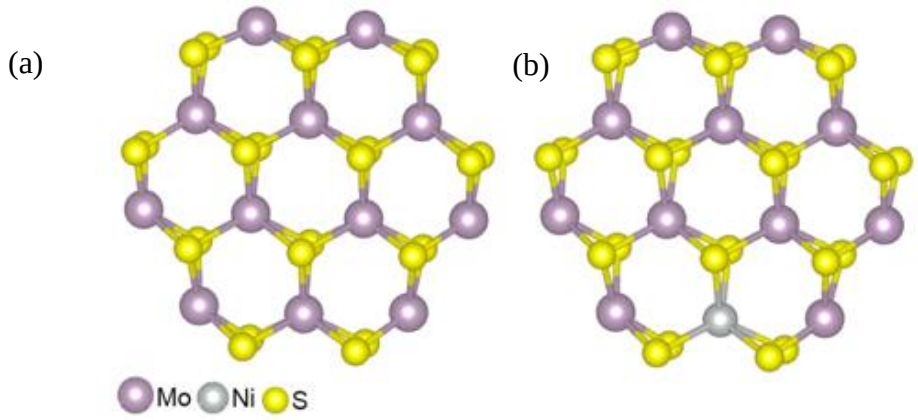

Figure 9. (a) $Mo_{12}S_{24}$ (b) $NiMo_{11}S_{24}$ clusters.

Despite the relevance of the sulfur metallic sites in hydrocracking, the hydrogenation rates are almost the same both in hydrocracking as well as in hydroreating; and also, that hydrogenation is not the rate determining step in hydrocracking [33]. With this in mind, and also considering that the inhibitory effect caused by nitrogenates is considerably stronger for the acid sites than for the metallic active sites [33], attention should be placed in understanding firstly the steps of the hydrocracking mechanisms which occur on the Brønsted acid sites. Different types of zeolites have been modeled in order to simulate the Brønsted acidity, but it is very important to define the size of the system, i.e. just considering a zeolite fragment completing the terminal atoms with hydrogens (Figure 10a), a silica-alumina cluster of one cavity of the zeolite (Figure 10b), or the whole unit cell taking into account periodic boundary conditions (Figure 10c) [86]. For aspects related to the geometry, the cluster approach against the periodic one, leads to very similar results, in fact even studying the transition states, the elementary steps remain the same [86]. But the energy estimation depends strongly on the considered approach, for which the periodic approach leads to a better estimation of the energy value [86]. And this could be appreciated as long as the number of atoms increases in the cluster approach, the bigger the cluster the better the estimation [74]. Highlighting, that working with the periodic approach, despite it leads to very good results,

will demand a lot of computational effort, because of the large amount in the number of atoms. For that reason, when periodic structures are considered, is expected the use of pseudopotentials, which aim to reduce the complexity of the calculation, by considering only the valence shell electrons, and the others are considered as an effective core potential [94].

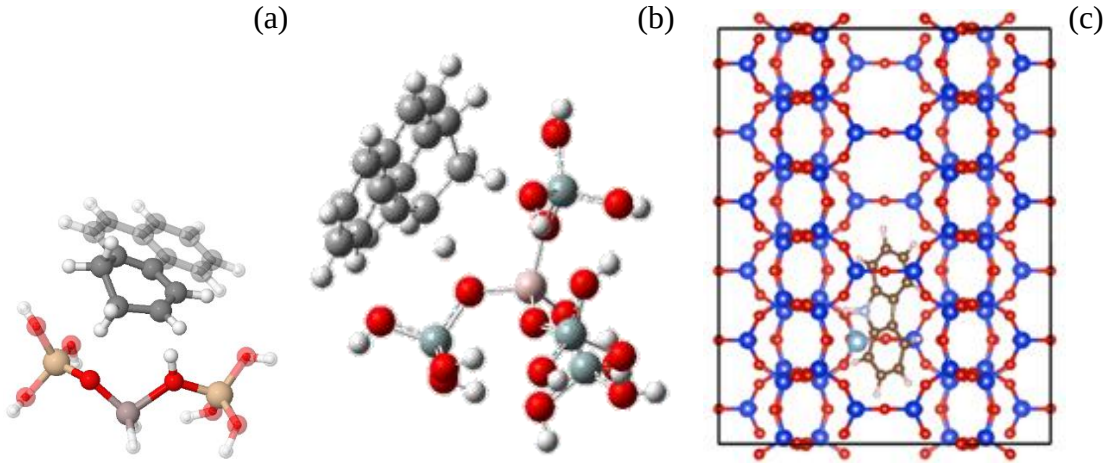

Figure 10. Representations of different approaches for modeling (a) a zeolite fragment, (b) a zeolite cluster of a cavity and (c) the bulk zeolite unit cell with periodicity.

Perspectives of this work

In light of the evidence, in this work, the aim was to measure the impact in the hydrocracking stage, in terms of catalytic activity, and the selectivities toward the different products. For such reason, the first chapter of this book concerns the characterization of a Vacuum Gas Oil obtained from the Colombian refinery. This fraction was characterized before and after hydrotreating, achieving small amounts of total nitrogen content, in a way to identify the most refractory nitrogen-containing compounds which will be present at the subsequent hydrocracking stage. To that end, the Electron Spray Ionization coupled with the Fourier Transform Ion Cyclotron Resonance Mass Spectrometry was used, in the positive and negative modes, for detecting the basic and weakly basic nitrogen-containing, respectively. Results from this analysis, allowed to identify carbazole and tetrahydrocarbazole, as molecules which fairly represent these highly refractory to

hydrodenitrogenation compounds. Hence, an assessment of the effect over the catalyst performance in the phenanthrene hydrocracking reaction, when these weakly basic nitrogenated compounds are present in different ratios was performed. Chapter two offers a discussion from a statistical point of view to evaluate the effect of the operational variables, i.e.: temperature, liquid hourly space velocity, and the relative concentration of weakly basic nitrogen-containing within the feed, over the activity and the selectivity towards the different hydrocracking products of the phenanthrene reaction. An additional exploratory study was performed to raise some affairs concerning the contribution to the inhibition caused by weakly basic compounds in presence of a severe basic atmosphere. Results from this study showed that these weakly basic nitrogen-containing significantly inhibit the hydrocracking reactions on the catalyst tested and suggested that these molecules are preferentially adsorbing on the Brønsted acid sites of the catalyst, thus affecting one of the postulated routes of the phenanthrene hydrocracking. To describe the interactions of the N-containing compounds which are present during the hydrocracking, with the active sites of the catalyst, chapter three addresses the thermodynamics and mechanistic issues of the hydrocracking of phenanthrene from a theoretical approach, based on the DFT. A surface Brønsted site is modeled on a zeolite, considering the same level of theory for the complete unit cell, using the Perdew-Burke-Ernzernhof functional, plane wave functions, pseudopotentials, and periodic boundary conditions. Activation energies, enthalpies, intermediates and transition states were determined for the phenanthrene reaction; in addition, the discussion about the adsorption energies of some polynuclear aromatic hydrocarbons and nitrogenates are included herein, in order to discern if the magnitude of the computed adsorption energies of nitrogenates is significant to make a correlation with the inhibitory effects experimentally observed. The last chapter of this book, chapter four, concerns the development of a methodology for measuring *in situ* the

adsorption process of nitrogenated probe molecules in the liquid phase with infrared spectroscopy. Data correlation based on DFT calculations was performed, for helping the assignments of the observed bands, to determine if these weakly basic nitrogen-containing compounds are physically adosorbing or chemisorbing on the zeolite acid sites. Results from this assessment showed that the weakly basic nitrogenated molecule hereof studied strongly interact with the silanol and Brønsted acid sites of the catalyst, as predicted with the theoretical calculations, and suggested with the reactivity tests. In conclusion, this work makes a contribution which is of interest to the catalytic industry, and also suggests considering new factors in the development of materials destined for hydrocracking.

References

[1] Hsu, C.S. Hydrotreating and hydrocracking: Fundamentals. Practical advances in *petroleum processing*. (Eds.) Robinson, P.R. Springer **2006**, p. 866.

[2] Liu, Y.; Gao, L.; Wen, L.; Zong, B. Recent Advances in Heavy Oil Hydroprocessing Technologies. *Recent Pat. Chem. Eng*. **2009**, 2, (1), 22-36.

[3] Speight, J.G. New approaches to hydroprocessing. *Catal. Today* **2004**, 98, (1–2), 55-60.

[4] Speight, J.G. Chapter 7 - Heavy Feedstock Refining—The Future. In: *Heavy and Extra-heavy Oil Upgrading Technologies.* Boston: Gulf Professional Publishing; **2013**, p. 149-62.

[5] Speight, J.G. Chapter 5 - Hydrocracking. In: *Heavy and Extra-heavy Oil Upgrading Technologies.* Boston: Gulf Professional Publishing; **2013,** p. 95-128.

[6] Kim, D.; Gautam, M.; Gera, D. Parametric studies on the formation of diesel particulate matter via nucleation and coagulation modes. *J. Aerosol Sci.* **2002,** 33, (12), 1609-21.

[7] Yao, Q.; Li, S.Q.; Xu, H.W.; Zhuo, J.K.; Song, Q. Studies on formation and control of combustion particulate matter in China: A review. *Energy* **2009**, 34, (9), 1296-309.

[8] W.H.O. Air Quality Guidelines for Europe. Second ed.; **2000.**

[9] Saavedra Trujillo, N.F.; Jiménez Inocencio, F.Y. Necesidades de Innovación y Tecnología para la industria de petróleo y gas en Colombia. *Revista de Ingeniería* **2014**, 40, 50-6.

[10] Motaghi, M.; Ulrich, B. Subramanian Slurry-phase hydrocracking—possible solution to refining margins. *Hydrocarbon Process* **2011**, 90, 37-43.

[11] Sau, M.; Basak, K.; Manna, U.; Santra, M.; Verma, R.P. Effects of organic nitrogen compounds on hydrotreating and hydrocracking reactions. *Catal. Today* **2005**, 109, (1–4), 112-9.

[12] Prins, R. Catalytic hydrodenitrogenation. *Advances in Catalysis.* Academic Press; **2001,** p. 399-464.

[13] Furimsky E.; Massoth, F.E. Deactivation of hydroprocessing catalysts. *Catal. Today* **1999**, 52, (4), 381-495.

[14] Dufresne, P.; Quesada, A.; Mignard, S. Influence of Nitrogen Feed Content On The Performances of A Zeolite Hydrocracking Catalyst. In: *Studies in Surface Science and Catalysis.* Elsevier **1989,** p. 301-15.

[15] Kobayashi, M.; Togawa, S.; Ishida, K. Effects of Small Amounts of Nitrogen Compounds in Feedstock on Performance of Hydrocracking Catalyst. . *J. Japn. Petrol. Inst* **2007**, 50, (1), 44-52.

[16] Rana, M.S.; Sámano, V.; Ancheyta, J.; Diaz, J.A.I. A review of recent advances on process technologies for upgrading of heavy oils and residua. *Fuel* **2007**, 86, (9), 1216-31.

[17] Leyva, C.; Ancheyta, J.; Travert, A.; Maugé, F.; Mariey, L.; Ramírez, J. Activity and surface properties of NiMo/SiO2–Al2O3 catalysts for hydroprocessing of heavy oils. *Appl. Catal., A* **2012**, 425–426, 1-12.

[18] Francis J.; Guillon, E.; Bats, N.; Pichon, C.; Corma, A.; Simon, L.J. Design of improved hydrocracking catalysts by increasing the proximity between acid and metallic sites. *Appl. Catal., A* **2011**, 409–410, 140-7.

[19] Kouzu, M.; Kuriki, Y.; Uchida, K.; Sakanishi, K.; Sugimoto, Y.; Saito, I. Catalytic Hydrocracking of Petroleum Residue over Carbon-Supported Nickel−Molybdenum Sulfides. *Energy Fuels* **2005**, 19, (3), 725-30.

[20] Ali, M.A.; Tatsumi, T.; Masuda, T. Development of heavy oil hydrocracking catalysts using amorphous silica-alumina and zeolites as catalyst supports. *Appl. Catal., A* **2002**, 233, (1–2), 77-90.

[21] Furimsky E. Selection of catalysts and reactors for hydroprocessing. *Appl. Catal., A* **1998**, 171, (2), 177-206.

[22] Akmaz, S.; Caglayan, P.A. Effect of Catalyst, Temperature, and Hydrogen Pressure on Slurry Hydrocracking Reactions of Naphthalene. *Chem. Eng. Technol*. **2015**, 38, (5), 917-30.

[23] Liu, D.; Kong, X.; Li, M.; Que, G. Study on a Water-Soluble Catalyst for Slurry-Phase Hydrocracking of an Atmospheric Residue. *Energy Fuels* **2009**, 23, (2), 958-61.

[24] Liu, D.; Li, M.; Deng, W.; Que, G. Reactivity and Composition of Dispersed Ni Catalyst for Slurry-Phase Residue Hydrocracking. *Energy Fuels* **2010**, 24, (3), 1958-62.

[25] Zhang, S.; Liu, D.; Deng, W.; Que, G. A Review of Slurry-Phase Hydrocracking Heavy Oil Technology. *Energy Fuels* **2007**, 21, (6), 3057-62.

[26] Gómez-Vargas, L.E.; Baldovino-Medrano, V.G.; Pérez-Martínez, D.J. Influence of solids in slurry hydrocracking for upgrading of heavy crude oils. *Int. Symp. Adv. Hydroprocessing Oil Fractions. ISAHOF*. México; **2017**:135–6.

[27] Agudelo J.L.; Hensen E.J.M.; Giraldo, S.A.; Hoyos, L.J. Influence of steam-calcination and acid leaching treatment on the VGO hydrocracking performance of faujasite zeolite. *Fuel Process. Technol.* **2015**;133:89-96.

[28] Barzetti, T.; Selli, E.; Moscotti, D.; Forni, L. Pyridine and ammonia as probes for FTIR analysis of solid acid catalysts. Journal of the Chemical Society, *Faraday Trans* **1996,** 92, (8), 1401-7.

[29] Gruia A. Distillate hydrocracking. In: Jones DSJS, Pujadó PR, editors. Handbook of Petroleum Processing. Dordrecht: Springer Netherlands; **2006,** p. 287-320.

[30] Restrepo-Garcia, J.R.; Baldovino-Medrano, V.G.; Giraldo, S.A. Improving the selectivity in hydrocracking of phenanthrene over mesoporous Al-SBA-15 based Fe–W catalysts by enhancing mesoporosity and acidity. *Appl. Catal., A* **2016**, 510, 98-109.

[31] Barbosa, F.A.; Santos, A.C.B., Silva, M.I.P., Stumbo A.M. Resistance to poisoning by nitrogen compounds of NiMo/Al-MCM-41 hydrocracking catalysts. *Catal. Today* **2004**, 98, (1–2), 109-13.

[32] Herrera, J.M; Reyes, J.; Roquero, P.; Klimova, T. New hydrotreating NiMo catalysts supported on MCM-41 modified with phosphorus. *Microporous Mesoporous Mater.* **2005**, 83, (1–3), 283-91.

[33] Korre, S.C.; Klein, M.T.; Quann, R.J. Hydrocracking of Polynuclear Aromatic Hydrocarbons. Development of Rate Laws through Inhibition Studies. *Ind. Eng. Chem. Res.* **1997**, 36, (6), 2041-50.

[34] Lemberton, J-L, Guisnet, M. Phenanthrene hydroconversion as a potential test reaction for the hydrogenating and cracking properties of coal hydroliquefaction catalysts. *Appl. Catal.* **1984**, 13, (1), 181-92.

[35] Baltanas, M.A.; Van Raemdonck, K.K.; Froment, G.F.; Mohedas, S.R. Fundamental kinetic modeling of hydroisomerization and hydrocracking on noble metal-loaded faujasites. 1. Rate parameters for hydroisomerization. *Ind. Eng. Chem. Res.* **1989**, 28, (7), 899-910.

[36] Jongpatiwut, S.; Li, Z.; Resasco, D.E.; Alvarez, W.E.; Sughrue, E.L.; Dodwell, G.W. Competitive hydrogenation of poly-aromatic hydrocarbons on sulfur-resistant bimetallic Pt-Pd catalysts. *Appl. Catal., A* **2004**, 262, (2), 241-53.

[37] Pawelec, B.; Castaño, P.; Arandes, J.M.; Bilbao, J.; Thomas, S.; Peña, M.A. Factors influencing the thioresistance of nickel catalysts in aromatics hydrogenation. *Appl. Catal., A* **2007**, 317, (1), 20-33.

[38] Jokuty, P.L.; Gray, M.R. Resistant nitrogen compounds in hydrotreated gas oil from Athabasca bitumen. *Energy Fuels* **1991**, 5, (6), 791-5.

[39] Wiwel, P.; Hinnemann, B.; Hidalgo-Vivas, A.; Zeuthen, P.; Petersen, B.O.; Duus, J.Ø. Characterization and Identification of the most Refractory Nitrogen Compounds in Hydroprocessed Vacuum Gas Oil. *Ind. Eng. Chem. Res.* **2010**, 49, (7), 3184-93.

[40] Rodgers, R.P.; Schaub, T.M.; Marshall, A.G. Petroleomics: MS Returns to Its Roots. *Anal. Chem.* **2005**, 77, (1), 20 A-7 A.

[41] Hsu, C.S.; Hendrickson, C.L.; Rodgers, R.P.; McKenna, A.M.; Marshall, A.G. Petroleomics: advanced molecular probe for petroleum heavy ends. *J. Mass Spectrom.* **2011**, 46, (4), 337-43.

[42] Kekäläinen, T.; Pakarinen, J.M.H.; Wickström, K.; Vainiotalo, P. Compositional Study of Polar Species in Untreated and Hydrotreated Gas Oil Samples by Electrospray Ionization Fourier Transform Ion Cyclotron Resonance Mass Spectrometry (ESI FTICR−MS). *Energy Fuels* **2009**, 23, (12), 6055-61.

[43] Li, X.; Zhu, J.; Wu, B.; Mao, X. Characterization of Acidic Compounds in Vacuum Gas Oils and Their Dewaxed Oils by Fourier Transform-Ion Cyclotron Resonance Mass Spectrometry. *Energy Fuels* **2012**, 26, (9), 5646-54.

[44] Li, Z-k.; Gao, J-s.; Wang, G.; Shi, Q.; Xu, C-m. Influence of Nonbasic Nitrogen Compounds and Condensed Aromatics on Coker Gas Oil Catalytic Cracking and Their Characterization. *Ind. Eng. Chem. Res.* **2011**, 50, (15), 9415-24.

[45] Al-Hajji, A.A.; Muller, H.; Koseoglu, O.R. Caractérisation par spectrométrie de masse par résonance cyclotronique ionique à transformée de Fourier des composés azotés et soufrés dans les charges d'alimentation d'hydrocraquage. *Oil Gas Sci. Technol. – Rev* **2008**, 63, (1), 115-28.

[46] Belaya, L.A; Doronin, V.P.; Sorokina, T.P.; Gulyaeva, T.I. Thermal stability of zeolites Y and ZSM-5 in matrices of various compositions. *Russ. J. Appl. Chem.* **2009**, 82, (2), 236-42.

[47] Wei, Q.; Wen, S.; Tao, X.; Zhang, T.; Zhou, Y.; Chung, K. Hydrodenitrogenation of basic and non-basic nitrogen-containing compounds in coker gas oil. *Fuel Process. Technol.* **2015**, 129, 76-84.

[48] Hinman, R.L.; Lang, J. The Protonation of Indoles. Basicity Studies. The Dependence of Acidity Functions on Indicator Structure. *J. Amer. Chem. Soc.* **1964**, 86, (18), 3796-806.

[49] Liu, D.; Fu, Y.; Deng, W.; Shi, Q.; Ma, K.; Hou, T. FT-ICR MS Analysis of Nitrogen-Containing Compounds in the Products of Liaohe Atmospheric Residue Hydrocracking. *Energy Fuels* **2011**, 26, (1), 624-8.

[50] Yagil, G. The proton dissociation constant of pyrrole, indole and related compounds. Tetrahedron **1967**, 23, (6), 2855-61.

[51] Hinman, R.L.; Whipple, E.B. The Protonation of Indoles: Position of Protonation. *J. Amer. Chem. Soc.* **1962**, 84, (13):2534-9.

[52] Stratiev, D.S.; Shishkova, I.K.; Nikolaychuk, E.; Sharafutdinov, I.M.; Vely, A.; Mitkova, M. Relationship of the aromatic structural types in vacuum gas oil to empirical correlations based on bulk properties. *Petrol. Sci. Technol*. **2016**, 34, (9), 860-5.

[53] León, A-Y.; Parra, M-J. Determination of molecular weight of vacuum residue and their sara fractions. *Revista CT&F* **2010**, 4, 101-12.

[54] Corma, A.; Wojciechowski, B.W. Some ideas on cracking catalyst design. *Can. J. Chem. Eng.* **1982**, 60, (1), 11-6.

[55] Benazzi, E.; Leite, L.; Marchal-George, N.; Toulhoat, H.; Raybaud, P. New insights into parameters controlling the selectivity in hydrocracking reactions. *J. Catal.* **2003**, 217, (2), 376-87.

[56] Coonradt, H.L.; Garwood, W.E. Mechanism of Hydrocracking. Reactions of Paraffins and Olefins. *Ind. Eng. Chem. Process Des. Dev.* **1964**, 3, (1), 38-45.

[57] Rezaei, H.; Liu, X.; Ardakani, S.J.; Smith, K.J.; Bricker, M. A study of Cold Lake Vacuum Residue hydroconversion in batch and semi-batch reactors using unsupported MoS2 catalysts. *Catal. Today* **2010**, 150, (3–4), 244-54.

[58] Jeon, S.G.; Na, J-G.; Ko, C.H.; Yi, K.B.; Rho, N.S.; Park, S.B. Preparation and Application of an Oil-Soluble CoMo Bimetallic Catalyst for the Hydrocracking of Oil Sands Bitumen. *Energy Fuels* **2011**, 25, (10), 4256-60.

[59] Lababidi, H.M.S; AlHumaidan, F.S. Modeling the Hydrocracking Kinetics of Atmospheric Residue in Hydrotreating Processes by the Continuous Lumping Approach. *Energy Fuels* **2011**, 25, (5), 1939-49.

[60] Ancheyta, J.; Sánchez, S.; Rodríguez, M.A. Kinetic modeling of hydrocracking of heavy oil fractions: A review. *Catal. Today* **2005**, 109, (1–4), 76-92.

[61] Elizalde, I.; Rodríguez, M.A.; Ancheyta, J. Modeling the effect of pressure and temperature on the hydrocracking of heavy crude oil by the continuous kinetic lumping approach. *Appl. Catal., A* **2010**, 382, (2), 205-12.

[62] Martínez, J.; Ancheyta, J. Kinetic model for hydrocracking of heavy oil in a CSTR involving short term catalyst deactivation. *Fuel* **2012**, 100, 193-9.

[63] Laxminarasimhan, C.S.; Verma, R.P.; Ramachandran, P.A. Continuous lumping model for simulation of hydrocracking. *AIChE J.* **1996**, 42, (9), 2645-53.

[64] Fukuyama, H.; Terai, S. Kinetic Study on the Hydrocracking Reaction of Vacuum Residue Using a Lumping Model. *Petrol. Sci. Technol.* **2007**, 25, (1-2), 277-87.

[65] Elizalde, I.; Rodríguez, M.A.; Ancheyta, J. Application of continuous kinetic lumping modeling to moderate hydrocracking of heavy oil. *Appl Catal., A* **2009**, 365, (2), 237-42.

[66] Ayasse, A.R.; Nagaishi, H.; Chan, E.W.; Gray, M.R. Lumped kinetics of hydrocracking of bitumen. *Fuel* **1997**, 76, (11), 1025-33.

[67] Sadighi, S.; Ahmad, A.; Irandoukht, A. Kinetic Study on a Commercial Amorphous Hydrocracking Catalyst by Weighted Lumping Strategy. *Int. J. Chem. Reac. Eng.* **2010**, 8(1)

[68] Svoboda, G.D.; Vynckier, E.; Debrabandere, B.; Froment, G.F. Single-Event Rate Parameters for Paraffin Hydrocracking on a Pt/US-Y Zeolite. *Ind. Eng. Chem. Res* **1995**, 34, (11), 3793-800.

[69] Alwahabi, S.M.; Froment, G.F. Single Event Kinetic Modeling of the Methanol-to-Olefins Process on SAPO-34. *Ind. Eng. Chem. Res* **2004**, 43, (17), 5098-111.

[70] Kumar, H.; Froment, G.F. A Generalized Mechanistic Kinetic Model for the Hydroisomerization and Hydrocracking of Long-Chain Paraffins. *Ind. Eng. Chem. Res* **2006**, 46, (12), 4075-90.

[71] Kumar, H.; Froment, G.F. Mechanistic Kinetic Modeling of the Hydrocracking of Complex Feedstocks, such as Vacuum Gas Oils. *Ind. Eng. Chem. Res* **2007**, 46, (18), 5881-97.

[72] Daudin, A.; Lamic, A.F.; Pérot, G.; Brunet, S.; Raybaud, P.; Bouchy, C. Microkinetic interpretation of HDS/HYDO selectivity of the transformation of a model FCC gasoline over transition metal sulfides. *Catal. Today* **2008**, 130, (1), 221-30.

[73] Nurkowski, D.; Klippenstein Stephen, J.; Georgievskii, Y.; Verdicchio, M.; Jasper Ahren, W.; Akroyd, J. Ab initio Variational Transition State Theory and Master Equation Study of the Reaction (OH)3SiOCH2 + CH3 ⇌ (OH)3SiOC2H5. *Z. Phys. Chem.* **2015**, 229:691.

[74] García-Serrano, L.A.; Flores-Sandoval, C.A.; Zaragoza, I.P. Theoretical study of the adsorption of isobutane over H-mordenite zeolite by ab initio and DFT methods. *J. Mol. Catal., A* **2003**, 200, (1–2), 205-12.

[75] Chen, M.; Wayne Goodman, D. Chapter 5 Oxide-supported metal clusters. In: Woodruff DP, editor The Chemical Physics of Solid Surfaces. Elsevier; **2007,** p. 201-69.

[76] Naoki, T.; Toshiharu, T. Preparation, Characterization, and Properties of Bimetallic Nanoparticles. *Catalysis and Electrocatalysis at Nanoparticle Surfaces*. CRC Press; **2003.**

[77] Ferrando, R.; Jellinek, J.; Johnston, R.L. ChemInform Abstract: Nanoalloys: From Theory to Applications of Alloy Clusters and Nanoparticles. ChemInform **2008,** 39, (24), 845–910.

[78] Zakharov, I.I.; Voroshina, O.V.; Startsev, A.N. The molecular and electronic structure of the Mo12S24 macromolecule as a model of the active component of a hydrodesulfurization catalyst. *Russ. J. Phys. Chem.* **2006**, 80, (7), 1083-7.

[79] Orita, H.; Uchida, K.; Itoh, N. Ab initio density functional study of the structural and electronic properties of an MoS2 catalyst model: a real size Mo27S54 cluster. *J. Mol. Catal., A* **2003**, 195, (1–2), 173-80.

[80] Faye, P.; Payen, E.; Bougeard, D. Density Functional Approach of a γ-Alumina Supported MoS2Hydrotreating Catalyst. *J. Catal.* **1998**, 179, (2), 560-4.

[81] Song, T.; Zhang, Z.; Chen, J.; Ring, Z.; Yang, H.; Zheng, Y. Effect of Aromatics on Deep Hydrodesulfurization of Dibenzothiophene and 4,6-Dimethyldibenzothiophene over NiMo/Al2O3 Catalyst. *Energy Fuels* **2006**, 20, (6), 2344-9.

[82] Travert, A.; Dujardin, C.; Maugé, F.; Veilly, E.; Cristol, S.; Paul, J.F. CO Adsorption on CoMo and NiMo Sulfide Catalysts: A Combined IR and DFT Study. *J. Phys. Chem., B* **2006**, 110, (3), 1261-70.

[83] Hossain, M.M. Co–Pd/γ-Al2O3 catalyst for heavy oil upgrading: Desorption kinetics, reducibility and catalytic activity. *Can. J. Chem. Eng.* **2012**, 90, (4), 946-955.

[84] Aprà, E.; Fortunelli, A. Density-Functional Calculations on Platinum Nanoclusters: Pt13, Pt38, and Pt55. *J Phys Chem., A* **2003**, 107, (16), 2934-42.

[85] Celis-Cornejo, C.M.; Gómez-Ballesteros, J.L; Giraldo S.A. Factors influencing the charge distribution on PdxPty bimetallic nanoparticles, *Revista ION*, **2013**, 26, (2), 65-72.

[86] Rozanska, X.; Santen, R.Av. Chapter 6 - Reaction mechanisms in protonic zeolites. *Computer Modelling of Microporous Materials*. London: Academic Press; **2004,** p. 165-200.

[87] Gounder, R.; Iglesia, E. Catalytic hydrogenation of alkenes on acidic zeolites: Mechanistic connections to monomolecular alkane dehydrogenation reactions. *J. Catal.* **2011**, 277, (1), 36-45.

[88] Milas, I.; Chaer Nascimento, M.A. A density functional study on the effect of the zeolite cavity on its catalytic activity: The dehydrogenation and cracking reactions of isobutane over HZSM-5 and HY zeolites. *Chem. Phys. Lett.* **2006**, 418, (4–6), 368-72.

[89] Milas, I.; Chaer Nascimento, M.A. The dehydrogenation and cracking reactions of isobutane over the ZSM-5 zeolite. *Chem. Phys. Lett.* **2003**, 373, (3–4), 379-84.

[90] Bucko, T.; Benco, L.; Demuth ,T.; Hafner J. Ab initio density functional investigation of the (001) surface of mordenite. *J. Chem. Phys.* **2002**, 117, (15), 7295-305.

[91] Tuxen, A.; Kibsgaard, J.; Gøbel, H.; Lægsgaard, E.; Topsøe, H.; Lauritsen, J.V. Size Threshold in the Dibenzothiophene Adsorption on MoS2 Nanoclusters. *ACS Nano* **2010**, 4,(8), 4677-82.

[92] Morales-Valencia, E.M.; Baldovino-Medrano, V.G.; Giraldo, S.A. Reactivity of olefins and inhibition effect on the hydrodesulfurization of a model FCC naphtha. *Fuel* **2015**, 153, (Supplement C):294-302.

[93] Michel, V.; Dorothée, L.; Christophe, G. Use of competitive kinetics for the understanding of deep hydrodesulfurization and sulfide catalysts behavior. *Appl Catal., B* **2012**, 128, 3-9.

[94] Paier, J.; Hirschl, R.; Marsman, M.; Kresse, G. The Perdew–Burke–Ernzerhof exchange-correlation functional applied to the G2-1 test set using a plane-wave basis set. *J. Chem. Phys.* **2005**, 122, (23), 234102.

CHAPTER 1: Identification of Refractory Weakly Basic Nitrogen-Containing Compounds in a Hydrotreated Vacuum Gas Oil and Their Effect Over a Ni-MoS_2/Y-Zeolite␣Alumina Catalyst Aimed for Two-stage Hydrocracking

Abstract

Heavy crude oils processing leads the way in current refining. These crudes yield larger amounts of heavy fractions such as Vacuum Gas Oil (VGO). VGO must be treated in at least two refining units: a hydrotreating unit where sulfur, nitrogen, and other heteroatoms are removed, and a hydrocracking unit where suitable fuels are obtained. Removal of heteroatoms during hydrotreating; particularly, nitrogen, dictate the efficiency of hydrocracking. In the first part of this work, the nature of nitrogen species refractory to hydrotreating was analyzed. To achieve this goal, both a vacuum gas oil and its hydrotreated counterpart were studied using Electrospray Ionization with Fourier Transform Ion Cyclotron Resonance Mass Spectrometry. Weakly basic nitrogenated compounds; namely, heavy pyrrolic like compounds and their partially hydrogenated derivatives were found to be the most refractory to hydrotreating. These compounds are weakly basic compared to conventionally tested nitrogenated compounds. Considering this finding, the effect of carbazole and of tetrahydrocarbazole on the reactivity of phenanthrene over Ni-MoS_2/Y-zeolite␣alumina two-stage hydrocracking catalyst was investigated to assess the effect of pyrroles in the second part of the work. Tests were carried out in a fixed-bed reactor and with mixtures of carbazole and tetrahydrocarbazole. Results showed that these weakly basic nitrogenated compounds can affect the catalytic performance. Furthermore, an increase in the relative concentration of tetrahydrocarbazole inhibited catalytic selectivity to hydrocracking products. Overall, these findings contribute to understanding the factors behind the catalytic performance of new hydrocracking units installed to upgrade heavy crude oils.

Keywords: Vacuum gas oil, ESI FT-ICR-MS, weakly basic nitrogen compounds, hydrocracking.

Nomenclature

%C	Conversion
%S	Selectivity
ANOVA	Analysis of Variance
APPI	Atmospheric Pressure Photoionization
DBE	Double Bond Equivalent
DFT	Density Functional Theory
ESI	Electrospray Ionization
FT-ICR-MS	Fourier Transform Ion Cyclotron Resonance Mass Spectrometry
GC	Gas Chromatography
HCK	Hydrocracking
HDT	Hydrotreatring
HDT-VGO	Hydrotreated Vacuum Gas Oil
ISTD	Internal Standard for GC
LHSV	Liquid Hourly Space Velocity
$\mathbf{S^{EXT}}$	Selectivity to hydrogenation of external rings leading to naphthalenes and tetralins
$\mathbf{S^{INT}}$	Selectivity to hydrogenation of internal rings which leads to biphenyls
$\mathbf{S^{MIX}}$	Selectivity which follows the route in which both an intermediate and an external ring are hydrogenated
VGO	Vacuum Gas Oil
WBN	Weakly Basic Nitrogen-Containing
$\mathbf{X_{WBN}}$	Carbazole to tetrahydrocarbazole molar ratio

1. Identification of Refractory Weakly Basic Nitrogen-Containing Compounds in a Hydrotreated Vacuum Gas Oil and Their Effect Over a Ni-MoS_2/Y-Zeolite␣Alumina Catalyst Aimed for Two-stage Hydrocracking

1.1. Introduction

Heavy crude oils production is on the rise and will continue so for the upcoming years. These crude oils are characterized for their high content of heteroatoms; namely, nitrogen, sulfur, and oxygen [1]. The conversion of such feedstocks to clean fuels requires more intensive heteroatoms; sulfur, nitrogen and metals, removal via hydrotreating (HDT) before processing via hydrocracking (HCK). Particularly, even small amounts of nitrogen-containing compounds; e.g. less than 100 ppm, can poison hydrocracking catalysts [2-5]. Vacuum gas oil (VGO); whose production is on the raise due to processing heavy crude oils, have high contents of nitrogen and are now common feedstock for hydrocracking. Nitrogenates present in this fraction are mainly anilines, pyridines, and pyrroles [2, 6]. Compounds such as pyridine and aniline are classified as basic while pyrroles are considered as acidic or non-basic [7-10] even though their acid-base properties confer them a weakly basic character [11].

Though the effect of basic nitrogenated compounds on the performance of hydrocracking catalysts is rather well established [2, 12, 13], the impact of weakly basic nitrogen-containing compounds remains largely unexplored in open literature. This can be partly due to the belief that pyrroles are easier to remove than pyridines during HDT because their heat of hydrogenation is significantly lower as compared to pyridines [2]. Therefore, pyrroles are hydrogenated at greater rates as compared to pyridines [2]. The hydrogenation is a required step for the

hydrodenitrogenation of pyridines and pyrroles [14-16]. However, one must be careful to differentiate between hydrogenation and hydrodenitrogenation since the latter encompasses the complete removal of the nitrogen heteroatom from the feedstock and not only the hydrogenation of the heterocyclic structures that contain it. On the other hand, basic nitrogenated compounds are known for poisoning and inhibiting hydrocracking even in very low amounts [4, 17, 18]. Poisoning can be explained because basic nitrogen compounds such as pyridine adsorb strongly on Brønsted acid sites forming protonated species [19] which are stable and H-bonded to the solid [20]. Despite the later, in a kinetic study for the hydrodenitrogenation of a coker gas oil, it was found that weakly basic nitrogen-containing compounds may control the removal of nitrogen during hydrotreating. In addition, the authors postulated that the hydrogenation of these weakly basic compounds were rate determining for the removal of their nitrogen heteroatom [10]. Therefore, pyrroles might be slowly hydrogenated as compared to pyridines, and their partially hydrogenated products, which are refractory to hydrodenitrogenation, may alter the behavior of hydrocracking catalysts.

Before studying the possible effect of weakly basic nitrogen-containing compounds on the performance of hydrocracking catalysts, it is important to identify key nitrogen-containing components present in the hydrotreated feed aimed to upgrading. Jokuty and Gray reported on the characterization of a hydrotreated gas oil from a bitumen using Field Ionization Mass Spectroscopy and Nuclear Magnetic Resonance (NMR). Authors found that the most abundant species of this product were pyrroles; namely, carbazole with alkyl substituents and partially hydrogenated benzocarbazoles [6]. The presence of carbazole and tetrahydrocarbazole was also detected, but with a very low relative abundance. The same was true for basic compounds such as quinolines and benzoquinolines, whose relative abundances were also low. These results confirm that basic nitrogen-containing compounds are easier to remove during hydrotreating as compared to weakly

basic. Similar results have been reported for an atmospheric residue, vacuum residue, and heavy coker gas oil using Atmospheric Pressure Photoionization and Electrospray Ionization with Fourier Transform Ion Cyclotron Resonance Mass Spectrometry (ESI FT-ICR-MS) [7, 21]. Wiwel *et al.* [22] studied a hydrotreated fraction by NMR and performed theoretical DFT calculations for analyzing the molecular structure and reactivity of this refinery stream. Authors found that tetrahydrocycloheptacarbazol; a partially hydrogenated pyrrole, was highly refractory to HDN [22]. Considering the above evidence, more attention should be paid to the possible influence of weakly basic nitrogen-containing compounds on hydrocracking catalysts. As far the authors of this thesis know, only Kobayashi et al. [25] have reported that a weakly basic nitrogenated molecule such as carbazole can inhibit hydrocracking catalysts even at concentration as low as 2 ppm.

Considering the above, the experimental strategy of this contribution consisted first on characterizing a vacuum gas oil fraction obtained from the distillation of a Colombian heavy crude oil and its hydrotreated counterpart (HDT-VGO). Fourier Transform Ion Cyclotron Resonance Mass Spectrometry was used for following the transformation of the nitrogenated species present in both samples after hydrotreating. The ESI negative and positive modes allowed differentiating nitrogenates according to their acid-base properties. Other works [8] have used the same technique for this same purpose but analyzing hydrotreated samples with total nitrogen contents above 700 ppm, which is common for the so-called mild hydrocracking, but still too high for the nitrogen slip used during a two-stage hydrocracking process [25]; the latter being the one to be implemented in Colombian refineries. Furthermore, in this case, recommendations from catalysts suppliers are to operate this process at concentrations of total nitrogen near 30 ppm [17]. Accordingly, this work particularly focused on identifying refractory nitrogen species remaining at concentrations about 20 ppm. In this regard, carbazole and its partially hydrogenated tetrahydrocarbazole counterpart

were identified as relevant model molecules for studying the effect of weakly basic nitrogen-containing compounds on a conventional hydrocracking catalyst. The hydrocracking of phenanthrene was performed as a model reaction. The collected evidence from these experiments indicated that though carbazole and tetrahydrocarbazole do not largely change the conversion of phenanthrene under the reaction conditions employed herein, they alter the catalytic selectivity to a most important extent. These results thus call for a re-evaluation of the role of weakly basic nitrogen-containing compounds during two-stage hydrocracking processes.

1.2. Experimental

1.2.1. Macroscopic characterization of the VGO sample before and after hydrotreating

Table 1.1.

Physicochemical properties of the analyzed Colombian VGO sample and of its hydrotreated counterpart.

VGO Sample				
Property	**Value**	**Method**	**SARA**	
Density (g/cm3)	0.951	D 4052	Fractional characterization (wt.%)	
API gravity	17.2	D 4052	Saturated	65.27
Total Sulfur (wt.%)	1.04	D 4294	Aromatics	31.62
Total Nitrogen (wt.%)	0.143	D 4629	Resins	3.11
Basic nitrogen (wt.%)	0.032	UOP 269	Asphaltenes	0
Hydrotreated VGO				
Property	**Value**	**Method**	**SARA**	
Density (g/cm3)	0.910	D 4052	Fractional characterization (wt.%)	
API gravity	23.7	D 4052	Saturated	N/A*
Total Sulfur (µg/g)	43	D 4294	Aromatics	N/A*
Total Nitrogen (µg/g)	23	D 4629	Resins	N/A*
Basic nitrogen (µg/g)	N/A*	UOP 269	Asphaltenes	N/A*

*N/A=Not available.

A vacuum gas oil sample with a boiling range between 550 – 821 K was provided by Ecopetrol S.A. Table 1.1 presents the density, API gravity, total sulfur, total nitrogen, basic nitrogen, SARA

distribution, and aromatic content of the sample and of its hydrotreated counterpart. The sample was hydrotreated at 643 K, 13.6 Mpa of H_2, and using a LHSV of 1 h^{-1} over a commercial catalyst.

1.2.2. Analysis by ESI FT-ICR Mass Spectrometry. FT-ICR MS analysis of vacuum gas oil and the hydrotreated-VGO samples were performed using a 15 T SolariX FT-ICR mass spectrometer from Bruker Daltonics (Billerica, MA). Nitrogen was used as drying and nebulizing gas whereas argon was employed in the collision cell. Prepared samples were directly injected with a syringe pump (Harvard, Holliston, MA). Stock sample solutions were prepared by dissolving samples to a concentration of ~10 mg/mL in toluene (99.5%, Merck). For ESI analysis, 0.2 mg/mL was used and spiked with 1 vol.% ammonium hydroxide (28%, Sigma-Aldrich) and 1.0 vol.% formic acid (98%, Sigma-Aldrich) before sample loading to improve ion detection in the (-) ESI and (+) ESI ion modes, respectively. External calibration was performed using a 0.05 mg/mL sodium trifluoroacetate solution in methanol. A flow rate of 450 µL/h, a drying gas temperature of 473 K, and a time-of-flight window of 0.7 ms were employed. The resolving power reached for all mass spectra was higher than 400000 at m/z 400. The RMS error of the calibration and the RMS error for molecular formula calculations were below 0.1 and 0.5 ppm, respectively. Data were acquired in broadband mode using 4 megaword data sets, with each mass spectrum resulting from the sum of 100 scans. Internal spectral calibration was performed using two homologous series: N1 DBE = 12 for (-) ESI and + N1 DBE = 9 for (+) ESI. The Data Analysis version 4.0 (Bruker Daltonics) software was used for data treatment. Peaks with relative abundances higher than 10 times the signal-to-noise ratio were exported to Excel for further analyses. Compositional assignment was done using the Composer software version 1.0.6 (Sierra Analytics, Modesto, CA, USA) with 1 ppm tolerance.

1.2.3. Expression of the FT-ICR MS results. The aromaticity of the heteroatom-containing species was expressed as the Double Bond Equivalent (DBE). DBE represents the number of aromatic rings plus the carbon double bonds in the molecule and is calculated from the formula:

$$DBE = c - h/2 + n/2 + 1 \quad (1.1)$$

Where, *c*, *h*, and *n* are the stoichiometric amounts of carbon, hydrogen, and nitrogen in the molecule, respectively. The classes of the species which contain the nitrogen, sulfur, and oxygen heteroatoms are represented according to the elements content, e.g. the N1 class represents the family of compounds which contains one nitrogen atom in their stoichiometric formula.

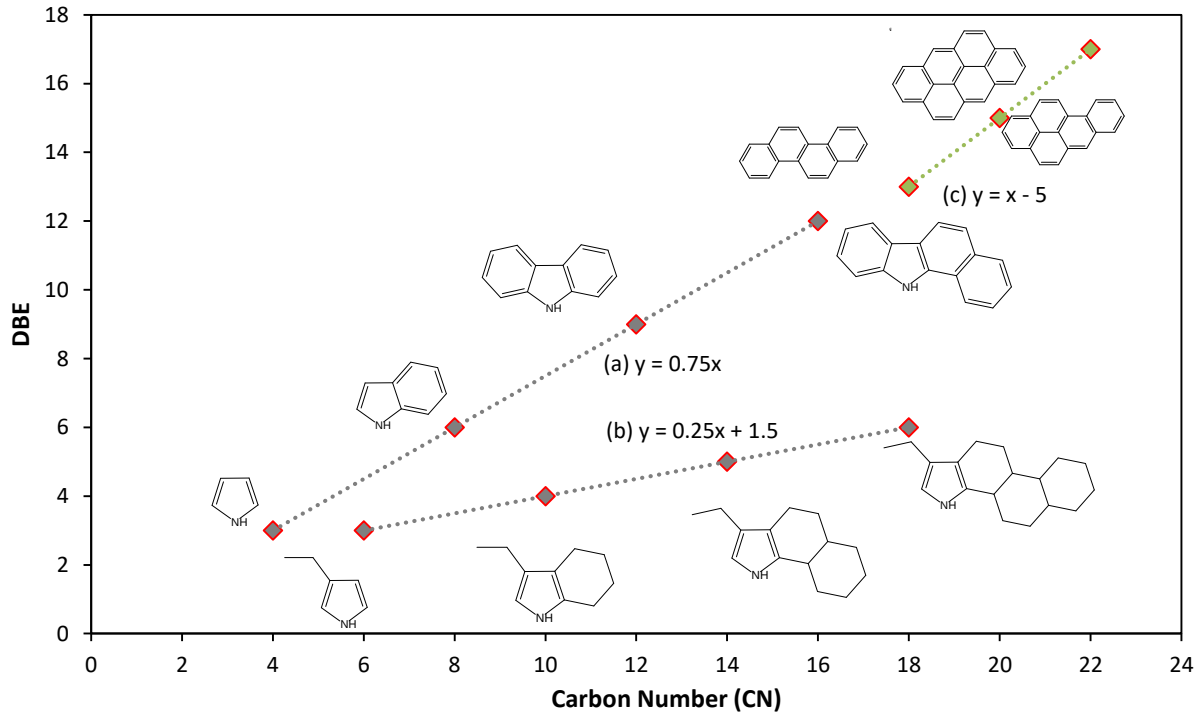

Figure 1.1. Examples of planar limits when the molecular weight increase by adding (a) aromatic rings linerly (b) saturated cycles linerly (c) and condesed aromatic rings, as proposed by Cho *et al* [26].

On the other hand, the concept of Planar Limits [26] was applied to correlate the aromatic and saturated nature of the studied families of compounds following the methodology developed by Cho et al. [26]. In brief, these authors proposed correlating the slopes and intercepts of regression lines derived from the contour plots of DBE versus Carbon Number (CN) with the chemical structure of the species analyzed by FT-ICR MS. They postulated that the larger the slope of these curves were, the higher the number of aromatic rings could be associated to the detected molecules. Therefore, Cho et al. [26] they proposed that slopes near 0.75 correspond to the successive addition of aromatic rings to a base ring. Meanwhile, slopes near 0.25 and with intercepts near 1.5 are to be associated to the addition of either alkyl of chains or saturated rings to the base ring. Figure 1.1 illustrates the above interpretations.

1.2.4. Catalyst preparation. A conventional hydrocracking catalyst was prepared following a similar procedure to that proposed by Agudelo et al. [27]. The support was prepared by extrusion of a paste consisting of a homogeneous mixture of 75 wt.% of boehmite (Catapal B, Sasol) and 25 wt.% of a commercial Y-zeolite (CBV 760, Zeolyst, 720 m2/g with a Si/Al ratio of 30). The paste was prepared at ambient conditions using a solution of 1.0 wt.% of HNO3 (65% p.a., Merck) as peptizing agent. The peptizing agent was added dropwise while kneading manually for 1 h until obtaining a plastic consistency [28]. Thereafter, the as obtained 2 mm diameter extrudates were dried at 378 K for 15 h and calcined for 6 h at 823 K under static air in a muffle furnace. Extrudates were crushed and sifted for obtaining particles of sizes between 0.3 and 0.6 mm. The calcined catalytic support was sequentially impregnated with appropriate amounts of ammonium heptamolybdate tetrahydrate (99 wt.%, Merck) and nickel nitrate hexahydrate (99 wt.%, Merck) in order to obtain catalysts loaded with 3.0 wt.% NiO and 15.0 wt.%. MoO3. Molybdenum was impregnated first by immersion of the solid in a volume of six times the solid

pore volume of the aqueous solution of ammonium heptamolybdate tetrahydrate. The wetted solid was aged for 24 h until reaching an equilibrium pH value. The obtained slurry was vacuum dried in a rotary evaporator (Heidolph) at 328 K, 100 mbar, and rotation speed of 60 rpm during 1 h. Afterwards, the dried solid was calcined at 773 K under an air flow of 100 ml/h for 6 h. The same procedure was repeated for the impregnation of nickel. The catalyst was denoted as Ni-MoS2/Y-zeolite_alumina, with the symbol _. Representing the fact that alumina is a binder.

1.2.5. Catalytic tests. Catalysts were tested in the hydrocracking of phenanthrene. The latter is conventionally used as a model molecule for hydrotreated vacuum gas oils [29, 30]. Carbazole (> 95%, Sigma-Aldrich) and tetrahydrocarbazole (99%, Sigma-Aldrich) were selected as representative nitrogenated model molecules present in the hydrocracking stage following results obtained by FT-ICR MS (Sections 3.1 and 3.2). For the catalytic tests, 0.15 g of catalyst diluted in 2.5 cm3 of quartz sand (1.0 – 0.7 mm); for preventing thermal spots [31], were placed in a fixed bed reactor. After drying for 1 h under a nitrogen flow of 100 ml/h, the catalyst was activated by flowing 10.65 wt.% of dimethyl disulfide (DMDS, 99.0%, Sigma-Aldrich) diluted in cyclohexane (99.5%, Sigma-Aldrich) at 673 K and under a hydrogen flow of 105 ml/min during 4 h. Reactions were carried out at 653 K, 6.9 Mpa, and at a (500 NL hydrogen)/(l L feed) ratio. The reaction feed consisted of a flow of 20 ml/h (LHSV = 1.3 h-1) of 2 wt.% phenanthrene (98%, Sigma-Aldrich) in cyclohexane (99.8%, Sigma-Aldrich). Carbazole and tetrahydrocarbazole were added in a total concentration of 50 ppm, which approximately corresponds to 5 ppm of total nitrogen content in the feed. A carbazole to tetrahydrocarbazole molar ratio (XWBN) was defined as presented in Equation (1.2):

(1.2)

$$X_{WBN} = \frac{n_{Carb}}{n_{Carb} + n_{THCarb}}$$

Where, n_{Carb} and n_{THCarb} represent the moles of carbazole and tetrahydrocarbazole, respectively. X_{WBN} was varied from 0.00; 0.23; 0.52; 0.89; to 1.00. Catalytic tests were replicated twice. The order of execution of the experiments was randomized for reducing systematic errors. Liquid samples were taken each hour until reaching steady state. Steady state was defined for conversion varing less than 1.0 % (conversion vs time on stream plots are available in Annex A, Figure A1). The test proposed by Le Page [32], for ruling out external diffusion limitations, was performed (results are featured in Annex A, Figure A2). The hydrocracking of phenanthrene in the absence of nitrogenates was performed under the same conditions mentioned above over the Ni-MoS_2/Y-zeolite␣alumina catalyst prepared herein and over a commercial NiMo/γ-Al_2O_3 catalyst (*Procatalyse*).

Reaction liquid products were identified by gas chromatography coupled to mass spectrometry (GC-MS) in an Agilent GC 7890A – MSD 5975C instrument. The GC-MS apparatus was provided with a HP-1 column. In general, ca. 87.9 % of the reaction products present in the liquid samples were assigned. The non-assigned products were considered hydrocracking products because they appeared in chromatograms at earlier retention times. Further analysis using Gas Chromatography in an Agilent 6890 apparatus served to quantify reaction products. The GC was provided with a Flame Ionization Detector and an HP-1 column from Agilent. 2.0 wt.% hexadecane (ReagentPlus® 99%, Sigma-Aldrich) was used as a chromatography internal standard. A sample volume of 1.0 µL was injected in a split liner at 373 K (split ratio 75:1) using a helium flow of 1.1 ml/min as carrier gas. Calibration curves were made for the following compounds, using the

corresponding standards for such purpose: phenanthrene, 9,10-dihydrophenanthrene, 1,2,3,4-tetrahydronaphthalene, naphthalene, biphenyl, cyclohexyl benzene, and hexadecane (all bought from Sigma). The response factor used for some compounds derived from hydrocracking was taken from the calibrated species, depending on their chemical nature. In addition, carbon mass balances were performed.

Catalytic results were expressed in terms of phenanthrene conversion (%C) and selectivities (%S) using equations 1.3 and 1.4.

$$\%C = \frac{(n_{PHE}^{0} - n_{PHE}^{E})}{n_{PHE}^{0}} * 100 \quad (1.3)$$

$$\%S = \frac{\sum_j n_j}{\sum_i n_i} * 100 \quad (1.4)$$

Where, n_{PHE}^{0}, n_{PHE}^{E}, $\sum n_j$ and $\sum n_i$ are the initial moles of phenanthrene, the steady state moles of phenanthrene during the reaction, the sum of moles of the products which belong to a certain designated reaction route, and the sum of moles of the total products from all considered reaction routes, respectively. Selectivities were defined following the hydrogenation order of the aromatic rings. According to literature [18,29], the hydrogenation of phenanthrene may proceed via three reaction routes: namely, the hydrogenation of internal rings which leads to biphenyls. For this route, a selectivity termed S^{INT} was thus defined; the hydrogenation of external rings leading to naphthalenes and tetralins, whose selectivity was defined as S^{EXT}; and a route in which both the intermediate and an external ring of the molecule are hydrogenated. The selectivity to the latter route was defined as S^{MIX}.

1.3. Results and discussion

1.3.1. Analysis of the basic species for the vacuum gas oil before and after hydrotreating.

Results presentation will focus on the N1 family in both ESI modes because such species were found to be the most abundant in the vacuum gas oil before and after hydrotreating. Figure 1.2 shows the relative abundances for the classes that contain nitrogen, sulfur, and oxygen as measured in the (+) ESI mode of FT-ICR MS. Polar basic species are detected in this mode of analysis [33].

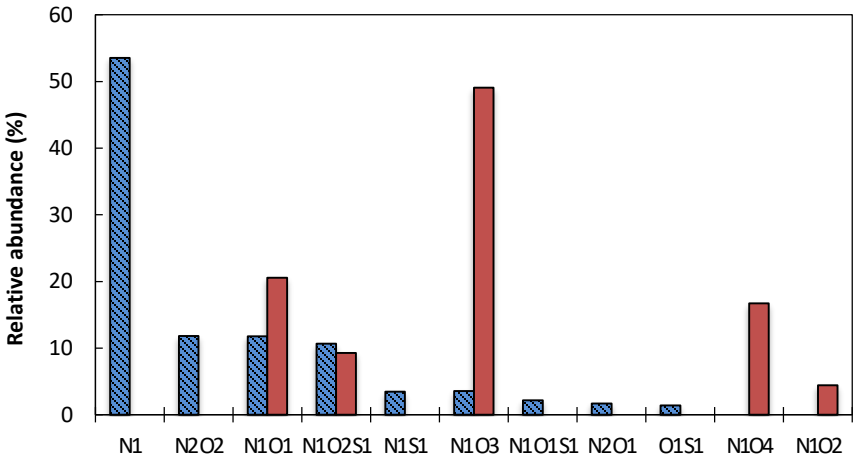

Figure 1.2. Positive ESI relative abundances of the heteroatom-containing families in the (▨) vacuum gas oil and (■) hydrotreated VGO at 643 K, 13.6 Mpa of H_2, LHSV of 1 h^{-1} and using a commercial catalyst.

For the vacuum gas oil, the N1 class had the higher relative abundance: 55 %, followed by the N2O2 and the N1O1 classes, both with a relative abundance of 11%. The N1 class was not detected in the hydrotreated VGO. These results must be seen considering that the amount of basic nitrogen in the hydrotreated VGO was two orders of magnitude less than the one corresponding to the vacuum gas oil. Since in ESI, or in whatever ionization source, only relative abundances are detected, what results from Figure 1.2 mean is that the remaining nitrogen is distributed into the classes N1O3, N1O1, N1O4, N1O2, and N1O2S1. Despite an analysis of the influence of these oxygenated species on the performance of hydrocracking catalysts is out of the scope of the present

work, further enquiries in this direction should be envisaged since they might also be relevant to the performance of hydrocracking units. In addition, results suggest that pyridines; the most basic nitrogen-containing compounds from the N1 family, were effectively removed by hydrotreating.

Zhang et al. [34] hydrotreated a Shale Oil with a NiMo based catalyst, until reaching 800 ppm of total nitrogen in the hydrotreated product. They suggested that N1O1 type compounds are more prompted to react than N1 type compounds during hydrotreating because the furan ring is easier to hydrogenate and to further release its oxygen heteroatom as compared to the nitrogen heteroatom bind to an aromatic ring. However, herein, all remaining basic nitrogenated compounds contained oxygen. Establishing the origin of such families of compounds is beyond the scope of this work. What is completely clear from present results is that the basic N1 class of nitrogenated molecules were removed from the vacuum gas oil to levels below the limit of detection of the FT-ICR MS technique.

The DBE distribution of the N1 class in the vacuum gas oil is depicted in Figure 1.3. Higher values for the relative abundance were between 6 and 13 DBE. As these are polar species, these nitrogen-containing compounds are usually attributed to basic molecules of the pyridine type [35]. DBE values of 7, 10, and 13 are ascribed to quinolones, acridines, and benzoacridines, respectively. Intermediate DBE values between 7 and 13 correspond to partially hydrogenated species of the above-mentioned species, e.g., partially hydrogenated quinolines (see insert in Figure 1.3 featuring DBE = 7, 8, and 9).

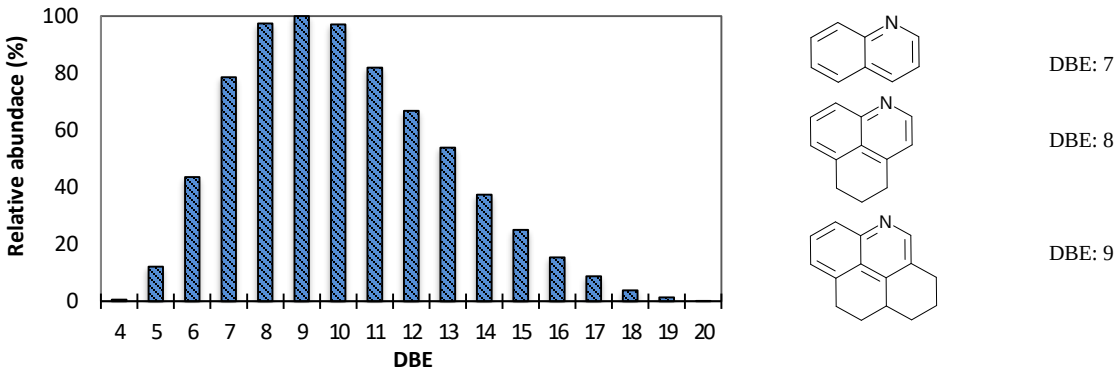

Figure 1.3. DBE distributions of the N1 class obtained by positive ESI, and its relative abundances in the vacuum gas oil. Compounds depicted at the right part, are quinoline derivates with their corresponding DBE values.

Figure 1.4 features a contour plot of DBE as a function of the Carbon Number (CN) for the N1 class. The more abundant species were those with CNs between C_{27} and C_{43} (red dots in the corresponding plot). Thus, for example, for the DBE 10 series, possible structures could be long chain alkyl substituted acridines. Taking the planar limit between C_{19} and C_{30}, a slope of 0.59 was estimated. This value can be considered closer to 0.75 than to 0.25, which suggests that pyridines would most likely grow preferentially linearly by addition of aromatic rings as a function of the DBE value. This confirms the aromatic character of the basic N1 class contained in the vacuum gas oil.

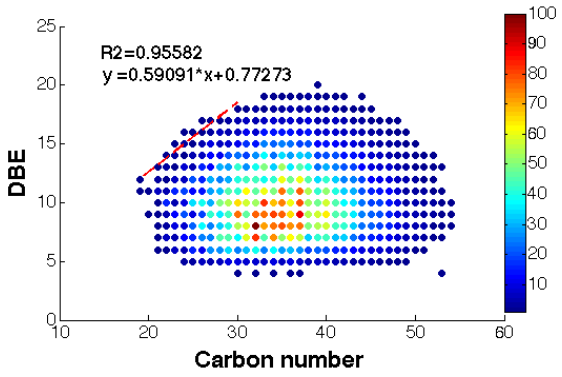

Figure 1.4. Positive ESI contour plot of the N1 family in the vacuum gas oil. Colors represent the relative abundances of the different species.

In conclusion, analysis of the hydrotreated vacuum gas oil showed that basic species from the N1 class; which correspond to those compounds associated with strong inhibition effects for hydrocracking catalysts [2,4], are effectively removed under the conditions employed herein for hydrotreating. In the next section, results will illustrate what happened to weakly basic nitrogen-containing compounds after hydrotreating.

1.3.2. Analysis of the acidic and weakly basic species for the vacuum gas oil before and after hydrotreating. The relative abundances of the classes which contain nitrogen, oxygen, and sulfur detected by (-) ESI are depicted in Figure 1.5. Species detected in this mode of FT-ICR MS are to be considered weakly basic or acidic in nature. The most abundant class in the VGO was N1 with approximately 43%, followed by the O2 and O1 classes with 17% and 10%, respectively. After hydrotreating, the most abundant family was O1; relative abundance of 31%, followed closely by O2 and N1; relative abundances of 27% and 26%, respectively. The classes which contain oxygen thus appeared more refractory to hydrotreating.

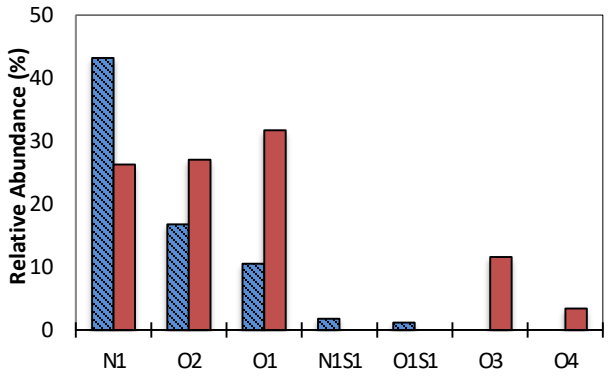

Figure 1.5. Negative ESI relative abundances of the heteroatom-containing families in the (▨) vacuum gas oil and (■) hydrotreated VGO at 643 K, 13.6 Mpa of H_2, LHSV of 1 h^{-1} and using a commercial catalyst.

These acidic species are normally attributed to phenolic and naphthenic acids [8]. On the other hand, and comparing the present results with those discussed for (+) ESI, species belonging to the N1 class and detected in the (-) ESI mode appeared more refractory to hydrotreatment. Hence, it can be said that most of the remaining nitrogenated species are weakly basic in nature. Likewise, these species have been found to be removed in lower rates during hydrotreating when compared to basic nitrogen-containing compounds [10].

The DBE distribution of the (-) ESI N1 class is shown in Figure 1.6. Higher relative abundances were registered between DBE 9 and 15. DBE values of 9, 12, and 15 are usually attributed to carbazoles, benzocarbazoles, and dibenzocarbazoles, respectively. Meanwhile, DBE values of 10, 11, 13, and 14 may be attributed to partially hydrogenated species from benzocarbazole and dibenzocarbazole.

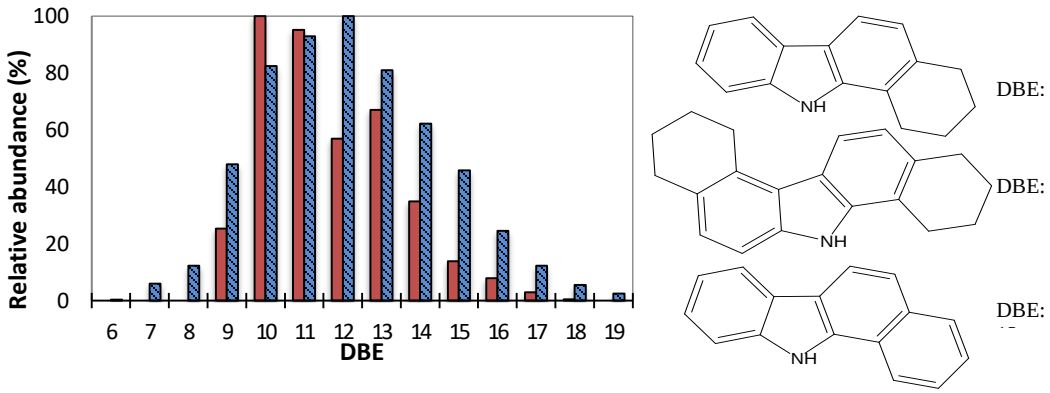

Figure 1.6. DBE distributions of the N1 class obtained by negative ESI, and its relative abundances in the (▨) vacuum gas oil and (■) hydrotreated VGO at 643 K, 13.6 Mpa of H_2, LHSV of 1 h^{-1} and using a commercial catalyst.

Comparing the vacuum gas oil before and after hydrotreating, DBE distribution for the latter appeared skewed to the right as compared to the seemingly *Gaussian* distribution found for the vacuum gas oil. Furthermore, there was an increase in the relative abundances of DBE 10, 11, and

13 that are ascribed to partially hydrogenated derivatives of benzocarbazole and dibenzocarbazoles (see Figure 1.6 insert for an illustration of DBE 10, 11, and 12). Therefore, the weakly basic nitrogen-containing compounds were found to be refractory to hydrotreating. Furthermore, these molecules were mostly partially hydrogenated without further elimination of the nitrogen heteroatom. This trend agrees with literature reports showing that condensed aromatics are rapidly hydrogenated during hydrotreating thus lowering the aromaticity of the hydrotreated product [18, 36].

Contour plots for the N1 class from the vacuum gas oil before and after hydrotreating are presented in Figure 1.7. For the vacuum gas oil, Figure 1.7(a), the most abundant species were those with carbon numbers within the range C_{22} – C_{38} (red dots). Such species can be ascribed to alkylated molecules [26]. After hydrotreating, Figure 1.7(b), the most abundant species had lower carbon numbers; specifically, within the range C_{18}-C_{33}. These species are said to have shorter alkyl chains. A similar trend was reported by Kekäläinen et al. [8]. Results featured in Figure 1.7(b) suggest that the resistance of these molecules to hydrodenitrogenation cannot only be attributed to steric effects. Otherwise, the most abundant species should appear, at least, at the same carbon number range. By considering the shape of the polyaromatics, compounds such as those corresponding to DBE 9 and DBE 12, which have planar shapes, may interact better with the surface of the catalyst. In addition, *ab-initio* calculations indicate that the presence of alkyl substituents could induce buckling in some partially hydrogenated species [37]. In partially hydrogenated compounds, the planar shape is almost lost because of the configuration of the aliphatic carbons. With carbons in the sp3 configuration bonded to the aromatic rings the planarity of the core is lost in such a way that the interaction with the catalyst is hindered for the subsequent removal of the nitrogen heteroatom. The shift to lower carbon numbers of the more abundant

nitrogenated species observed after hydrotreating could thus be a consequence of the hydrocracking of some alkyl groups occurring under current process conditions [38]. The estimated slope for the planar limit of the vacuum gas oil was ca. 0.73. According to Cho *et al* [26], such a value corresponds to weakly basic nitrogen-containing compounds growing linearly by addition of aromatic rings. After hydrotreating, the slope of the planar limit decreased to 0.25. Such a change hints to the linear addition of cyclic saturated rings [26]. This result further supports the fact that the remaining nitrogenated compounds might be a mixture of weakly basic species and their partially hydrogenated products, with a relatively higher abundance of the latter.

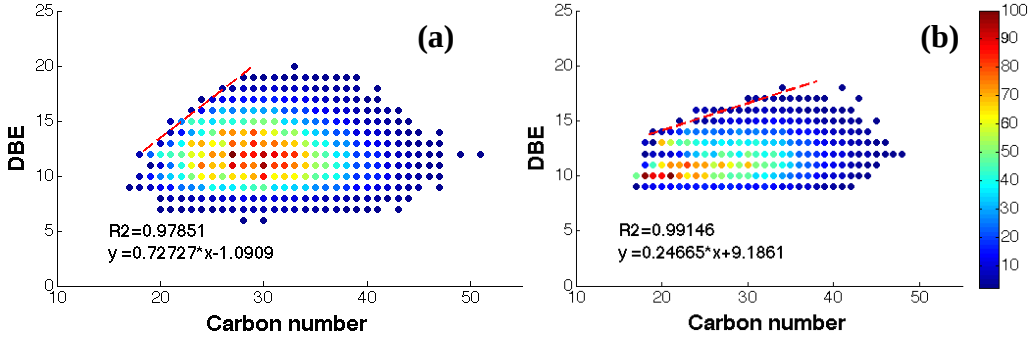

Figure 1.7. Negative ESI contour plot of the N1 family, in the (a) VGO and (b) the hydrotreated VGO at 643 K, 13.6 Mpa of H_2, LHSV of 1 h^{-1} and using a commercial catalyst. Colors represent species relative abundances.

To summarize, the above results indicate that weakly basic nitrogenated polyaromatics present in a hydrotreated vacuum gas oils are the most refractory nitrogenated molecules to hydrodenitrogenation. These molecules are partially hydrogenated during the process, but they are the main nitrogenated species for a vacuum gas oil with total nitrogen contents around 20 ppm which are subjected to two-stage hydrocracking processes for upgrading. Consequently, it was deemed important to study the effect of this type of compounds over the performance of a conventional Ni-MoS_2/Y-zeolite␣alumina in hydrocracking. Carbazole and its partially hydrogenated product; tetrahydrocarbazole, were selected as models for weakly basic nitrogenated

compounds while phenanthrene was selected as a model polyaromatic to be hydrocracked. Results for the corresponding catalytic tests are presented next.

1.3.3. Catalytic results. First, results from phenanthrene hydrocracking in the absence of nitrogenates will be presented as a reference to assess the effect of carbazole and tetrahydro carbazole on the catalytic performance. Second, results from hydrocracking in the presence of the selected weakly basic nitrogen-containing compounds will be discussed.

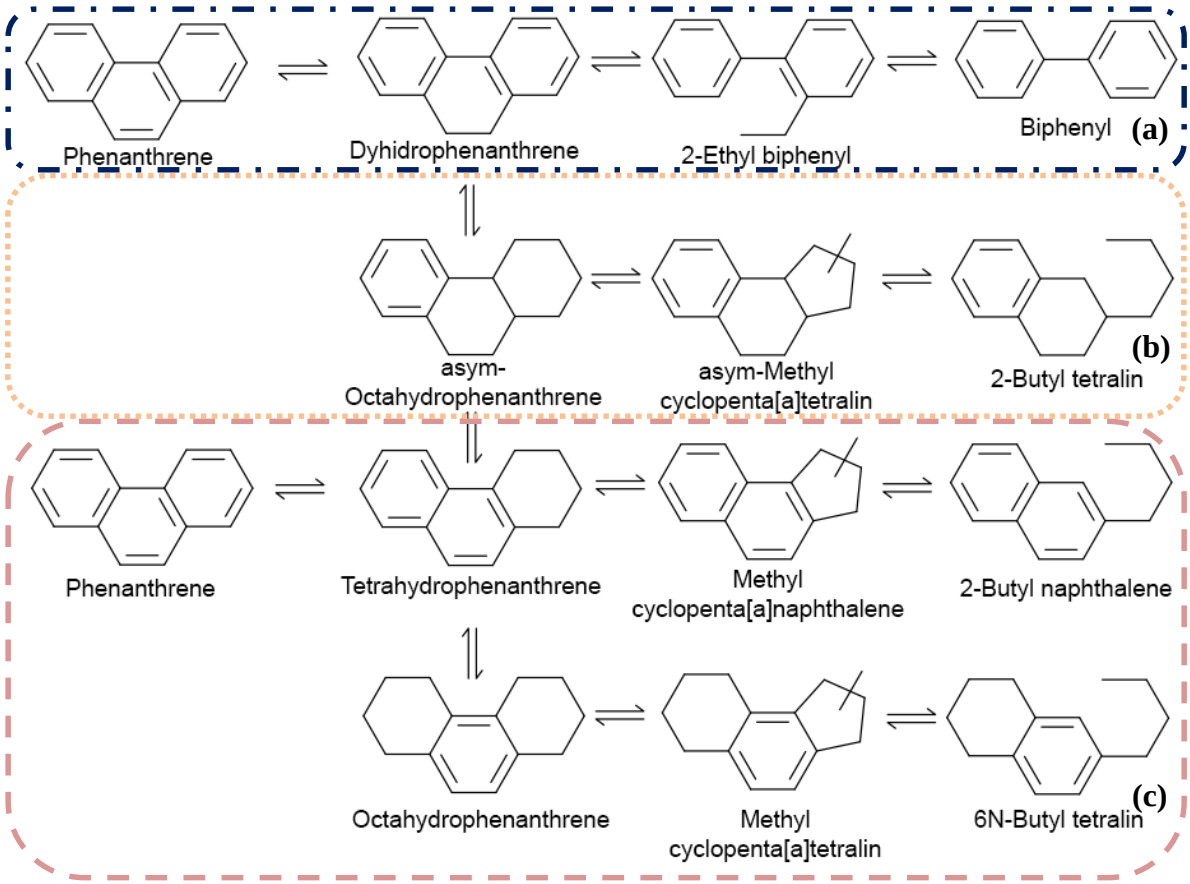

Scheme 1.1. Proposed reaction scheme for the hydrocracking of phenanthrene over a Ni-MoS_2/Y-zeolite␣alumina catalyst. Reaction conditions: 653 K, 6.9 Mpa, and LHSV of 1.3 h^{-1}. Highlighted pathways follow the hydrogenation of: (a) an intermediate ring, (b) and intermediate and an external ring, and (c) the hydrogenation of external rings. Further reaction products are not included.

Table 1.2.

Experimental data for phenanthrene hydrocracking carried out in the absence of weakly basic nitrogen-containing compounds over a Ni-MoS_2/Y-zeolite␣alumina catalyst. Reaction conditions: 653 K, 6.9 MPa, and LHSV = 1.3 h^{-1}. Cyclohexane was used as solvent and hexadecane as standard for GC.

Cyclohexane (wt.%)	Hexadecane (wt.%)	Reactant	Acronym	wt.% in feed	Conversion (%)
96.09	1.94	Phenanthrene	PHE	1.97	80.1±0.2

Primary Hydrogenation Products

Route	Acronym	Compound	Average equivalent % in carbon mass balance	Selectivities (%)
INT	DHP	Dihydrophenanthrene	0.1499	
EXT	THP	Tetrahydrophenanthrene	0.1428	
	OHP	Octahydrophenanthrene	0.0489	
MIX	asym-OHP	asym-Octahydrophenanthrene	0.0462	
		Others†	0.0374	
		Total	0.4253	37.1±0.2*

Primary Isomerization Products

Route	Acronym	Compound	Average equivalent % in carbon mass balance	Selectivities (%)
EXT	MCPTL	Methylcyclopenta[a]tetralin	0.0279	
	MCPNP	Methylcyclopenta[a]naphthalene	0.0660	
MIX	asym-MCPTL	iso-Methylcyclopenta[a]tetralin	0.0073	
		Total	0.1012	8.8±0.1*

Hydrocracking Products

Route	Acronym	Compound	Average equivalent % in carbon mass balance	Selectivities (%)
INT	BP	Biphenyl	0.0077	22.2±0.2
	CHB	Cyclohexyletilbenzene	0.0113	
	EBP	2 Ethyl biphenyl	0.0294	
	DMBP	Dimethyl biphenyl	0.0187	
EXT	IN	Indane	0.0240	72.5±0.2
	MIN	Methyl indane	0.0196	
	TL	Tetrahydronaphthalene (tetralin)	0.0566	
	NP	Naphthalene	0.0245	
	MTL	5-Methyl tetrahydronaphthalene	0.0197	
	MNP	2-Methylnaftaleno	0.0128	
	BTL	6N-Butyl tetrahydronaphthalene	0.0369	
	BNP	2-Butyl-naphthalene	0.0261	
MIX	i-BTL	2-Butyl tetrahydronaphtlane	0.0077	5.3±0.1
		Others†	0.3167	
		Sum of listed hydrocracking products ($\sum_i n_i$)	0.3037	
		Total	0.6204	54.0±0.2*

* Overall selectivity as compared to all detected and quantified reaction products.

† The set of products named as Others accounted for compounds whose quantity in the equivalent % carbon mass balance was 0.35±0.01. This group contains species that were not assigned with GC-MS as well as products related to further hydrogenations, dealkylation, and isomerizations that occurred. Others thus include products such as indane, methyl indane, methyl naphthalene, methyl tetralin, ethyl naphthalene, ethyl tetralin, toluene, butyl benzene, dimethyl cyclohexane and methyl cyclohexane. A complete list of these products and their corresponding relative concentrations is presented in Table A1.

1.3.3.1. Hydrocracking of phenanthrene in the absence of nitogen-containing compounds. Following catalytic tests in the absence of nitrogenates, the reactivity of phenanthrene, average %conversion at steady state = 80.1±0.2%, over Ni-MoS2/Y-zeolite␣alumina allowed establishing a reaction scheme for the primary steps involved in its hydrocracking under the process conditions employed herein. Scheme 1.1 presents such a reaction scheme.

The postulated scheme was based on the detected reaction products (See Annex A, Figures A3 and A4) and inspired by previous literature reports [18, 29] except as for the so-called perhydrophenanthrene route [29, 39]. The reason for the latter was that this product and its derivatives were not detected during GC-MS analyses. According to the proposed reaction scheme, phenanthrene is initially hydrogenated to dihydrophenanthrene (a), and tetrahydrophenanthrene. The relative concentrations of these compounds in the liquid product are shown in Table 1.2. After these hydrogenations, three main conversion routes are proposed. (a) Ring opening of the internal ring of dihydrophenanthrene leading to the production of 2-ethylbiphenyl and further hydrocracking to biphenyl. (b) Hydrogenation of the internal and one external ring of dihydrophenanthrene to asym-octahydropheanthrene and further isomerization and ring opening to asym-methylcyclopenta[a]tetralin and 2-butyl tetralin, respectively. This route may also proceed via the hydrogenation of 1,2,3,4-tetrahydrophenanthrene. (c) Hydrogenation of the external ring of tetrahydrophenanthrene to produce octahydropheanthrene followed by isomerization to methyl cyclopenta[a]tetralin and ring opening to 6N-butyl tetralin. Within (c), tetrahydrophenanthrene can also be isomerized to methyl cyclopenta[a]naphthalene and later ring opened to 2-butyl naphthalene. Considering these results, isomerization was considered as a necessary intermediate step before ring opening and dealkylation reactions leading to the hydrocracking products listed in

Table 1.2. In this Table, the set of products named as Others accounted for compounds whose quantity in the equivalent % carbon mass balance was 0.35±0.01. This group contains species that were not assigned with GC-MS as well as products related to further hydrogenations, dealkylation, and isomerizations that occurred. Others thus include products such as indane, methyl indane, methyl naphthalene, methyl tetralin, ethyl naphthalene, ethyl tetralin, toluene, butyl benzene, dimethyl cyclohexane and methyl cyclohexane.

A complete list of these products and their corresponding relative concentrations is presented in Table A1. Due to the fact that Others mostly disappeared during the reaction tests performed in the presence of the weakly basic nitrogen-containing compounds, it was decided to focus the analysis of the effect of these compounds on the catalytic performance on products presented in Scheme 1.1.

Besides the products from the phenanthrene reaction, it was found that cyclohexane, used as solvent, was isomerized to methylcyclopentane. The conversion for this reaction did not exceed 1.6%. Other authors have found similar results over Pt/HY zeolite and Pt/mordenite catalysts [39, 40]. In general, it can be considered that this reaction does not significantly inhibit hydrocracking. Theoretical calculations show that the adsorption energy of polynuclear aromatic hydrocarbons over acidic and hydrogenating sites is one order of magnitude higher than that estimated for monoaromatic hydrocarbons [18, 36].

Based on Scheme 1.1, the selectivities, S^{INT}, S^{EXT}, S^{MIX}; were expressed as defined in equation 1.4 but considering the different compounds involved in the routes featured in Scheme 1.1 The following specific formulas were thus applied (Equations 1.5, 1.6, and 1.7):

$$S^{INT} = \frac{n_{BP} + n_{CHB} + n_{EBP} + n_{DMB}}{\sum_i n_i} \quad (1.5)$$

$$S^{EXT} = \frac{n_{IN} + n_{MIN} + n_{TL} + n_{NP} + n_{MTL} + n_{MNP} + n_{BTL}}{\sum_i n_i} \quad (1.6)$$

$$S^{MIX} = \frac{n_{i-BTL}}{\sum_i n_i} \quad (1.7)$$

Where, BP = biphenyl, CHB = dyclohexylbenzene EBP = 2-ethylbiphenyl, DMBP = dimethylbiphenyl, IN = indane, MIN = methylindane, TL = tetralin (tetrahydronaphthalene), NP = naphthalene, MTL = methyltetralin, MNP = methylnaphthalene, BTL = 6-butyltetralin, i-BTL = 2-butyltetralin. The overall selectivity to isomerization and hydrocracking products were respectively 8.8%±0.1and 54.0%±0.2 and. The ratio of selectivities, S^{EXT}/S^{INT}, for the reaction in the absence of nitrogenated compounds was about 3.3 hence indicating a preference to the production of tetralins and naphthalenes under the current reaction conditions.

It is worth comparing the results obtained over Ni-MoS_2/Y-zeolite␣alumina to those obtained over a commercial NiMo/γ-Al_2O_3 catalyst. The reason for this test was that NiMo/γ-Al_2O_3 possesses mostly Lewis acid sites and either scarce or none Brønsted acid sites [41-44]. Figure A4 (in Annex A) shows a typical chromatogram for the phenanthrene reaction over the NiMo/γ-Al_2O_3 formulation. The average steady conversion of phenanthrene over this catalyst was 73% with a selectivity to hydrocracking products of about 7% and a selectivity of ca. 93% to partially hydrogenated products. These results were expected as from previous literature reports [29] but it is interesting noticing that the most abundant detected hydrocracking products (2-ethyl biphenyl and biphenyl) belonged to the route which follows the hydrogenation of intermediate rings (see Scheme 1), i.e. S^{INT}. This may be due to the type of acidity that the catalyst support material possesses.

The results obtained for the hydrocracking of phenanthrene in the absence of the weakly based nitrogenated compounds over the catalyst employed herein can thus be summarized as follows. First, the conversion was very close to equilibrium. Second, the reaction proceeded through three primary routes. Among these routes, the catalyst mostly favored the route which is selective to naphthalenes and tetralins (Scheme 1.1c), followed by that which is derived from the internal ring hydrogenation and leads to biphenyl-like compounds (Scheme 1.1a), whereas the route which proceeds with the simultaneous hydrogenation of one external and one internal ring of the phenanthrene, was the least favored.

1.3.3.2. Hydrocracking of phenanthrene in the presence of weakly basic nitrogenated compounds

1.3.3.2.1. *Conversion.* The conversion of phenanthrene as a function of the XWBN ratio is shown in Figure1.8. The dotted line corresponds to the average conversion of phenanthrene under steady state conditions in the absence of the nitrogenated compounds at 653 K (conversion data as a function of time on stream is presented in Annex A, Figure A1). In addition, Table A2 (in Annex A) shows numerical values for the limits of 95% Student's-t confidence intervals included in Figure 1.8). A decrease in the conversion of phenanthrene was observed after with the addition of the nitrogenated compounds regardless of the ratio XWBN (95% confidence interval for the mean hydrocracking conversion = 70.6 ± 1.7 as based on a Student's-t distribution with 4 and 15 degrees of freedom, F4,15) On the other hand, the conversion of phenanthrene was not affected by the XWBN ratio (p-value = 0.4 as based on Student's-t distribution with 4 and 15 degrees of freedom, F4,15). This finding differs from the common conception in literature that weakly basic nitrogen-containing compounds do not affect hydrocracking.

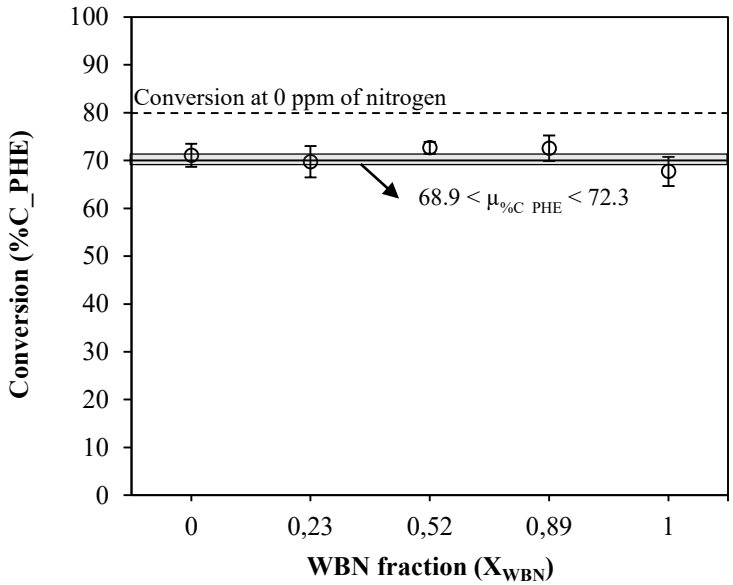

Figure 1.8. Phenanthrene average steady state conversions over a Ni-MoS_2/Y-zeolite␣alumina catalyst as a function of the X_{WBN}^* molar ratio (5 ppm of total nitrogen). Reaction conditions: 653 K, 6.9 MPa, and LHSV of 1.3 h^{-1}. The dotted line denotes the average phenanthrene conversion in the absence of nitrogenated compounds. A Student's-t 95% confidence interval for the mean phenanthrene conversion ($\mu_{\%C\text{-}Phe}$) = 70.6 ± 1.7 is also presented. Raw data for elaborating this figure are available in Table A2. *X_{WBN} = moles of carbazole/(moles of carbazoles + moles of tetrahydrocarbazole).

Furimsky and Massoth [2] in an extensive review about the deactivation of hydroprocessing catalysts proposed that weak basic nitrogen-containing compounds were presumably easy to remove during hydrotreating hence disregarding their possible negative impact on hydroprocessing. Authors further supported their affirmation on analyzing tendencies on the heats of hydrogenation for the nitrogenated compounds which led them to conclude that weakly basic nitrogen-containing compounds could be hydrogenated at large rates assuming that their subsequent hydrodenitrogenation would be promoted [2]. Notwithstanding, results obtained herein clearly differ from such analysis. Furthermore, it will be demonstrated next that the catalytic selectivity for the phenanthrene reaction was importantly modified in the presence of these compounds.

1.3.3.2.2. *Selectivity.* The influence of the XWBN ratio over the average catalytic selectivities is shown in Figure 1.9a (selectivity data is summarized in Annex A, Table A3); error bars depict sample variances. The selectivity to products that simultaneously follow the hydrogenation of internal and external rings, SMIX, is represented on the secondary axis in Figure 1.9a. For the selectivity to the hydrogenation of the external rings of phenanthrene, SEXT (◇), which further leads to hydrocracking products such as naphthalenes, a rather linear increase with the increase in the XWBN ratio was observed. The opposite trend was obtained for the selectivity to the hydrogenation of internal rings leading to biphenyl, SINT. The maximum SEXT value was observed in the absence of tetrahydrocarbazole (i.e. XWBN = 1), and the SEXT/SINT ratio was approximately 2.2 (see Figure 1.9b). This value was lower than (3.7) the one determined for the reaction performed in the absence of nitrogenated compounds. As seen in Fig 1.9b, the SEXT/SINT ratio decreased with an increase in the relative fraction of tetrahydrocarbazole (p-value = 4.47x10-7 for SEXT and a p-value = 1.17x10-5 for SINT found from one-way ANOVA tests with 4 and 15 degrees of freedom, F4,15). Table A4 (in Annex A) shows the corresponding one-way ANOVA tables. Validation tests for the assumptions of the ANOVA linear model as suggested by [45-47] are also available in Annex A, Figures A5 to A8. On the other hand, the hydrogenation of internal and external rings, SMIX, did not change at a significant level (p-value = 0.205, F4,15 –Table A4–).

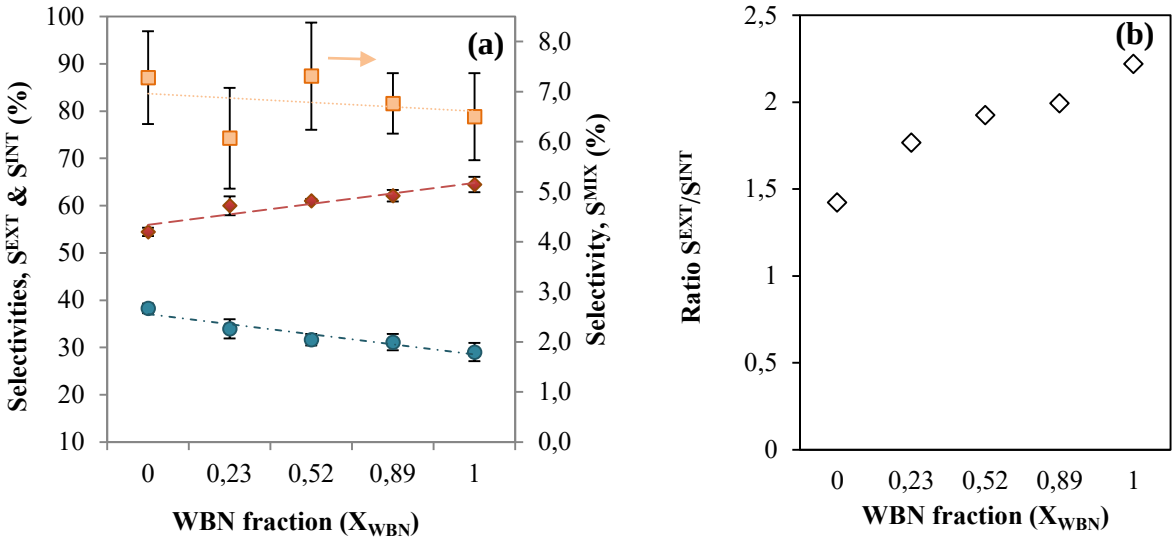

Figure 1.9. (a) Selectivities to the hydrogenation of the external rings of phenanthrene (S^{EXT}) (♦), the hydrogenation of the internal rings of phenanthrene (S^{INT}) (●), and to the simultaneous hydrogenation of the external and internal rings of the molecule (S^{MIX}) (■) observed during the hydrocracking of phenanthrene over a Ni-MoS_2/Y-zeolite␣alumina catalyst as a function of the X_{WBN}* molar ratio (5 ppm of total nitrogen). (b) Ratio of selectivities S^{EXT}/S^{INT} as a function of the ratio X_{WBN}. *X_{WBN} = moles of carbazole/(moles of carbazoles + moles of tetrahydrocarbazole). Reaction conditions: 653 K, 6.9 Mpa, and LHSV of 1.3 h^{-1}.

Next, the above trends will be compared to the results obtained over the Ni-MoS_2/γ-Al_2O_3 catalyst. Particularly, it is important to recall the high selectivity of Ni-MoS_2/γ-Al_2O_3 to the products belonging to the S^{INT} route which was the route affected by the weakly basic nitrogen-containing compounds over the Ni-MoS_2/Y-zeolite␣alumina. From the point of view of acidity, Ni-MoS_2/γ-Al_2O_3 lacks the strong Brønsted acid sites [41-44] present in zeolites and which are required for the isomerization and cracking of external rings, i.e. the route over which the naphthalenes and tetralins are produced [29]. Therefore, one may lay the hypothesis that weakly basic nitrogen-containing compounds preferentially inhibit the Brønsted acid sites of the catalyst. As a plausible support for this hypothesis, Choi *et al.* [48] aimed to selectively remove nitrogen from shale oil by using Lewis acid solids. Authors found that the affinity of weakly basic nitrogen-

containing compounds with some Lewis acids was weak. On the other hand, there is some evidence about the protonation of weakly basic compounds, observed in salts of indole, whose N-protonated species has been detected in FT-IR spectra of by following the presence, or absence, of bands corresponding to ammonium groups [24]. Furthermore, there are some reports arguing for a strong adsorption of weakly basic nitrogen-containing compounds over the acid sites of the support of hydrotreating catalysts [49, 50]. In this regard, Laredo *et al.* [50] studied the distribution of basic and weakly basic nitrogenated compounds in some middle and light oil fractions. For such a purpose, they extracted the basic compounds by using acidified silica. They found that weakly basic nitrogen-containing compounds tended to adsorb strongly on the acidified silica. They hence suggested that weakly basic molecules were capable of inhibiting hydrodesulfurization reactions. Finally, recent DFT calculations [51] performed for the adsorption of carbazole and the tetrahydrocarbazole over a model Brønsted acid site in the pore mouth of Y-zeolite led to conclude that these compounds become protonated upon adsorption. Furthermore, the calculated adsorption energies for both compounds were found to be higher than those obtained for the adsorption of polynuclear aromatic hydrocarbons with 2, 3 and 4 rings, hence indicating that both compounds might influence the performance of conventional hydrocracking catalysts.

1.4. Conclusions

This work showed that weakly basic nitrogenated compounds are highly refractory to hydrotreating even when the total concentration of nitrogen species in a hydrotreated vacuum gas oil decreases below 20 ppm. Among these compounds, carbazole and its partially hydrogenated compound: tetrahydrocarbazole, were determined to be suitable for assessing the effect of these species over catalysts; herein, a conventional Ni-MoS_2/Yzeolite␣alumina formulation, for two

stage hydrocracking processes. Particularly, phenanthrene hydrocracking was studied. Results showed that both selected weakly basic nitrogenated compounds affect the catalytic activity and selectivity. Concerning the latter, an increase in the relative concentration of tetrahydrocarbazole was found to exert a negative effect on the hydrocracking route derived from the hydrogenation of the internal ring of phenanthrene. Results presented in the chapter thus contribute to considering new factors in the design of hydrocracking processes and catalysts for heavy crude oils.

References

[1] Motaghi, M.; Ulrich, B.; Subramanian, A. Slurry-phase hydrocracking—possible solution to refining margins. *Hydrocarbon Process* **2011,** 90, 37-43.

[2] Furimsky, E.; Massoth, F.E. Deactivation of hydroprocessing catalysts. *Catal. Today* **1999,** 52, (4), 381-495.

[3] Osipov, L.N.; Agafonov, A.V.; Khavkin, V.A.; Rogov, S.P. Effect of nitrogen compounds on the hydrocracking of heavy distillates. *Chem. Tech. Fuels Oils* **1965,** 1, (8), 581-585.

[4] Sau, M.; Basak, K.; Manna, U.; Santra, M.; Verma, R.P. Effects of organic nitrogen compounds on hydrotreating and hydrocracking reactions. *Catal. Today* **2005,** 109, (1–4),112-9.

[5] Speight, J.G. Chapter 1 – Refining Heavy Oil and Extra-heavy Oil. In: *Heavy and Extra-heavy Oil Upgrading Technologies.* Boston: Gulf Professional Publishing, **2013**, p. 1-13.

[6] Jokuty, P.L.; Gray, M.R.; Resistant nitrogen compounds in hydrotreated gas oil from Athabasca bitumen. *Energy Fuels* **1991,** 5, (6), 791-5.

[7] Liu, D.; Fu, Y.; Deng, W.; Shi, Q.; Ma, K.; Hou, T. FT-ICR MS Analysis of Nitrogen-Containing Compounds in the Products of Liaohe Atmospheric Residue Hydrocracking. *Energy Fuels* **2011,** 26, (1), 624-8.

[8] Kekäläinen, T.; Pakarinen, J.M.H.; Wickström, K.; Vainiotalo, P. Compositional Study of Polar Species in Untreated and Hydrotreated Gas Oil Samples by Electrospray Ionization

Fourier Transform Ion Cyclotron Resonance Mass Spectrometry (ESI FTICR−MS). *Energy Fuels* **2009,** 23, (12), 6055-61.

[9] Revellin, N.; Dulot, H.; López-García, C.; Baco, F.; Jose, J. Specific Nitrogen Boiling Point Profiles of Vacuum Gasoils. *Energy Fuels* **2005,** 19, (6), 2438-44.

[10] Wei, Q.; Wen, S.; Tao, X.; Zhang, T.; Zhou, Y.; Chung, K. Hydrodenitrogenation of basic and non-basic nitrogen-containing compounds in coker gas oil. *Fuel Process. Technol* **2015,** 129, (0), 76-84.

[11] Hinman, R.L.; Lang, J. The Protonation of Indoles. Basicity Studies. The Dependence of Acidity Functions on Indicator Structure. *J. Amer. Chem. Soc*., **1964,** 86, (18), 3796-806.

[12] Fu, C.M.; Schaffer AM. Effect of nitrogen compounds on cracking catalysts. *Ind. Eng. Chem. Prod. Res. Dev* **1985,** 24, (1), 68-75.

[13] Nagai, M.; Sato, T.; Aiba, A. Poisoning effect of nitrogen compounds on dibenzothiophene hydrodesulfurization on γ-NiMoAl2O3 catalysts and relation to gas-phase basicity. *J. Catal.* **1986,** 97, (1), 52-8.

[14] Prins, R. Catalytic hydrodenitrogenation. *Advances in Catalysis.* Academic Press, **2001,** 399-464.

[15] Bachrach, M.; Marks, T.J.; Notestein, J.M. Understanding the Hydrodenitrogenation of Heteroaromatics on a Molecular Level. *ACS Catal.* **2016,** 6, (3), 1455-76.

[16] Ferdous, D.; Dalai, A.K.; Adjaye, J. Comparison of Hydrodenitrogenation of Model Basic and Nonbasic Nitrogen Species in a Trickle Bed Reactor Using Commercial NiMo/Al2O3 Catalyst. *Energy Fuels* **2003,** 17, (1), 164-71.

[17] Dufresne, P.; Quesada, A.; Mignard, S. Influence of Nitrogen Feed Content On The Performances of A Zeolite Hydrocracking Catalyst. *Studies in Surface Science and Catalysis*. Elsevier, **1989,** p. 301-15.

[18] Korre, S.C.; Klein, M.T.; Quann R.J. Hydrocracking of Polynuclear Aromatic Hydrocarbons. Development of Rate Laws through Inhibition Studies. *Ind. Eng. Chem. Res* **1997,** 36, (6), 2041-50.

[19] Barzetti T, Selli E, Moscotti D, Forni L. Pyridine and ammonia as probes for FTIR analysis of solid acid catalysts. Journal of the Chemical Society, *Faraday Trans* **1996,** 92, (8), 1401-7.

[20] Castellà-Ventura M, Akacem Y, Kassab E. Vibrational Analysis of Pyridine Adsorption on the Brønsted Acid Sites of Zeolites Based on Density Functional Cluster Calculations. *J. Phys. Chem. C* **2008,** 112, (48), 19045-54.

[21] Al-Hajji A, A., Muller H, Koseoglu O, R. Caractérisation par spectrométrie de masse par resonance cyclotronique ionique à transformée de Fourier des azotés et soufrés dans les charges d'alimentation d'hydrocraquage. *Oil Gas Sci. Technol. – Rev. IFP* **2008,** 63, (1), 115-28.

[22] Wiwel, P.; Hinnemann, B.; Hidalgo-Vivas, A.; Zeuthen, P.; Petersen, B.O.; Duus, J.Ø. Characterization and Identification of the most Refractory Nitrogen Compounds in Hydroprocessed Vacuum Gas Oil. *Ind. Eng. Chem. Res* **2010,** 49, (7), 3184-93.

[23] Yagil, G. The proton dissociation constant of pyrrole, indole and related compounds. *Tetrahedron* **1967,** 23, (6), 2855-61.

[24] Hinman, R.L. Whipple EB. The Protonation of Indoles: Position of Protonation. *J. Amer. Chem. Soc.* **1962,** 84, (13), 2534-9.

[25] Kobayashi, M.; Togawa, S.; Ishida, K. Effects of Small Amounts of Nitrogen Compounds in Feedstock on Performance of Hydrocracking Catalyst. *J. Japn. Petrol. Inst* **2007,** 50, (1), 44-52.

[26] Cho, Y.; Kim, Y.H.; Kim, S. Planar Limit-Assisted Structural Interpretation of Saturates /Aromatics /Resins /Asphaltenes Fractionated Crude Oil Compounds Observed by Fourier Transform Ion Cyclotron Resonance Mass Spectrometry. Anal. Chem **2011,** 83, (15), 6068-73.

[27] Agudelo, J.L.; Hensen, E.J.M.; Giraldo S.A.; Hoyos, L.J. Influence of steam-calcination and acid leaching treatment on the VGO hydrocracking performance of faujasite zeolite. *Fuel Process. Technol* **2015,** 133, 89-96.

[28] Jirátová, K.; Janáček, L.; Schneider, P. Influence Of Aluminium Hydroxide Peptization On Physical Properties Of Alumina Extrudates. *Stud. Surf. Sci. Catal* **1983,** 16, 653-63.

[29] Lemberton, J.L.; Guisnet, M. Phenanthrene hydroconversion as a potential test reaction for the hydrogenating and cracking properties of coal hydroliquefaction catalysts. *Appl. Catal.* **1984,** 13, (1), 181-92.

[30] Restrepo-Garcia, J.R.; Baldovino-Medrano, V.G.; Giraldo, S.A. Improving the selectivity in hydrocracking of phenanthrene over mesoporous Al-SBA-15 based Fe–W catalysts by enhancing mesoporosity and acidity. *Appl. Catal., A* **2016,** 510, (Supplement C), 98-109.

[31] Perego, C.; Peratello, S. Experimental methods in catalytic kinetics. *Catal. Today* **1999,** 52, 133-145.

[32] Le Page JF. Applied Heterogeneous Catalysis. Paris; **1987.**

[33] Wilm, M. Principles of Electrospray Ionization. *Mol. Cell. Proteomics* **2011,** 10, (7), M111.009407.

[34] Zhang, K.; Yu, J.; Gao, S.; Li, C.; Xu, G. Understanding Shale Oil Hydrotreatment with Composition Analysis Using Positive-Ion Mode Atmospheric Pressure Photoionization Fourier Transform Ion Cyclotron Resonance Mass Spectrometry. *Energy Fuels* **2017,** 31, (2), 1362-9.

[35] McKay, J.F.; Weber, J.H.; Latham, D.R. Characterization of nitrogen bases in high-boiling petroleum distillates. *Anal. Chem* **1976,** 48, (6), 891-8.

[36] Song, T.; Zhang, Z.; Chen J, Ring Z, Yang H, Zheng Y. Effect of Aromatics on Deep Hydrodesulfurization of Dibenzothiophene and 4,6-Dimethyldibenzothiophene over NiMo/Al2O3 Catalyst. *Energy Fuels* **2006,** 20, (6), 2344-9.

[37] Sayan, Ş.; Paul, J. Hydrogenation of naphthalene and methylnaphthalene: modeling and spectroscopy. *J. Mol. Catal. A: Chem* **2002,** 185, (1), 211-22.

[38] SA Rincon Ortiz, J Rodriguez Pereira, VG Baldovino-Medrano. An investigation on the cracking of dibenzothiophene over Pd-Pt/aluminosilicate. *13th EuropaCat.* Florence, Italy; 2017.

[39] Benazzi, E.; Leite, L.; Marchal-George, N.; Toulhoat, H.; Raybaud, P. New insights into parameters controlling the selectivity in hydrocracking reactions. *J. Catal.* **2003,** 217, (2), 376-87.

[40] Allan, D.E. The Dehydrogenation and Isomerization of Cyclohexane Over a Platinum Alumina Mordenite Catalyst. Chemical Engineering doctoral dissertation. Louisiana: Louisiana State University and Agricultural & Mechanical College; **1970,** 356.

[41] Morterra, C.; Chiorino, A.; Ghiotti, G.; Garrone, E. Surface acidity of [small eta]-alumina. Part 1.-Pyridine chemisorption at room temperature, *J. Chem. Soc., Faraday Trans*, **1979,** 75, 271-288

[42] Gafurov, M.R.; Mukhambetov, I.N.; Yavkin, B.V.; Mamin, G.V.; Lamberov, A.A.; Orlinskii, S.B. Quantitative Analysis of Lewis Acid Centers of γ-Alumina by Using EPR of the Adsorbed Anthraquinone as a Probe Molecule: Comparison with the Pyridine, Carbon Monoxide IR, and TPD of Ammonia, *J. Phys. Chem., C*, **2015,** 119, 27410-27415.

[43] Mora-Vergara ID, Hernández Moscoso L, Gaigneaux EM, Giraldo SA, Baldovino-Medrano VG. Hydrodeoxygenation of guaiacol using NiMo and CoMo catalysts supported on alumina modified with potassium. *Catal. Today* **2017,** (In Press).

[44] Baldovino-Medrano, VG.; Centeno, A.; Giraldo, S.A. Evaluating the functionalities of NiMo/□-Al2O3B2O3 catalysts in naphthalene hydrodearomatization and dibenzothiophene hydrodesfulfurization. *CT&F* **2010,** 4, 91-9.

[45] Montgomery, D. C.; Runger, G. C. Applied Statistics and Probability for Engineers, 6th Edition, Wiley, **2013,** 836 p**.**

[46] Quinn, G.P.; Keough, M.J. Experimental design and data analysis for biologists. Cambridge University Press, Cambridge, UK, **2002,** 527 p.

[47] Kutner, M.H.; Nachtsheim, C; Neter, J.; Li, W. Applied linear statistical models. 5th Edition, McGraw-Hill/Irwin, **2004,** 1396 p.

[48] Choi, H.W.; Dines, M.B. Selective removal of nitrogen compounds from shale oil. *Fuel* **1985,** 64, (1), 4-8.

[49] Dong, D.; Jeong, S.; Massoth, F.E. Effect of nitrogen compounds on deactivation of hydrotreating catalysts by coke. *Catal. Today* **1997,** 37, (3), 267-75.

[50] Laredo, G.C; Leyva, S.; Alvarez, R.; Mares, M.T.; Castillo, J.; Cano, J.L. Nitrogen compounds characterization in atmospheric gas oil and light cycle oil from a blend of Mexican crudes. *Fuel* **2002,** 81, (10), 1341-50.

[51] Celis-Cornejo C.M.; Mantilla, M.M.G.; Baldovino-Medrano V.G.; Ramírez-Caballero G.E. A quantum chemical study for exploring the inhibitory effect of nitrogen containing species on the adsorption of polynuclear aromatic hydrocarbons over a Brønsted acid site. *J. Phys. Conf. Ser* **2016,** 743, (1), 012010.

CHAPTER 2: Weakly Basic Nitrogen-Containing Compounds Inhibit Catalytic Two-Stage Hydrocracking Processes

Abstract

Under the common assumption that only basic nitrogenated compounds significantly inhibit the catalytic performance (activity and selectivity) during the hydrocracking, information about the inhibition caused by weakly basic nitrogen-containing compounds is very meager. Notwithstanding, these weakly basic nitrogen-containing compounds were found to be more refractory to the hydrotreating. Therefore, the goal in this chapter was to study the effect of small amounts of weakly basic molecules, carbazole and tetrahydrocarbazole, in the phenanthrene hydrocracking reaction over a Ni-MoS_2/Y-zeolite␣alumina catalyst. For such purpose, an unreplicated 3^3 factorial experiment was designed for studying the effect of temperature, liquid hourly space velocity and relative concentration of weakly basic nitrogen-containing compounds. The first set of experiments was carried out considering only the effect of carbazole, meanwhile, the second group of experiments was executed under similar conditions but evaluating the effect of a mixture of carbazole and tetrahydrocarbazole in 1:1 ratio. The latter, because it fairly represents the remaining nitrogen compounds in a hydrotreated heavy oil fraction aimed for a two-stage hydrocracking reactor. The significance of the two-way and three-way interactions between the studied factors was assessed with the analysis of interaction plots. Results were complementary studied with an analysis of variance (ANOVA) for an un-replicated factorial design for corroborating the results from the main effects and interaction plots. Results from the ANOVA showed that temperature and relative concentration of weakly basic nitrogen-containing compounds were the individual factors which predominantly affected the selectivity towards the hydrocracking products. In addition, it was found that some two-way interactions predicted as negligible with the ANOVA, were considered to be nonremovable effects with the analysis of the interaction plots. In the last section, the effect of weakly basic nitrogen-containing compounds under a severe basic atmosphere was explored in order to determine if the presence of weakly basic molecules contributes to exert a higher inhibition on the catalyst performance, than the observed in absence of them. Interestingly, the addition of 20 ppm of weakly basic nitrogen-containing compounds significantly inhibited the number of isomerization products, thus contributing to a higher inhibition.

Keywords: hydrocracking, weakly basic nitrogen-containing compounds, inhibition, Ni-MoS_2/Y-zeolite␣alumina, experimental design, interaction plots, ANOVA.

Nomenclature

%C_PHE	Phenanthrene Conversion
%S	Selectivity
ANOVA	Analysis of Variance
DFT	Density Functional Theory
ESI	Electrospray Ionization
FT-ICR-MS	Fourier Transform Ion Cyclotron Resonance Mass Spectrometry
GC	Gas Chromatography
GC-MS	Gas Chromatography coupled with Mass Spectrometry
HCK	Hydrocracking
HDT	Hydrotreatring
ISTD	Internal Standard for GC
LHSV	Liquid Hourly Space Velocity
MS	Mass Spectrometry
S^{HCK}	Selectivity towards the hydrocracking products
S^{EXT}	Selectivity to the route derived from the cracking of partially hydrogenated external rings
S^{INT}	Selectivity to the route derived from the cracking of a partially hydrogenated internal ring
S^{MIX}	Selectivity which follows the route in which both an intermediate and an external ring are hydrogenated
VGO	Vacuum Gas Oil
WBN	Weakly Basic Nitrogen-containing compounds

2. Weakly Basic Nitrogen-Containing Compounds Inhibit Catalytic Two-Stage Hydrocracking Processes

2.1. Introduction

Heavy crude oils require hydrocracking for upgrading [1, 2]. There is a direct link between the characteristics of a crude oil and its content of heteroatoms: the heavier the crude oil, the higher its contents of nitrogen, sulfur, oxygen and other heteroatoms [3]. Hydrotreating is the primary process for removing heteroatoms from oil fractions. However, complete removal of heteroatoms is technically unfeasible. Among heteroatoms, nitrogen is critical for the performance of catalysts for hydrocracking. The inhibitory effect of the nitrogen-containing hetero compounds over the hydroprocessing catalyst has been copiously investigated [4-9].

As previously discussed in the introductory chapter, for the hydrodenitrogenation of heavy feedstocks, the evidence suggests that the nitrogenated compounds of basic character are easier to remove than the weakly basic ones [10-15]. In this regard, Jokuty and Gray [10] used the retention chromatographic method for concentrating the nitrogen fraction of a hydrotreated coker gas oil sample. FT-IR, NMR, and Mass Spectrometry were used for studying the nature of refractory nitrogenates. They found a high concentration of weakly basic carbazole, benzocarbazoles, and tetrahydrobenzocarbazoles in the hydrotreated fraction. As exemplified in chapter 1 the implementation of high-resolution mass spectrometry for describing the constituents of hydrotreated fractions pointed to a similar conclusion [11-13]. Kekäläinen *et al.* [12] using Fourier Transform Ion Cyclotron Resonance Mass Spectrometry (FT-ICR-MS) analyzed a hydrotreated vacuum gas oil fraction, with specifications of 700 ppm of total N content. They observed a significant reduction in the basic nitrogenated compounds as compared to the weakly basic ones.

Notwithstanding, the N content studied in the previous works is common in mild hydrocracking units but still too high for accomplishing the nitrogen slip suggested by the catalyst suppliers for the two-stage hydrocracking configuration [16]. In chapter 1, we employed Electrospray Ionization coupled with the FT-ICR-MS to identify the most refractory nitrogenated compounds in a hydrotreated vacuum gas oil with a total N content of about 20 ppm [17]. Interestingly, none of the basic nitrogen-containing compounds were detected, whereas a high relative abundance of weakly basic nitrogen-containing compounds with the N1 stoichiometry was evidenced. Moreover, the relative abundance of partially hydrogenated nitrogen-containing molecules; namely, tetrahydrocarbazoles and benzocarbazoles, was prominently higher in the hydrotreated fraction than in the untreated vacuum gas oil.

Studies by Sau *et al.* [18] showed that the inhibition exerted by the organic nitrogen present in a hydrotreated oil fraction on a hydrocracking catalyst was larger compared to the inhibition observed under the presence of pyridine; which is a strongly basic molecule. Kobayashi *et al.* [19] suggested that even small amounts of weakly basic nitrogen-containing compounds; ca. 2 ppm of total N, specifically carbazole can inhibit hydrocracking catalysts. In chapter 1, we also found evidence of inhibition effects by weakly basic nitrogen-containing compounds on hydrocracking catalysts [17]. Particularly, the performance of a conventional Ni-MoS_2/Y-zeolite␣alumina catalyst in the hydrocracking of phenanthrene was affected by the incorporation of mixtures of carbazole and tetrahydrocarbazole to the reaction feed. Evidence of a decrease in the selectivity to products derived from the hydrocracking of partially hydrogenated external rings was presented [17].

Continuing our studies on this phenomenon, the present chapter makes a more systematic evaluation of the effect of small amounts of weakly basic nitrogen-containing compounds on the

catalytic performance of a Ni-MoS_2/Y-zeolite␣alumina material employed for hydrocracking. Carbazole, tetrahydrocarbazole, and mixtures of these compounds were used as representative models for weakly basic nitrogen-containing compounds [17], whereas phenanthrene was selected as a representative molecule of the polynuclear aromatic fraction of a common hydrocracking feedstock [20-23]. Reaction test were carried out by varying temperature, liquid hourly space velocity (LSHV), and the concentration of nitrogenates. Considering these variables, an un-replicated full 3^3 factorial experiment was designed to evaluate their effect on the catalytic performance. Using such a strategy, the estimation of possible combined effects (i.e. interactions) on the response variables; conversion and selectivities, can be assessed by statistical methods. In addition, the effect of the weakly basic nitrogen-containing compounds on the catalytic performance under an ammonia reaction atmosphere was also investigated. The goal of these tests was to discern if small amounts (20 ppm of total N) of the 50/50 wt.%/wt.% mixture of carbazole and tetrahydrocarbazole could significantly affect the remaining activity of the Ni-MoS_2/Y-zeolite␣alumina catalyst under an ammonia atmosphere. Results provided strong evidence that calls for no longer disregarding the effect of weakly basic nitrogen-containing compounds on heavy oil hydrocracking. Thenceforward, an improvement of catalytic formulations for hydrocracking is called upon to tackle challenges in current fuels processing and purification.

2.2. Experimental

2.2.1. Catalyst preparation. The oxide precursor of the Ni-MoS2/Y-zeolite␣alumina catalyst was prepared adapting the methods presented by Agudelo et al. [24]. Extrudates containing 75 wt.% of an alumina precursor (Bohemite, Catapal B, Sasol) and 25 wt.% of a commercial Y-zeolite (CBV 760, Zeolyst, 720 m2/g with a Si/Al ratio of 30) were used as supports. Shaped bodies were

dried at 378 K for 15 h and further calcined for 6 h at 823 K under static air in a muffle furnace. Extrudates were crushed and sifted for obtaining particles of sizes between 0.3 and 0.6 mm. These particles were sequentially impregnated with appropriate amounts of ammonium heptamolybdate tetrahydrate and nickel nitrate hexahydrate; both 99 wt.%, Merck, in order to obtain catalysts loaded with 3.0 wt.% NiO and 15.0 wt.%. MoO3. More details concerning the catalyst preparation can be found in chapter 1 [17]. Sulfidation was performed in situ before catalytic tests (Section 3.2.2). The catalyst was denoted as Ni-MoS2/Y-zeolite␣alumina, with the symbol ␣ representing the fact that alumina is a binder.

2.2.2. Reactivity tests. Phenanthrene (98%), carbazole (> 95%), tetrahydrocarbazole (99%), dimethyl disulfide (DMDS, 99.0%), cyclohexane (99.5%), and hexadecane (ReagentPlus® 99%) were all purchased from Sigma-Aldrich and used without further purification. On the other hand, aniline (>99%) was kindly supplied by the Laboratorio de Química Orgánica y Biomolecular, (LQOBio) from Universidad Industrial de Santander. Reactions were performed in fixed bed reactors packed with 0.15 g of the oxide precursors of the Ni-MoS2/Y-zeolite␣alumina catalyst diluted in 2.5 cm3 of quartz sand (1.0 – 0.7 mm) for preventing thermal spots [25]. Two catatests were employed for the experiments allowing to establish the reproducibility of the results [26] (pictures of these set-ups are presented in Figure B1, Annex B). The absence of external diffusion limitations was ruled out as from chapter 1 [17]. Once placed in the reactor and mounted on the catatest, the oxide precursor of the catalyst was dried for 1 h under a nitrogen flow of 100 ml/h. Thereafter, it was activated using 10.65 wt.% of DMDS diluted in cyclohexane at 673 K under a hydrogen flow of 105 ml/min during 4 h. Reactions were performed at a (500 NL hydrogen)/(l L feed) ratio and 6.9 MPa. The feed consisted on a flow of 20 ml/h of 2 wt% phenanthrene in cyclohexane. An un-replicated full 33 factorial experimental design was implemented for

performing two sets of reactions. Temperature, LHSV, and total concentration of weakly basic nitrogen-containing compounds ([WBN]) were taken as input variables of the design. The corresponding levels for temperature were 623, 638 and 653 K; for LHSV were 1.3, 1.8 and 2.2 h-1; and for total concentration of weakly basic nitrogen-containing compounds three levels between 0 and 5 ppm were chosen (0, 0.8, and 3.6 for the first set of experiments, and 0, 1.0, and 5.0 for the second set). The first set of catalytic tests was carried out by adding carbazole to the reaction feed, while a 50/50 wt.%/wt.% mixture of carbazole and tetrahydrocarbazole was added for the second set. It is important to highlight that the total concentration of nitrogen for the second set of reactions was higher (0, 1.0 and 5.0 ppm of total N) as compared to the first set (0, 0.8 and 3.6 ppm of total N). The reason for such a choice was to investigate the effect of both low and middle ranges of weakly basic nitrogen-containing compounds concentrations over hydrocracking. In addition, results for catalytic tests at 0 ppm of total nitrogen were considered for the statistical analyses of both sets of reactions without further replication.

Finally, a set of tests under an ammonia atmosphere was carried out. 1 wt.% aniline was added to the reaction feed to produce the ammonia atmosphere. These tests were planned according to an un-replicated 2^2 full factorial design choosing temperature; namely, 653 and 673 K, and the total concentration of nitrogen from the weakly basic compounds; namely, 0 and 20 ppm, as input variables.

2.2.3. Identification and quantification of reaction products. Gas chromatography coupled to quadrupole ion trap mass spectrometry (GC-MS) was employed for the identification of reaction liquid products. An Agilent GC 7890A - MSD 5975C instrument was used. The GC-MS apparatus was equipped with an HP-1 column (Agilent, ID: 0.18 mm, length: 100 m).

Samples were diluted in cyclohexane using a 1:10 volume ratio before injection. A solvent delay time of 12 min and a detection range of 15 to 350 Da were employed for mass spectrometry. The analysis method consisted of a heating ramp of 5 K min^{-1} starting from 363 K to 503 K, then keeping constant the latter temperature for 14 min. A helium flow of 1.1 $ml \cdot min^{-1}$ was used as carrier gas. The Wiley 8.0 mass spectra library was used for the assignment of the spectra obtained from the GC-MS, and this was confirmed by a data quality of mass spectra obtained of 95%. In general, ca. 87.9 % of the reaction liquid products was identified by the implemented method. Un-identified peaks appeared in chromatograms at earlier retention times. They were thus considered to correspond to lighter hydrocracking products; specifically, mono and di-aromatics. During the catalytic tests, the quantification of the reaction products was carried out by gas chromatography in an Agilent 6890 apparatus provided with a Flame Ionization Detector and a HP-1 column of the same characteristics of the one employed for GC-MS. 2.0 wt% hexadecane was used as a chromatography internal standard. A sample volume of 1.0 µL was injected in a split liner at 373 K (split ratio 75:1). The method was the same as described for the GC-MS. Chromatographic standards were used for making the calibration curves of the following compounds: phenanthrene, 9,10-dihydrophenanthrene, 1,2,3,4-tetrahydronaphthalene, naphthalene, biphenyl, cyclohexyl benzene, and hexadecane (all bought from Sigma-Aldrich). The response factor used for some compounds derived from hydrocracking was taken from the calibrated species depending on their similarities with respect to the chemical structures. A list of the response factors, specifying those which were made equal to the ones determined from standards, are available in Annex B Figure B2.

2.2.4. Expression of catalytic results. Catalytic results were expressed in terms of phenanthrene conversion (%C_{PHE}) and overall selectivity to hydrocracking products (%S^{HCK}) as defined in equations 2.1 and 2.2.

$$\%C_{PHE} = \frac{n_{PHE}^{Feed} - n_{PHE}^{Product}}{n_{PHE}^{Feed}} * 100 \quad (2.1)$$

$$\%S^{HCK} = \frac{\sum n_i^{HCK}}{\sum n_i^{HYD} + \sum n_i^{HCK}} * 100 \quad (2.2)$$

Where, n_{PHE}^{Feed}, $n_{PHE}^{Product}$, $\sum n_i^{HCK}$, $\sum n_i^{HYD}$ are the initial moles of phenanthrene, the moles of phenanthrene in the liquid product, the sum of identified and quantified hydrocracking products, and the sum of primary hydrogenation products. Isomerization products were accounted for the overall selectivity to hydrocracking. Primary hydrogenated products were: dihydrophenanthrene, tetrahydrophenanthrene, octahydrophenanthrene, and asym-octahydrophenanthrene. Neither perhydrophenanthrene nor decalin were detected under the reaction conditions employed herein as in contrast to other published works [22, 27]. Full conversion data is available in Annex B in the form of Time on Stream plots (Figures B3-B5). The mean of the carbon mass balance (μ_{mC}) of the catalytic tests was estimated to be within the 95% confidence interval: $17.3 \leq \mu_{mC} \leq 23.7$ as based on a Student's-t distribution with 26 degrees of freedom.

2.2.5. Statistical analysis. Reaction results were analyzed following the graphical procedures suggested by [28-30]. In addition, analysis of variance (ANOVA) models were formulated and their parameters statistically tested for significance. All models were of the fixed effects type and included the effects of the principal variables: temperature, LHSV, and [WBN] as well as two-way and three-way interactions of these variables. For the analysis of the data from the un-replicated 33 designs, ANOVA calculations were performed according to the method proposed by Yang [31].

Details of the statistical development and tests for checking the assumptions of normality, constant variance, and error independency, of the ANOVA model, can be found in the Annex B. In general, these tests were considered satisfactory hence evidencing the appropriateness of the statistical tests.

2.3. Results and discussion

The effect of carbazole on the activity and selectivity of the Ni-MoS_2/Y-zeolite␣alumina catalyst for phenanthrene hydrocracking is presented and discussed first followed by the effect of the mixture of carbazole and tetrahydrocarbazol. Finally, the effect of the weakly basic nitrogen-containing compounds under an ammonia atmosphere is presented and discussed.

2.3.1. Phenanthrene hydrocracking in the presence of carbazole

2.3.1.1. ***Effect on conversion.*** Table B1 in Annex B summarizes the conversion data at steady state for the first experimental design at the studied three different levels of temperature, LHSV, and relative concentration of carbazole. Steady state conversion data is represented in the form of main effects plots in Figure 2.1(a)-(c) to analyze the effect of each one of the principal variables. Error bars correspond to two tail 95% confidence intervals calculated with the Student's t-distribution (with 8 degrees of freedom, $\boldsymbol{t_{0.025,8}}$). According to results, conversion increased with temperature and decreased with LHSV. This could be expected in a way that temperature and LHSV directly affect kinetics. Although it is clear that the hydrogenation and hydrocracking reactions are mostly exothermic, at these conditions the hydrogenation reactions in steady state are close to the equilibrium [20, 32], without considering the formation of perhydrophenanthrene. In this regard, at temperatures above the range studied herein, the thermodynamic equilibrium is more affected, adversely affecting the conversion. On the other hand, increasing LHSV implies a shorter

contact time and consequently the conversion decreases. From Figure 2.1(c), the presence of carbazole exerts a slight effect over phenanthrene conversion under the tested conditions. However, the effect of the concentration of carbazole on conversion is not significant. This could indicate that confidence interval is too strict for the number of experiments carried out.

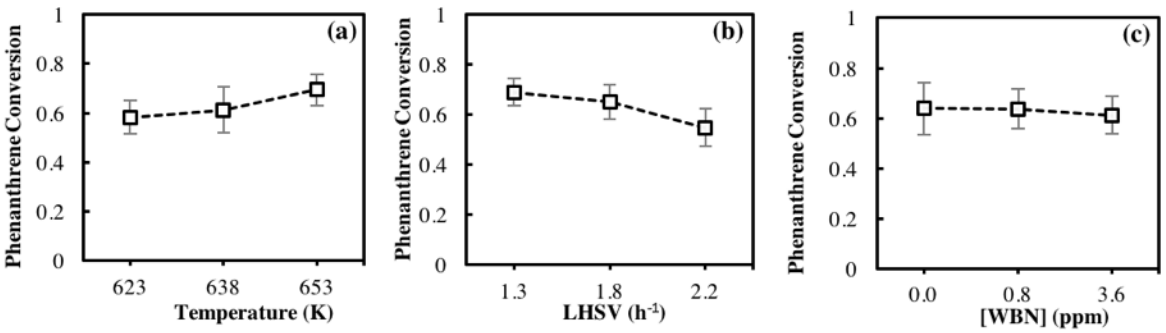

Figure 2.1. Main effects plot for phenanthrene conversion as a function of (a) temperature, (b) LHSV and (b) relative concentration of carbazole ([WBN]). Reactions were carried out at 6.9 MPa and (500 NL hydrogen)/(l L feed) ratio.

The assessment of interactions from a statistical point of view of the factors considered in the experiment provides information about whether these variables are related, allowing to establish how the effect of a certain factor over the dependent variable is linked to the level of the other interacting factor. In general, the existence of statistical interactions implies that the corresponding statistical model contains non-linear terms (of first and second order). Additionally, the implementation of the A-against B plot, and its reciprocal, B-against A plot, brings interesting information about synergetic or antagonistic effects, which are not possible to observe by analyzing only one of the interaction plots [28]. When referring to a removable or non-removable variable, it is implied whether these terms can be dropped out from the models after a suitable transformation of the response variable is applied. Therefore, after the analysis of these plots what must be concluded is the statistical model may or not contain such nonlinear terms.

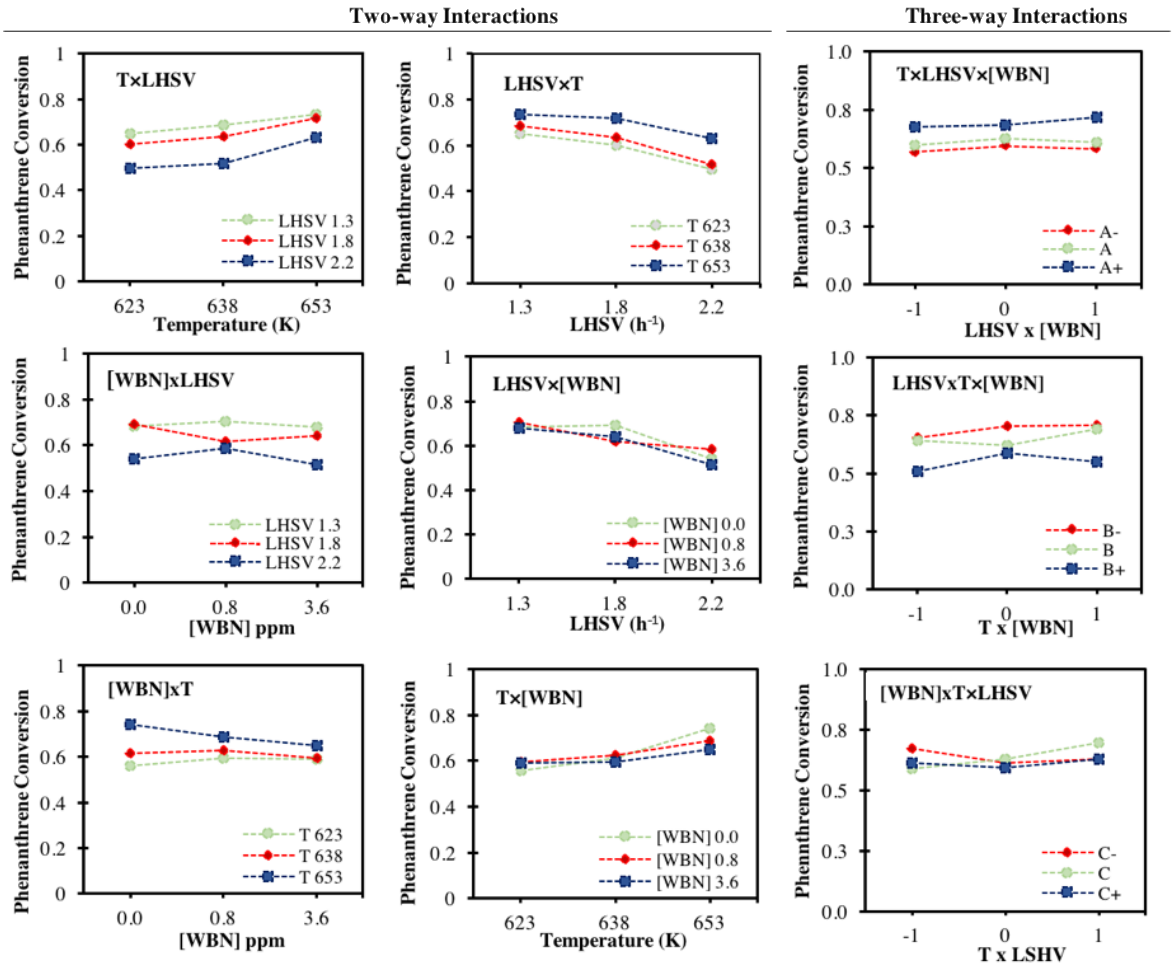

Figure 2.2. Two-way and three-way interactions for phenanthrene conversion of temperature (K), LHSV (h^{-1}), and relative concentration of carbazole ([WBN] in ppm). Reactions were carried out at 6.9 MPa and (500 NL hydrogen)/(l L feed) ratio.

Two-way and three-way interaction plots are presented in Figure 2.2. Starting with the two-factor interactions, T×LHSV and its reciprocal is possible to observe that these interactions do not cross in any value, being a removable effect from the ANOVA model [33]. However, is interesting to see that there exists a synergistic effect of temperature and LHSV on the conversion, at higher values of temperature, and lower values of LHSV, the conversion is favored. When this trend is clearly observable, then the existence of external diffusional limitations is ruled out [25, 34]. On the other hand, plots for the interactions [WBN]×LHSV exhibited borderline interaction, while its

reciprocal, showed a crossover interaction. Despite the main effect of the relative concentration of carbazole apparently has a weak significance, is not enough reason for eliminating the two-way interaction from the model [33, 35]. Moreover, if the interaction exhibits an interpretable effect, as it could be evidenced in the synergistic effect which the plot describes. This could be interpreted as if decreasing the LHSV then the effect of the relative concentration of carbazole is less significant over the conversion. In other words, at lower space velocities a larger accumulation of the reactant takes place into the mesopores of the catalyst binder (alumina), where the sulfide active phases should be supported [36], making less evident the effect of the weakly adsorbed nitrogen-containing compounds on the conversion, due to a promotion of the hydrogenation reactions of phenanthrene which occur on these active centers. Considering that the adsorption of carbazole on the active sites of the catalyst is a faster process than the reaction of polynuclear aromatic hydrocarbons, is possible to infer that an increase in LHSV favors the mass transfer coefficient of nitrogenates towards the catalytic surface [37, 38], consequently increasing the adsorption of these molecules on the active sites of the catalyst. This assumption is valid for an adsorbate in dilute concentration which diffuses on a single catalyst particle [37]. In third place, the interaction of [WBN]×T and its reciprocal also show borderline interaction, whereas the T×[WBN] plot showed a cross-interaction. Higher temperatures favor the kinetics and promote the desorption of weakly adsorbed nitrogen-containing compounds from the acid sites. Additionally, a slight antagonistic effect is observed for the interaction [WBN]×T. This shows that for higher values of temperature and relative concentration of carbazole, the conversion is decreased. Meanwhile, at lower values of temperature and higher concentrations of carbazole, the conversion is promoted. This may indicate that the inhibitory effect of carbazole on the conversion of phenanthrene, at the studied concentrations, is very sensitive to the operational variables, T and

LHSV. Moreover, these interactions indicate the presence an underlying effect of the concentration of carbazole which is not clearly visible under the conditions studied. Observing the three-way interactions only the [WBN]xTxLHSV presents a cross and a border line interaction, by the principles of sparsity and hierarchy, higher order interactions are considered to be less significant for dominating the system [28].

To corroborate the statistical significance of the trends described above, an ANOVA of the data collected was performed. The same analysis also allowed to detect the possible presence of effects linked to the interaction of the studied variables. The effects observed in Figure 2.1(a) and (b) for temperature and LHSV, respectively, over the conversion were confirmed (*p-value* = 6.27×10^{-6} for temperature and a *p-value* = 2.48×10^{-6} for LHSV found from ANOVA tests with 2 and 16 degrees of freedom, $F_{2,16}$). On the contrary, for the relative concentration of carbazole the ANOVA test corroborated that it does not have a significant effect over the conversion (*p-value* = 0.624, with 2 and 16 degrees of freedom, $F_{2,16}$). Likewise, the combined effects of temperature and LHSV, relative concentration of carbazole and temperature, LHSV and relative concentration of carbazole, and the triple effect of T-[WBN]xLHSV were not statistically significant. It is important to note that although there is no significant interaction between temperature and LHSV is consistent with the absence of diffusional limitations and the absence of heat transport [34]. Going back to the point, the negligible effect of carbazole on the conversion under the studied conditions is reasonable, due to it may not exert an inhibition on the phenanthrene hydrogenation reactions but probably in some further transformation on the acid sites of the catalyst. Thus, the conversion is not affected, but, as observed in chapter 1 [17], the distribution of cracking products.

In order to validate the assumptions of normality and independence of the statistical model proposed in the ANOVA, an analysis of residuals was made to establish its utter fulfillment (see Figure B6, in Annex B). Taking this into account, the statistical model that describes the conversion of phenanthrene according to the statistically significant effects of the studied variables is expressed as:

$$Y_{ijk} = \mu_0 + (\tau_T)_i + (\tau_{LHSV})_k + \varepsilon_{ijk} \quad (1.3)$$

Where, μ_0 is the population mean that is estimated from the global mean of the experiment data at 64.6; τ_T is the effect of temperature; τ_{LHSV} is the effect of the LHSV and ε_{ijk} is the experimental error.

In summary, for the conversion of phenanthrene, the main effects of temperature and LHSV were found to be more significant than the two-way interactions of LHSVx[WBN] and [WBN]xT, according to the ANOVA test, and with the principle of hierarchy [28]. However, this not imply that the observed two-way interactions are negligible. In fact, this suggest that an underlying effect of the relative concentration of carbazole over the conversion is linked to the operational variables, T and LHSV. In the next section the effect of this variables over the selectivity towards the hydrocracking is discussed in terms of the same analysis, and similar trends are observed.

2.3.1.2. Effect on selectivity. To make a discussion about this aspect, it is important to begin by describing the scheme of the phenanthrene reaction over a Ni-MoS2/Y-zeolite␣alumina catalyst, shown in Scheme 2.1. In a first stage, the internal or external rings of phenanthrene could be partially hydrogenated, as well as both simultaneously. Dihydrophenanthrene is obtained from the partial hydrogenation of the internal ring. Meanwhile, tetrahydrophenanthrene and

octahydrophenanthrene are obtained from the partial hydrogenation of external rings. The product denoted as asym-octahydrophenantrhene is originated by the simultaneous partial hydrogenation of an internal and external ring. Isomerization takes place over the external partially hydrogenated rings to form a 5-membered ring with a methyl substituent i.e. methylcyclopenta -naphthalene and -tetralin. Notwithstanding, direct ring opening of the 6-membered partially hydrogenated ring could simultaneously occur [21]. The further phenanthrene cracking steps (ring opening and dealkylation) follows three main routes. One that encompasses the products derived from the cracking of the tetrahydro and octahydrophenanthrene, partially hydrogenated external rings, i.e. Butylnaphthalene, butyltetralin, naphthalene, tetralin, methylindane, indane. As mentioned, this route favors the butane production. A second route in which the partially hydrogenated internal ring of dihydrophenanthrene is cracked into alkylbiphenyls, biphenyl, and cyclohexylbenzene. Ethane and methane are produced from the dealkylation of the ring-opened products. The last route encompasses the products derived from the asym-octahydrophenanthrene, which is produced by the simultaneous hydrogenation of one external and one internal ring. However, the selectivity to this route, in the range of the studied conditions, is very low as compared to the two first mentioned above [17]. A complete carbon mass balance is shown in Table 2.1 for one reaction in absence of weakly basic nitrogen-containing compounds, and another one at same conditions but in presence of these nitrogenated molecules. When doping with weakly basic nitrogen-containing compounds what is observed is a noticeable decrease in the cracking products. Even more, the ratio of non-assigned products in the hydrocracking region is considerably lower. With this information, the effect of carbazole on the selectivity towards the hydrocracking products will be addressed first.

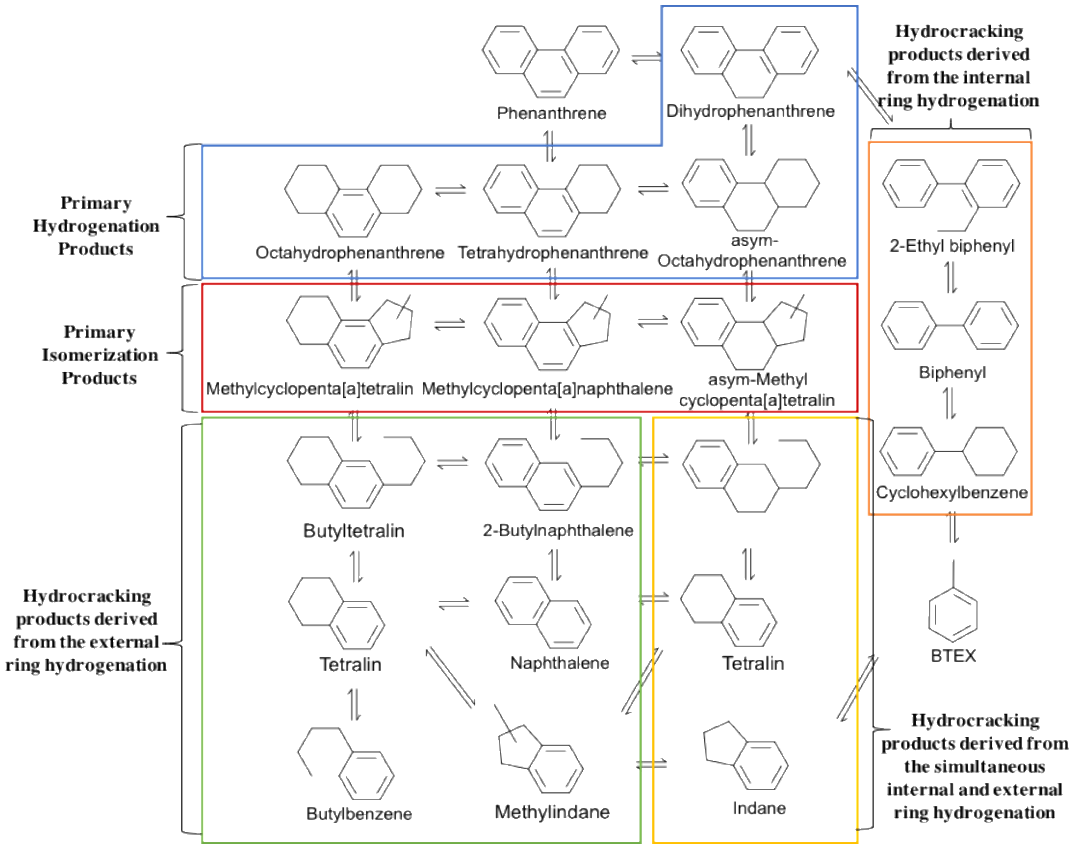

Scheme 2.1. Reaction scheme for the hydrocracking of phenanthrene over a Ni-MoS_2/Y-zeolite␣alumina catalyst and its routes as proposed in chapter 1 [17]. BTEX, account for the mixture of monoaromatic hydrocarbons i.e. Methylcyclohexane, dimethylcyclohexane, ethylcyclohexane, toluene and butyl benzene.

Results of the selectivity towards the hydrocracking products, as defined in equation 2.2, are available in Table B2 in Annex B. Mentioning that primary isomerization products accounted for the sum of hydrocracking products as explained in the methodology is worth. Figure 2.3 shows the main effects plots for the selectivity towards the hydrocracking products with respect to (a) temperature, (b) LHSV and (c) relative concentration of carbazole. The error bars correspond to a confidence interval calculated with the Student's t-distribution (with 8 degrees of freedom, and alpha level of 0.05, $t_{0.05/2,8}$).

Table 2.1.

Carbon mass balance equivalent % for the assigned products detected with GC-MS, and the non-assigned products, for the reactions containing a relative concentration of weakly basic nitrogen-containing compounds ([WBN]) of 0 and 5 ppm at 653 K, 6.9 MPa, LHSV = 1.3 h^{-1}, and (500 NL hydrogen)/(l L feed) ratio. The WBN encompasses the mixture of carbazole and tetrahydrocarbazole in a 1:1 ratio.

Equivalent % in C mass balance					
Compound name	**[WBN] 0 ppm**	**[WBN] 5 ppm**	**Compound name**	**[WBN] 0 ppm**	**[WBN] 5 ppm**
Primary Hydrogenation Products			**Hydrocracking Products**		
Dihydrophenanthrene	0.1571	0.2565	Methyl Naphthalene	0.0134	0.0000
Tetrahydrophenanthrene	0.1496	0.2462	Methyl Tetralin	0.0207	0.0000
Octahydrophenanthrene	0.0513	0.0891	Naphthalene	0.0257	0.0025
asym-Octahydrophenantrhene	0.0484	0.0399	Tetralin	0.0593	0.0066
Primary Isomerization Products			Methyl Indane	0.0206	0.0000
Methylcylopenta Naphthalene	0.0691	0.0819	Indane	0.0252	0.0039
Methylcylopenta Tetralin	0.0293	0.0239	Octahydroantrhacene	0.0060	0.0000
i-Methylcylopenta Tetralin	0.0076	0.0048	Tetrahydroanthracene	0.0129	0.0000
Hydrocracking Products			Ethylidene bisbenzene	0.0136	0.0105
Dimethyl Biphenyl	0.0196	0.0093	Cyclopentyl propylbenzene	0.0073	0.0053
Ethyl Biphenyl	0.0308	0.0168	Butylbenzene	0.0045	0.0000
Cyclohexyl Benzene	0.0119	0.0060	Ethylcyclohexane	0.0035	0.0000
Biphenyl	0.0081	0.0099	Dimethylcyclohexane	0.0072	0.0000
2-Butyl Naphthalene	0.0273	0.0140	Toluene	0.0088	0.0000
6-Butyl Tetralin	0.0387	0.0082	Methylcyclohexane	0.0191	0.0058
2-Butyl Tetralin	0.0169	0.0025	non asigned in HYD region	0.0168	0.0000
Ethyl Naphthalene	0.0062	0.0027	non asigned in HCK region	0.2546	0.0555
Ethyl Tetralin	0.0044	0.0000	Phenantrhene in product	0.3763	0.7510
			Total	1.5717	1.6526
			Equivalent % in C mass for Phenantrhene in feed	1.8594	1.8221
			Weight loss %C	0.2877	0.1694
			Phenanthrene Conversion (%C_PHE)	79.8	58.8

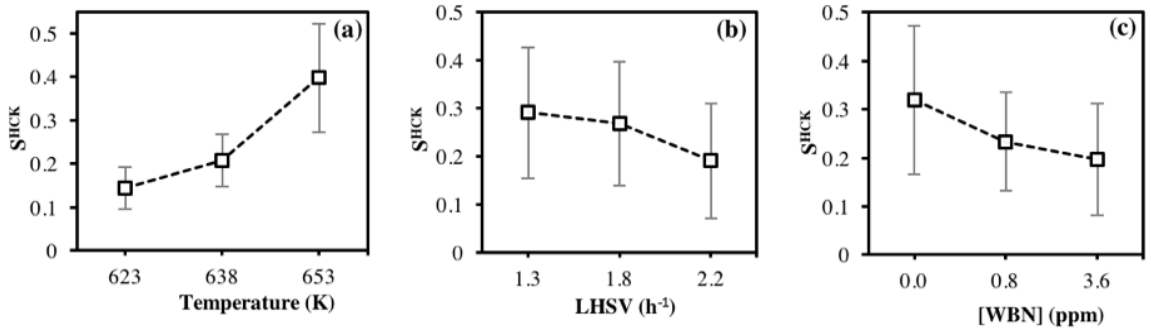

Figure 2.3. Main effects plot for selectivity towards the hydrocracking products (S^{HCK}), as a function of (a) temperature, (b) LHSV and (b) relative concentration of carbazole ([WBN]). Reactions were carried out at 6.9 MPa and (500 NL hydrogen)/(l L feed) ratio.

The effects of the three variables studied over the selectivities are notorious. At high temperatures, the selectivity towards the hydrocracking products was favored. The kinetics of the cracking reactions is assisted by an increase in temperature, being more remarkable than the adverse effect on the thermodynamic equilibrium. Meanwhile, the increase in LHSV decreases the selectivity towards the hydrocracking, being this effect more notorious at high values. On the other hand, it is possible to see in Figure 2.3.c an effect of the relative concentration of carbazole on selectivity. In particular, the increase in [WBN] appears to disadvantage the selectivity towards the hydrocracking products. Thence, although the observed effect of carbazole on the conversion was not significant, it seems that it exerts a marked effect on selectivity.

Figure 2.4 shows two-way and three-way interactions of the studied factors. Following the same order, the interaction of TxLHSV and its reciprocal, is removable from the model [33]. As well as the interaction of [WBN]xT. However, a crossover interaction of [WBN]xLHSV is observed, due to a low variation observed on selectivity at different concentrations of carbazole and LHSV of 1.8 h^{-1}.

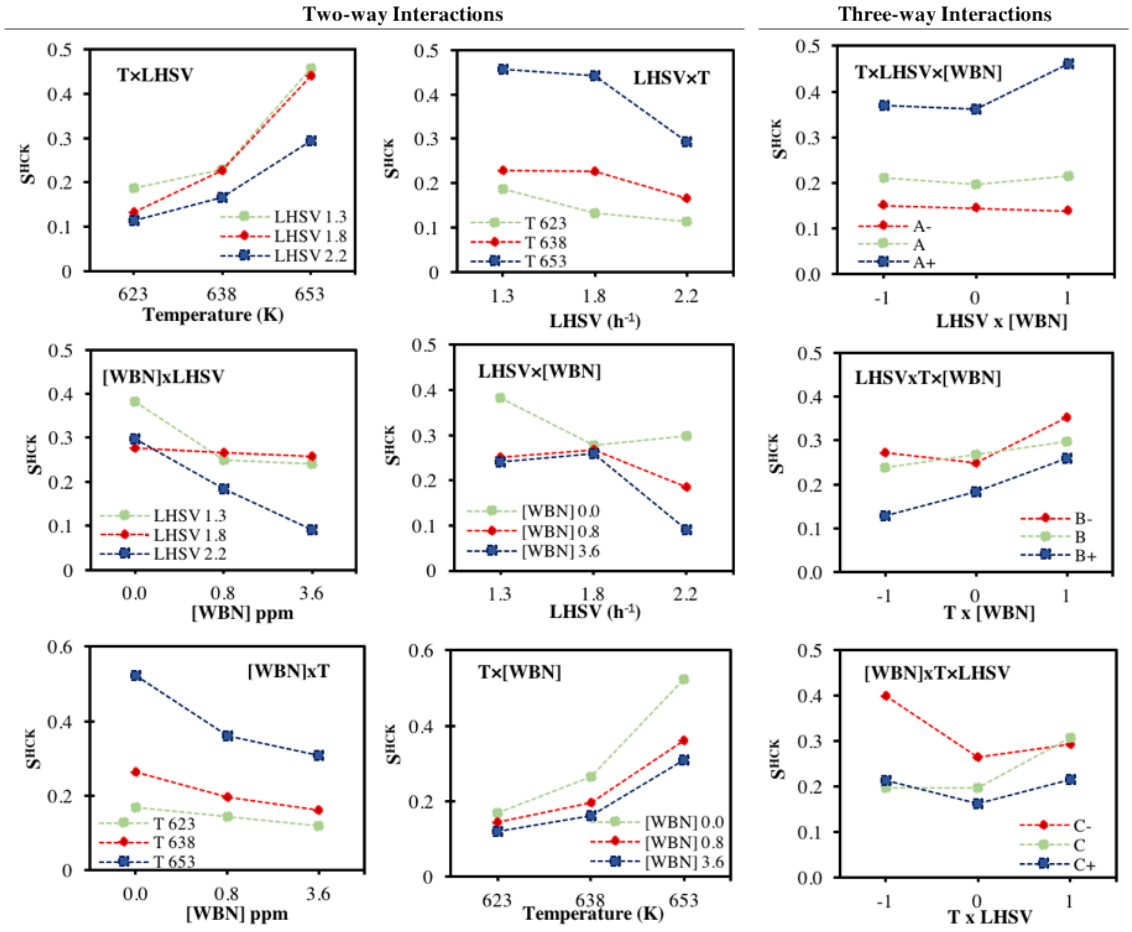

Figure 2.4. Two-way and three-way interactions for selectivity towards the hydrocracking products (S^{HCK}) of temperature (K), LHSV (h^{-1}), and relative concentration of carbazole ([WBN] in ppm). Reactions were carried out at 6.9 MPa and (500 NL hydrogen)/(l L feed) ratio.

At this point is important to mention that selectivity is dependent on conversion, and this trend is illustrated in Figure 2.5. This suggests an underlying effect of conversion over selectivity. For such reason, two-way interactions observed for selectivity could be explained in terms of the same analysis made on conversion. Thus, the synergetic interaction [WBN]xLHSV evidenced an inhibition of selectivity towards the hydrocracking products at high concentrations of carbazole and LHSV. This inhibitory effect was ascribed to the adsorption of carbazole on the active acid sites of the catalyst, which is promoted by the increase in the space velocity [37]. The three-way

interaction observed, results from a collinearity of the main, first-order and second-order contributions. However, based on the principles of sparsity and hierarchy, this high order contribution may not significantly dominate the system [28].

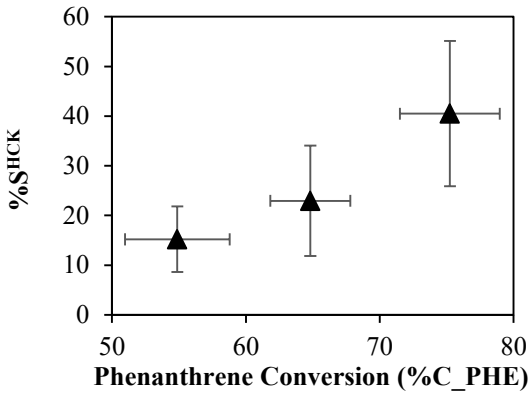

Figure 2.5. Selectivity towards the hydrocracking products in % (%S^{HCK}) vs phenanthrene conversion in % (%C_PHE) for the set of reactions in presence of carbazole, carried out at 6.9 MPa and (500 NL hydrogen)/(l L feed) ratio.

Results from the ANOVA confirm the statistical significance of the main effects temperature, LHSV and relative concentration of carbazole on selectivity (*p-value* = 1.20×10^{-8} for temperature, 4.24×10^{-4} for carbazole concentration and 5.46×10^{-4} for LHSV, with 2 and 16 degrees of freedom in all cases, $F_{2,16}$). Raising the temperature favors the kinetics, thus increasing the formation of partially hydrogenated products, which favors the subsequent transformation to hydrocracking products. On the other hand, an increase in the LHSV directly affects the hydrocracking of phenanthrene because if the contact time decreases, this implies that the partially hydrogenated molecules do not sufficiently interact with the acid sites of the catalyst. Additionally, an increase in the concentration of carbazole causes a negative effect on the selectivity towards the hydrocracking products. In general, the degree of basicity of the nitrogen compounds could be correlated with the inhibition of the catalyst [4, 18]. While pyridine behaves as a base which can

get easily protonated on Brønsted acid sites of the catalyst, as a consequence of the ion-pair donor [39], the pyrrolic-like compounds such as indole and carbazole have a weak basic character [40]. Nevertheless, the inhibitory effect observed in selectivity towards the hydrocracking products could be explained in terms of a blockage of the Brønsted acid sites of high acidity, promoted by the carbazole molecules present in the liquid moiety. A DFT theoretical work [41], evidenced the protonation of carbazole when interacts with a Brønsted acid site. The formation of N-protonated species in indole like compounds has been observed with IR in salts of these compounds by locating the ammonium band in the spectra [42]. In addition, Laredo *et al.* [43], observed a strong adsorption of these weakly basic nitrogen-containing compounds present in a heavy oil fraction over the acid sites of a material, used in order to separate the basic nitrogenates from the sample. Thereafter, in a further study regarding the inhibition over the hydrodesulfurization reaction of dibenzothiophene in presence of nitrogenated compounds, they observed inhibition exerted by these weakly basic compounds was attributed to the observed affinity of these molecules with the acid sites [44, 45]. All this supports the observed trend of the relative concentration of carbazole on selectivity.

In contrast to what was observed in the two-way interactions plots, the combined effects of temperature with relative concentration of carbazole, and temperature with LHSV affected the hydrocracking selectivity (*p-value* = 3.54×10^{-3} and *p-value* = 3.15×10^{-3}, respectively with $F_{1,16}$). This results from the strong significance observed for temperature in the ANOVA (*p-value* = 1.20×10^{-8}) which consequently exert a direct influence on the significance of its derived two-way interactions. On the one hand, an increase in temperature favors the desorption of carbazole from the acid sites of the catalyst, hence favoring the selectivity towards the hydrocracking, hinted by the [WBN]xT interaction. On the other hand, a significant effect of the two-factor interaction

TxLHSV for selectivity is understandable, since at higher temperatures the effect of the LHSV is less visible because a rise in temperature promotes the cracking reactions on the active acid sites. Being consistent with what is stated in the interaction plots, it could be affirmed that these interactions that the ANOVA test shows as significant, can be removed from the model by making an appropriate transformation of the data. Meanwhile, the interaction of LHSV and relative concentration of carbazole is meaningless (*p-value* = 0.103, $F_{1,16}$). However, the low significance of the two-way interaction of LHSV and relative concentration of carbazole probably is obtained due to the restrictions considered in the ANOVA model. Else, the crossover interaction observed is a consequence of the low variation on selectivity at LHSV of 1.8 h^{-1} with respect to the different levels of carbazole. Thereby, although this interaction was considered to be nonremovable from the model, its trend on selectivity is uninterpretable for the data of LHSV at 1.8 h^{-1}. All this suggest that an underlying effect is hidden in this interaction, which was not visible under the studied levels of carbazole concentration. Finally, a low significance was also obtained for the three-factor interaction (*p-value* = 0.247, $F_{1,16}$). The later result, confirm that the three-way interaction could be neglected. Likewise, the assumptions of normality and independence of the statistical ANOVA model were satisfactorily verified in this case (See Figure B7). The statistical model describing the hydrocracking selectivity is:

$$Y_{ijk} = \mu_0 + (\tau_T)_i + (\tau_{[WBN]})_j + (\tau_{LHSV})_k + (\tau_{T-[WBN]})_{i,j} + (\tau_{T-LHSV})_{i,k} + \varepsilon_{ijk} \qquad (2.4)$$

Where μ_0 = 25,6; $(\tau_T)_i$, $(\tau_{[WBN]})_j$ y $(\tau_{LHSV})_k$ are the individual effects; $(\tau_{T-[WBN]})_{i,j}$ and $(\tau_{T-LHSV})_{i,k}$ are the combined effects, respectively and ε_{ijk} is the experimental error. These results corroborate what is known of the hydrocracking process due to the fact that the cracking is favored at higher temperatures and lower spatial velocity (i.e. longer contact time) but, at the same time,

confirms that carbazole exerts a negative effect on selectivity, despite the fact that it does not affect phenanthrene conversion.

To summarize, even if carbazole does not affect the conversion under the studied conditions, it significantly affects the hydrocracking selectivity. Between carbazole and tetrahydrocarbazole, a previous exploratory study concerning the inhibition of these compounds [17], found that the influence of carbazole over the conversion and selectivity of the same reaction was lower than the observed for the tetrahydrocarbazole, but still significant at 5 ppm of total N content. Temperature was found to be the variable which more affects the conversion and the selectivity towards the hydrocracking. In this way, an increase in temperature besides favoring the kinetics of hydrocracking, it possibly facilitates the desorption of the weakly basic nitrogen molecules from the catalyst acid sites, key pieces to molecular cracking. Regarding the two-way interaction plots which pointed to consider the two-factor interaction of LHSV and relative concentration of carbazole, the ANOVA showed the opposite conclusion. It may imply that under the studied intervals for the relative concentration of carbazole, was not possible to establish a clear relationship between the two-way interaction of LHSVxWBN and their effect on selectivity. In the further part of this chapter, the effect of a mixture of carbazole and tetrahydrocarbazole in 1:1 ratio is discussed based on the same statistical assessment.

2.3.2. Phenanthrene hydrocracking in presence of a mixture of weakly basic nitrogen-containing compounds

2.3.2.1. Effect on conversion. As mentioned in the experimental section, the second set of experiments were performed using a mixture of carbazole and tetrahydrocarbazole in 1:1 ratio. Different amounts of this mixture were added to the feed in order to obtain 1 and 5 ppm of total N

content for completing the levels of the factorial experimental design. A foregoing finding suggested that after hydrotreating the heavy oil fraction to obtain low nitrogen specification aimed for a two-stage hydrocracking configuration, the residual nitrogen content is rich in partially hydrogenated compounds of this type [17]. In addition, apropos of the inhibitory effect measured for the tetrahydrocarbazole, it was slightly higher than that determined for the carbazole solely [17]. Table B3 shows the results of conversion as a function of the temperature, LHSV and relative concentration of weakly basic nitrogen-containing compounds. Additionally, Figure 2.6(a)-(c) present the main effects plots (error bars indicating a t-based confidence interval, $\boldsymbol{t_{0.05/2,8}}$). From this descriptive statistic is clearly visible that all the variables seem to affect the conversion. Comparatively with respect to the reactions in presence of carbazole alone, the [WBN] mixture of 50/50 wt.%/wt% of tetrahydrocarbazole and carbazole apparently exert an evident significant effect over the conversion (Figure 2.6c). It is important to mention that also the high level of the experimental design was increased from 3.6 to 5.0. The same trend as observed for carbazole is obtained for the mixture of nitrogenates regarding the temperature and the LHSV; the higher the temperature and the lower the LHSV, the higher the conversion.

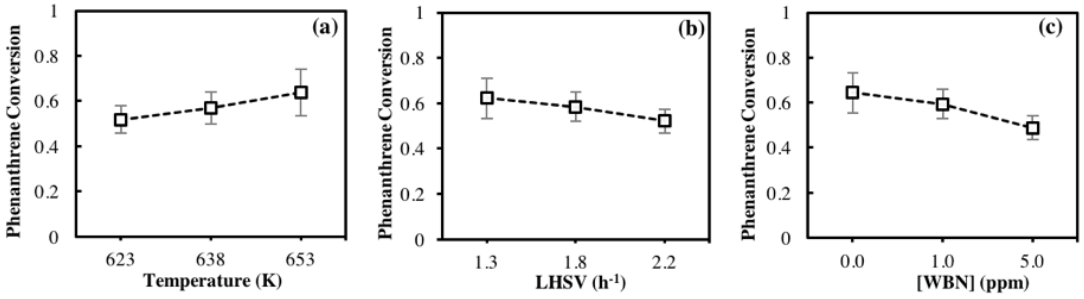

Figure 2.6. Main effects plot for phenanthrene conversion as a function of (a) temperature, (b) LHSV and (b) relative concentration of weakly basic nitrogen-containing compounds ([WBN] in ppm). The WBN consisted of a mixture of carbazole and tetrahydrocarbazole in 1:1 ratio. Reactions were carried out at 6.9 MPa and (500 NL hydrogen)/(l L feed) ratio.

Figure 2.7 shows the two-way and three-way interaction plots for the studied factors on conversion in presence of the mixture of carbazole and tetrahydrocarbazole.

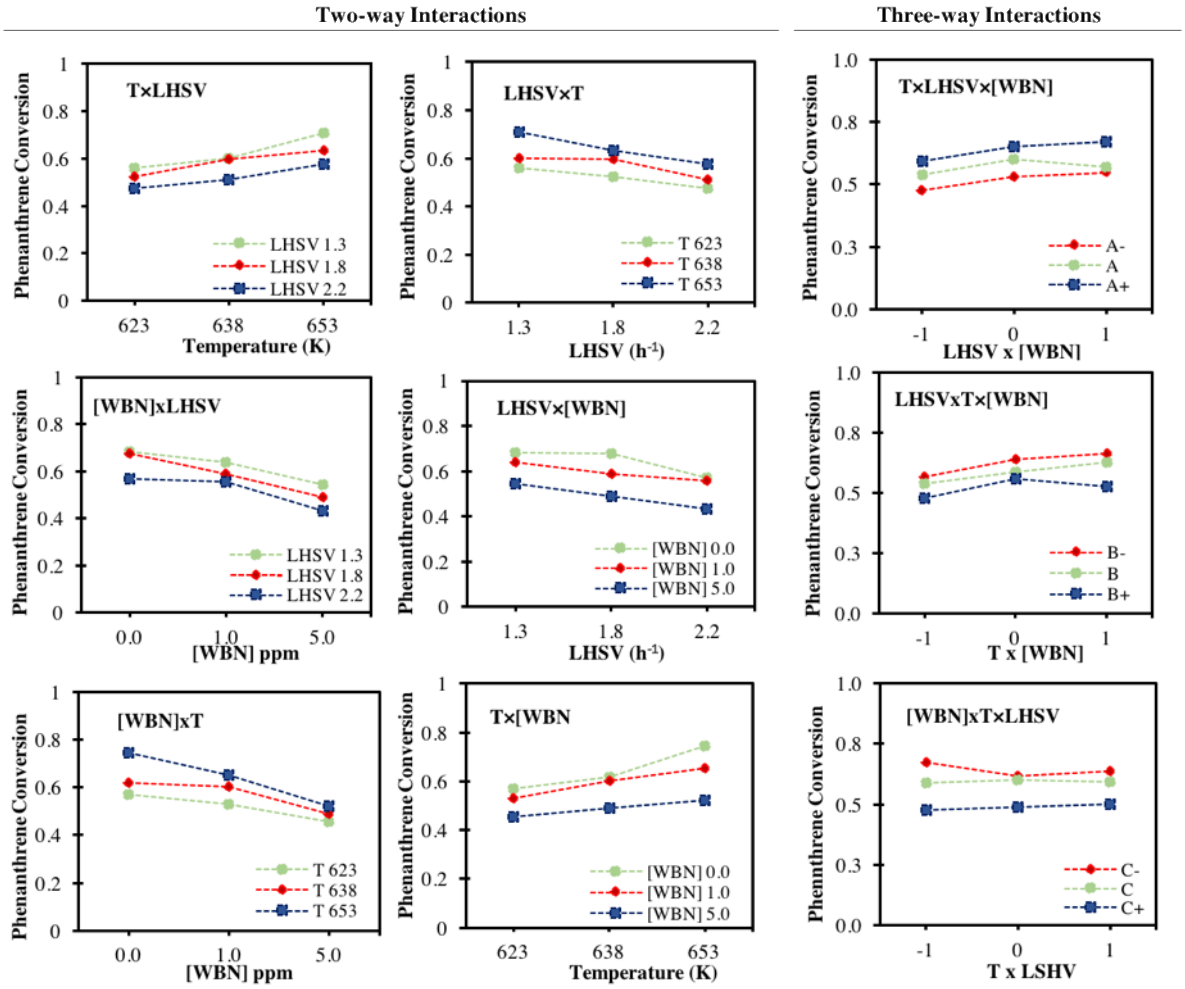

Figure 2.7. Two-way and three-way interactions for phenanthrene conversion of temperature (K), LHSV (h^{-1}), and relative concentration of weakly basic nitrogen-containing compounds ([WBN] in ppm). The WBN consisted of a mixture of carbazole and tetrahydrocarbazole in 1:1 ratio. Reactions were carried out at 6.9 MPa and (500 NL hydrogen)/(l L feed) ratio.

Only some border line interactions were observed in TxLHSV and [WBN]xLHSV. These synergistic interactions observed are probably a consequence of the collinearity of the two-factors interactions with respect to the main effects of its parents. However, the two-way interaction of [WBN]xLHSV once more suggests that at high values of space velocity, the mass transfer of

nitrogenated molecules into the catalytic surface is promoted [37], hence increasing the blockage of active sites. Despite, both interactions of TxLHSV and [WBN]xLHSV are considered to be nonremovable interaction effects [33], based on the sparsity principle, the system is mainly dominated by the main effects [28]. Finally, no three-factor interaction was evidenced.

The ANOVA test for the conversion confirmed the aforesaid trend (*p-value*=3.29×10^{-6} for temperature, 2.62×10^{-5} for LHSV, and 9.75×10^{-8} for relative concentration of weakly basic nitrogen-containing compounds, $F_{2,16}$). Notwithstanding, the interaction between temperature and relative concentration of weakly basic nitrogen-containing compounds is significant also (*p-value*=4.36×10^{-3}, $F_{1,16}$). In this case, from a statistical point of view, the strong significance of the relative concentration of nitrogen-containing compounds on the ANOVA model influences a trend on its derived nonlinear terms of first order, in line with the heredity principle. Furthermore, the absence of parallelism observed in the [WBN]xT plot and its reciprocal, suggests the presence of an interaction. By considering the synergistic effect observed in both interaction plots, the physical interpretation of this interaction relies on the effect of temperature on the adsorption/desorption process of nitrogen-containing compounds on the active sites of the catalyst, which has a direct implication on conversion. In addition, no interaction between the temperature and the LHSV is observed (*p-value*=0.288, $F_{1,16}$), supported by the parallelism which is visible in both interaction plots, of TxLHSV and its reciprocal interaction. These results confirm the absence of external diffusional limitations in the experiments [34]. The tests for validation of the model assumptions are available in Figure B8. With this, the model which describes the conversion in presence of small amounts of weakly basic nitrogen-containing compounds (carbazole and tetrahydrocarbazole mixture) is:

$$Y_{ijk} = \mu_0 + (\tau_T)_i + (\tau_{[WBN]})_j + (\tau_{LHSV})_k + (\tau_{T-[WBN]})_{i,j} + \varepsilon_{ijk} \quad (2.5)$$

Where μ_0 = 57.6; $(\tau_T)_i$, $(\tau_{[WBN]})_j$ y $(\tau_{LHSV})_k$ are the individual effects; $(\tau_{T-[WBN]})_{i,j}$ is the combined effect of temperature and weakly basic nitrogen-containing compounds relative concentration, and ε_{ijk} is the experimental error.

The main effect of the concentration of weakly basic nitrogen-containing compounds on conversion was statistically significant in these experiments for two main reasons: (i) as shown in chapter 1 [17], the presence of tetrahydrocarbazole makes more visible the inhibitory effect exerted by the relative concentration of the mixture of weakly basic nitrogen-containing compounds; and (ii) because the levels of the concentration of weakly basic nitrogen-containing compounds were increased from 0, 0.8 and 3.6 to 0, 1.0 and 5.0 ppm of total N. Results here exposed support the fact that carbazole and tetrahydrocarbazole are adsorbing on the acid sites of the catalyst blocking them and in consequence, causing inhibition of the cracking reactions of partially hydrogenated polyaromatic hydrocarbons. Considering that the hydrogenation reactions of phenanthrene in steady state are close to the equilibrium at these conditions [20, 32], but the further transformation of the hydrogenated products in the acid sites is lowered, the conversion is adversely affected. Effects on selectivity are shown next.

2.3.2.2. Effect on selectivity. The data of selectivity towards the hydrocracking products is available in Table B4, as well as the main effects plots for each factor considered in the experiment (Figure 2.8a-c, with a t-based confidence interval, $\boldsymbol{t_{0.05/2,8}}$). In this case, the evident effects are seen for temperature and concentration of weakly basic nitrogen-containing compounds. When increasing temperature, selectivity towards the hydrocracking products is favored; whilst, for relative concentration of weakly basic nitrogen-containing compounds, at higher values,

selectivity is negatively affected. However, the effect of LHSV on selectivity apparently is negligible (Figure 2.8b), as no trend is observed in the main effect plot. This is contrary to what was observed in the reaction with carbazole only. Seems reasonable that LHSV does not exert a significant effect on the selectivity in so far as the other variables exerted a considerably higher effect.

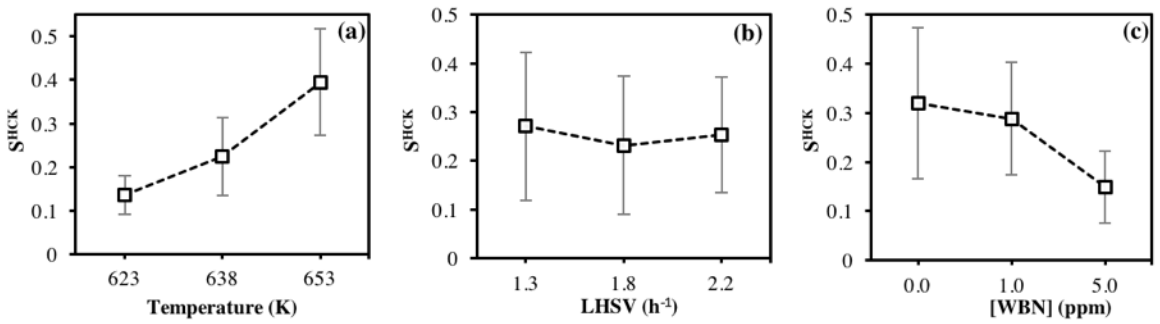

Figure 2.8. Main effects plot for selectivity towards the hydrocracking products (%S^{HCK}), as a function of (a) temperature, (b) LHSV and (b) relative concentration of weakly basic nitrogen-containing compounds ([WBN]). The [WBN] consisted on a mixture of carbazole and tetrahydrocarbazole in 1:1 ratio. Reactions were carried out at 6.9 MPa and (500 NL hydrogen)/(l L feed) ratio.

Figure 2.9 shows the two-way and three-way interaction plots of temperature, LHSV, and relative concentration of weakly basic nitrogen-containing compounds, on selectivity towards the hydrocracking products. Crossover interactions are observed for TxLHSV, [WBN]xLHSV and its reciprocal, and Tx[WBN]. Again, this results confirm that the inhibitory effect exerted by the mixture of nitrogenates on selectivity is sensitive to the operational variables, T and LHSV. The crossover interaction of TxLHSV indicates that at high temperatures the effect of LHSV on selectivity is less marked. On the other hand, the nonremovable effect of the two-way interaction of [WBN]xLHSV exhibits a synergistic effect. From the reciprocal plot LHSVx[WBN], an interpretation of this relationship is understandable for a high value of the concentration of

nitrogenates (5.0 ppm), in which the effect of LHSV on the selectivity is less appreciable. In absence of nitrogenates, the lower the LHSV the higher the contact time which assists the selectivity towards the hydrocracking.

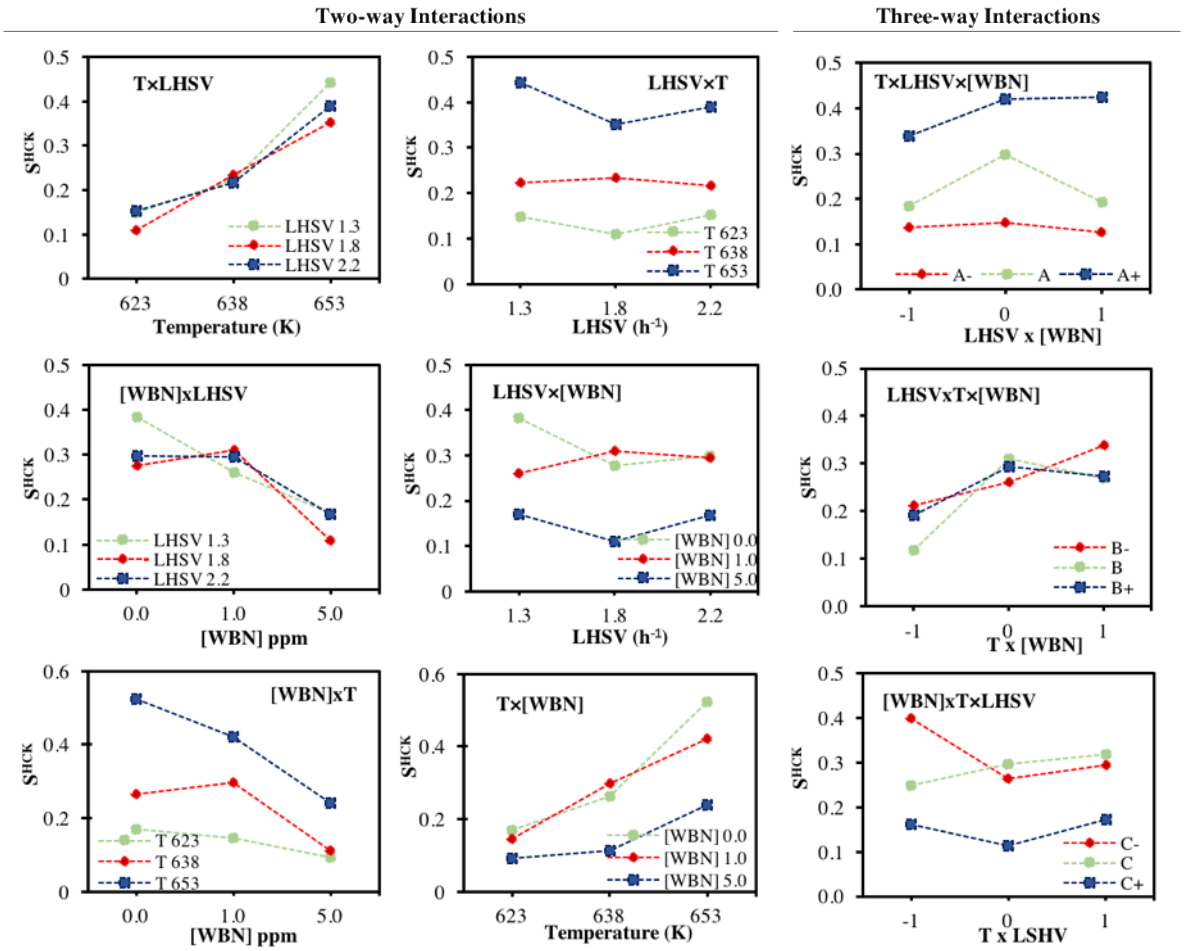

Figure 2.9. Two-way and three-way interactions for selectivity towards the hydrocracking products (%S^{HCK}) of temperature (K), LHSV (h^{-1}), and relative concentration of weakly basic nitrogen-containing compounds ([WBN] in ppm). The WBN consisted of a mixture of carbazole and tetrahydrocarbasole in 1:1 ratio. Reactions were carried out at 6.9 MPa and (500 NL hydrogen)/(l L feed) ratio.

As commented before, the selectivity is dependent on the conversion, this trend is visible in Figure 2.10. The lower the conversion, the lower the selectivity towards the hydrocracking products. This trend hints the existence of a hidden effect caused by the variables, temperature, LHSV and relative concentration of weakly basic nitrogen-containing compounds. So the observed

two-way interactions for selectivity are directly linked with conversion. In the [WBN]xLHSV plot, in presence of weakly basic nitrogen-containing compounds, from 1.0 to 5.0 ppm of total N, the slope of the lines is marked at higher LHSV values (1.8 and 2.2 h^{-1}). This confirms that an increase in space velocity in presence of nitrogenates adversely affect the selectivity towards hydrocracking due to the promotion of the adsorption of nitrogenates on the active acid sites of the catalyst. Additionally, due to the collinearity of the main, first and second-order effects, a three-way cross interaction is also observed. Notwithstanding, due to the principle of sparsity and hierarchy, the effect of this high order interaction is expected to be negligible [28]. In this sense, is expected that a rise in temperature and a reduction in LHSV in presence of weakly basic nitrogen-containing compounds influence a lower inhibitory effect of these compounds on the selectivity which will be visible in an improvement in the conversion.

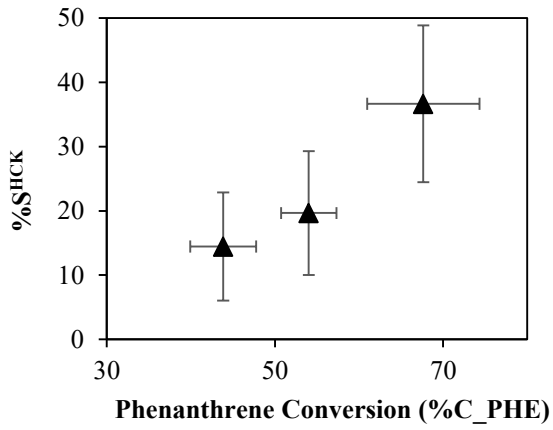

Figure 2.10. Selectivity towards the hydrocracking products in % (%S^{HCK}) vs phenanthrene conversion in % (%C_PHE) for the set of reactions in presence of the mixture of weakly basic nitrogen-containing compounds. The WBN consisted of a mixture of carbazole and tetrahydrocarbasole in 1:1 ratio. carried out at 6.9 MPa and (500 NL hydrogen)/(l L feed) ratio.

The description of the main effects was confirmed by the ANOVA test (*p-value*=1.21×10^{-7} for temperature, *p-value*=0.35 for LHSV, and *p-value*=1.47×10^{-5} for weakly basic nitrogen-containing compounds relative concentration, $F_{2,16}$). In addition, the interaction between temperature and relative concentration of weakly basic nitrogen-containing compounds was also significant (*p-value*=1.80×10^{-3}, $F_{1,16}$), it explains the fact that raising the temperature, desorption of weakly basic compounds from the acid sites of the catalyst is promoted.

The model obtained from the ANOVA test for the selectivity towards the hydrocracking products in presence of the mixture of weakly basic nitrogen-containing compounds is presented in equation 2.6. As for all, the model assumptions were validated (Figure B9).

$$Y_{ijk} = \mu_0 + (\tau_T)_i + (\tau_{[WBN]})_j + (\tau_{T-[WBN]})_{i,j} + \varepsilon_{ijk} \qquad (2.6)$$

Where μ_0 = 25.2; $(\tau_T)_i$, $(\tau_{[WBN]})_j$ y $(\tau_{LHSV})_k$ are the individual effects; $(\tau_{T-[WBN]})_{i,j}$ is the combined effect of temperature and weakly basic nitrogen-containing compounds relative concentration, and ε_{ijk} is the experimental error.

Apparently, the mixture of carbazole and tetrahydrocarbazole exert a clearer inhibitory effect over the hydrocracking reaction in general. This finding is in accordance with the observation made in chapter 1, which suggested that tetrahydrocarbazole may inhibit more the activity and selectivity of the phenanthrene hydrocracking reaction [17]. The importance of this lies in the fact that after hydrotreating the heavy oil fraction for accomplishing the low nitrogen specifications needed for the two-stage hydrocracking reactor, the amount of partially hydrogenated weakly basic nitrogen-containing compounds of this type significantly increase [12, 17]. In consideration of this finding, then is expected some inhibition of this compounds even in small amounts, as claimed in an earlier report by Kobayashi *et al*. [19]. In the next section, a brief discussion about the effects

of the mixture of carbazole and tetrahydrocarbazole on the hydrocracking routes of the phenanthrene reaction are analyzed, in order to better understand the interactions of these inhibitors with the Brønsted acid sites of the catalyst.

2.3.3. Effect of the weakly basic nitrogen-containing compounds over the hydrocracking routes. As explained in Scheme 2.1, phenanthrene after hydrogenated could follow three routes when it further reacts on acid sites. One derived from the ring opening and dealkylation of external hydrogenated rings, whose selectivity is denoted as SEXT. A second route when the partially hydrogenated internal ring of dihydrophenanthrene is opened to form alkyl biphenyls; the term SINT is used to describe this selectivity. And a route derived from the asym-octahydrophenanthrene which has suffered a simultaneous hydrogenation of an internal and external ring, SMIX is employed for describing this selectivity. Based on this description, three selectivities are defined for the cracking products derived from each route, being in order:

$$S^{EXT} = \frac{n_{IN} + n_{MIN} + n_{TL} + n_{NP} + n_{MTL} + n_{MNP} + n_{BTL}}{\sum_i n_i} \quad (2.7)$$

$$S^{INT} = \frac{n_{BP} + n_{CHB} + n_{EBP} + n_{DMBP}}{\sum_i n_i} \quad (2.8)$$

$$S^{MIX} = \frac{n_{i-BTL}}{\sum_i n_i} \quad (2.9)$$

Where, IN = indane, MIN = methylindane, TL = tetralin (tetrahydronaphthalene), NP = naphthalene, MTL = methyltetralin, MNP = methylnaphthalene, BTL = 6-butyltetralin, BP = biphenyl, CHB = dyclohexylbenzene EBP = 2-ethylbiphenyl, DMBP = dymethylbiphenyl, i-BTL = 2-butyl tetralin, and $\sum_i n_i$ is the sum of the listed products.

Particularly, the selectivities S^{MIX} and S^{EXT}, are an indirect measure of the selectivity towards butane production, considering that the ring opening and dealkylation of the internal ring of dihydrophenanthrene mainly produces ethane and methane (See Scheme 2.1). This is important from an economic point of view, since the products derived from the cracking of external rings are easier to hydrogenate [46, 47], thus increasing the cetane number; and also, because butane is one of the main constituents of the LPG [48].

The analysis of the aforementioned hydrocracking routes is developed for the set of experiments in presence of the mixture of carbazole and tetrahydrocarbazole instead of carbazole only. The above, in consideration of the results from the statistical assessment for determining the inhibitory effect of carbazole and the mixture of weakly basic nitrogen-containing compounds, which conclusively found that in the experiments with the mixture of carbazole and tetrahydrocarbazole in a 1:1 ratio, the effect on the catalyst performance was clearer. Also taking into account that the mixture employed fairly represents the remaining nitrogen in hydrotreated heavy oil fractions aimed for a two-stage hydrocracking reactor. A detailed description regarding the effect of different mixtures of carbazole and tetrahydrocarbazole at similar nitrogen content is treated in chapter 1 [17].

Table B5 summarizes the results for each selectivity to the different routes as postulated in Scheme 2.1, for the three factors of the experimental design, i.e. temperature, LHSV and relative concentration of weakly basic nitrogen-containing compounds. Henceforth, each factor is individually analyzed. The plots of main effects for selectivities vs temperature are shown in Figures 2.11(a)-(c). All the main effects plots are presented with t-based confidence intervals ($t_{0.05/2,8}$).

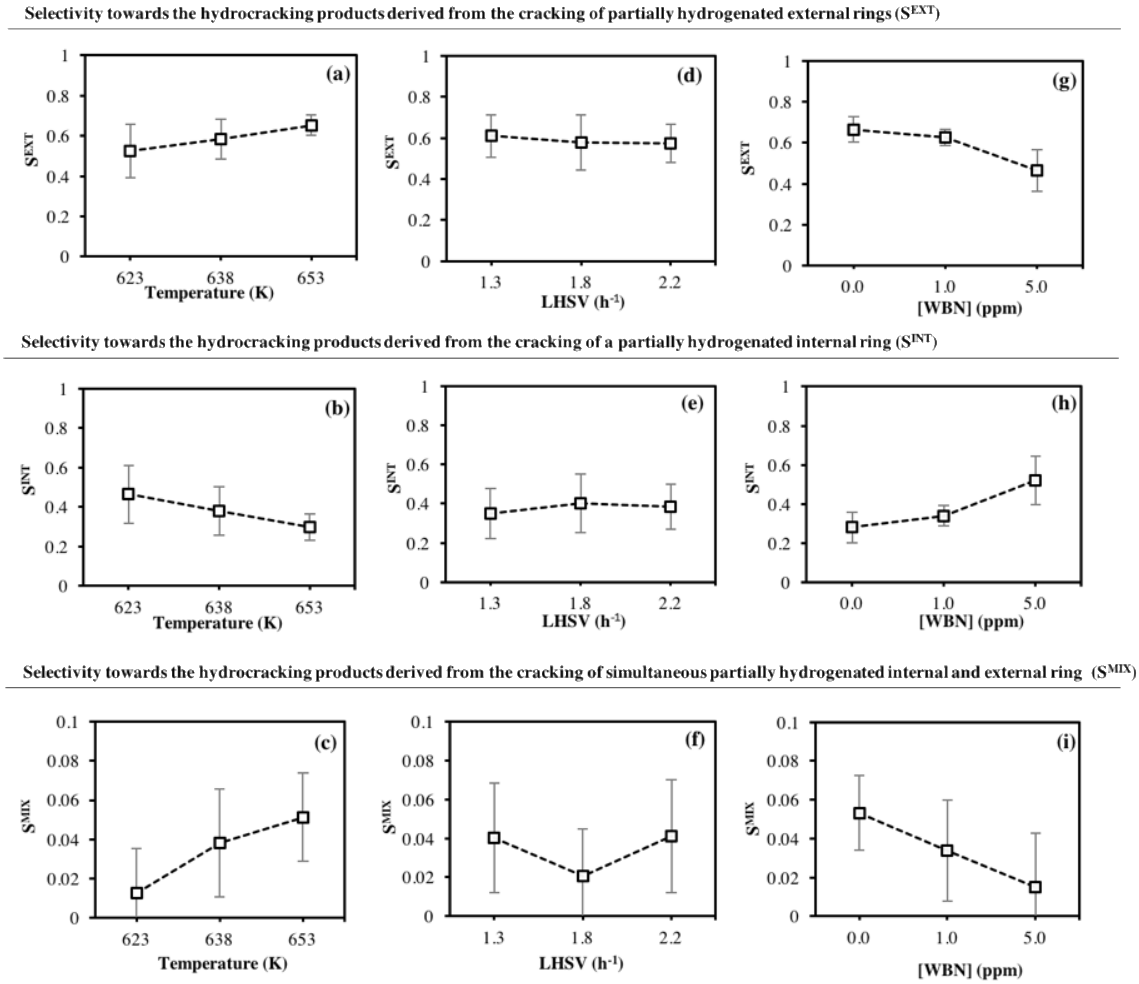

Figure 2.11. Main effects plot for selectivity towards the hydrocracking routes derived from hydrogenated external rings, S^{EXT}, internal ring, S^{INT}, and simultaneous external and internal hydrogenated rings, S^{MIX}, as a function of (a-c) temperature, (d-f) LHSV, and (g-i) relative concentration of weakly basic nitrogen-containing compounds ([WBN] in ppm). Reactions were carried out at 6.9 MPa and (500 NL hydrogen)/(l L feed) ratio

Analyzing the selectivity towards the products derived from the cracking of hydrogenated external rings, S^{EXT}, is clearly appreciable that an increase in temperature favors this route (Figure 2.11a). The same trend was observed for the cracking reaction of the products derived from the asym-octahydrophenanthrene, S^{MIX} (Figure 2.11c). Nonetheless, the opposite trend was described for the selectivity towards the products derived from the cracking of a partially hydrogenated internal ring, S^{INT} (Figure 2.11b). Thereby, temperature activates the catalytic cracking on

Brønsted sites, thus favoring the ring opening and dealkylation of partially hydrogenated external rings. Leite *et al.* [49], in a study of phenanthrene hydrocracking over Pt bifunctional catalyst, observed that selectivity to the cracking of the isomerization products was highly influenced by temperature, being greater at higher temperatures. On the other hand, the cracking reaction of the internal ring could proceed through acid cracking and hydrogenolysis of the C-C bond [20]. Also, the hydrogenolysis route is suggested to proceed preferentially on highly dehydrogenated species, attributed to badly sulfide Ni and Mo [20]. The cracking reaction of a partially hydrogenated internal ring, as it does not depend on an intermediate isomerization step, is less affected by temperature as compared to the cracking of partially hydrogenated external rings. In the descriptive statistic of LHSV no trend is appreciable, for any of the studied routes (Figures 2.11d-f), and this is further confirmed by the ANOVA test, LHSV does not exert a significant effect on the selectivities. This is congruent with what was observed for the overall hydrocracking selectivity (in section 2.3.2.2). Figures 2.11(g)-(i) depicts the effect of relative concentration of weakly basic nitrogen-containing compounds among the studied routes. Products derived from the cracking of partially hydrogenated external rings, S^{EXT} (Figure 2.11g), which includes that derived from the cracking of the asym-octahydrophenanthrene external ring, S^{MIX} (Figure 2.11i), are apparently more affected with the increase in the relative concentration of weakly basic nitrogen-containing compounds than those products derived from the partially hydrogenated internal ring cracking, S^{INT} (Figure 2.11h). As previously discussed, an increase in the [WBN] causes a significant reduction of the overall selectivity to hydrocracking products, and this is clearly noticeable in the carbon mass balance reported in Table 1 when comparing 0 and 5 ppm of [WBN]. Many of the hydrocracking products detected in absence of weakly basic nitrogen-containing compounds disappeared at 5 ppm of [WBN], and this is comparatively reflected in the amount of non-assigned

by GC-MS products in the hydrocracking region. However, the proportion of products derived from the cracking of partially hydrogenated internal ring, S^{INT}, increased when increasing the relative concentration of weakly basic nitrogen-containing compounds. This may indicate that carbazole and tetrahydrocarbazole are selectively inhibiting a certain type of acid sites. In an exploratory theoretical work [41], in which a Brønsted acid site of a mordenite was modeled with the DFT, the formation of an ion-pair complex of carbazole and tetrahydrocarbazole on the Brønsted acid site was observed as similarly occur for pyridine. This evidences a trend of these compounds to strongly interact with Brønsted acid sites. On the other hand, Choi et al. [50], aiming to separate the nitrogen compounds from a shale oil by using acid solids, observed that these weakly basic nitrogen-containing compounds have a weak affinity with the Lewis acid sites. All this evidence points to the fact that carbazole and tetrahydrocarbazole preferentially inhibit the Brønsted acid sites of the catalyst.

Observing Figure 2.11 is possible to see that certain interdependence of the routes exists. That is to say, higher temperatures and relative concentration of weakly basic nitrogen-containing compounds cause a decrease in selectivity towards the products derived from the cracking of partially hydrogenated external rings, S^{EXT}, meanwhile, the proportion of products route derived from the cracking of a partially hydrogenated internal ring, S^{INT}, is favored. In this sense, this interdependence of the defined selectivities influences in the interaction effects observed for the two-factor and three-factor interactions. In other words, the obtained interaction effects for one route are basically the same for the others. For such reason, Figure 2.12 only depicts the two-way and three-way interaction plots for the route derived from the cracking of partially hydrogenated external rings, S^{EXT}.

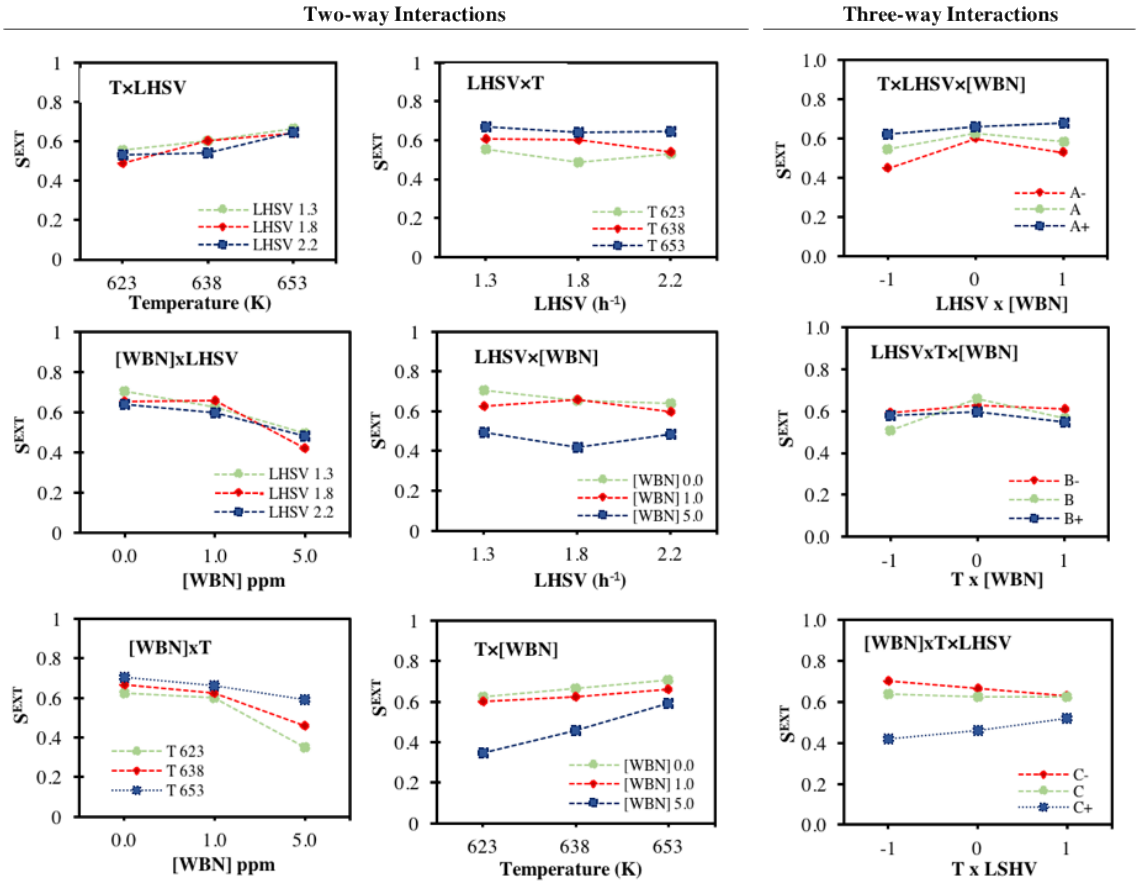

Figure 2.12. Two-way and three-way for selectivity towards the hydrocracking routes derived from hydrogenated external rings, S^{EXT}, of temperature (K), LHSV (h^{-1}), and relative concentration of weakly basic nitrogen-containing compounds ([WBN] in ppm). The WBN consisted of a mixture of carbazole and tetrahydrocarbazole in 1:1 ratio. Reactions were carried out at 6.9 MPa and (500 NL hydrogen)/(l L feed) ratio.

Two-way crossover interactions of TxLHSV and [WBN]xLHSV are observed, as well as three-way crossover and borderline interactions. This describes the same trend as observed for the overall selectivity towards the hydrocracking product, S^{HCK} in Figure 2.9. The implications of these effects will be further discussed once exposed the results from the ANOVA. Once more, the three-way interaction is considered to be less significant applying the principle of hierarchy and sparsity [28].

The ANOVA test for the three selectivities were similar. Temperature and relative concentration of weakly basic nitrogen-containing compounds were the main factors whose effects were significant (*p-value*=3.05×10^{-4} for temperature, *p-value*=7.99×10^{-7} for [WBN], in S^{EXT}; *p-value*=1.32×10^{-4} for temperature, *p-value*=1.12×10^{-6} for [WBN], in S^{INT}; *p-value*=5.23×10^{-3} for temperature, *p-value*=6.65×10^{-3} for [WBN], in S^{MIX}; all of them with degrees of freedom: $F_{2,16}$). These results agree with the discussion made in previous sections, mentioning that for these selectivities the effect of LHSV was not significant. For S^{EXT} and S^{INT} only the interaction between temperature and relative concentration of weakly basic nitrogen-containing compounds was significant (*p-value*=1.28×10^{-3} for S^{EXT}; *p-value*=3.74×10^{-3} for S^{INT}, with $F_{1,16}$). This is in accordance to what was observed for the overall selectivity towards the hydrocracking products, S^{HCK}. However, as shown in the interaction plots, the two-way interactions of TxLHSV and [WBN]xLHSV were found to be nonremovable effects [33]. As it was shown for the overall selectivity towards the hydrocracking products, S^{HCK}, the TxLHSV and [WBN]xLHSV interactions induce a slight effect on the selectivity to products derived from the cracking of partially hydrogenated external rings, S^{EXT}. Specifically, at high values of LHSV, an increase in temperature causes a slightly smaller positive effect on selectivity (S^{EXT}) than observed at low values of space velocity. For the other effect, high values of LHSV slightly promotes the inhibition on selectivity (S^{EXT}) by weakly basic nitrogen-containing compounds, explained in terms of an increase in the mass transfer of the nitrogenated molecules towards the catalytic surface. Finally, a weak significance of the triple interaction of temperature, LHSV, and [WBN] was observed for S^{MIX} (*p-value*=0.018, $F_{1,16}$), conversely, as this p-value is very close to the alpha level, is not clear the effect of this interaction over the predicted model. The tests for validating the assumptions of

normality and independence for the model are available in Figure B10-B12 in Annex B. The predicted models for the selectivities are shown in equations 2.10-2.12.

$$S^{EXT}:\ Y_{ijk} = \mu_0^{\mathrm{EXT}} + (\tau_T)_i + (\tau_{[WBN]})_j + (\tau_{T-[WBN]})_{i,j} + \varepsilon_{ijk} \quad (2.10)$$

$$S^{INT}:\ Y_{ijk} = \mu_0^{\mathrm{INT}} + (\tau_T)_i + (\tau_{[WBN]})_j + (\tau_{T-[WBN]})_{i,j} + \varepsilon_{ijk} \quad (2.11)$$

$$S^{MIX}:\ Y_{ijk} = \mu_0^{\mathrm{MIX}} + (\tau_T)_i + (\tau_{[WBN]})_j + (\tau_{T-LHSV-[WBN]})_{i,j,k} + \varepsilon_{ijk} \quad (2.12)$$

Where μ_0^{EXT} = 58.6; μ_0^{INT} = 38.0; μ_0^{MIX} = 3.4; $(\tau_T)_i$, $(\tau_{[WBN]})_j$ y $(\tau_{LHSV})_k$ are the individual effects; $(\tau_{T-[WBN]})_{i,j}$ is the combined effect of temperature and weakly basic nitrogen-containing compounds relative concentration, $(\tau_{T-LHSV-[WBN]})_{i,j,k}$ is the combined effect of the triple interaction, and ε_{ijk} is the experimental error. The analysis of the models herein exposed leads to the following conclusions: (i) Increasing the temperature favors the cracking of partially hydrogenated external rings, which is desired among the cracking of the internal ring. (ii) The presence of carbazole and tetrahydrocarbazole in a 1:1 ratio at small amounts of total nitrogen content (from 0 to 5.0 ppm) caused a marked inhibition of the hydrocracking route derived from the external ring opening. (iii) Desorption of carbazole and tetrahydrocarbazole from the Brønsted acid sites is promoted by increasing the temperature, thus favoring the hydrocracking of partially hydrogenated external rings. (iv) Despite the ANOVA model does not predict first-order interactions of the factors TxLHSV and [WBN]xLHSV clearly observed in the interaction plots, these are considered to be nonremovable effects. Thus, although the main effect of LHSV is negligible, the crossover effects with temperature and relative concentration of weakly basic nitrogen-containing compounds suggest that LHSV has a significant influence over the observed effect of T and [WBN] on the selectivities. Sau *et al.* [18], reported that the organic nitrogen within the heavy oil fraction exerted a higher inhibition than the nitrogen-free heavy oil fraction doped

with pyridine at the same amount of total nitrogen. Notwithstanding, they attributed this behavior to the complexity of the nitrogenated hetero compounds which probably make them more basic than the pyridine itself. It is worth asking if this higher inhibition observed by the nitrogenated hetero compounds within the heavy oil fractions as compared to that caused by basic nitrogenated species, could be attributed also to the presence of weakly basic nitrogen-containing compounds. If so, would be this effect measurable even under a severe basic atmosphere? The last section of this article attempts to shed a light on these affairs.

2.3.4. Effect of weakly basic nitrogen-containing compounds under a severe basic atmosphere. In view hereof, an exploratory study for catching a sight of a possible significant contribution to the inhibition caused by nitrogenates, of weakly basic compounds over the Ni-MoS2/Y-zeolite␣alumina catalyst under a severe basic atmosphere, is further developed below. A severe ammonia atmosphere was created by adding 1 wt.% aniline into the feed. Reactions were carried out at 653 and 673 K, with 0 and 20 ppm of the relative concentration of the weakly basic nitrogen-containing compounds (carbazole and tetrahydrocarbazole mixture at 1:1 ratio), a pressure of 6.9 MPa and (500 NL hydrogen)/(l L feed) ratio.

Table 2.2 displays the results of the experiments in terms of phenanthrene conversion, selectivity towards the hydrocracking products, S^{HCK}, and selectivity to the route derived from the cracking of partially hydrogenated external rings, S^{EXT}. Averages and standard deviations were calculated taking two steady state points of the Time on Stream curves. At the conditions employed, not all the aniline was transformed into ammonia, hence, the ammonia partial pressure is also reported for each experiment, calculated with the remaining aniline detected in the liquid

products. In this regard, an increase in temperature causes a greater decomposition of aniline, generating a higher ammonia partial pressure.

Table 2.2.

Phenanthrene conversion (%C_PHE), selectivity to hydrocracking products (%S^{HCK}), selectivity of products derived from the cracking of partially hydrogenated external rings (%S^{EXT}), and NH_3 partial pressure, for experiments in NH_3 atmosphere carried out at LHSV = 1.3 h^{-1}, 6.9 MPa and (500 NL hydrogen)/(l L feed) ratio. Averages and standard deviations were computed taking the data from the steady state points.

		[WBN] (ppm)	
Variable	**T (K)**	**0**	**20**
%C_PHE	653	51.0 ± 0.3	48.1 ± 1.0
	673	47.4 ± 0.3	53.3 ± 0.2
%S^{HCK}	653	8.1 ± 0.1	6.9 ± 0.3
	673	11.7 ± 0.5	8.6 ± 0.1
%S^{EXT}	653	47 ± 1.0	44 ± 2.0
	673	58 ± 1.0	47 ± 1.0
NH_3 partial pressure (kPa)	653	41.4 ± 0.3	35.1 ± 0.5
	673	45.6 ± 0.2	45.3 ± 0.2

In general, an increase in temperature (20 K) apparently does not affect the conversion, in the absence or not of weakly basic nitrogen-containing compounds. This could be due to the increase in the ammonia partial pressure which accompanied the rise in temperature. Dufresne *et al.* [16], in the hydrocracking reaction of n-heptane over a commercial NiMo-S_2/USY catalyst, determined that the activity reached a pseudo-plateau over an ammonia partial pressure of 10 kPa at 390 K. Ammonia partial pressure herein is about 3 times that value, being reasonable that an increase in temperature does not level off the conversion. Moreover, the adsorption constant of ammonia over the hydrogenation sites was estimated to be one order of magnitude higher than that for the polynuclear aromatic hydrocarbons [21], thus inhibiting also the hydrogenation functionalities of the catalyst. Notwithstanding, in absence of weakly basic nitrogen-containing compounds, the increase in temperature rather affects the overall hydrocracking selectivity (S^{HCK}) and the selectivity towards the hydrocracking products derived from the external ring opening (S^{EXT}).

Specifically, the number of products derived from the isomerization of an external ring considerably increased (from 15 wt.% of isomerization compounds in hydrocracking products at 653 K, to 45% of isomerization compounds in hydrocracking products at 673 K). This suggests that an increase in temperature promotes the ammonia desorption from some Brønsted acid sites. When adding weakly basic nitrogen-containing compounds to the feed, the overall hydrocracking selectivity (S^{HCK}), as well as the selectivity towards the hydrocracking products derived from the external ring opening (S^{EXT}) exhibited lower values. The interesting fact is that no isomerization products were detected at 653 K and only a 6% of isomerization compounds in hydrocracking products were observed at 673 K. This may suggest that the inhibition caused by introducing 20 ppm of the carbazole and tetrahydrocarbazole mixture over the Brønsted acid sites is higher than the observed in absence of weakly basic nitrogen-containing compounds. This result agrees with the observation made by Sau *et al.* [18], that the organic nitrogen within the heavy oil fractions inhibited more the acid functionalities of the catalyst than the pyridine itself. However, this effect may not be explained in terms of a higher basicity of those compounds, but probably due to the presence of weakly basic nitrogen-containing compounds which could cause an additional effect, as observed herein. These results draw the attention to consider the effect of weakly basic nitrogen-containing compounds even in presence of basic compounds, such as pyridine or quinoline, over the catalytic performance of acid materials.

2.4. Conclusions

The statistical assessment allowed to evidence the significant effects on conversion and selectivity of small amounts of weakly basic nitrogen-containing compounds in the phenanthrene hydrocracking over a Ni-MoS_2/Y-zeolite␣alumina catalyst. The relative concentration of carbazole

did not significantly affect the conversion under the studied conditions. However, despite the main effect of carbazole concentration was meaningless, the combined effects with temperature and LHSV were significant on conversion, as shown by crossover interactions in the plots of two-factors. Moreover, the presence of carbazole caused a significant effect on the overall hydrocracking selectivity. The mixture of carbazole and tetrahydrocarbazole in 1:1 ratio inhibited more the selectivity towards the hydrocracking products than the carbazole solely, even the activity was significantly affected. Additionally, was suggested that carbazole and tetrahydrocarbazole preferentially inhibit the Brønsted acid sites of the catalyst. The aforesaid affinity of these weakly basic compounds with the Brønsted acid sites affects the cracking route which follows the ring opening and dealkylation of partially hydrogenated external rings. In general, the ANOVA tests confirmed that temperature and relative concentration of weakly basic nitrogen-containing compounds were the main factors which predominantly influences the overall hydrocracking selectivity. Even, the ANOVA predictions of the interaction between temperature and relative concentration of weakly basic nitrogen-containing compounds was significative enough, allowing to discern that an increase in temperature is also promoting the desorption of weakly basic nitrogen-containing compounds from the acid sites. In all cases, some two-way interactions that were predicted to be negligible with the ANOVA test, in the interaction plots described crossover and borderline interactions. In this way, while the main effect of LHSV on selectivity towards the hydrocracking products which was meaningless, its interaction with T and concentration of weakly basics exhibited a nonremovable effect. The possibility that the weakly basic nitrogen-containing compounds could exert a significant effect even in presence of basic nitrogenated molecules was explored herein. Conclusively, the addition of weakly basic nitrogenates caused a higher inhibition of the Brønsted acid sites, in a way that isomerization reactions were considerably inhibited under

the studied conditions. Results from this work call the attention to consider new aspects in the developing of new materials aimed for hydrocracking.

References

[1] Speight, J.G. Chapter 5 - Hydrocracking, in: *Heavy and Extra-heavy Oil Upgrading Technologies*, Gulf Professional Publishing, Boston, **2013**, pp. 95-128.

[2] Hsu, CS. Hydrotreating and hydrocracking: Fundamentals, in: *Practical advances in petroleum processing*, Springer, **2006**, pp. 866.

[3] Motaghi, M.; Ulrich, B.; Subramanian, A. Slurry-phase hydrocracking—possible solution to refining margins. *Hydrocarbon Process* **2011,** 90, 37-43.

[4] Furimsky, E.; Massoth, F.E. Deactivation of hydroprocessing catalysts, *Catal. Today*, 1999, 52, 381-495.

[5] Barbosa, F.A.; Santos, A.C.B.d.; Silva, M.I.P.d.; Stumbo, A.M. Resistance to poisoning by nitrogen compounds of NiMo/Al-MCM-41 hydrocracking catalysts, *Catal. Today*, **2004,** 98, 109-113.

[6] Gallo, P. Del; Pham-Huu, C.; York, A.P.E.; Ledoux, M.J. Comparison of the Effects of Nitrogen Poisoning on Molybdenum Oxycarbide and Pt/β-Zeolite Catalysts in the Isomerization of n-Heptane, *Ind. Eng. Chem. Res*., **1996,** 35, 3302-3310.

[7] Fu, C.M.; Schaffer, A.M. Effect of nitrogen compounds on cracking catalysts, *Ind. Eng. Chem Prod. Res. Dev*., **1985**, 24, 68-75.

[8] Dong, D.; Jeong, S.; Massoth, F.E. Effect of nitrogen compounds on deactivation of hydrotreating catalysts by coke, *Catal. Today*, **1997,** 37, 267-275.

[9] Li, Z.-k.; Gao, J.-s.; Wang, G. ; Shi, Q.; Xu, C.-m. Influence of Nonbasic Nitrogen Compounds and Condensed Aromatics on Coker Gas Oil Catalytic Cracking and Their Characterization, *Ind. Eng. Chem. Res*, **2011,** 50, 9415-9424.

[10] Jokuty, P.L.; Gray, M.R. Resistant nitrogen compounds in hydrotreated gas oil from Athabasca bitumen, *Energy Fuels*, 1991, 5, 791-795.

[11] Al-Hajji A, A., Muller H, Koseoglu O, R. Caractérisation par spectrométrie de masse par résonance cyclotronique ionique à transformée de Fourier des composés azotés et soufrés dans les charges d'alimentation d'hydrocraquage. *Oil Gas Sci. Technol. – Rev. IFP* **2008,** 63, (1), 115-28.

[12] Kekäläinen, T.; Pakarinen, J.M.H.; Wickström, K.; Vainiotalo, P. Compositional Study of Polar Species in Untreated and Hydrotreated Gas Oil Samples by Electrospray Ionization Fourier Transform Ion Cyclotron Resonance Mass Spectrometry (ESI FTICR−MS), *Energy Fuels*, **2009,** 23, 6055-6061.

[13] Li, X.; Zhu, J.; Wu, B.; Mao, X. Characterization of Acidic Compounds in Vacuum Gas Oils and Their Dewaxed Oils by Fourier Transform-Ion Cyclotron Resonance Mass Spectrometry, *Energy Fuels*, **2012,** 26, 5646-5654.

[14] Wei, Q.; Wen, S.; Tao, X.; Zhang, T.; Zhou, Y.; Chung, K. ; Xu, C. Hydrodenitrogenation of basic and non-basic nitrogen-containing compounds in coker gas oil, *Fuel Process.Technol.*, **2015,** 129, 76-84.

[15] Wiwel, P.; Hinnemann, B.; Hidalgo-Vivas, A. ; Zeuthen, P.; Petersen, B.O.; Duus, J.Ø. Characterization and Identification of the most Refractory Nitrogen Compounds in Hydroprocessed Vacuum Gas Oil, *Ind. Eng. Chem. Res.*, **2010,** 49, 3184-3193.

[16] Dufresne, P.; Quesada, A.; Mignard, S. Influence of Nitrogen Feed Content On The Performances of A Zeolite Hydrocracking Catalyst, in: *Studies in Surface Science and Catalysis*, Elsevier, **1989,** pp. 301-315.

[17] Celis-Cornejo, C.M.; Perez-Martínez, D.J.; Orrego-Ruiz, J.A.; Baldovino-Medrano, V.G. Identification of Refractory Weakly Basic Nitrogenates in a Hydrotreated Vacuum Gas Oil and Their Effect Over a Ni-MoS2/Y-Zeolite␣Alumina Catalyst Aimed for Two-stage Hydrocracking, (Submitted) *Energy Fuels*, (2017).

[18] Sau, M.; Basak, K.; Manna, U.; Santra, M.; Verma, R.P. Effects of organic nitrogen compounds on hydrotreating and hydrocracking reactions, *Catal. Today*, **2005,** 109, 112-119.

[19] Kobayashi, M.; Togawa, S.; Ishida, K. Effects of Small Amounts of Nitrogen Compounds in Feedstock on Performance of Hydrocracking Catalyst, *J. Jpn. Petrol. Ins.*, **2007,** 50, 44-52.

[20] Lemberton, J.-L.; Guisnet, M. Phenanthrene hydroconversion as a potential test reaction for the hydrogenating and cracking properties of coal hydroliquefaction catalysts, *Appl. Catal.*, **1984,** 13, 181-192.

[21] Korre, S.C.; Klein, M.T.; Quann, R.J. Hydrocracking of Polynuclear Aromatic Hydrocarbons. Development of Rate Laws through Inhibition Studies, *Ind. Eng. Chem. Res.*, **1997,** 36, 2041-2050.

[22] Benazzi, E.; Leite, L.; Marchal-George, N.; Toulhoat, H.; Raybaud, P. New insights into parameters controlling the selectivity in hydrocracking reactions, *J. Catal*, **2003,** 217, 376-387.

[23] Restrepo-Garcia, J.R.; Baldovino-Medrano, V.G.; Giraldo, S.A. Improving the selectivity in hydrocracking of phenanthrene over mesoporous Al-SBA-15 based Fe–W catalysts by enhancing mesoporosity and acidity, Applied Catalysis A: General, **2016,** 510, 98-109.

[24] Agudelo, J.L.; Hensen, E.J.M.; Giraldo, S.A.; Hoyos, L.J. Influence of steam-calcination and acid leaching treatment on the VGO hydrocracking performance of faujasite zeolite, *Fuel Process. Technol*., **2015,** 133, 89-96.

[25] Perego, C.; Peratello, S. Experimental methods in catalytic kinetics, *Catal. Today*, 1999, 52, 133-145.

[26] Medina, N.S.; Roa, J.S. Efecto de inhibición del carbazol sobre el hidrocraqueo de fenantreno, in: Escuela de Ingeniería Química, Universidad Industrial de Santander, Bucarmanga, Colombia, **2017.**

[27] Jongpatiwut, S.; Li, Z.; Resasco, D.E.; Alvarez, W.E.; Sughrue, E.L.; Dodwell, G.W. Competitive hydrogenation of poly-aromatic hydrocarbons on sulfur-resistant bimetallic Pt-Pd catalysts, *Appl. Catal. A.*, **2004,** 262, 241-253.

[28] Wu, C.F.J.; Hamada, M.S. Experiments: Planning, Analysis, and Optimization, 2nd Edition, **2009.**

[29] Kutner, M.H.; Nachtsheim, C.; Neter, W., J.L. Applied linear statistical models. 5th Edition, **2004.**

[30] Montgomery, D.C.; Runger, G.C. Applied Statistics and Probability for Engineers, 6th Edition., **2013.**

[31] Yang, M. Statistical Analysis of Unreplicated Factorial Designs Using Contrasts. M.Sc. Theses, Electronic Theses & Dissertations, in, Georgia Southern University, Statesboro, Georgia, **2014.**

[32] Frye, C.G. Equilibria in the Hydrogenation of Polycyclic Aromatics, *J. Chem. Eng. Data*, **1962,** 7, 592-595.

[33] Wagenmakers, E.-J.; Krypotos, A.-M.; Criss, A.H.; Iverson, G. On the interpretation of removable interactions: A survey of the field 33 years after Loftus, *Mem. Cognition*, **2012,** 40, 145-160.

[34] C.N. Satterfield, Mass transfer in heterogeneous catalysis, Cambridge, Mass., **1970.**

[35] Rosnow, R. L.; Rosenthal, R. If You're Looking at the Cell Means, You're Not Looking at Only the Interaction (Unless All Main Effects Are Zero), *Psychol. Bull.*, **1991,** 110, 574–576.

[36] Thybaut, J.W.; Marin, G.B. Chapter Two - Multiscale Aspects in Hydrocracking: From Reaction Mechanism Over Catalysts to Kinetics and Industrial Application, in: *Advances in Catalysis*, Academic Press, **2016,** pp. 109-238.

[37] Fogler, H.S. Elements of Chemical Reaction Engineering, 5th Edition. Prentice Hall, **2016.**

[38] Bird, R.B.; Stewart, W.E.; Lightfoot, E.N. Transport phenomena, 2nd Edition. Wiley, American Institute of Chemical Engineers, New York, **2006.**

[39] Davantès, A.; Costa, D.; Sallman, B.; Rakshit, S.; Lefèvre, G. Surface Polymerization of Mo(VI) and W(VI) Anions on Hematite Revealed by in Situ Infrared Spectroscopy and DFT+U Theoretical Study, *J. Phys. Chem. C*, **2017,** 121, 324-332.

[40] Hinman, R.L.; Lang, J. The Protonation of Indoles. Basicity Studies. The Dependence of Acidity Functions on Indicator Structure, *J. Amer. Chem. Soc.*, **1964,** 86, 3796-3806.

[41] Celis-Cornejo, C.M.; Mantilla, M.M.G.; Baldovino-Medrano, V.G.; Ramírez-Caballero, G.E. A quantum chemical study for exploring the inhibitory effect of nitrogen containing species on the adsorption of polynuclear aromatic hydrocarbons over a Bronsted acid site, *J. Phys. Conf. Ser.*, **2016,** 743, 012010.

[42] Hinman, R.L.; Whipple, E.B. The Protonation of Indoles: Position of Protonation, *J. Amer. Chem. Soc,* **1962,** 84, 2534-2539.

[43] Laredo, G.C.; Leyva, S.; Alvarez, R.; Mares, M.T.; Castillo, J.; Cano, J.L. Nitrogen compounds characterization in atmospheric gas oil and light cycle oil from a blend of Mexican crudes, *Fuel*, **2002,** 81, 1341-1350.

[44] Laredo, G.C.; Altamirano, E.n.; De los Reyes, J.A. Inhibition effects of nitrogen compounds on the hydrodesulfurization of dibenzothiophene: Part 2, *Appl. Catal. A.*, **2003,** 243, 207-214.

[45] Laredo G.C., De los Reyes, J.A.; Luis Cano, J.; Jesús Castillo, J.; Inhibition effects of nitrogen compounds on the hydrodesulfurization of dibenzothiophene, *Appl. Catal. A,* **2001,** 207, 103-112.

[46] Hydrogenation of the Aromatic Ring, in: *Metal-Catalysed Reactions of Hydrocarbons*, Springer US, Boston, MA, **2005,** pp. 437-471.

[47] Morales-Valencia, E.M.; Castillo-Araiza, C.O.; Giraldo, S.A.; Baldovino-Medrano, V.G. Kinetic assessment of the simultaneous hydrodesulfurization of dibenzothiophene and the hydrogenation of diverse polyaromatic structures, 2017.

[48] Owen, K.; Coley, T.; Weaver, C.S. Automotive Fuels Reference Book, **1995.**

[49] Leite, L.; Benazzi, E.; Marchal-George, N. Hydrocracking of phenanthrene over bifunctional Pt catalysts, *Catal. Today*, **2001,** 65, 241-247.

[50] Choi, H.W.; Dines, M.B. Selective removal of nitrogen compounds from shale oil, *Fuel*, **1985,** 64, 4-8.

CHAPTER 3: First-Principles Assessment of Polynuclear Aromatic Hydrocarbons Reaction Mechanism Over a Brønsted Acid Site and Their Inhibition by Nitrogen-Containing Compounds

Abstract

The inhibition exerted by nitrogenated compounds and the role of Brønsted acidity on the hydroprocessing of heavy oil derived fuels is an important issue to produce cleaner fuels. In this work, density functional theory (DFT) calculations with the Nudged Elastic Bands theory (NEB) were performed to explore the isomerization mechanism of tetrahydrophenanthrene, which is a partially hydrogenated intermediate compound produced during hydrocracking. In addition, the effect of different nitrogenated molecules on the adsorption of polynuclear aromatic hydrocarbons was studied on the same system. Mordenite was chosen as a suitable structure for modeling a Brønsted acid site. The character of the acid site was confirmed by both a vibrational frequency calculation and a Bader charge analysis. For the isomerization mechanisms, a set of realistic intermediates and transition states were determined, leading to a probable mechanism which could occur under elevated H_2 pressure and in presence of a hydrogenating sulfided catalyst. These results also showed that for the proposed mechanism, ring-opening is the rate-determining step. Otherwise, regarding the adsorption of polynuclear aromatic hydrocarbons, the energies were found to increase with the number of rings, that is from highest to lowest: tetrahydrochrysene > tetrahydrophenanthrene > tetrahydronaphthalene. Additionally, by analyzing the computed energies, regardless of their basic character, the nitrogenated compounds strongly inhibit the adsorption of polynuclear aromatic hydrocarbons on Brønsted sites, being the basic compounds stronger inhibitors. Finally, the formation of ion-pair complexes of the nitrogenated compounds was determined for all the molecules, even for those molecules with a weakly basic character. This explains the inhibitory effect observed even at small amounts of nitrogen content during the two-stage hydrocracking operation, and provides a better understanding of hydrocarbon hydroprocessing in refineries.

Keywords: DFT, Polynuclear aromatic hydrocarbons, nitrogenated compounds, transition states, Mordenite, external surface, pore mouth.

Nomenclature

ΔE_{ads}	Adsorption energy
DFT	Density Functional Theory
DFT-D3	Zero Damping Density Functional Theory Dispersive Energy Correction
ESI	Electrospray Ionization
FT-ICR-MS	Fourier Transform Ion Cyclotron Resonance Mass Spectrometry
FT-IR	Fourier Transform Infrared Spectroscopy
GGA	General Gradient Approximation
GC-MS	Gas Chromatography with Mass Spectrometry
HCK	Hydrocracking
MS	Mass Spectrometry
NEB	Nudged Elastic Bands Theory
PAH	Polynuclear Aromatic Hydrocarbon
PBE	Perdew–Burke–Ernzerhof exchange correlation functional
TS	Transition State
TST	Transition State Theory
VASP	Vienna Ab-initio Simulation Package
VGO	Vacuum Gas Oil

3. First-Principles Assessment of Polynuclear Aromatic Hydrocarbons Reaction Mechanism Over a Brønsted Acid Site and Their Inhibition by Nitrogen-Containing Compounds

3.1. Introduction

Hydrocracking has become a key technology for upgrading heavy oil feedstocks into gasoline and diesel. Industrial hydrocracking catalysts employ a shaped mixture of zeolite and alumina as a support of a sulfided active phase whose role is to promote hydrocarbon hydrogenation [1-3]. The incorporated metals are mostly distributed outside the microporous structure of the zeolite and along the alumina binder [4]. Thus, primary hydrogenation reactions must take place in the external area of the zeolite. Moreover, the diffusion of molecules into the micropores of the zeolite is driven by molecular activation after adsorption on the external surface [5]. In addition, due to the large size of the molecules present in the heavy oil fractions, some of them are not able to diffuse inside the pores of the zeolite [6]. Consequently, the acid sites on the pore mouth of zeolites play an important role in the catalytic performance since they promote intermediate reactions such as isomerization [7].

Aiming to understand the fundamentals of this complex of the process, phenanthrene and naphthalene are used as representative models for studying the hydroprocessing of heavy oil fractions over different catalysts [8-10]. These studies have helped establishing reaction schemes for phenanthrene at different conditions. Lemberton *et al.* [9] proposed a scheme of reaction for phenanthrene hydrogenation at 10 MPa and 703 K over a Ni-MoS_2/γ–Al_2O_3 catalyst. Phenanthrene undergoes partial hydrogenation into four products depending on the rings that are hydrogenated. Another partially hydrogenated product of the reaction; perhydrophenanthrene, has only been

detected over highly hydrogenating noble metal catalysts [11]. Considering the above and our studies on the reactivity of phenanthrene exposed in chapter 1 and 2 [12], we have proposed a reaction scheme for the reaction when performed over a Ni-MoS_2/Y-zeolite_alumina catalyst. Scheme 2.1 in chapter 2 shows it. According to the scheme, it is only after the partial hydrogenation of the rings that the isomerization, ring opening, and dealkylation steps proceed.

Despite the above works, an assessment of the reaction mechanism of phenanthrene hydrocracking is missing in the literature. Particularly, the role of the active sites of the catalyst is far from being established. However, the cracking mechanisms of aliphatic compounds over Brønsted and Lewis acid sites have been described [13-16]. Normally, reaction steps are based on the chemistry of the carbenium ion and the ß-scission (see Figure 3.1) [16-19]. On the contrary, specific mechanisms for alicyclic and aromatic hydrocarbons are not broadly described from a molecular point of view [18].

Figure 3.2 shows two possible primary hydrogenated products from the hydrogenation of the external ring of phenanthrene; namely, 1,2-dihydrophenanthrene and 1,2,3,4-tetrahydrophenanthrene. It has been hypothesized that 1,2-Dihydrophenanthrene could be produced by dehydrogenation of 1,2,3,4-tetrahydrophenanthrene in dehydrogenating functionalities of the catalyst [9]. As shown in Figure 3.2, proton donation to the double bond located in the partially hydrogenated ring of 1,2-dihydrophenanthrene may proceed as first step for the hydrocracking of the ring (the mechanism is depicted in Figure 3.1). Notwithstanding, considering the hydrogenating properties of sulfided Ni-Mo catalysts and the elevated H_2 pressure, the detection of 1,2-dihydrophenanthrene under the usual reaction conditions of model hydrocracking studies has not been reported [9, 10, 12, 20, 21]. Usually, only partially

hydrogenated hydrocarbons such as 9,10-dihydrophenanthrene, 1,2,3,4-tetrahydrophenanthrene, octahydrophenanthrene, and in less proportion asym-octahydrophenanthrene (those presented in Scheme 2.1 of chapter 2 are detected, see Annex 1 Figure A4) [12]. Despite arguing that under such circumstances considering these early steps in the reaction mechanism might be kinetically irrelevant, a true comprehension of the mechanism must consider such possibilities for providing a feasible explanation for the ring-opening and isomerization steps.

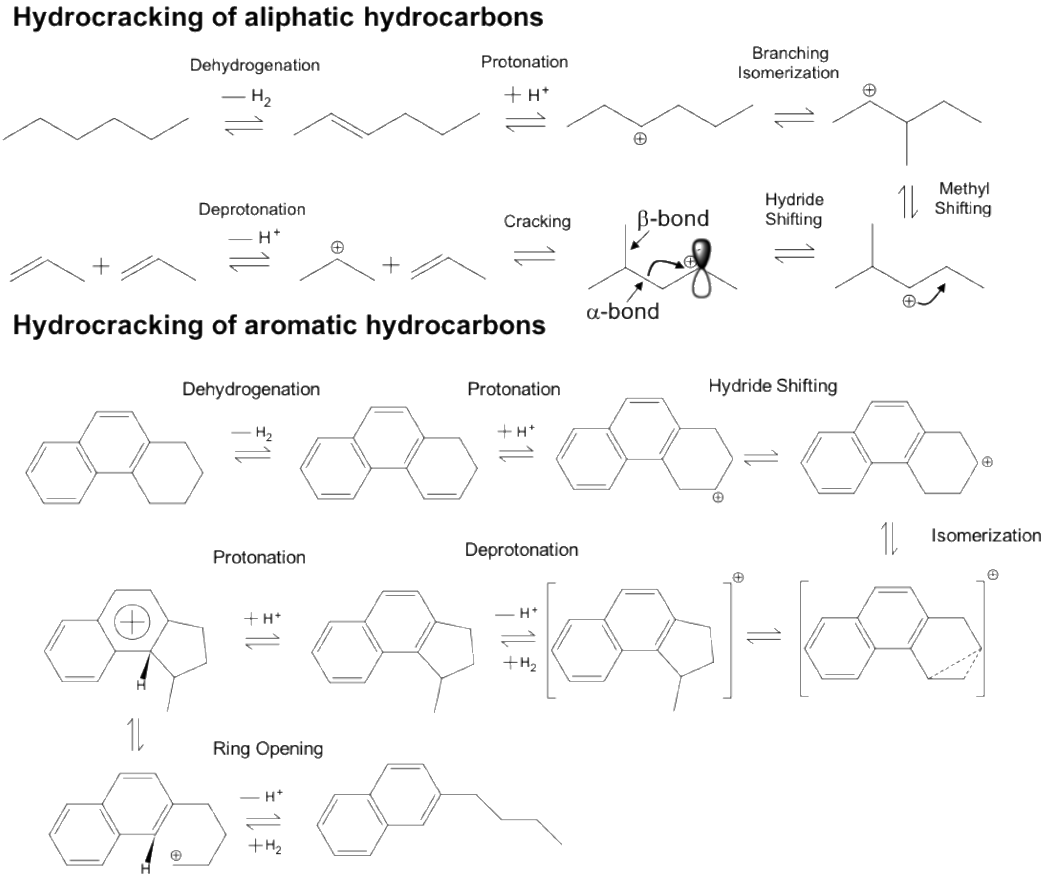

Figure 3.1. Hydrocracking mechanism of alkanes through the carbenium ion elementary steps as described by Froment and coworkers [16, 17, 19]. The mechanism of ß-scission is drawn in the cracking step. Hydrocracking of partially hydrogenated polynuclear aromatic hydrocarbons as suggested by Lemberton et al [9].

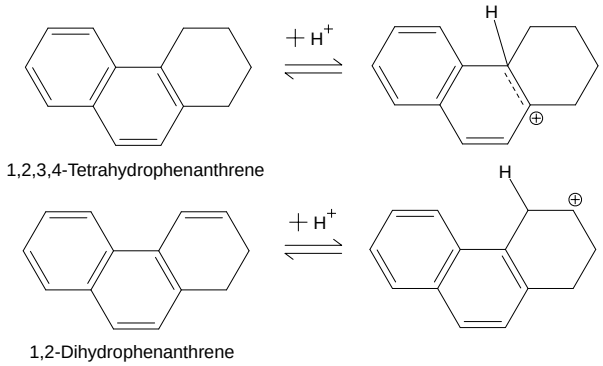

Figure 3.2. Chemical structures of the theoretical intermediate compound, the 1,2-dihydro phenanthrene, and the 1,2,3,4-tetrahydrophenanthrene, and their further protonated conformations.

Heavy crude oils have a large amount of heterocompounds [22, 23]. Thus, the hydrocracking unit is usually preceded by hydrotreating in which sulfur, nitrogen, and metal heteroatoms are removed [24] due to their ability for inhibiting the hydrocracking catalysts [25]. After hydrotreating, refractory heteroatom containing compounds persist [26-28] nonetheless. The inhibitory effect of basic nitrogenated compounds has been broadly documented [29-31] and this is reviewed in the introductory chapter and in chapters 1 and 2. In this regard, in chapter 1 [12], we found that when the total nitrogen concentration in a hydrotreated heavy fraction is below 20 ppm, the most abundant nitrogenates are weakly basic compounds; consisting mainly of pyrrolic type structures such as carbazoles and benzocarbazoles, whose effect on hydrocracking catalysts has been scarcely studied. This might partly be due to the strong inhibition of basic nitrogenates which leads many authors to jump into the conclusion that weakly basic nitrogen-containing compounds are minor players in hydrocracking [32]. In chapters 1 and 2, We have systematically studied the effect of carbazole and tetrahydrocarbazole on phenanthrene hydrocracking over a Ni-MoS_2/Y-zeolite␣alumina catalyst. Findings from this work showed that weakly basic nitrogen-containing compounds inhibited the phenanthrene conversion and the selectivity towards the reactions which preferentially take place on Brønsted acid sites.

Up to this point, the above discussion points out two important facts: (ii) the study of a feasible reaction mechanism to explain the hydrocracking mechanism of partially hydrogenated molecules representative of a heavy oil fraction on the pore mouth of zeolites; and (ii) understanding the inhibitory effect exerted by non-weakly basic nitrogenated molecules on the adsorption and reactivity of polynuclear aromatic hydrocarbons is necessary for upgrading heavy crude oils. Consequently, we decided to perform Density Functional Theory (DFT) calculations with the Nudged Elastic Band Theory for assessing the isomerization and ring-opening mechanisms of 1,2,3,4-tetrahydrophenanthrene π-adsorbed on a model Brønsted acid site located on the external surface of a mordenite type structure. Despite Y-zeolites are widely used as part of the supporting material in the hydrocracking catalyst [10, 12, 33], as this study aimed to model the reaction in the external surface of the zeolite, mordenite results suitable for modeling the interactions on a Brønsted acid site. A recent publication showed that the Si/Al ratio influences more on the adsorption energy of different basic molecules on Brønsted acid sites, than the framework type of the zeolite [34]. Afterwards, we analyzed the π-adsorption of two, three, and four ring polynuclear aromatic hydrocarbons; namely, tetrahydronaphthalene, tetrahydrophenanthrene, and tetrahydrochrysene, on the same catalytic site. Subsequently, the adsorption of both basic; specifically, pyridine and quinoline, and weakly basic; namely, tetrahydrocarbazole, carbazole, indole, and tetrahydroindole, nitrogenated molecules, over the Brønsted site was also analyzed. These calculations to establish molecular level causes for the inhibitory effect of nitrogenated compounds over hydrocracking.

3.2. Molecular modeling

In this section, the aspects concerning the DFT method, the procedure for modeling the Brønsted acid site, the external catalyst surface, the isomerization mechanism of 1,2,3,4-tetrahydrophenanthrene, and the theoretical adsorption of the studied molecules are presented.

3.2.1. Computational details. The software Vienna Ab-Initio Simulation Package (VASP) was used for calculations considering periodic boundary conditions. The Projector-Augmented Wave (PAW) and the Perdew–Burke–Ernzerhof exchange-correlation functional (PBE) were considered in all cases. A smearing of zero and a sigma parameter of 0.05 were taken for calculations performed for the bulk system and for the external surface of the zeolitic material. Plane waves up to an energy cut off of 600 eV was chosen after a convergence study. A Γ-point Brillouin-zone sampling was considered due to the large size of the unit cell. An additional support grid was considered which adds 8 times more more points than the standard grid. A correction to the dispersion energy contribution was made using the Grimme's parametrization of density functional dispersion correction (DFT-D3) [35, 36], as implemented in VASP, taking into account the fact that the DFT method within the GGA approach does not correctly estimate the energy for these modeled systems [37].

3.2.2. DFT modelling of a Bronsted acid site in mordenite. Pure silica mordenite was taken for modelling the basic structure of mordenite, following a similar procedure as Demuth et al. [38, 39], and Bucko et al. [40]. The selected structure has an orthorhombic morphology, with a Cmcm space group and crystallography unit cell parameters: a = 18.052-18.168 Å, b = 20.404-20.527 Å, and c = 7.501-7.537 Å [41]. For calculations, the bulk CIF file was taken from the Database of Zeolite Structures [41]. Initial unit cell parameters of the pure silica mordenite were a

= 18.194 Å, b = 20.470 Å, and c = 7.506 Å. After optimizing the bulk unit cell parameters (a = 18.260 Å, b = 20.702 Å, and c = 7.581 Å), it was duplicated in z-axis, and a surface was created adding a vacuum space of 10 Å in the same direction and cutting the surface over the (001) plane aiming to expose the 12-membered ring. For stabilizing the charge, terminal oxygen atoms were completed with hydrogen atoms. From this methodology some terminal silanol groups were obtained. Following this procedure, we obtained a structure with 193 atoms. This procedure restricts the results presented herein to reactions carried out in the pore mouth of the zeolite. For the sake of convenience, the interactions of the studied compounds with the mordenite sites were carried out over the 12-membered ring which has a cross-section between 12.16 Å and 11.25 Å. Figure 3.3 shows the aforementioned structural dimensions and the main cavity of the model zeolite. The effect of confinement into the pore of the zeolite over the adsorption energy was determined for carbazole adsorption, because among the studied nitrogen-containing compounds it has the greater molecule size. A small increase in the computed value was observed (see Annex C, Figure C1), in accordance with other studies [42]. An isomorphic substitution of one silicon atom by one aluminum atom in the T2 position (Figure 3.4), was made for modeling the Brønsted acid site, getting a Si/Al ratio of 47, corresponding to a very dealuminated zeolite [41], possessing a strong acidity [43-45]. The position chosen for placing the aluminum atom was based on the work by Demuth et al. [39] who found that such a position was more energetically stable. As mentioned in the introductory part, theoretically, the strength of the acidity of a zeolite, which is directly related with the adsorption energy of basic molecules on Brønsted sites, depends more on the Si/Al ratio and the atomic composition than on the framework. A vibrational frequency calculation considering only Al-O-H atoms within the structure was made to confirm the acid character of the modeled Brønsted site. An additional parameter that indicates the acid character

of the modeled site is the accumulated charge of the hydrogen atoms in the mordenite surface. An analysis of this property was carried out with a Bader charge analysis using the algorithms published by Henkelman and coworkers [46]. From this calculation the punctual charge of all the atoms in the zeolite framework is obtained. The information that these algorithms require is contained in the CHGCAR file which provides the atomic positions, the lattice vectors, the product of the total charge density and the volume on the augmented fine FFT-grid (NGXF×NGYF×NGZF), and the PAW one-center occupancy matrices [47].

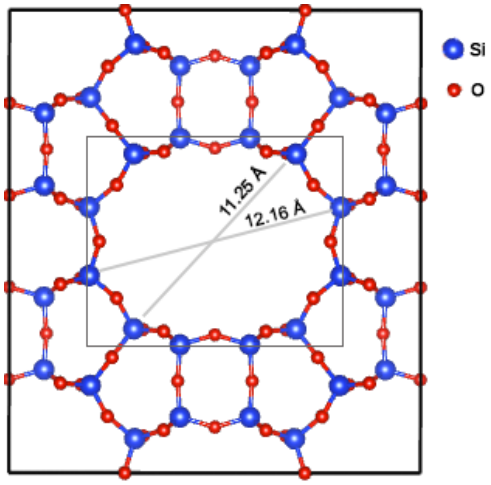

Figure 3.3. Optimized mordenite bulk 144 atom unit cell from a top view.

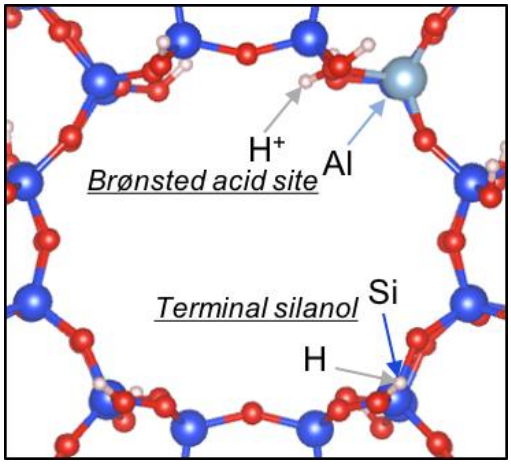

Figure 3.4. Isomorphic substitution of aluminum for the modeled Brønsted acid site, and terminal silanol groups in the pore mouth of a mordenite, from the top view of the (001) plane.

3.2.3. Simulation of the isomerization mechanism. A set of 10 images was used for the Nudged Elastic Bands (NEB) analysis to find the transition states between the proposed intermediate compounds. The structural arrangements for all the intermediates and transition states of the studied steps are reported in the supplementary information Figure C2.

3.2.4. Adsorption of polyaromatic hydrocarbons and nitrogen-containing compounds on the model Bronsted acid site. The adsorption of the following PAHs over the model Bronsted acid site was analyzed: tetrahydrchrysene, tetrahydrophenanthrene, tetrahydronaphthalene. Concerning the adsorption of nitrogenated molecules, pyridine and quinoline representing basic nitrogenates were selected for the study while carbazole, 1,2,3,4-tetrahydrocarbazole, indole, and 1,2,3,4-tetrahydroindole were selected to represent the behavior of weakly basic compounds. Each adsorbate was optimized before adsorption using a cube cell with edge length of 25 Å to avoid interactions between the periodic images. These calculations of the isolated molecules were performed using the same input parameters as described in section 3.2.1. The energy of the optimized adsorbates was defined as the gas phase energy ($\boldsymbol{E_m}$). Equation 3.1 corresponds to the general expression used for computing the adsorption energy ($\Delta \boldsymbol{E_{ads}}$) of the model molecules:

$$\Delta E_{ads} = E_{m-zeo} - (E_m + E_{zeo}) \tag{3.1}$$

Where, E_{zeo} and E_{m-zeo} represent the mordenite external surface and the mordenite-adsorbate complex energies, respectively.

The adsorption of partially hydrogenated polynuclear aromatic hydrocarbons with the Brønsted acid site was considered by the carbon atom located in the aromatic ring adjacent to the partially hydrogenated ring, in a π-stacking adsoption (see Figure 3.5.a). In addition, the basic and weakly basic nitrogenated compounds were adsorbed by the nitrogen atom, as it concentrates a higher negative charge (see Figure 3.5.b). This is ideal for the formation of acceptor-donor type complexes or adsorbed ion-pair complexes. Additionally, interactions with terminal silanol groups were studied for the nitrogenated compounds. The tested silanol group was chosen in the position

shown in Figure 3.4. This position was selected due to the hydrogen atom of the chosen silanol group does not present hydrogen-bond interactions with other oxygen atoms of the framework. Bucko *et al.* [40], theoretically demonstrated that these silanol groups which does not interact with other oxygen atoms of the framework, fairly describes the experimental behavior of a silanol group, regarding the O-H stretching frequency. For the polynuclear aromatic hydrocarbons, the initial distance between the adsorbate and the site were set at 2.0 Å, which is found to be a suitable distance for aromatic hydrocarbon adsorption [37]; while for the nitrogenated compounds it was set at 1.5 Å, as it is expected a strong interaction of the nitrogen atom with the proton of the zeolite [48, 49]. All calculations were relaxed considering Van de Waals interactions until all adsorbates reached an optimum distance from the acid site.

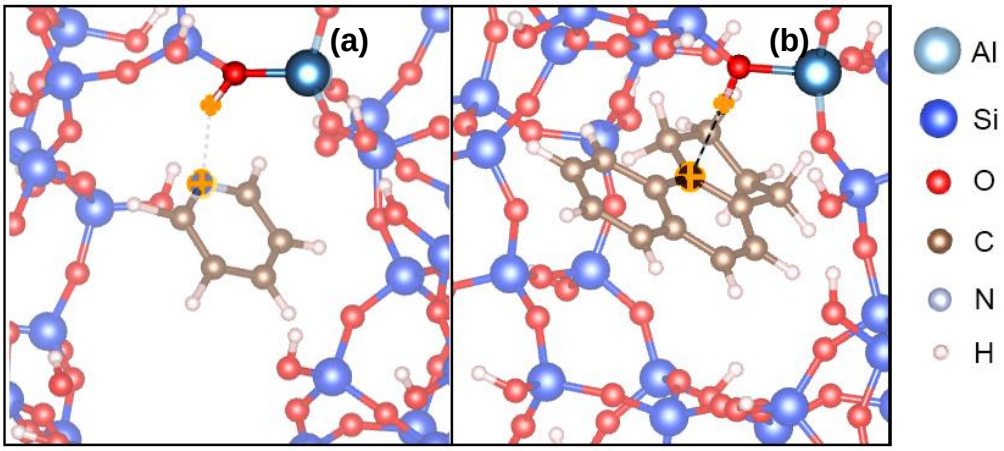

Figure 3.5. Adsorption initial conformations: (a) pyridine and (b) tetrahydrophenanthrene

3.3. Results and discussion

In this section, a brief description of the Brønsted acid site of mordenite is presented first. This Brønsted acid site is further demonstrated to act as an active site for tetrahydrophenanthrene isomerization. Afterward, the study of the hydrocracking mechanism of the tetrahydrophenanthrene over a Brønsted acid site. Once the latter is established, the adsorption of other selected polynuclear aromatic hydrocarbons and nitrogenates over the active Brønsted acid site is analyzed giving special importance on the inhibition effects that nitrogen-containing compounds exert over hydrocracking.

3.3.1. Brønsted acid site modelling . After optimization, the obtained lattice constants for the modeled zeolite surface with the Brønsted acid site were a = 18.257 Å, b = 20.718 Å, and c = 21.2 Å. These parameters were very similar to those reported by Demuth et al. [39] within the GGA approach, for a pure silica mordenite (a = 18.260 Å and b = 20.706 Å). From the frequency calculation of the Al-O-H atoms, a stretching frequency of 3603.9 cm-1 was obtained for the O-H. This value was in good agreement with the one reported by FT-IR characterization of Brønsted acid sites in a mordenite (3608 cm-1) [40]. From the Bader charge analysis, the hydrogen atom of the terminal silanol groups exhibited an average charge of +0.64 ±0.11. For the Brønsted site, the assigned punctual charge of the calculation for the hydrogen atom bonded to the oxygen adjacent to the aluminum was ca. +0.75. Comparing the punctual charge of the hydrogen atom of the Brønsted site with the average charge of the hydrogen atom of silanols, this was found to be higher, confirming an acid character of the modeled site. However, some isolated hydrogen atoms of terminal silanol groups exhibited a greater positive charge even around the same value as obtained for the hydrogen atom of the Brønsted site. Despite these terminal silanol groups behaves as weak

Brønsted sites, they do not have the ability for protonating a nucleophile molecule such as ammonia [50]. Thereby, their role in the isomerization mechanism is expected to be less significant. Once a suitable model for the Brønsted acid site was obtained by confirming its characteristic properties such as the O-H stretching frequency and a positive charge in the hydrogen atom, the isomerization mechanism of tetrahydrophenanthrene is studied next.

3.3.2. Isomerization of tetrahydrophenanthrene over the simulated Brønsted acid site. Figure 3.6 presents the ring-opening mechanism proposed for the isomerization of tetrahydrophenanthrene to methylcyclopentanaphthalene over the modeled Brønsted acid site. This mechanism was chosen based on the consideration that there is no unsaturation in the partially hydrogenated ring, otherwise 1,2-dihydrophenanthrene was selected as reactant for the isomerization reaction. Lemberton et al. [9], proposed a mechanism for the ring-opening of tetrahydrophenanthrene to produce butylnaphthalene, starting from the protonation of one carbon of the intermediate aromatic ring, adjacent to the partially hydrogenated cycle. However, the neglected this mechanism considering that the primary carbocation formed is very unstable, making that mechanism unfeasible. However, in this hypothesized mechanism the interaction of the intermediates and transition states with the zeolite was not considered. In this regard, the role of zeolites is crucial in the stabilization of intermediates and transition states formed during the reaction [34, 42, 51, 52]. The mechanism involves: (1) protonation of the carbon belonging to the aromatic ring adjacent to the saturated ring (as depicted also in Figure 3.2) followed by (2) ring opening of partially hydrogenated cycle, (3) hydride shift to the carbon bonded to the oxygen atom of the zeolite, (4) cyclization of the positively charged butyl chain, and (5) donation of the proton to the zeolite for recovering the Brønsted site.

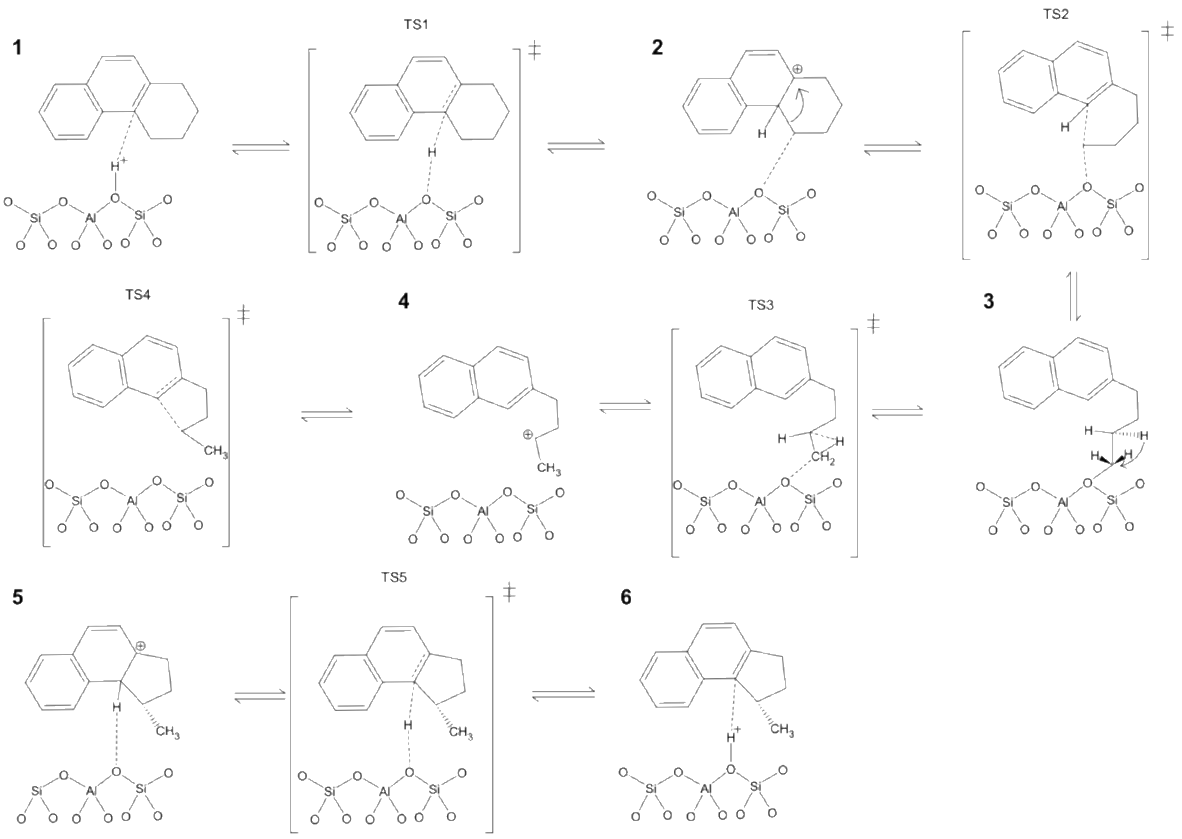

Figure 3.6. Mechanism of isomerization for the tetrahydrophenanthrene to methylcyclopentanaphthalene.

For the mechanism, the initial adsorbed configuration of tetrahydrophenanthrene on the Brønsted acid site is considered to be a π-interaction, as shown in step 1 in Figure 3.6. When cyclization into a 5-membered ring occurs, step (5) in Figure 3.6, methyl was chosen in that position as long as, only with this configuration, the ring opening of this compound leads to 2-butylnaphthalene which was a very abundant product detected on our previous studies [9, 12]. The structural arrangements of the transition states for the postulated mechanism are shown in Figure 3.7. Where, TS1, corresponds to the proton donation to the π-adsorbed complex; TS2, represents the ring opening step, while aromaticity is restored; TS3, is the hydride shifting for generating a secondary carbocation in the alkyl chain; TS4, is the subsequent cyclization of the butyl chain for

stabilizing the secondary carbocation; and TS5, is the deprotonation of the 5-membered ring favored by the steric hindrance caused by the methyl group.

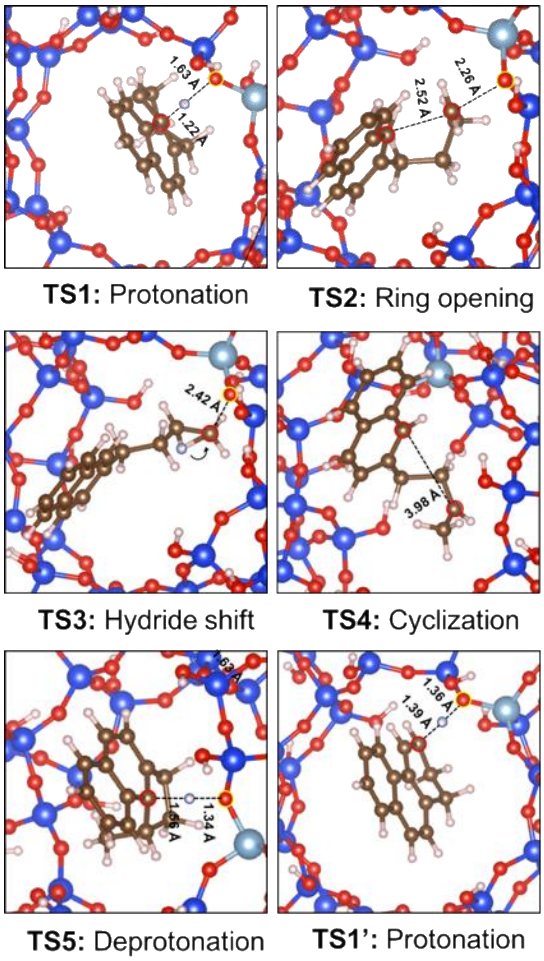

Figure 3.7. Configurations of the transition states calculated from the NEB study for the mechanism depicted in Figure 3.6 for the tetrahydrophenanthrene. The TS1' is the hypothetical transition states of the protonated 1,2-dihydrophenanthrene.

Despite the isomerization reaction may occur under high hydrogen pressure, no intermediate hydrogenation/dehydrogenation steps were considered to occur on the Brønsted acid site of the zeolite. Such an assumption was based on previous literature reports [12, 53]. A study analyzing the catalytic cracking mechanism of isobutene suggested that a Haag-Dessau mechanism could

take place on the Brønsted acid sites of zeolites [54]. This mechanism involves an initial dehydrogenation step. The nature of the mechanism is similar for alkanes and alicyclic compounds. Accordingly, we decided to perform the modelling of such a mechanism for tetrahydrophenanthrene over the Brønsted acid site of mordenite. The energy profile and the transition state conformations for the Haag-Dessau mechanism on tetrahydrophenanthrene are available in the Annex C, Figure C3. The estimated activation energy for the dehydrogenation reaction was 176 $kJ \cdot mol^{-1}$. This value was found to be near the values reported by Gounder and Iglesia [55] for the monomolecular dehydrogenation of alkanes. Considering the energy barrier associated to the calculated activation energy, a very slow rate of reaction can be expected as in correspondence to what is observed in monomolecular alkane reactions on mordenite [56].

The energy profile estimated by the NEB study for the isomerization mechanism of tetrahydrophenanthrene is presented in Figure 3.8. This profile shows the relative energies determined with respect to the energy calculated for tetrahydrophenanthrene in the gas phase. The red line is the protonation step of 1,2-dihydrophenanthrene, which was also modeled aiming to compare the feasibility of this step in our postulated mechanism. On the contrary the black line is the complete energy profile calculated for the postulated mechanism. For the protonation of the carbon closer to the acid center of tetrahydrophenanthrene (Step 1 in Figure 3.6), an activation energy of 56.8 $kJ \cdot mol^{-1}$ was obtained. This energetic barrier was moderately larger as compared to the protonation of the double bond of 1,2-dihydrophenanthrene (activation energy = 30.5 $kJ \cdot mol^{-1}$). The calculated adsorption energies for both compounds were almost the same: namely, -101.2 $kJ \cdot mol^{-1}$ for 1,2,3,4-tetrahydrophenanthrene and -101.4 $kJ \cdot mol^{-1}$ for 1,2-dihydrophenanthrene, regardless of the fact that different adsorption configurations were obtained after relaxation. These results show the feasibility of the conceived mechanism. Thus, the

protonation of the carbon located in the aromatic ring of tetraydrophenanthrene, as considered in the mechanism featured in Figure 3.6, will slightly cost more (26.3 $kJ \cdot mol^{-1}$) than the classical protonation of a double bond in an aliphatic hydrocarbon [9]. The ring opening step (Step 2 in Figure 3.6) was determined to have an activation energy of 119.4 $kJ \cdot mol^{-1}$. This was the largest energetic value for the proposed mechanism. Therefore, this step is possibly rate-determining. Furthermore, this is the energetic cost for the ß-scission of the C-C bond which leads to ring opening. Note that for this mechanism to occur the ring opening step is necessary. The oxygen adjacent to the aluminum plays the role of a basic site and it stabilizes the primary carbocation obtained in the ring-opened transition state (TS2 in Figure 3.7) by the formation of an alkoxide. At this point, the reaction may follow two routes: (i) hydrogen transfer from a neighbor carbon in the alkyl chain to an oxygen adjacent to the aluminum atom, and (ii) a hydride shift (step 3 in Figure 3.6) from an adjacent carbon to the carbon bonded to the oxygen, thus breaking the C-O bond, and forming a secondary carbocation in the alkyl chain. Route (i) leads to the direct production of butenylnaphthalene [9]. However, this product has not been identified in studies concerning the hydrocracking of phenanthrene [12]. Therefore, the energy profile for this case was not developed in this work. It is possible though that butenylnaphthalene could be very rapidly hydrogenated by the Ni-MoS_2 active phase to butylnaphthalene, which has been said to be a common hydrocracking product detected by GC-MS [12]. Route (ii) corresponds to step 3 of the proposed mechanism and its energetic barrier was estimated to be 108.3 $kJ \cdot mol^{-1}$. This step involves the scission of the formed C-O bond, due to the hydride shifting, and, in consequence, it leads to the formation of a secondary carbocation. The shifted hydrogen atom is in an initial position so the migration occurs from the opposite side of the C-O bond (see also Figure C2 in Annex C). Thereafter, cyclization of the alkyl group for obtaining a 5-membered ring (step 4 in

Figure 3.6) was determined to involve an activation energy of 36.9 kJ·mol^{-1}, but also an enthalpy of cyclization of -90.2 kJ·mol^{-1} (enthalpies are available in Annex C, Table C1), hence suggesting the formation of a very stable intermediate. A mechanism of isomerization from octahydrophenanthrene to octahydroanthracene was studied by Nie *et al.* [57] using a mechanical embedded two-layer ONIOM(DFT:UFF) method for modeling mordenite and faujasite clusters. A similar conformation of the alkoxide intermediate to what is proposed here for the cyclization was modeled. However, the authors considered the formation of a primary carbocation in the carbon bonded to the oxygen. In consequence, the cyclization step derived in a 6-membered cycled anthracene-like intermediate with a higher energy (enthalpy of cyclization = 43.9 kJ·mol^{-1}) [57]. The characterization of the isomerization products derived from tetrahydrophenanthrene produced during the hydrocracking of phenanthrene over a Ni-MoS_2/Y-zeolite catalyst formulation showed that the amount of methylcyclopenta-naphthalene amounted to a 4.4 wt.% of the total liquid products, yet, anthracene-like isomers were not observed [12]. The cyclization into a 5-membered ring in a phenanthrene-like structure seems to be more feasible than the formation of an anthracene one insofar as the attacked carbon is facing the aluminum over which the reaction takes place. Otherwise, an additional rotation of the aromatic nucleus is required in order to proceed with the deprotonation step (step 4 in Figure 3.6, TS4 in Figure 3.7). Moreover, from the secondary carbocation formed after the shifting of the hydride, the distance between the carbocation and the carbon facing the aluminum atom is shorter than the distance from the other adjacent carbon, and is observed also in the cyclization transition state (See Figure 3.7 or Figure C2 conformation TS4). That implies a rotation of the alkyl chain thence favoring cyclization to the phenanthrene-like compound (all the intermediate compounds are available in Annex C Figure C2). In consequence, after cyclization, the hydrogen atom which is facing the aluminum center moves toward the basic

oxygen adjacent to the aluminum atom. Finally, the deprotonation step is performed with a very low barrier of 36.9 kJ·mol^{-1}. The energy change between gas phase reactive and product is about 8.6 kJ·mol^{-1}.

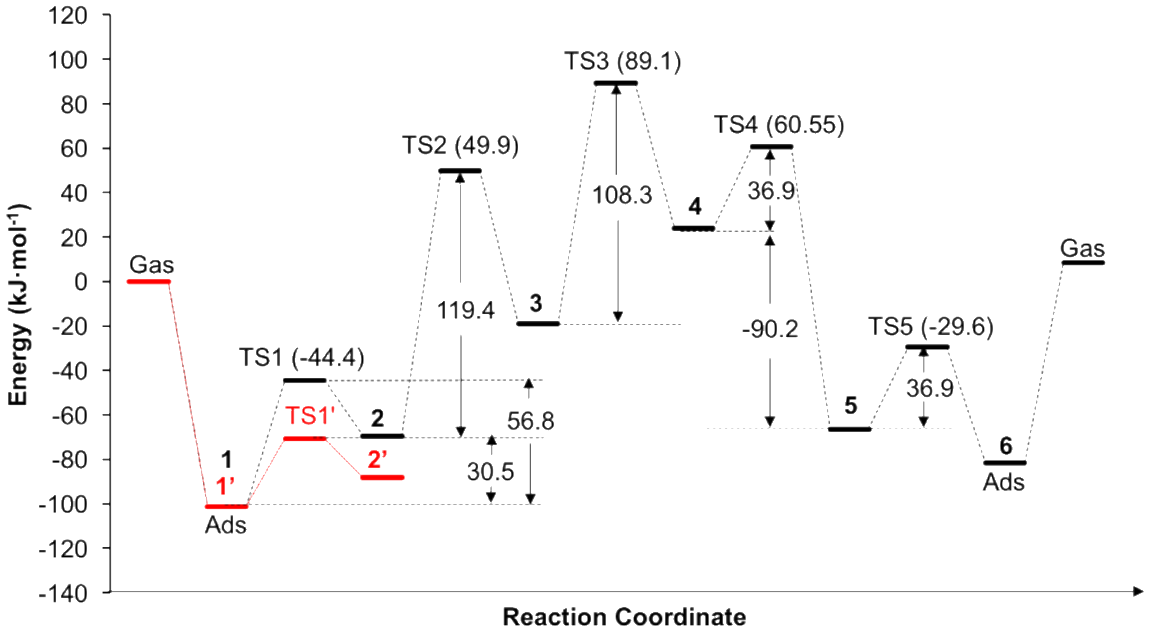

Figure 3.8. Relative energy profiles for the isomerization mechanism of the tetrahydrophenanthrene to methycyclopentanaphthalene over a Brønsted acid site. Energy difference between the product and the reactive in gas phase: $E_{Prod} - E_{Reac}$ = 8.6 kJ·mol^{-1}. The red dotted line is the energy profile for the protonation step of the 1,2-dihydrophenanthrene, transition state is indicated as TS1'. In accordance with the mechanism described in Figure 3.6, transition states correspond in order to TS1, protonation, TS2, ring opening step, TS3, hydride shifting, TS4, cyclization, and TS5, deprotonation.

To summarize, a mechanism starting from the protonation of a π-adsorbed complex of tetrahydrophenanthrene was studied. To the best of our knowledge, this mechanism has not been studied at a molecular point of view because most authors assume an initial dehydrogenation step to form an unsaturation of the alicyclic ring [9]. An analysis of the Haag-Dessau mechanism allowed to conclude that it could take place at a very slow rate of reaction. Afterwards, the second

step modeled corresponded to the ring-opening step, which was found to be the rate-determining step of the mechanism with an energy barrier of -119.4 kJ·mol^{-1}. When cyclization into a 5-membered occurs, the formation of anthracene-like isomers was found to be less probable. Once the above mechanism has been proven feasible, we will now focus our attention to analyzing the competitive π-adsorption of polynuclear aromatic hydrocarbons containing 2, 3, and 4-rings and of nitrogenated compounds over the modeled Brønsted acid site.

3.3.3. Adsorption of polynuclear aromatic hydrocarbons over a Brønsted acid site and competitive adsorption of nitrogen-containing compounds.

The π-adsorption of tetrahydronaphthalene, tetrahydrophenanthrene and tetrahydrochrysene on the Brønsted active site is addressed first. Then a further discussion about the competitive adsorption of nitrogenates on Brønsted acid sites based on the analysis of the adsorption energies is raised on the subject.

As postulated for the mechanism of isomerization presented in the above section, the π-adsorption on the modeled Brønsted acid site, of the polynuclear aromatic hydrocarbons is performed considering similar arrangements (see Annex C, Figure C4). The optimized adsorption configurations and adsorption energies (ΔH_{ads}) are shown in Figure 3.9 for each case. Despite the fact that the proton of the acid site points in the direction closer to the carbon atom of the adsorbates, the distance between the carbon and the proton was found to be greater than 2.07 Å. Accordingly, the binding of the molecules can be considered to correspond to π-stacking ion-acceptor complexes, taking into account that at the equilibrium distance no protonation of the π-adsorbed complexes is observed [34]. That is to say, no migration of the hydrogen atom of the Brønsted acid site towards the polynuclear aromatic hydrocarbons is evidenced.

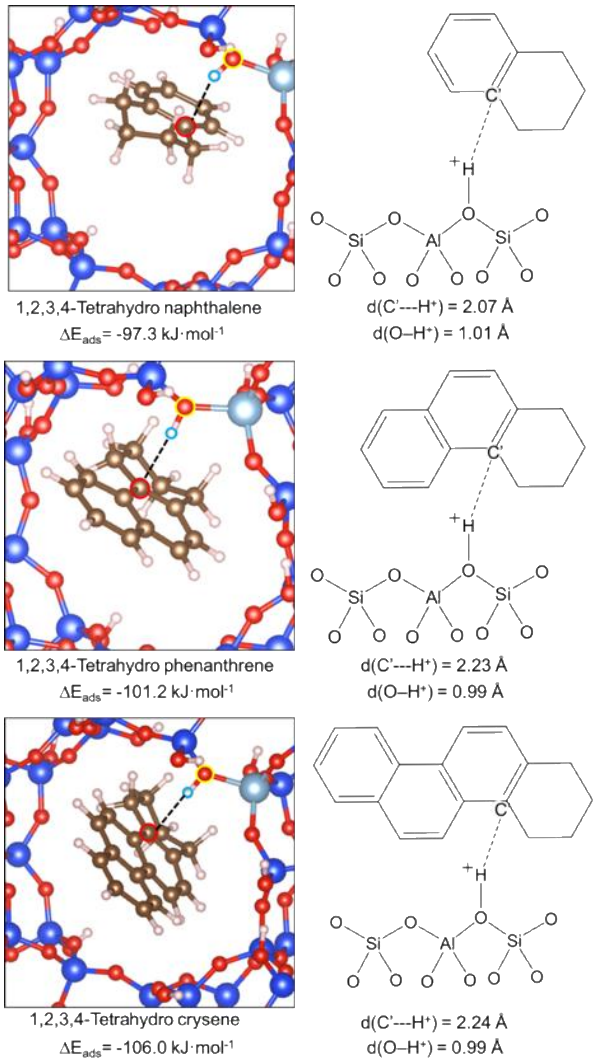

Figure 3.9. Structural arrangement for the optimized adsorbed polynuclear aromatic hydrocarbons complexes on the Brønsted site and their corresponding adsorption energies (ΔE_{ads}).

For polynuclear aromatic hydrocarbons, adsorption energies decreased with the number of rings; namely, ΔE_{ads} tetrahydrochrysene = -106.0 kJ·mol^{-1} > ΔE_{ads} tetrahydrophenanthrene = -101.2 kJ·mol-1 > ΔE_{ads} tetrahydronaphthalene = .97.3 kJ·mol^{-1}. This trend agrees with previous theoretical [58] and experimental works [10]. These adsorption energy values are considered to be in the range of chemisorption, upon 80 kJ·mol^{-1} [59, 60], upporting the above discussed idea. In addition, results thus imply that compounds with 3 and 4-rings preferentially react on the Brønsted active site as over the 2 rings compounds [10]. The magnitude of the calculated adsorption energies

is close to some theoretical data (-116 kJ·mol^{-1}) reported for toluene adsorption on Brønsted sites situated inside the channel of a mordenite [37]. It is important to remember that present calculations were performed on the external surface of the zeolite thus such differences are expected. In a recent theoretical study based on Monte Carlo simulations, Janda *et al.* [42], demonstrated for the adsorption of alkanes onto Brønsted sites that interaction in the external surface will exhibit lower magnitudes for the adsorption energies, and higher values for the activation energies as compared to the adsorption process into the pores od zeolites [42]. Authors ascribed this to the confinement effects, because in zeolites with higher confinements, the adsorption energies were higher and the activation energies lowered. An example of this is shown in Figure C1 in Annex C. This might be explained in terms of the Van der Waals interactions of the adsorbates with the zeolite neighbor atoms.

Up to this point, π-stacking adsorption configurations for 2, 3 and 4 rings partially hydrogenated polynuclear aromatic hydrocarbons on a Brønsted acid site located in the pore mouth of a mordenite was modeled. Findings here exposed suggest that the adsorption of tetrahydrochrysene is energetically favored, followed by the adsorption of tetrahydrophenanthrene, and tetrahydronaphthalene was the one with the lowest adsorption energy. Next, the adsorption energies of basic and weakly basic nitrogenated compounds are computed in order to correlate them with possible inhibitory effects on the hydrocracking of polynuclear aromatic hydrocarbons.

As discussed in section 3.3.1, some isolated silanol groups exhibit a positive charge similar to the value obtained for the Brønsted site (+0.75). Bucko *et al.* [50], theoretically described, by modeling ammonia adsorption on a mordenite, that some silanol groups behaves as weak Brønsted acis sites, despite their poor ability to donate protons. In this regard, the adsorption of nitrogen-

containing compounds was also performed on a terminal silanol group for studying the interaction of these compounds with a weak Brønsted acid site, in order to stablish the nature of this interaction for weakly and basic nitrogen-containing compounds. Optimized conformations of the adsorbed nitrogenated compounds are available in supplementary information, Figure C4. Table 3.1 shows the computed adsorption energies (ΔE_{ads}) obtained from the optimized conformations over both the Bronsted and the silanol sites. For the Brønsted site, the adsorption energies obtained, in kJ·mol^{-1}, from highest to lowest were: quinoline, ΔE_{ads} = -163.3 > pyridine, ΔE_{ads} = -149.7 > carbazole, ΔE_{ads} = -129.6 > tetrahydrocarbazole, ΔE_{ads} = -111.2 > indole, ΔE_{ads} = -111.2 > tetrahydroindole, ΔE_{ads} = -104.8.

Table 3.1.

Adsorption energies calculated from Equation 3.1 for the interaction of the nitrogenated compounds with the Brønsted site and the silanol group.

Molecule	$\Delta E_{ads}^{Brønsted}$ (kJ·mol^{-1})	$\Delta E_{ads}^{Silanol}$ (kJ·mol^{-1})
Quinoline	-163.6	-26.6
Pyridine	-149.7	-28.9
Carbazole	-129.6	-63.1
Tetrahydro carbazole	-112.2	-60.7
Indole	-111.2	-47.8
Tetrahydro indole	-104.8	-49.2

This is consistent with reports on the inhibition of hydrocracking catalysts by basic nitrogenates [25, 30, 31]. On the other hand, all weakly basic nitrogen-containing compounds showed adsorption energies larger than those determined for polynuclear aromatic hydrocarbons. This suggests that their adsorption is thermodynamically favored over that of the polyaromatic compounds. This provides theoretical support to experiments showing that these nitrogenates inhibit hydrocracking reactions by selectively disfavoring the production of isomerization intermediates [12]. The inhibitory effect exerted by weakly basic nitrogen-containing compounds

on the hydrocracking of polynuclear aromatic hydrocarbons in order from highest to lowest is: carbazole > tetrahydrocarbazole > indole > tetrahydroindole. In previous experimental works [12], the inhibition of hydrocracking reaction of phenanthrene over a Ni-MoS_2/Y-zeolite_alumina catalyst by carbazole and tetrahydorcarbazole was studied. Carbazole and tetrahydrocarbazole, used in a concentration as low as 5 ppm, were found to negatively affect the catalytic conversion to a similar extent. Regarding selectivity, carbazole and tetrahydrocarbazole tended to specifically inhibit the reaction route derived from the hydrogenation of external rings that leads to naphthalenes and tetralins (Scheme 2.1 in Chapter 2). The mechanism studied hereof belongs to the aforesaid route. As isomerization and ring opening occur preferentially on Brønsted acid sites [9, 18, 61], the inhibition of this route suggested a blockage of Brønsted acid sites by strongly adsorbed carbazole and tetrahydrocarbazole [12]. The distances obtained for the adsorbed complexes for all the nitrogenated compounds over the Brønsted acid site and the terminal silanol group are listed in Table 3.2. Structural arrangements are available in Figures C4 and C5. Protonation of the nitrogen heteroatom was observed, in so far as the hydrogen atom from the Brønsted acid site migrated to the nitrogen atom of the compounds. N-H bond length of 1.03–1.04 Å for basic compounds and 1.12 –1.13Å for weakly basic ones, were obtained over the Brønsted site. All the weakly basic compounds remain adsorbed at a short distance (1.45 – 1.49 Å), except the basic ones for which distances of 1.76 and 2.31 Å were obtained after relaxation for pyridine and quinoline, respectively. It is well-known that pyridine gets protonated when interacting with a Brønsted site. This is indeed the principle for measuring acidity by FT-IR analysis of adsorbed probe molecules where the vibrational frequencies of the adsorbed species are followed [49, 62]. However, this trend has not been described for indoles and carbazoles. In this sense, the existence of protonated weakly basic nitrogenated species observed in indole salts has been documented, by

the detection of the ammonium and immonium characteristic bands with FT-IR [63]. Nonetheless, this behavior is not widely reported in the literature.

Table 3.2.

Distances for the interactive atoms in the adsorbed complexes after geometry optimization for all of the nitrogen-containing compounds over Brønsted sites and terminal silanol groups.

Molecule	Interaction	Brønsted (Å)	Silanol (Å)
Carbazole	N---H^+	1.13	2.04
	H^+---O	1.45	0.98
Tetrahydro carbazole	N---H^+	1.12	2.01
	H^+---O	1.45	0.98
Indole	N---H^+	1.12	2.12
	H^+---O	1.46	0.98
Tetrahydro indole	N---H^+	1.12	2.15
	H^+---O	1.49	0.98
Pyridine	N---H^+	1.04	2.03
	H^+---O	1.76	0.98
Quinoline	N---H^+	1.03	2.10
	H^+---O	2.31	0.98

On the other hand, weakly basic nitrogen-containing compounds exhibited an interesting behavior when interacting with silanol groups. A higher energy was displayed by the weakly basic molecules as compared to basic nitrogenates. Nonetheless, the calculated adsorption energies are closer to the values reported for physical adsorption than to chemical adsorption, less than 80 $kJ \cdot mol^{-1}$ [59, 60]. The selective adsorption of nitrogenates on silica based materials is a matter of interest when aim to pretreat the oil fractions before the deep hydrodesulfurization or hydrocracking stages [64-66]. For the adsorption of carbazole on a silica surface, characterized by NMR, Kim *et al.* [64], suggested that small amounts of this compound was adsorbed on the material as long as the isolated signal of silanol was vanished, even proposing a strong interaction of carbazole with the silica surface. Other authors reported a similar trend for the adsorption of nitrogenated compounds within a heavy oil fraction on acidified silica-based materials [66]. This evidence suggests that weakly basic nitrogen-containing compounds have a marked affinity with

weak or strong Brønsted acid sites. Concerning the distances calculated for silanol interactions (Table 3.2), these are characteristic of physisorbed species. In addition, as expected, no migration of the hydrogen atom of the silanol group was obtained in the optimized conformations. In fact, a weak interaction is observed as the hydrogen atom of the silanol group directly points to the nitrogen atom in all cases (see Figure C5). This results confirms the inability of the tested silanol groups located on the external surface of a mordenite type zeolite for donating the proton to nucleophile species.

Summarizing, the formation of ion-pair complexes of weakly basic nitrogen-containing compounds on the theoretical model of a Brønsted acid site located in the pore mouth of a modenite type zeolite were obtained. The adsorption energies also suggest a strong interaction of these compounds when adsorbed on the Brønsted acid site, and even with the silanol groups, as described in this work, may explain the documented interactions of these compounds with Brønsted acid sites [12, 64-66]. Moreover, in light of the evidence, some studies concerning the development of new materials which resist the poisoning caused by nitrogenates, may not disregard the inhibitory effect of weakly basic nitrogen-containing compounds. All these, by considering also the evidence which points that these weakly basic nitrogenated compounds are by far the most refractory to the hydrotreating [12, 26-28]. Finally, the magnitude of the adsorption energies calculated herein for these weakly basic nitrogen-containing compounds also indicate that probably some of these compounds influence a reversible effect over the hydrocracking of polynuclear aromatic hydrocarbons. This trend is confirmed in a previous experimental work, in which the influence of temperature over the adsorption/desorption process of weakly basic nitrogen-containing compounds on the Brønsted site of the catalyst was evidenced. In other words, an increase in the temperature promotes the desorption of weakly basic nitrogen-containing compounds.

3.4. Conclusions

An interpretation of the hydrocracking reactions of polynuclear aromatic hydrocarbons in the zeolite pore mouth was assessed, by modeling a Brønsted acid site on the external surface of a mordenite using the density functional theory calculations with dispersion correction. A feasible mechanism for the isomerization reaction of the tetrahydrophenanthrene was developed herein, without including hydrogenation/dehydrogenation reactions. This study also hinted that π-adsorption of partially hydrogenated polynuclear aromatic hydrocarbons could lead to further isomerization reactions. Regarding the steps of the studied mechanism, the ring opening of the partially hydrogenated ring was found to be the rate-determining step of the mechanism with an activation energy of 119 $kJ \cdot mol^{-1}$. The adsorption energies calculated for the polynuclear aromatic hydrocarbons with 2, 3 and 4-rings clearly show a trend, the higher the aromaticity, the stronger the adsorption. Another remarkable aspect concerning the adsorption of these polynuclear aromatic hydrocarbons is that the proposed mechanism could be extended for all of them taking into account that all the adsorbed π-complexes exhibited a similar geometrical arrangement. Regarding the inhibitory effect exerted by nitrogenated compounds, the adsorption energies for basic compounds were visibly higher than the calculated for the weakly basic. Notwithstanding, the weakly basic compounds tend to form ion-pair complexes as well as the basic ones. Moreover, these compounds theoretically displayed a higher affinity when physisorbed on silanol groups than the basic molecules. The trend observed concerning the inhibition of weakly basic compounds was high as long as the aromaticity of the molecules increased. These results draw attention to include

the effect of the weakly basic nitrogenated compounds in the development of new supporting materials and hydrocracking catalysts.

References

[1] Mohanty, S.; Kunzru, D.; Saraf, D.N.; Hydrocracking: a review. *Fuel*, **1990,** 69, 12, 1467-73.

[2] Scherzer, J.A.; Gruia, A.J. Hydrocracking Science and Technology. New York; **1996.**

[3] Aitani AM. Catalysts in petroleum refining and petrochemicals. *Oil Gas European Magazine* **2001,** 27, 1, 42-3.

[4] Thybaut, J.W.; Marin, G.B. Chapter Two - Multiscale Aspects in Hydrocracking: From Reaction Mechanism Over Catalysts to Kinetics and Industrial Application. In: *Advances in Catalysis*. Academic Press, **2016,** p. 109-238.

[5] Auerbach, S.M.; Henson, N.J.; Cheetham, A.K.; Metiu, H.I. Transport Theory for Cationic Zeolites: Diffusion of Benzene in Na-Y. *J. Phys. Chem.,* **1995,** 99, 26, 10600-8.

[6] Ren, W.; Chen, H.; Yang, C.; Shan, H. Molecular size characterization of heavy oil fractions in vacuum and solution by molecular dynamic simulation. *Front. Chem. Eng. China*, **2010,** 4, 3, 250-6.

[7] Souverijns, W.; Martens, J.A.; Froment, G.F.; Jacobs, P.A. Hydrocracking of Isoheptadecanes on Pt/H–ZSM-22: An Example of Pore Mouth Catalysis. *J. Catal.* **1998,** 174, 2, 177-84.

[8] Restrepo-Garcia, J.R.; Baldovino-Medrano, V.G.; Giraldo, S.A. Improving the selectivity in hydrocracking of phenanthrene over mesoporous Al-SBA-15 based Fe–W catalysts by enhancing mesoporosity and acidity. *Appl. Catal. A,* **2016,** 510, 98-109.

[9] Lemberton, J-L; Guisnet, M. Phenanthrene hydroconversion as a potential test reaction for the hydrogenating and cracking properties of coal hydroliquefaction catalysts. *Appl. Catal.* **1984,** 13, 1, 181-92.

[10] Korre, S.C.; Klein, M.T.; Quann, R.J. Hydrocracking of Polynuclear Aromatic Hydrocarbons. Development of Rate Laws through Inhibition Studies. *Ind. Eng. Chem. Res.* **1997,** 36, 6, 2041-50.

[11] Benazzi, E.; Leite, L.; Marchal-George, N.; Toulhoat, H.; Raybaud, P. New insights into parameters controlling the selectivity in hydrocracking reactions. *J. Catal.,* **2003,** 217, 2, 376-87.

[12] Celis-Cornejo, C.M.; Perez-Martínez, D.J.; Orrego-Ruiz, J.A.; Baldovino-Medrano, V.G. Identification of Refractory Weakly Basic Nitrogenates in a Hydrotreated Vacuum Gas Oil and Their Effect Over a Ni-MoS2/Y-Zeolite␣Alumina Catalyst Aimed for Two-stage Hydrocracking. *(Submitted) Energy Fuels* **2017.**

[13] Gruia, A. Distillate hydrocracking. In: *Handbook of Petroleum Processing.* Dordrecht: Springer Netherlands; **2006,** p. 287-320.

[14] Corma, A.; Wojciechowski, B.W. Some ideas on cracking catalyst design. *Can. J. Chem. Eng.* **1982,** 60, 1, 11-6.

[15] Kumar, H.; Froment, G.F. A Generalized Mechanistic Kinetic Model for the Hydroisomerization and Hydrocracking of Long-Chain Paraffins. *Ind. Eng. Chem. Res.* **2006,** 46, 12, 4075-90.

[16] Baltanas, M.A.; Van Raemdonck, K.K.; Froment, G.F.; Mohedas, S.R. Fundamental kinetic modeling of hydroisomerization and hydrocracking on noble metal-loaded faujasites. 1. Rate parameters for hydroisomerization. *Ind. Eng. Chem. Res.* **1989,** 28, 7, 899-910.

[17] Alwahabi, S.M.; Froment, G.F. Single Event Kinetic Modeling of the Methanol-to-Olefins Process on SAPO-34. In *Ind. Eng. Chem. Res.,* **2004,** 43, 17, 5098-111.

[18] Weitkamp J. Catalytic Hydrocracking—Mechanisms and Versatility of the Process. *ChemCatChem,* **2012,** 4, 3, 292-306.

[19] Svoboda, G.D.; Vynckier, E.; Debrabandere, B.; Froment, G.F. Single-Event Rate Parameters for Paraffin Hydrocracking on a Pt/US-Y Zeolite. *Ind. Eng. Chem. Res.* **1995,** 34, 11, 3793-800.

[20] Frye, C.G. Equilibria in the Hydrogenation of Polycyclic Aromatics. *J. Chem. Eng. Data,* **1962,** 7, 4, 592-5.

[21] Restrepo-Garcia, J.R.; Baldovino-Medrano, V.G.; Giraldo, S.A. Improving the selectivity in hydrocracking of phenanthrene over mesoporous Al-SBA-15 based Fe–W catalysts by enhancing mesoporosity and acidity. *Appl. Catal. A* **2016,** 510, (Supplement C), 98-109.

[22] Motaghi, M.; Ulrich, B.; Subramanian, A. Slurry-phase hydrocracking—possible solution to refining margins. **2011,** 90, 2, 37-43.

[23] Speight, J.G. Chapter 1 - Refining Heavy Oil and Extra-heavy Oil. In: *Heavy and Extra-heavy Oil Upgrading Technologies.* Boston: Gulf Professional Publishing, **2013,** p. 1-13.

[24] Hsu C.S. Hydrotreating and hydrocracking: Fundamentals. Practical advances in petroleum processing. Springer; **2006,** p. 866.

[25] Furimsky E, Massoth FE. Deactivation of hydroprocessing catalysts. *Catal. Today* **1999,** 52, 4, 381-495.

[26] Al-Hajji, A.A.; Muller, H.; Koseoglu, O.R.; Caractérisation par spectrométrie de masse par résonance cyclotronique ionique à transformée de Fourier des composés azotés et soufrés dans les charges d'alimentation d'hydrocraquage. *Oil Gas Sci. Technol. - Rev IFP,* **2008,** 63, 1, 115-28.

[27] Jokuty, P.L.; Gray, M.R. Resistant nitrogen compounds in hydrotreated gas oil from Athabasca bitumen. *Energy Fuels,* **1991,** 5, 6, 791-5.

[28] Kekäläinen, T.; Pakarinen, J.M.H.; Wickström, K.; Vainiotalo, P. Compositional Study of Polar Species in Untreated and Hydrotreated Gas Oil Samples by Electrospray Ionization Fourier Transform Ion Cyclotron Resonance Mass Spectrometry (ESI FTICR−MS). *Energy Fuels,* **2009,** 23, 12, 6055-61.

[29] Dufresne, P.; Quesada, A.; Mignard, S. Influence of Nitrogen Feed Content On The Performances of A Zeolite Hydrocracking Catalyst. In: *Studies in Surface Science and Catalysis.* Elsevier; **1989,** p. 301-15.

[30] Barbosa, F.A.; Santos, A.C.Bd; Silva, M.I.Pd; Stumbo, A.M. Resistance to poisoning by nitrogen compounds of NiMo/Al-MCM-41 hydrocracking catalysts. *Catal. Today* **2004,** 98, 1, 109-13.

[31] Sau, M.; Basak, K.; Manna, U.; Santra, M.; Verma, R.P. Effects of organic nitrogen compounds on hydrotreating and hydrocracking reactions. *Catal. Today,* **2005**, 109, 1–4, 112-9.

[32] Barzetti, T.; Selli, E.; Moscotti, D.; Forni, L. Pyridine and ammonia as probes for FTIR analysis of solid acid catalysts. Journal of the Chemical Society, *Faraday Trans.* **1996,** 92, 8, 1401-7.

[33] Lercher, J.A.; Gründling, C.; Eder-Mirth, G. Infrared studies of the surface acidity of oxides and zeolites using adsorbed probe molecules. *Catal. Today,* **1996,** 27, 3, 353-76.

[34] Prins R. Catalytic hydrodenitrogenation. Advances in Catalysis. Academic Press; **2001,** p. 399-464.

[35] Kobayashi, M.; Togawa, S.; Ishida, K. Effects of Small Amounts of Nitrogen Compounds in Feedstock on Performance of Hydrocracking Catalyst. *J. Jpn. Petrol. Ins.,* **2007,** 50, 1, 44-52.

[36] Agudelo, J.L.; Hensen, E.J.M.; Giraldo, S.A.; Hoyos, L.J. Influence of steam-calcination and acid leaching treatment on the VGO hydrocracking performance of faujasite zeolite. *Fuel Process. Technol.*, **2015,** 133, 89-96.

[37] Liu, C.; Tranca, I.; van Santen R.A.; Hensen, E.J.M.; Pidko, E.A. Scaling Relations for Acidity and Reactivity of Zeolites. *J. Phys. Chem. C,* **2017,** 121, 42, 23520-30.

[38] Grimme, S.; Antony, J.; Ehrlich, S.; Krieg, H. A consistent and accurate ab initio parametrization of density functional dispersion correction (DFT-D) for the 94 elements H-Pu. *J. Chem. Phys.*, **2010,** 132, 15, 154104.

[39] Grimme, S.; Ehrlich, S.; Goerigk, L. Effect of the damping function in dispersion corrected density functional theory. *J. Comp.Chem.,* **2011,** 32, 7, 1456-65.

[40] Rozanska, X.; van Santen R.A.; Hutschka, F.; Hafner, J. A Periodic DFT Study of Intramolecular Isomerization Reactions of Toluene and Xylenes Catalyzed by Acidic Mordenite. *J. Amer. Chem. Soc*. **2001,** 123, 31, 7655-67.

[41] Demuth, T.; Benco, L.; Hafner, J.; Toulhoat, H.; Hutschka, F. Ab initio investigation of the adsorption of benzene in mordenite. *J. Chem. Phys.* **2001,** 114, 8, 3703-12.

[42] Demuth, T.; Hafner, J.; Benco, L.; Toulhoat, H. Structural and Acidic Properties of Mordenite. An ab Initio Density-Functional Study. *J. Phys. Chem. B*, **2000,** 104, 19, 4593-607.

[43] Bucko, T.; Benco, L.; Demuth, T.; Hafner, J. Ab initio density functional investigation of the (001) surface of mordenite. *J. Chem. Phys.*, **2002,** 117, 15, 7295-305.

[44] Baerlocher, C.; McCusker, L.B. Database of Zeolite Structures; 2017. Available from: http://www.iza-structure.org/databases/. **2017**].

[45] Janda, A.; Vlaisavljevich, B.; Lin, L-C.; Smit, B.; Bell, A.T. Effects of Zeolite Structural Confinement on Adsorption Thermodynamics and Reaction Kinetics for Monomolecular Cracking and Dehydrogenation of n-Butane. *J. Amer. Chem. Soc*, **2016,** 138, 14, 4739-56.

[46] Jia M, Lechert H, Förster H. I.r. studies on the acidity of dealuminated Y zeolite with different probe molecules. *Zeolites* **1992,** 12, 1, 32-6.

[47] Simon-Masseron, A.; Marques, J.P.; Lopes, J.M.; Ribeiro, F.R.; Gener, I.; Guisnet, M. Influence of the Si/Al ratio and crystal size on the acidity and activity of HBEA zeolites. *Appl. Catal. A*, **2007,** 316, 1, 75-82.

[48] Derouane, E.G.; Védrine, J.C.; Pinto, R.R.; Borges, P.M.; Costa, L.; Lemos, M. The Acidity of Zeolites: Concepts, Measurements and Relation to Catalysis: A Review on Experimental and Theoretical Methods for the Study of Zeolite Acidity. *Catal. Rev.* **2013,** 55, 4, 454-515.

[49] Tang, W.; Sanville, E.; Henkelman, G. A grid-based Bader analysis algorithm without lattice bias. *J. Phys. Condens. Matter,* **2009,** 21, 8, 084204.

[50] Kresse, G.; Marsman, M.; Furthmüller, J. VASP the GUIDE. Computational Materials Physics; **2016.** Available from: http://cms.mpi.univie.ac.at/vasp/vasp/vasp.html.

[51] Ferwerda, R.; van der Maas, J.H.; van Duijneveldt, F.B. Pyridine adsorption onto metal oxides: an ab initio study of model systems. *J. Mol. Catal. A.,* **1996,** 104, 3, 319-28.

[52] Castellà-Ventura, M.; Akacem, Y.; Kassab, E. Vibrational Analysis of Pyridine Adsorption on the Brønsted Acid Sites of Zeolites Based on Density Functional Cluster Calculations. *J. Phys. Chem. C,* **2008,** 112, 48, 19045-54.

[53] Bucko, T.; Hafner, J.; Benco, L. Adsorption and vibrational spectroscopy of ammonia at mordenite: Ab initio study. *J. Chem. Phys.,* **2004,** 120, 21, 10263.

[54] Rozanska, X.; Santen, R.Av. Chapter 6 - Reaction mechanisms in protonic zeolites. Computer Modelling of Microporous Materials. London: Academic Press; **2004,** p. 165-200.

[55] Gounder, R.; Iglesia, E. The Roles of Entropy and Enthalpy in Stabilizing Ion-Pairs at Transition States in Zeolite Acid Catalysis. *Acc. Chem. Res., 2012,* 45, 2, 229-38.

[56] Milas, I.; Chaer Nascimento M.A. A density functional study on the effect of the zeolite cavity on its catalytic activity: The dehydrogenation and cracking reactions of isobutane over HZSM-5 and HY zeolites. *Chem. Phys. Lett.,* **2006,** 418, 4–6, 368-72.

[57] Gounder, R.; Iglesia, E. Catalytic hydrogenation of alkenes on acidic zeolites: Mechanistic connections to monomolecular alkane dehydrogenation reactions. *J. Catal.* **2011,** 277, 1, 36-45.

[58] Gounder, R.; Iglesia, E. Effects of Partial Confinement on the Specificity of Monomolecular Alkane Reactions for Acid Sites in Side Pockets of Mordenite. Angewandte Chemie International Edition **2010,** 49, 4, 808-11.

[59] Nie, X.; Janik, M.J.; Guo, X.; Song, C. A computational investigation of ring-shift isomerization of sym-octahydrophenanthrene to sym-octahydroanthracene catalyzed by acidic zeolites. *PCCP*, **2012,** 14, 48, 16644-53.

[60] Song, T.; Zhang, Z.; Chen, J.; Ring, Z.; Yang, H.; Zheng, Y. Effect of Aromatics on Deep Hydrodesulfurization of Dibenzothiophene and 4,6-Dimethyldibenzothiophene over NiMo/Al2O3 Catalyst. *Energy Fuels,* **2006,** 20, 6, 2344-9.

[61] Davis, M.E.; Davis, R.J. Fundamentals of Chemical Reaction Engineering. McGraw-Hill. **2003.**

[62] Webb PA, Orr C. Analytical Methods in Fine Particle Technology. Micromeritics. **1997.**

[63] Leite, L.; Benazzi, E.; Marchal-George, N. Hydrocracking of phenanthrene over bifunctional Pt catalysts. *Catal. Today*, **2001,** 65, 2, 241-7.

[64] Hinman, R.L.; Whipple, E.B. The Protonation of Indoles: Position of Protonation. *J. Amer. Chem. Soc.*, **1962,** 84, 13, 2534-9.

[65] Kim, H.J.; Lee, C.H.; Shul, Y.G.; Min, W.S. Adsorption Characteristics of Nitrogen Compounds on Silica Surface. *Adsorpt. Sci. Technol.,* World Scientific; **2011,** p. 584-8.

[66] García-Martínez, J.C.; González Uribe, H.A.; González-Brambila, M.M.; Colín-Luna, J.A.; Escobedo-García, Y.E.; López-Gaona, A. Selective adsorption of nitrogen compounds using silica-based mesoporous materials as a pretreatment for deep hydrodesulfurization. *Catal. Today,* **2017.**

[67] Laredo, G.C.; Leyva, S.; Alvarez, R.; Mares, M.T.; Castillo, J.; Cano, J.L. Nitrogen compounds characterization in atmospheric gas oil and light cycle oil from a blend of Mexican crudes. *Fuel*, **2002,** 81, 10, 1341-50.

CHAPTER 4: Development of a Liquid-Solid ATR-IR Methodology for Studying Inhibitory Effects of Nitrogen-Containing Molecules in the Liquid Phase

Abstract

In situ approaches for studying the adsorption phenomena, are key for understanding the inhibitory effects on hydroprocessing catalyst. Considering the limitations that some IR *in situ* cells have to operate some probe molecules in the gas phase, a continuous flow ATR-IR cell was employed for studying the adsorption of pyridine and indole dissolved in n-hexane, on a USY zeolite film. An essential aspect that was overcome herein, was the possibility to follow the indole adsorption, which due to its low vapor pressure, present an inherent difficulty to operate in gas phase. Despite some noise was observed in the spectra due to water present in the vapor phase, the characteristic peaks for pyridine and indole adsorbed on silanol and Brønsted sites were distinguished. The implementation of quantum chemical calculations based on the DFT, for predicting the vibrational frequencies of the adsorbates over a zeolite surface, assisted the assignation of the observed signals. In addition, the analysis of the low-frequency region (>900 cm^{-1}) provided accurate information of the type of interaction. For pyridine the signals at 700 and 750 cm^{-1}, were associated to indole on silanol, meanwhile, the band at 684 cm^{-1}, was suggested to be proper of pyridine on Brønsted site. Similarly, for indole, the peak at 738 cm^{-1}, was important to follow the adsorption process. A weak signal located at 789 was attributed to the vibrational mode of indole on Brønsted sites. For both molecules, strong interactions were observed after flushing the solid film with n-hexane flow. Findings here exposed are crucial for studying inhibitory effects exerted by nitrogenated compounds on acidic materials.

Keywords: ATR IR *in situ*, liquid-solid, indole, pyridine, zeolite, Brønsted acidity, hydrocracking, inhibition, DFT, modeling.

Nomenclature

ATR-IR	Attenuated Total Reflectance Infrared Spectroscopy
DFT	Density Functional Theory
DFT-D3	Zero Damping Density Functional Theory Dispersive Correction
FT-IR	Fourier Transform Infrared Spectroscopy
GGA	Generalized Gradient Approximation
HCK	Hydrocracking
IR	Infrared Spectroscopy
IRE	Internal Reflection Element
MTC	Mercury Cadmium Telluride detector
PAW	Projector Augmented Wave Method
PBE	Perdew-Burke-Ernzerhof exchange-correlation functional
USY	Ultra-Stable Y Zeolite
VASP	Vienna Ab-initio Simulation Package
VGO	Vacuum Gas Oil
WBN	Weakly Basic Nitrogen-containing compounds

4. Development of a Liquid-Solid ATR-IR *in situ* Operando Methodology for Studying Inhibitory Effects of Nitrogen-Containing Molecules in the Liquid Phase

4.1. Introduction

The development of new methodologies and techniques for the characterization of materials under real operating conditions represents a primary issue for understanding adsorption at a molecular level. Infrared (IR) spectroscopy has been gaining importance as a basic analytical technique in experimental works in heterogeneous catalysis [1, 2]. Most of the scientific publications in catalysis in which IR spectroscopy characterizations are included make use of the transmission-adsorption and diffusive reflectance mode of analysis [3]. In this sense, IR cells for *in situ* studies working on transmission mode have been developed for characterizing materials under specific activation conditions [1]. These systems also enable the possibility to include probe molecules in the gas phase for obtaining information about the nature and physicochemical properties of specific catalytic surface sites. Lercher *et al.* [4] established a series of criteria for the selection of probe molecules for assessing key physicochemical properties of catalytic materials. Specifically, for studying acidic properties, the use of pyridine and ammonia has been extensively exploited [4, 5] as based on the principle of the interaction provided by the electron pair donor with the acid sites. Additionally, other nitrogenated probe molecules, such as lutidine and butylamine [6, 7], have been used for distinguishing Brønsted from Lewis acid sites. Nonetheless, compounds such as carbon monoxide are also widely used for studying acidity [8, 9].

A fundamental aspect of the characterization of the acidity of solids by IR analysis of adsorbed probe molecules is the possibility to discriminate whether the probe is in the gas phase or adsorbed

in the surface sites. Kubelkova *et al.* [10], published one of the first computational works regarding this topic. The Authors studied the formation of pyridine-zeolite complexes. The existence of an ion-pair complex H-bonded to the modeled zeolite cluster consisting of three tetrahedra (3T), $HOSiH_2(OH)AlH_2OSiH_3$, was determined. Figure 4.1 depicts the formation of the aforementioned ion-pair complex for the pyridine adsorbed on a model Brønsted site.

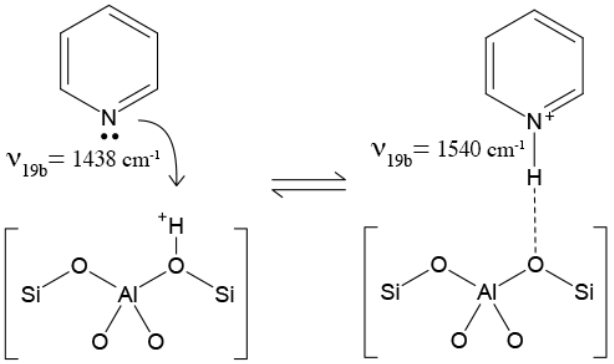

Figure 4.1. Formation of the pyridinium Ion-pair complex H-bonded to the oxygen adjacent to the aluminum atom.

In further studies, Ferwerda *et al.* [11] predicted the vibrational modes of H_2O-pyridine and HCl-pyridine complexes by means of the Hartree Fock method. Castellà-Ventura et al. [12] described the vibrational modes of pyridine adsorbed on a twelve tetrahedra (12T) cyclic cluster, for modeling the zeolite acid site. Authors draw attention to the importance of including dispersive interactions in the quantum mechanical model for future studies. Their results were in line with the formation of an ion-pair complex of pyridine H-bonded to the acid site, concluding that is energetically more stable than the non-protonanted hydrogen-bonded pyridine molecule. Thus, the accuracy of the theoretical assessment for predicting the characteristic bands in the IR spectrum for a specific interaction of probe molecules was clearly shown.

Certain signals of pyridine in the IR spectrum associated to specific vibrational modes, could shift when the molecule interact with the solid surface sites. In liquid phase, the ν_{19b} vibrational

mode of pyridine presents a characteristic IR at 1438 cm^{-1}. When pyridine becomes protonated over Brønsted acid sites this value shifts to ca. 1540 cm^{-1}. This also happens with other characteristic vibrational IR frequencies associated with Brønsted acid sites; namely, $\square_{19a}$, $\square_{8a}$, and $\square_{8b}$. Likewise, the frequencies associated to Lewis acid sites also exhibit specific shifting [11]. Despite such interesting possibilities, most of the IR cells for *in situ* studies concerning the analysis of adsorbed liquids are limited by the low vapor pressure of the probe molecules. For pyridine, the saturation of solid materials under vacuum conditions is relatively easy to perform because the vapor pressure of the molecule is about 2733 Pa at 298 K [13]. However, when the probe molecule exhibit low vapor pressure, its handling in the IR *in situ* cell becomes problematic, or unfeasible.

When the study in the vapor phase cannot be performed, the use of solvents for the characterization in liquid-solid systems with ATR-IR spectroscopy opened a wide range of possibilities for *in situ* studies under more realistic conditions [14]. Experimental setups concerning ATR-IR continuous flow [15-17], batch cells [18], and others [14] have been adapted for studying the adsorption of probe molecules in the liquid phase. Rivera *et al.* [15] performed pyridine adsorption in liquid phase over sol-gel films deposited over the ATR crystal with the aid of n-heptane and methanol as solvents. The experiment consisted in flowing a pyridine solution while several spectra were acquired following the accumulation of pyridine from a concentration of 0.3 to 580 mM. Despite some noise induced by the water present in the gas phase was observed, results were accurate enough; after subtraction of the solvent pattern, for describing the interactions displayed by the adsorbates and the solid films, using polar and nonpolar solvents. On the other hand, Panella *et al.* [18] using a liquid-solid ATR-IR batch cell studied the reactivity of amino functionalized silica coated magnetic nanoparticles of SiO_2/Fe_3O_4. This methodology provided a very accurate quantification of the pending groups attached to the soild, which are

available for reactivity with the organic molecules, even when the presence of water distorted the acquired spectra. In contrast, the other classical solid-state methods, such as XRD, overestimated the number of funcitonal groups, due to not all the pending groups are available for reactivity.

The aim hereof has been understanding the inhibitory effects exerted by nitrogen-containing compounds over the activity and selectivity of heterogeneous catalysts. In this regard, the inhibitory effects induced by basic nitrogen-containing molecules, those with the electron-pair donor ability, is broadly documented [19-21]. Nonetheless, the effect that weakly basic nitrogen-containing compounds (WBNs); e.g. indols, carbazoles, benzocarbazoles; exert over hydrocracking catalysts has only recently put in evidence [22]. Chpater 1 [22], confirmed that weakly basic nitrogen-containing compounds are the most abundant nitrogenates in a hydrotreated vacuum gas oil (VGO) with very low; ca. 20 ppm, total nitrogen content. With this background, the study of the effect ocassioned by carbazole and tetrahydrocarbazole on the performance of a Ni-MoS_2/Y-Zeolite␣Alumina catalyst was carried out in chapter 2, for the hydrocracking reaction of phenanthrene. Results from this study allow to conclude that even small amounts of these weakly basic nitrogen-containing compounds (<5 ppm of total N), exert a significant effect on the selectivity towards the hydrocracking products . Moreover, a blockage of the Brønsted acid sites of the catalyst was suggested, considering that an increase in the concentration of carbazole and tetrahydrocarbazole tend to inhibit more the cracking route which preferentially takes place on these sites.

In view of the foregoing, in this work, a methodology for analyzing the adsorption of pyridine and indole in a liquid solvent on a USY zeolite using a home-built continous flow ATR-IR cell is presented. Indole was selected as a model molecule for representing the behavior of weakly basic

nitrogen-containing compounds. It is worth mentioning that indole has a very low vapor pressure (1.6 Pa at 298 K). On the other hand, pyridine provides information of the acidic properties of the studied material, and may show how the basic compounds interact with the zeolite acid sites in the liquid phase. In addition, it helps validating the performed analyses. Experiments were complemented by density funcional theory (DFT) calculations to help interpretating results. A mordenite unit cell was employed for modeling a Brønsted acid site and associated terminal silanol groups, on the pore mouth of the zeolite. Periodic boundary conditions and a dispersive interaction correction were implemented during calculations. The findings of this work support the fact that weakly basic nitrogen-containing compounds adsorb strongly on the acid sites of zeolites. Moreover, the possible formation of protonated adsorbed indole species on the acid sites of the catalyst are also described herein.

4.2. Experimental section

In this section, the aspects concerning the setup of the continuous flow ATR-IR cell are first explained, followed by the description of the methodology and the conditions employed for spectra acquisition. Afterwards, the methods for DFT calculations are exposed. Methods comprise the methodology for modeling the mordenite system and the interactions between pyridine and indole with the model Brønsted acid site and a terminal silanol group are shown.

4.2.1. Continuous Flow Attenuated Total Reflectance Infrared Cell. Tests were carried out with a home-built continuous flow ATR-IR cell setup whose schematics are shown in Figure 4.2.

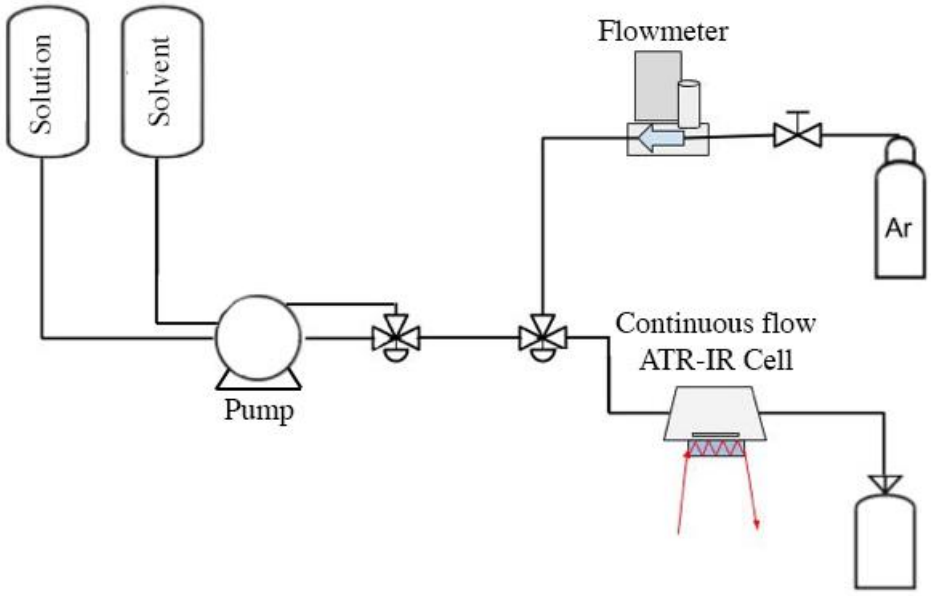

Figure 4.2. Continuous flow ATR-IR cell setup. The solution comprises the diluted probe molecule in n-hexane, the other recipient (solvent) contains pure n-hexane.

The cell consisted of a dome-like device mounted on the ATR-IR crystal which allows the entrance of gas and liquid flows, and is controlled by a 3-way valve. The Internal Reflection Element (IRE) was provided with a Specac Golden Gate ATR device along with a ZnSe crystal and one reflection beam. IRE was placed in a Nicolet iS50 FT-IR spectrometer equipped with a nitrogen cooled MCT detector under N_2 flow for purging. Two recipients, one containing the solution with indole and another containing the pure solvent were connected simultaneously to a multi-channel peristaltic pump (Ismatec). An additional 3-way valve was employed for switching from the flow from the solution to the solvent. The solvent employed was n-hexane (99%, Sigma-Aldrich), and the tests solutions were 1 wt.% of pyridine (99.9%, Merck) and 0.2 wt.% of indole (>99%, Sigma-Aldrich). The indole solution was less concentrated due to its low solubility in non-polar hydrocarbons (pKa=16.97 [23]). Finally, a recipient was employed for storing the liquid effluent from the cell before its final disposition.

4.2.2. Methodology and contitions for liquid-solid ATR-IR experiments. An IR background was always taken with the empty cell under a flow of argon 30 ml·min-1 before adsorption tests. Each spectrum was recorded after 32 scans using a resolution of 4 cm-1. Spectra from the liquid solution and the solvent were recorded after reaching steady state conditions. The latter were normally reached after feeding 3 ml·min-1 of both liquids separately for 10 min. For depositing of a solid film of the sample onto the ATR crystal the method proposed by Davantès et al. [16] was addapted. Accordingly, a droplet of a concentrated USY zeolite (CBV760, zeolyst) suspension was put on top of the ATR-IR crystal and left to dry. The acidic properties of the USY zeolite employed were measuered with pyridine adsorption in a IR in situ cell, the spectra and the information are available in Annex D, Figure D1. Thereafter, the deposited solid was dried in situ under an Argon flow of 30 ml·min-1 and 473 K during 2 h. A stable solid film fairly resisting the shear tension of the liquid flow was achieved. After drying, the n-hexane were put in contact with the sample. From this point onwards, a loop for the rapid acquisition of ATR-IR spectra, which takes spectra each 20 seconds, was used to follow the accumulation of the adsorbed n-hexane. The spectrum of the solid film saturated with n-hexane was taken as a reference to obtain the difference spectra, in order to eliminate the strong signals of the solid+n-hexane from spectra, to better watch the accumulation and flushing of the probe molecules. A factor of 1 was used for the subtraction of the reference spectrum. Afterwards, the flow was switched to the corresponding test solution containing the indole using the same flow rate until reaching saturation. Desorption of the weakly or non-adsroebd probe molecules was induced by switching back the liquid flow to n-hexane for several minutes. Finally, the solids were dried under argon flow at room temperature in order to analyze the adsorbed species remaining after these treatments.

4.2.3. Computational details. DFT calulations were carried out using the Vienna Ab-initio Simulation Package (VASP) considering periodic boundary conditions and pseudopotentials. The Projected Augmented Wave (PAW) method with the Perdew-Burke-Ernzerhof (PBE) exchange-correlation functional were implemented for all the calculations. An energy cut-off of 600 eV was set, with a □-point for sampling the Brillouin-zone. A smearing of 0 and a sigma parameter of 0.5 were chosen. Grimme's density functional dispersive correction with zero damping (DFT-D3) [24] was included to account for dispersive interactions [25]. A more detailed description is found in Chapter 3.

The external surface of the (001) plane of a mordenite zeolite was modeled following the procedure described in Chapter 3 [26]. Mordenite was chosen instead of faujasite due to the considerably smaller amount of atoms; 144 for mordenite and 600 for faujasite, within the unit cell of the latter, for saving computational resources. In addition, the adsorption is modeled in the pore mouth of the mordenite. In this regard, the choice of mordenite, which has a 12T main cavity, for predicting the vibrational frequencies instead of faujasite should not significantly affect the calculated frequencies. The later, based on a theoretical finding which evidenced that the stretching mode of the O-H group of Brønsted acid sites are not significantly affected by the position of the aluminum atom in the different cavities of the framework [27]. Additionally, IR *in situ* pyridine adsoprtion on different Y-zeolites and on mordenite showed the pyridine characterisic bands almost at the same frequency values [5]. Recent works have theoretically shown that the steric effects and the zeolite framework topology influence more on the stabilization of the transition states during reactions due to the different confinement [28, 29]. In this regard, was also shown that the strength in the acidity, which is well described by the adsorption energy of electron donor basic molecules, is more related to the chemical composition of the zeolite than the morphology

[28]. A Brønsted acid site was simulated by replacing one silicon atom for an aluminum one, and subsequently hydrogenating the adjacent oxygen atom for stabilizing the charge. The T2 position of the Brønsted acid site on the twelve tetrahedra principal cavity was chosen following Demuth's *et al.* [30] assumption that this represents the more stable conformation. Terminal silanol groups were created when completing with hydrogen atoms the unbonded oxygen atoms, that are generated when the zeolite unit cell is duplicated in z-axis and then is cut by the 001 plane and a vacuum of 10 Å in z-axis is added. The optimized 193-atom structure of the external surface of mordenite is shown in Annex D. Figure D2. The acid characteristics of the modeled Brønsted site in the pore mouth of the mordenite were validated in Chapter 3 [26], calculating the vibrational frequency of the O-H group adjacent to the aluminum atom, and the atomic charge of the the hydrogen atom. A charge of +0.75 and a frequency of 3603.9 cm^{-1}, which fairly represent the characteristics of a Brønsted acid site [27, 31].

Pyridine and indole were first optimized in a vacuum cube box with an edge length of 25 Å and a frequency calculation was subsequently performed for obtaining the data of the isolated gas phase molecules. For modeling the adsorption of pyridine and indole on the Brønsted acid site, the molecules were set at a distance of 1.5 Å from the hydrogen atom of the Brønsted site, interacting by the nitrogen atom, which is a suitable distance for the initial configuration [12, 26] in order to perform the geometry optimization of the interactive complexes. Figure 4.3 depicts the interactions evaluated in the case of indole. The ion-pair complexes were observed for both molecules when interacting with the Brønsted acid site, as reported in a previous work . Frequency calculations of the vibrational modes were performed for the interacting surface complexes and its neighbors, e.g.: pyridine-H^+---O-Al, indole-H^+---O-Al, pyridine---H-O-Si and indole---H-O-Si. Thereby, the

comparative calculated data for assessing the liquid phase adsorption of pyridine and indole on the zeolite was obtained.

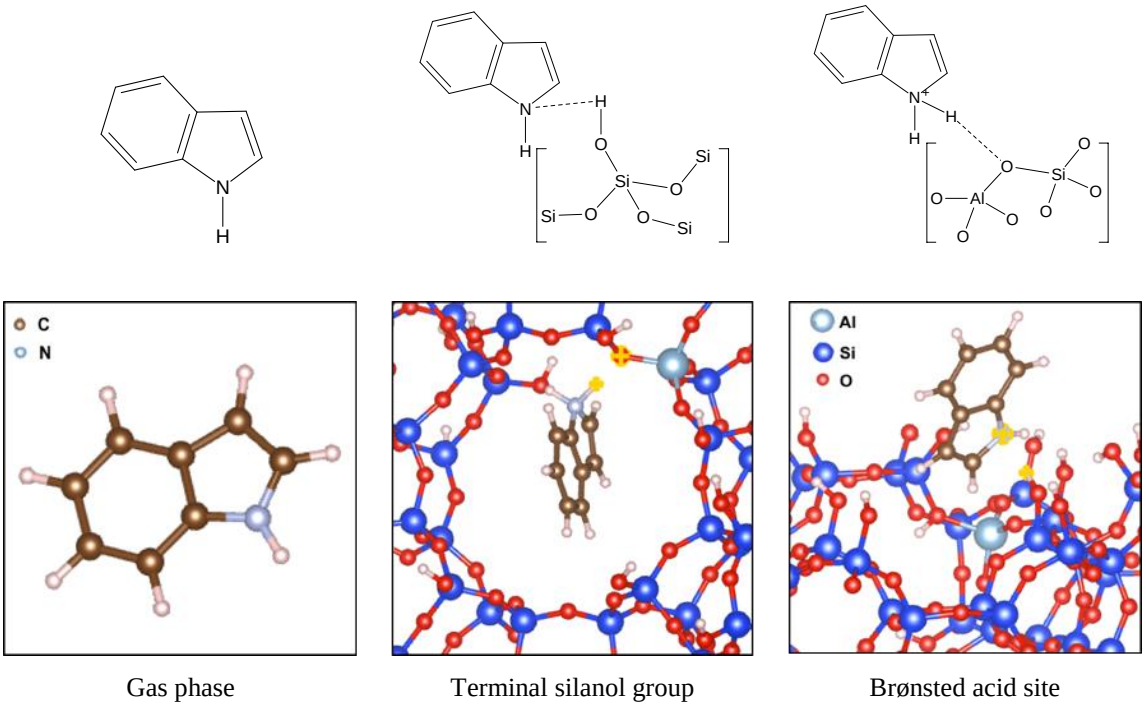

Gas phase Terminal silanol group Brønsted acid site

Figure 4.3. The three configurations evaluated for the calculation of the vibrational frequencies for indole. In yellow the interactin atoms.

4.3. Results and discussion

4.3.1. Theoretical predicted vibrational frequencies. Results from the theoretical calculations aiming to predict the vibrational frequencies of the adsorbed complexes are firstly discussed for pyridine and then for indole.

4.3.1.1. Adsorption of pyridine on a silanol group and a Brønsted acid site. In FT-IR in situ studies, pyridine adsorption is normally analyzed within the range between 1400 and 1700 cm-1 [11]. According to Wilson's vibrational mode numbers described for the benzene [32], pyridine vibrational modes located in this range are □8a, □8b, □19a and □19b. The corresponding atomic

displacements for the aforementioned vibrational modes correspond to in-plane motions, and it could be seen in Figure 4.4.

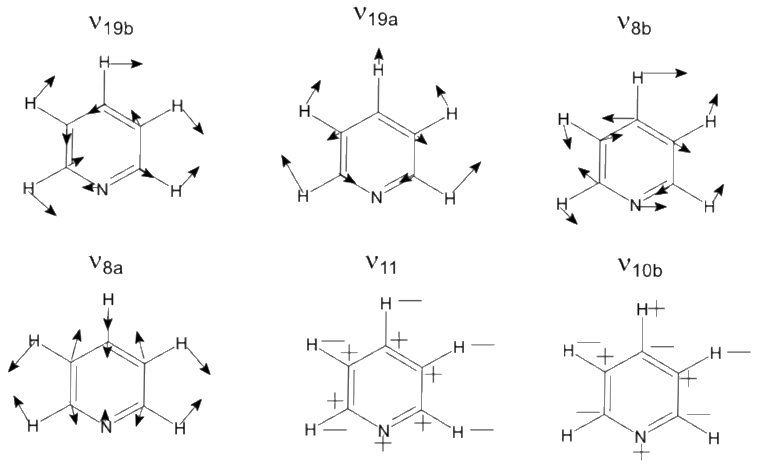

Figure 4.4. Atomic displacements for the commonly studied vibrational modes of pyridine.

Table 4.1.

Predicted values for the pyridine adsorption on silanol and Brønsted sites. Values reported in parentheses are the corresponding shifting values, the experimental data was obtained from ref. [33, 34].

	Pyridine frequencies (cm^{-1})						
Vibrational mode*	**Gas phase**		**Silanol group**		**Brønsted site**		
	Calc.	**Exp.**	**Calc.**	**Exp.**	**Calc.**	**Other [12]†**	**Exp.**
8a	1587	1590	1595 *(+7)*	1590–1600 *(0– +10)*	1634 *(+47)*	1643 *(+39)*	1640 *(+50)*
8b	1574	1581	1573 *(-1)*	1580–1590 *(-1– +9)*	1621 *(+47)*	1669 *(+78)*	1620 *(+39)*
19b	1432	1442	1437 *(+5)*	1440–1447 *(-2– +9)*	1547 *(+115*)	1563 (+118)	1540 *(+98)*
19a	1472	1483	1475 *(+3)*	1485–1490 *(+2– +7)*	1485 *(+13)*	1486 (0)	1485–1500 *(+2– +17)*
10b	699	700	706 *(+7)*	-	686 *(-13)*	-	680 *(-20)*
11	742	744	745 *(+3)*	-	721 *(-21)*	-	-

*Wilson's numbers for the vibrational modes of the benzene ring. † Theoretical data from other work, calculated for the pyridine interaction on a Brønsted acid site in a $12T_{OH}$ zeolite cluster using the *B3LYP/6-31G(d,p)*, as reported in reference [12].

Table 4.1 shows predicted (not scaled) and experimental values for each of these vibrational modes [33, 34]. Besides the 1400 and 1700 cm^{-1} region, the region between 670 and 850 cm^{-1} exhibits some intense bands [34] that may provide information about pyridine adsorption in the liquid-solid ATR-IR analysis. The later by considering the noise observed in spectra acquired in liquid-solid ATR-IR *in situ* operando cells, due to the presence of water in the gas phase [15, 18]. According to this, in the region of low frequency (900 – 600 cm^{-1}), is not visible the perturbation occasionated by water in the gas phase. The ν_{10b} and ν_{11} modes are two characteristic signals of pyridine within the low-frequency range, and they are attributed to out-of-plane motions (Figure 4.4).

Concerning the predicted values for pyridine in the gas phase presented in Table 4.1, a good prediction of the vibrational frequencies is observed, compared to experimental data [33]. The interaction of pyridine on silanol is characteristic of a physisorption, as the distance between the adsorbate and the H atom of the acid site is too large to be considered a chemical interaction (see optimized configurations provided in Annex D, Figure D3). The vibrational frequency shiftings predicted for pyridine in silanol, are in good agreement with those values experimentally obtained [34], except for the ν_{8b} mode, for which almost no shifting was obtained. In all cases, a slight vibration of the O-H group of silanol, which accompanied the vibrations of the pyridine atoms, is observed, except for the $\square_{8b}$ mode, for which the H atom remains motionless. There is no previous report in this regard. For this kind of physical interaction, the characteristic vibrations of the pyridine atoms are very similar to those observed for pyridine in the gas phase. Only when the interaction is strong enough, that is to say, a chemisorbed complex of pyridine in a Brønsted site, some changes are appreciable in the motions of the pyridine atoms [11, 12]. This changes could explain the observed shiftings which are characteristic of the ion-pair H-bonded complexes

described in the literature [10, 12]. For the interactions of pyridine on the Brønsted sites, the predicted shiftings of the vibrational modes are well replicated, but for the ν_{8b} and ν_{19b}, the predicted values are slightly high as compared to the experimental data, respectively. This trend has been described by Castellà-Ventura *et al.* [12], in an earlier theoretical work. In that study, the authors modeled the adsorption of pyridine on a Brønsted site, considering three different sizes of clusters, namely, three tetrahedra completed with hydrogen atoms ($3T_H$) $H_3Si(OH)AlH_2OSiH_3$, $12T_H$ cluster completed with hydrogen atoms, and $12T_{OH}$ cluster completed with hydroxyls. Better results were obtained for the $12T_{OH}$ size cluster, so they concluded that a cluster that contains a larger number of atoms is more appropriate for modeling the vibrational frequencies. These values are also reported in one column in Table 4.1. In line with this conclusion, the predicted values obtained in this work are more realistic than those predicted for the $12T_{OH}$ size cluster, taking into account that the adsorption was carried out on a Brønsted acid site located in the pore mouth of a 193-atom mordenite. Analyzing the region of low-frequency; i.e. 670 – 850 cm^{-1}, two intense bands are observed, ν_{10b} and ν_{11}, which correspond to out-of-plane vibrations. For the ν_{10b} mode in silanol, a small shift is observed, meanwhile, for interactions in Brønsted site, a characteristic band at 684 cm^{-1} of pyridinium is described [34]. This observed shifting which is particular of pyridine chemisorbed on Brønsted sites could be helpful for assessing the analysis of the liquid-solid ATR-IR acquired spectra in the region of low-frequency.

4.3.1.2. Adsorption of Indole on a silanol group and a Brønsted acid site . Next, the predicted vibrational frequencies (not scaled) for indole in the gas phase and interacting with a silanol terminal group and a Brønsted acid site of mordenite, are shown in Table 4.2.

Table 4.2.

Predicted values for the indole in the gas phase and adsorbed on silanol and Brønsted sites.

Indole Frequencies (cm^{-1})				
Vibrational modes	*Intensity**	*Gas Phase*	*Silanol Group*	*Brønsted Site*
N–H Stretching	vs	3509	3549	3144
Symmetric and Antisymmetric H Stretching	w	3203	3205	3211
	w	3185	3186	3185
	sh	3137	3138	3163
	s	3126	3128	3156
	s	3116	3120	3142
	sh	3110	3111	3130
N^+–H Stretching	-	-	-	1890
In-Plane Quadrant and Semicircular Stretching of the rings	w	1621	1618	1621
	-	-	-	1610
	m	1573	1574	1602
	vw	1508	1508	1560
	s	1485	1483	1474
	s	1446	1441	1449
	s	1416	1411	1401
	sh	1356	1352	1377
	s	1344	1343	1321
	-	-	-	1287
	s	1280	1271	1228
	m	1239	1238	1259
	vw	1196	1195	1157
H Scissoring	vw	1150	1149	1162
In-Plane Stretching of the ring	m	1121	1119	1080
In-Plane Stretching of the ring	s	1091	1085	980
H Scissoring	sh	1065	1064	1119
Rocking of the NH_2^+ group	-	-	-	1033
In-Plane Stretching of the ring	m	1016	1015	1023
Out-of-plane vibrations of the rings and H atoms	vw	957	957	989
	s	916	918	943
	sh	886	887, 880	871
	vw	864	862	837
	sh	840	858	912
	s	832	836	865
	sh	759	756	735
	vs	756	765	-
	vs	731	736	742,763
	w	709	726	700

*Intensities were assigned to the calculated modes in the gas phase, based on the IR spectra in the gas phase of indole reported in the NIST webbook [36], and contrasted with the IR spectra of indole [35, 37]. Abbreviations: vs, very strong, s, strong, m, medium, w, weak, vw, very weak, sh, shoulder

The solid spectrum compared to that in the gas-phase presents some discrepancies because it is slightly redshifted, but in consideration of this, the intensities fit well. Observing the assigned intensities of the computed frequencies for the gas phase, the strongest signals are located in three specific regions in the IR spectrum, namely, 700 to 1000 cm^{-1}, 1200 to 1500 cm^{-1}, and above 3000 cm^{-1} [37]. The first region from 700 to 1000 cm^{-1}, where some vibrational modes corresponding to out-of-plane motions are present, i.e. frequencies at 731 and 832 cm^{-1}.

Considering the noise in the spectra induced by water in the gas phase, which makes difficult the interpretation of the variability of the bands with weak intensities, the analysis of the low-frequency region again is key for following the indole adsorption process. The second region between 1000 and 1500 cm^{-1} has several peaks attributed to in-plane vibrational modes of the 6 and 5-membered rings; i.e. 1280, 1344, 1416 and 1446 cm^{-1}. Figure 4.5 depicts the displacements of the in-plane vibrational frequencies calculated for the indole in the gas phase. Callis *et al.* [38], theoretically calculated the vibrational frequencies of isolated indole with the perturbational *ab-initio* method MP2/6-31G(d). In their results, the mode at 1278 cm^{-1} whose intensity must be strong [39], was predicted at an appreciable lower value. In this work, the frequency at 1280 cm^{-1}, correctly matches with the vibrational mode of strong intensity (see Figure 4.5). Finally, the third region, above 3000 cm^{-1}, has signals with high intensity normally assigned to hydrogen stretching; specifically between 3110 and 3137 cm^{-1}, and the band attributed to N-H stretching at 3590 cm^{-1}.

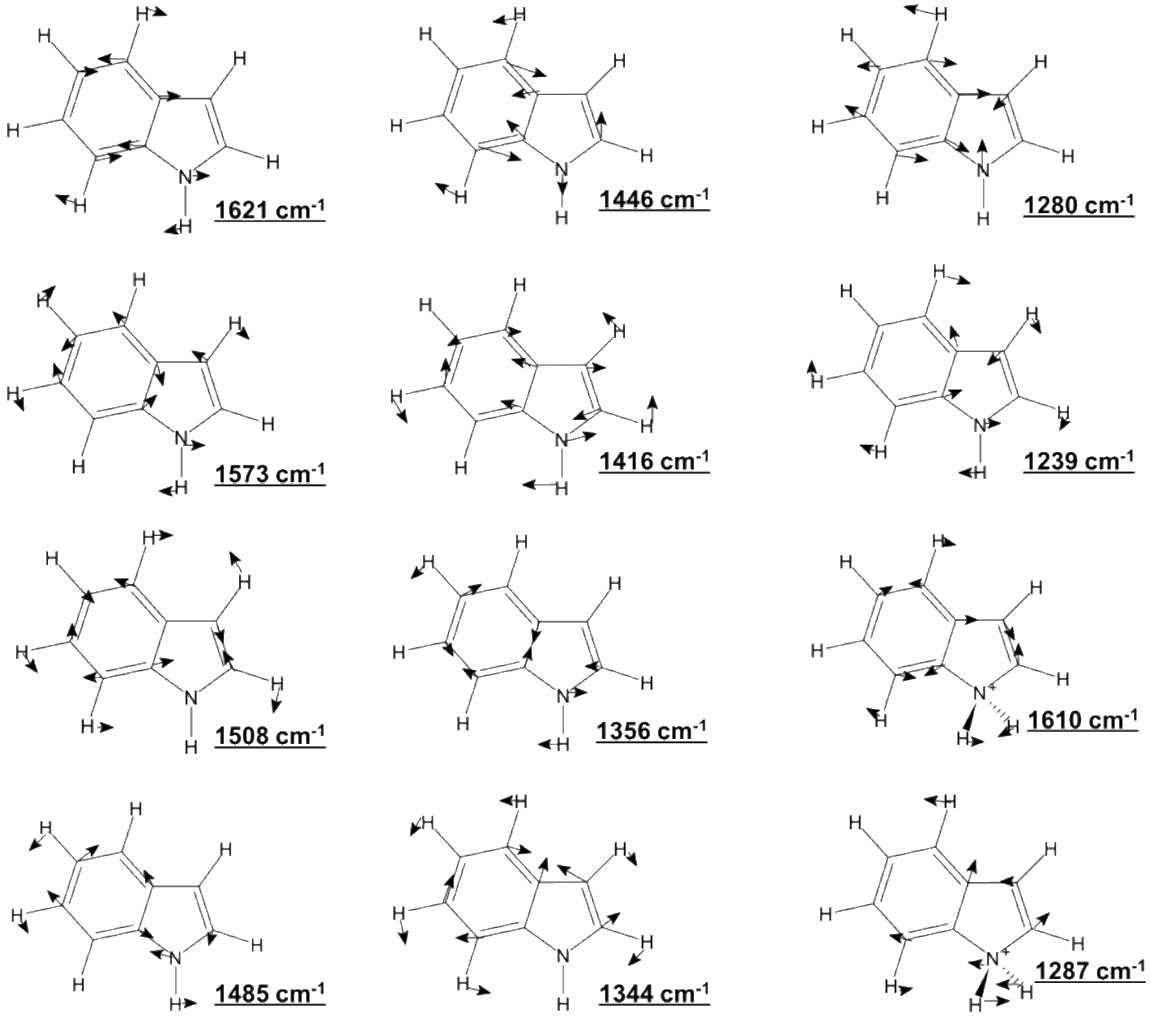

Figure 4.5. Atomic displacements for in-plane vibrational modes of indole in the gas phase from 1200 to 1700 cm^{-1}. Frequencies at 1287 and 1610 cm^{-1} correspond to additional in-plane modes calculated for indole adsorbed on a Brønsted acid site.

The predicted values of the vibrational frequencies for the interactions of indole with a silanol group exhibited some small shiftings as compared to the gas phase spectra. This obeys the fact that indole is physisorbed on silanol, as proposed in an earlier work. In this sense, indole physisorbed on a silanol group keeps the same atomic motions as in the gas phase. The highest shifting value was observed for the N-H stretching which changed from 3590 cm^{-1} in the gas phase to 3549 cm^{-1} in the interaction indole-silanol. This could be a consequence of the type of interaction N---H-O

which affects more the vibrational modes of the nitrogen atom. A similar trend regarding the marked shifting in the stretching mode of the N-H group was observed in a theoretical work focused on studying the ammonia adsorption on different silanol groups and Brønsted sites of a mordenite [40]. The N-H stretching modes of ammonia showed a higher shifting when interacting with silanol than that observed for the bending modes. Small shiftings are also observed for the most intense bands in the region between 1000 and 1500 cm^{-1}. Going to the region of low-frequency, the values at 731 and 756 cm^{-1} which in the spectra of indole in the gas phase have a very strong signal, for the indole-silanol interaction, are shifted to 736 and 765 cm^{-1} respectively. In addition, the frequency at 832 cm^{-1} has a strong intensity in the gas phase and this value is slightly shifted to 836 cm^{-1}. These small shiftings should be visible in the indole spectra obtained with the liquid-solid ATR-IR. On the contrary, for indole interacting with a Brønsted acid site, as for pyridine, the calculations predict marked shiftings in some frequencies with strong intensities. This could be attributed to indole protonation on Brønsted acid sites, as it was shown in a previous theoretical work , which causes an appreciable change in the vibrational modes of the adsorbed molecule. Even, some additional modes are predicted, e.g. 1033, 1287, 1610 and 1890 cm^{-1}. Frequencies at 1287 and 1610 cm^{-1} correspond to in-plane vibrations of the indole rings (see Figure 4.5), while the frequencies at 1033 and 1890 cm^{-1} are respectively rocking of the NH_2^+ group and N^+-H stretching modes. One noticeable fact that is worth mentioning, concern the N-H stretching band shifting from 3590 cm^{-1} in the gas phase to 3144 cm^{-1} for indole on a Brønsted acid site. In this region, the N-H stretching shifted signal will be overlapped by the signals of the hydrogen stretching modes. Larrubia *et al.* [41] suggested that the indole and carbazole are dissociatively adsorbed on the Brønsted sites of metal oxides, based on the observation of the disappearance of the characteristic N-H stretching band experimentally observed at 3420 cm^{-1} for solid indole. As

the theoretical calculation showed, the disappearance of the N-H stretching band could be also attributed to indole protonation on Brønste sites without breaking the N-H bond, which is a step suggested for dissociative adsorption. Another interesting behavior was obtained from the calculated frequencies of indole on a Brønsted acid site in the region of low-frequency, and it concerns the redshiftings of the frequency at 731 cm^{-1} in the gas phase to 742 and 763 cm^{-1}, both describing out-of-plane motions of the hydrogen atoms.

Results of the predicted vibrational frequencies for indole in the gas phase, and adsorbed on a silanol terminal group and a Brønsted site of a mordenite can be summarized as follows: (i) for interactions of indole with silanol groups small shiftings were obtained, and this could be helpful for describing indole adsorption on weak Brønsted acid sites; (ii) shifting of the vibrational modes in the low-frequency region could provide interesting information about the adsorption on the different acid sites of the zeolite in the liquid-solid ATR-IR experiments, considering the presence of very strong singals due to the out-of-plane vibrations; (iii) formation of an ion-pair complex resulting from the strong interactions of indole with Brønsted sites, influences the shifting of the N-H stretching to a lower value close to the region where the strong signals of the hydrogen stretching modes are located.

4.3.2. Liquid-solid ATR-IR experiments. In this section, the description of the experiments for pyridine and indole adsorption on a USY zeolite film in the liquid phase characterized with ATR-IR in situ is exposed.

4.3.2.1. Pyridine adsorption on USY zeolite. Figure 4.6 shows spectra for pyridine adsorption over the USY zeolite film in the liquid phase (solid line) and the spectrum of the adsorbed pyridine which remains after flushing the solid film with n-hexane for removing the weakly or non-adsorbed species (dashed line). Difference spectra were obtained by subtracting the spectrum of the n-hexane in the solid.

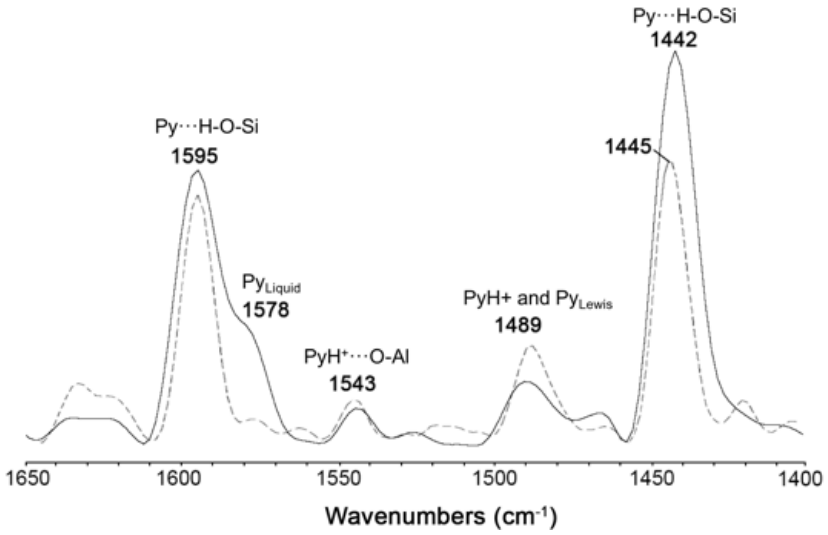

Figure 4.6. ATR-IR difference spectra of the pyridine in n-hexane adsorption in the USY zeolite film, obtained by subtracting the spectrum of solid saturated with pure n-hexane. The solid line is the steady state adsorption of the pyridine solution and the dashed line is the desorption of the weakly adsorbed species by passing through the solvent

Rivera *et al.* [15] reported a similar pattern for pyridine adsorption in the liquid phase on a silica, which allowed to observe the characteristic peaks of pyridine physisorbed and one weak attributed to pyridinium ions, indicating the presence of highly acidic silanols capable to transfer a proton. They also highlighted the presence of noise in the spectra ascribed to water in the vapor phase, which makes difficult to discern the peaks in the region between 1200 and 1600 cm^{-1}.

Peaks at 1578 and 1595 cm-1, in Figure 4.6, are attributed to the pyridine ν_{8a} mode in the liquid phase and to pyridine interacting with silanol groups, respectively, are clearly appreciable in the

spectrum described by the solid line, along with the peak located at 1442 cm^{-1} which was also attributed to pyridine adsorbed on silanol (ν_{19a}). After flushing with n-hexane (dashed line) to drag the weakly or non-adsorbed molecules, the shoulder observed at 1578 cm^{-1} disappeared and the band at 1442 cm^{-1} was shifted to 1445 cm^{-1}. The DFT calculations also predicted a small shifting of the band attributed to the ν_{19a} mode from pyridine in the gas phase, to pyridine physisorbed on silanol (see Table 4.1). These results confirm the remotion of pyridine in the liquid phase, showing also that after passing the solvent pyridine remained adsorbed. In addition, the characterization of the acidity with pyridine adsorption in the gas phase on the USY zeolite in the IR *in situ* apparatus (see Annex D), allowed to see the presence of strong Brønsted acidity was determined. In this sense, The peaks normally attributed to pyridinium species; 1543 cm^{-1} and 1489 cm^{-1}, are observed in similar positions. As mentioned, the noise induced by water in the gas phase distort the spectra in this region between 1200 and 1600 cm^{-1}. For such reason small bands are observed widespread across the spectra shown in Figure 4.6, representing a difficulty for making a correct estimation of the proportion of pyridinium species with respect to the physisorbed pyridine on silanol. A ratio of the areas of the peaks could give an idea of the proportion of pyridine adsorbed on silanols and Brønsted acid sites. Thus, the ratios of the areas of the peaks located at 1595 and 1543 cm^{-1}, for pyridine adsorption in the gas phase performed in the IR *in situ* apparatus and for the liquid-solid ATR-IR experiments give values of 4.0 and 6.5, respectively. Comparatively, this is a fair estimation of the ratios of the areas which describes the proportion of pyridine adsorbed on silanols and Brønsted acid sites. In this regard, other experimental works have made fair estimations of the number of active sites available for reaction, despite of the reported noise [15, 18].

Focusing on the region of low-frequency from 700-900 cm^{-1}, Figure 4.7 depicts the (a) evolution of the spectra for pyridine adsorption on the USY zeolite film, (b) flushing with n-hexane

flow, and (c) drying under argon flow at room temperature. In all stages, the presence of intense bands at 700 and 750 cm^{-1} is an evidence of pyridine adsorbed over silanol groups. These bands were predicted by the DFT calculations at 700 and 744 cm^{-1}, respectively (see Table 4.1). Additionally, a band at 684 cm^{-1} was observed in the spectrum of desorption under n-hexane flow (Figure 4.7b) and also after drying with argon (Figure 4.7c). This band could be assigned to an out-of-plane mode of pyridinium species, as predicted in the calculations (see Table 4.1). No other band was predicted between 650 and 700 cm^{-1} for the considered interactions of pyridine with a silanol group and a Brøsnted sited in the DFT calculations. The negative band at 830 cm^{-1} which changed to positive after drying the solid under argon flow, is normally attributed to Si-O stretchings of silanol groups [42]. The change in this signal is explained by the nature of the experiment. N-hexane is a non-polar solvent which is expected to present weak interactions with the active sites of the USY zeolite film, on the contrary, pyridine exhibits stronger interactions with the active sites of the solid film leading to a higher accumulation of these molecules into the pores of the solid and on the external surface. As a consequence, the intensity of the Si-O stretching signal is decreased when the solid is saturated with pyridine. As the spectra shown is differenced taking as reference the spectrum of the solid film saturated with n-hexane, a negative band is observed. While the remaining pyridine in liquid solution is flushed out with n-hexane flow, and after drying, the intensity of the Si-O stretching signal is recovered.

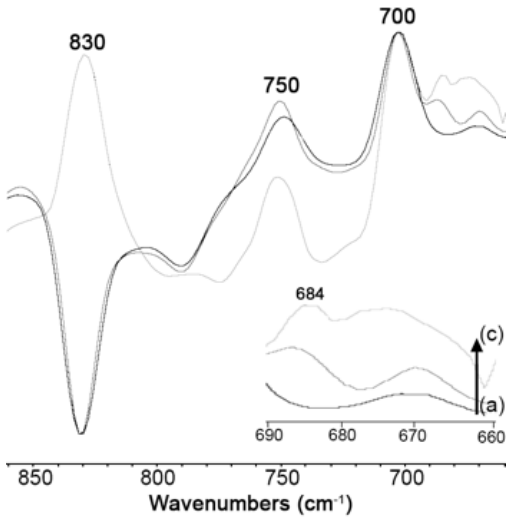

Figure 4.7. ATR-IR difference spectra in the region of low-frequency, obtained by subtracting the spectrum of solid saturated with pure n-hexane, of (a) pyridine adsorption in n-hexane, (b) desorption under pure n-hexane flow and (c) drying under Argon flow.

In summary, pyridine adsorption in the liquid phase on a USY zeolite was successfully characterized *in situ* using ATR-IR spectroscopy. The analysis in the region that comprises the range between 1200 and 1600 cm^{-1}, showed that despite the presence of noise induced by water in the gas phase, the intensity of the vibrational modes of pyridine is good enough to make a good estimation of the acidic properties of the solid film. The theoretical assessment based on the DFT calculations allow assigning a characteristic peak of pyridinium species at 684 cm^{-1}, in the region of low-frequency, which was attributed to out-of-plane motions of the atoms.

4.3.2.2. Indole adsorption. Difference spectra of the indole adsorption on the USY zeolite while flowing the indole solution until saturation is shown in Figure 4.8, for the regions between 3450 – 3510 cm-1 and 700 – 900 cm-1. The region comprising the values from 1200 – 1600 cm-1 is not studied herein, due to the noise induced by water vapor (see the spectra in Annex D, Figure D4).

Moreover, the indole bands located in the aforesaid region are not very strong, adding more difficulty to interpret the spectra. The spectra in Figure 4.8 correspond to subtraction of the spectrum of the solid film saturated with n-hexane from the spectra taken at different indole coverages (followed with the acquisition loop).

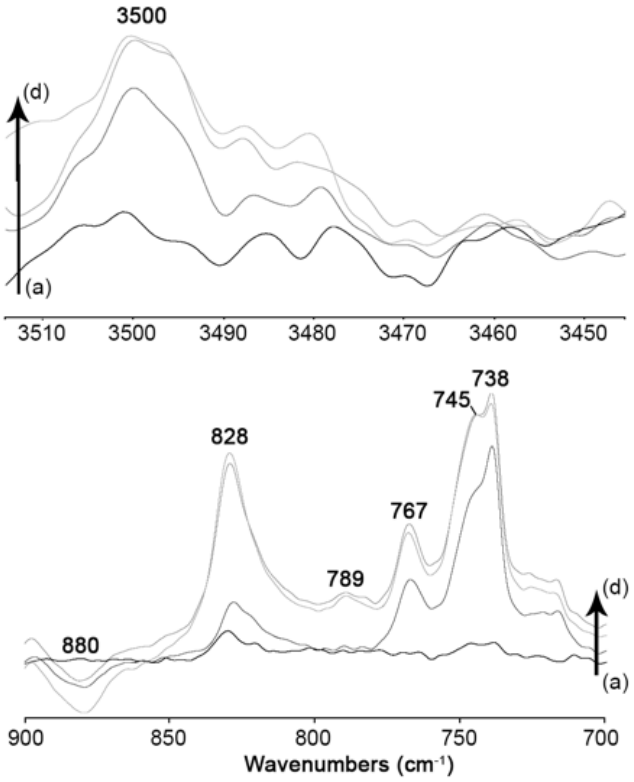

Figure 4.8. ATR-IR difference spectra of the indole adsorption on the USY zeolite at different coverages, obtained by subtracting the spectrum of solid saturated with pure n-hexane, from (a) initial time to (d) saturation, in the regions of high (3450 – 3510 cm^{-1}) and low frequency (700 – 900 cm^{-1}).

The high-frequency region, where the N-H stretching band of the indole should appear is also very affected by the noise induced by the water present in the vapor phase. Notwithstanding, a broadband around 3500 cm^{-1} starts to appear when flowing the indole solution, this may indicate the accumulation of indole in the liquid phase into the pores of the solid film. Going down to the low-frequency region, between 700 and 900 cm^{-1}, where no noise attributed to water in the vapor phase was present, the appearance of very strong indole signals (see Table 4.2) was observed. The

peaks at 738 and 828 cm^{-1} were ascribed to indole in n-hexane vibrational modes, experimentally assigned by subtracting the spectrum of pure n-hexane flowing, before the deposition of the solid film, from the spectrum of the indole solution at the same flow rate (see Annex D, Figure D5). However, the solid presents a characteristic band of Si-O stretchings at 830 cm^{-1}, and it could interfere in the analysis of the signal at 828 cm^{-1}. These bands, assigned to indole in the liquid phase, in the DFT calculations are predicted at 731 and 832 cm^{-1} (see Table 4.2) and correspond to out-of-plane vibrations of the hydrogen atoms. A shoulder is observed at 742 cm^{-1}, according to calculations, a shifting of the peak at 738 cm^{-1} is expected when indole interacts with a silanol group (+5) and a Brønsted site (+11 and +32). Hence, this shoulder is attributed to indole adsorbed on silanol or Brønsted acid sites. The peak observed at 767 cm^{-1} was described in previous works as an in-plane vibration of the indole, but the authors mentioned that it should correspond to an out-of-plane mode because its intensity is strong in the IR spectrum [37]. The calculations presented herein showed an out-of-plane vibration of the indole rings at 756 cm^{-1} in the gas phase and 765 cm^{-1} for the interaction of indole with silanol (see Table 4.2). Thus, the peak at 767 cm^{-1} could be attributed to indole physisorbed in the USY zeolite. The peak observed at 789 cm^{-1} increased with the indole accumulation in the solid film until saturation. As this signal has not been experimentally described for indole in liquid phase or in vapor [37], it could be attributed to an interaction of indole with the active sites of the USY zeolite. The DFT calculations also predicted an out-of-plane vibration mode for indole adsorbed in 763 cm^{-1} for indole adsorbed on a Brønsted acid site (see Table 4.2). This value was assigned to a shifting of the frequency at 731 cm^{-1} in the calculations for the gas phase, which is the strongest signal observed in the spectra of the vapor phase [35-37]. Considering the magnitude of the shifting and the deviation obtained in the theoretically predicted values, the band observed at 789 cm^{-1} could be attributed to a signal of

indole interacting with the Brønsted acid sites. The appearance of a negative band at 880 cm^{-1}, and considering that the spectrum of the solid saturated with n-hexane is subtracted from all spectra, is thought to be a consequence of the increasing indole concentration in the solid, thus affecting the n-hexane signal.

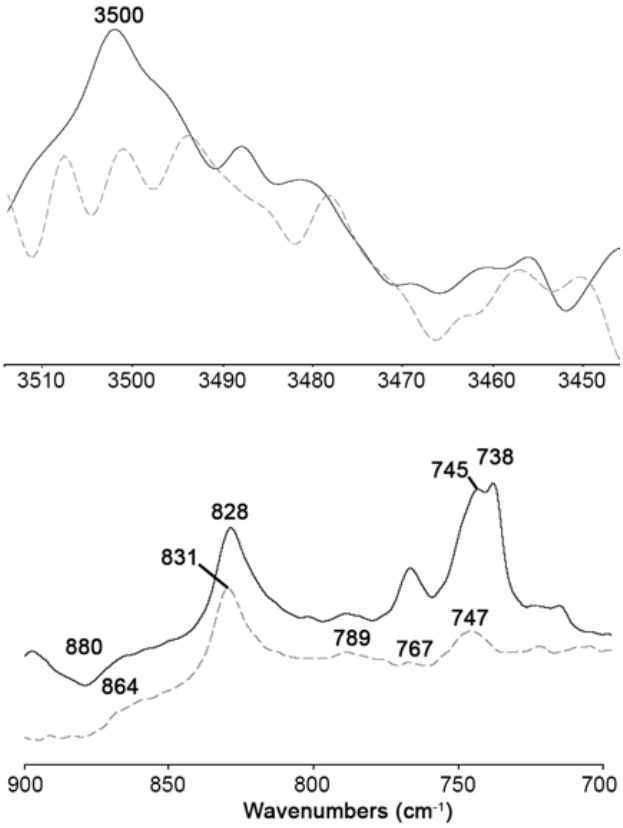

Figure 4.9. ATR-IR difference spectra of the indole adsorbed on the USY zeolite under flowing with n-hexane, obtained by subtracting the spectrum of solid saturated with pure n-hexane, at different coverages from initial time (solid line) to equilibrium in flow (dashed line), in the regions of high (3450 – 3510 cm^{-1}) and low frequency (700 – 900 cm^{-1}).

Figure 4.9 shows the changes in the difference spectrum after flushing with pure n-hexane (dashed line), in the regions of high (3450 – 3510 cm^{-1}) and low-frequencies (700 – 900 cm^{-1}).

This spectrum was obtained by subtracting from this the spectrum of the solid film saturated with n-hexane before indole adsorption.

Analyzing the high-frequency region, the broad band that was attributed to the N-H stretching mode of the indole (3500 cm^{-1}) is faded. It may indicate that non-adsorbed indole in the liquid phase was efficiently removed after flowing n-hexane. The indole desorption is more visible in the low-frequency region. The signal at 738 cm^{-1}, attributed to indole in the liquid phase, faded and only a small peak shifted to a value of 747 cm^{-1} was visible. According to calculations, this peak was attributed to indole adsorbed on silanol and on Brønsted sites. This suggests that indole remained adsorbed on the solid active sites after flushing with n-hexane. Another band which considerably decreased its intensity was the one located at 767 cm^{-1}. Calculations predicted an out-of-plane mode for indole in the gas phase at 756 cm^{-1}, and 765 cm^{-1} for indole adsorbed on silanol. As this band was significantly diminished, this evidences that the n-hexane flush induced the complete remotion of indole in the liquid phase, but also, of a part of the adsorbed indole on silanols. Interestingly, the intensity of the band at 828 cm^{-1} remains almost invariable and shifted to a value of 831 cm^{-1}. The calculations predicted an out-of-plane vibrational mode at 832 cm^{-1} for indole in the gas phase, and 836 cm^{-1} for indole adsorbed on silanol. The observed shifting to 831 cm^{-1} in the spectrum in Figure 4.9, is a consequence of the indole remotion in the liquid phase. It must be mentioned that the signal of the Si-O stretching mode, which appears at 830 cm^{-1}, is overlapped with this peak [42]. As discussed, the peak at 789 cm^{-1} was attributed to an out-of-plane mode of indole in Brønsted sites, despite the intensity of the band is weak, it remains the same after flowing n-hexane. This supports the fact that this is a signal of a strong interaction of indole with the active sites of the solid, probably with Brønsted acid sites.

The interaction of indole with the active sites of the USY zeolite was clearly evidenced in the ATR-IR *in situ* experiments in the liquid phase. When flushing with n-hexane after saturation with indole, the remaining bands observed at 747 cm^{-1} and 831 cm^{-1} supported the presence of indole adsorbed on the USY zeolite film, either in silanols or in Brønsted sites. Laredo *et al.* [43] attempted to separate basic from weakly basic nitrogen-containing compounds in a heavy oil fraction by using solid acids. The separation was not efficient and this was ascribed to a strong adsorption of the weakly basic compounds on the materials employed. In addition, the band observed at 789 cm^{-1} was attributed to an out-of-plane mode of indole in Brønsted sites. Moreover, the fact that the signal remained with almost the same intensity after flowing n-hexane, suggests that the interaction described by this signal is strong. Additionally, this frequency was theoretically predicted in the adsorption model of indole forming an ion-pair complex on a Brønsted acid site, as shown in Figure 4.3 In this way, the interaction of indole with Brønsted acid sites via the formation of an ion-pair complex is feasible , contrary to the suggested mechanism of dissociative adsorption [41]. In previous works [22], the inhibition of the Brønsted acidity induced by small amounts of carbazole and tetrahydrocarbazole, which are weakly basic nitrogenated compounds of the same family, over the hydrocracking reaction of phenanthrene was evident. This inhibitory effect was explained in terms of a blockage of the Brønsted acid sites due to the adsorption of these nitrogenates. The presence of N-protonated species in indole salts has been observed by examining the ammonium characteristic band with FT-IR [44]. As it was suggested, the presence of some weakly bands attributed to indole strongly adsorbed in Brønsted sites and due to the agreement with the theoretical results is highly probable the formation of an ion-pair complex even in these compounds.

4.4. Conclusions

Adsorption of nitrogenated probe molecules in the liquid phase, using n-hexane as a non-polar solvent, was characterized herein. Specifically, the study of indole adsorption on a USY zeolite, that is difficult for handling in the gas phase IR *in situ* cell, was successfully carried out in the liquid phase. Pyridine adsorption on a USY zeolite film was possible to follow, even in the region of the spectra which is distorted by the water present in the vapor phase (from 1200 to 1600 cm^{-1}). After saturation of the USY zeolite film with the nitrogenated probe molecules, desorption of weakly or non-adsorbed species by flowing n-hexane was corroborated. This was supported by the disappearance of bands ascribed to vibrational modes characteristics of the molecules in the liquid phase after flushing with n-hexane. The analysis of the spectra in the low-frequency region for both nitrogen-containing compounds provided specific information about the nature of the surface interactions of the adsorbates. For pyridine, the permanence of bands at 700 and 750 cm^{-1} after flowing n-hexane, indicate the presence of some adsorbed molecules on silanols. Meanwhile, the band at 684 cm^{-1}, could be attributed to pyridinium adsorbed species. The strongest band for indole in the gas phase is located at 738 cm^{-1}, which is shifted to 745 cm^{-1} for interactions of indole on silanol and Brønsted sites. As an important part of the methodology employed, the implementation of the Density Functional Theory for predicting the vibrational modes of the probe molecules when interacting with the surface sites, allowed to assign the appearance of bands associated with the adsorption phenomena. In this sense, a band attributed to indole adsorbed in Brønsted acid sites was evidenced in the region of low-frequency. Thus, the band at 789 cm^{-1}, was attributed to an out-of-plane mode of indole adsorbed on a Brønsted site. In this regard, the adsorption of indole via the formation of an ion-pair complex is a feasible mechanism. This is a hint of the inhibitory effect that these compounds may exert over the acidic functionalities of the catalyst, specifically

Brønsted sites. Results from this work are of interest for measuring inhibitory effects of nitrogenated compounds on acidic materials.

References

[1] Thibault-Starzyk, F.; Maugé, F. Infrared Spectroscopy. Characterization of Solid Materials and Heterogeneous Catalysts. Wiley-VCH Verlag GmbH & Co. KGaA; **2012,** p. 1-48.

[2] Vimont, A.; Thibault-Starzyk, F.; Daturi, M. Analysing and understanding the active site by IR spectroscopy. *Chem. Soc. Rev.*, **2010,** 39, 12, 4928-50.

[3] Ryczkowski, J. IR spectroscopy in catalysis. *Catal. Today*, **2001,** 68, 4, 263-381.

[4] Lercher, J.A.; Gründling, C.; Eder-Mirth, G. Infrared studies of the surface acidity of oxides and zeolites using adsorbed probe molecules. *Catal. Today*, **1996,** 27, 3, 353-76.

[5] Barzetti, T.; Selli, E.; Moscotti, D.; Forni, L. Pyridine and ammonia as probes for FTIR analysis of solid acid catalysts. *J. Chem. Soc*., *Faraday Trans.*, **1996,** 92, 8, 1401-7.

[6] Breysse, M.; Berhault, G.; Kasztelan, S.; Lacroix, M.; Maugé, F.; Perot, G. New aspects of catalytic functions on sulfide catalysts. *Catal. Today*, **2001,** 66, 1, 15-22.

[7] Healy, M.H.; Wieserman, L.F.; Arnett, E.M.; Wefers, K. Infrared spectroscopy and microcalorimetric investigations of .delta.-.theta. and .kappa. aluminas using basic probe molecules: acetonitrile, pyridine, 2,6-lutidine, and n-butylamine. *Langmuir* **1989,** 5, 1, 114-23.

[8] Ballinger, T.H.; Yates, J.T. IR spectroscopic detection of Lewis acid sites on alumina using adsorbed carbon monoxide. Correlation with aluminum-hydroxyl group removal. *Langmuir*, **1991,** 7, 12, 3041-5.

[9] Travert, A,; Dujardin, C.; Maugé, F.; Veilly, E.; Cristol, S.; Paul, J.F. CO Adsorption on CoMo and NiMo Sulfide Catalysts: A Combined IR and DFT Study. *J. Phys. Chem. B* **2006,** 110, 3, 1261-70.

[10] Kubelkova, L.; Kotrla, J.; Florian, J. H-Bonding and Interaction Energy of Acetonitrile Neutral and Pyridine Ion-Pair Surface Complexes in Zeolites of Various Acidity: FTIR and ab Initio Study. *J. Phys. Chem.*, **1995,** 99, 25, 10285-93.

[11] Ferwerda, R.; van der Maas, J.H.; van Duijneveldt, F.B. Pyridine adsorption onto metal oxides: an ab initio study of model systems. *J. Mol. Catal. A*, **1996,** 104, 3, 319-28.

[12] Castellà-Ventura, M.; Akacem, Y.; Kassab, E. Vibrational Analysis of Pyridine Adsorption on the Brønsted Acid Sites of Zeolites Based on Density Functional Cluster Calculations. *J. Phys. Chem. C*, **2008,** 112, 48, 19045-54.

[13] Meulen, P.Avd.; Mann, R.F. THE VAPOR PRESSURE OF PYRIDINE. *J. Amer. Chem. Soc.*, **1931,** 53, 2, 451-3.

[14] Andanson, J-M.; Baiker, A. Exploring catalytic solid/liquid interfaces by in situ attenuated total reflection infrared spectroscopy. *Chem. Soc. Rev.*, **2010,** 39, 12, 4571-84.

[15] Rivera, D.; Harris, J.M. In Situ Studies of Pyridine Adsorption to Bare and Cyano-Derivatized Silica Sol−Gel Films Using Attenuated-Total-Internal-Reflection Fourier-Transform Infrared Spectroscopy. *Langmuir*, **2001,** 17, 18, 5527-36.

[16] Davantès, A.; Costa, D.; Sallman, B.; Rakshit, S.; Lefèvre, G. Surface Polymerization of Mo(VI) and W(VI) Anions on Hematite Revealed by in Situ Infrared Spectroscopy and DFT+U Theoretical Study. *J. Phys. Chem. C*, **2017,** 121, 1, 324-32.

[17] Mudunkotuwa, I.A.; Minshid, A.A.; Grassian, V.H. ATR-FTIR spectroscopy as a tool to probe surface adsorption on nanoparticles at the liquid-solid interface in environmentally and biologically relevant media. *Analyst*, **2014,** 139, 5, 870-81.

[18] Panella, B.; Vargas, A.; Ferri, D.; Baiker, A. Chemical Availability and Reactivity of Functional Groups grafted to Magnetic Nanoparticles monitored In situ by ATR-IR Spectroscopy. *Chem. Mater.*, **2009,** 21, 18, 4316-22.

[19] Barbosa, F.A.; Santos, A.C.Bd; Silva, M.I.Pd.; Stumbo, A.M. Resistance to poisoning by nitrogen compounds of NiMo/Al-MCM-41 hydrocracking catalysts. *Catal. Today*, **2004,** 98, 1–2, 109-13.

[20] Sau, M.; Basak, K.; Manna, U.; Santra, M.; Verma, R.P. Effects of organic nitrogen compounds on hydrotreating and hydrocracking reactions. *Catal. Today*, **2005,** 109, 1–4, 112-9.

[21] Furimsky, E.; Massoth, F.E. Deactivation of hydroprocessing catalysts. *Catal. Today*, **1999,** 52, 4, 381-495.

[22] Celis-Cornejo, C.M.; Perez-Martínez, D.J.; Orrego-Ruiz, J.A.; Baldovino-Medrano, V.G. Identification of Refractory Weakly Basic Nitrogenates in a Hydrotreated Vacuum Gas Oil and Their Effect Over a Ni-MoS2/Y-Zeolite␣Alumina Catalyst Aimed for Two-stage Hydrocracking. (Submitted) *Energy Fuels,* **2017.**

[23] Yagil, G. The proton dissociation constant of pyrrole, indole and related compounds. Tetrahedron **1967,** 23, 6, 2855-61.

[24] Grimme, S.; Ehrlich, S.; Goerigk, L. Effect of the damping function in dispersion corrected density functional theory. *J. Comp. Chem*., **2011,** 32, 7, 1456-65.

[25] Rozanska, X.; van Santen, R.A.; Hutschka, F.; Hafner, J. A Periodic DFT Study of Intramolecular Isomerization Reactions of Toluene and Xylenes Catalyzed by Acidic Mordenite. *J. Amer. Chem. Soc.*, **2001,** 123, 31, 7655-67.

[26] Celis-Cornejo, C.M.; Mantilla, M.M.G.; Baldovino-Medrano, V.G.; Ramírez-Caballero, G.E. A quantum chemical study for exploring the inhibitory effect of nitrogen containing species on the adsorption of polynuclear aromatic hydrocarbons over a Bronsted acid site. *J. Phys. Conf. Ser.*, **2016,** 74, 1, 012010.

[27] Hafner, J.; Benco, L.; Bučko, T. Acid-based Catalysis in Zeolites Investigated by Density-Functional Methods. *Top. Catal*., **2006,** 37, 1, 41-54.

[28] Liu, C.; Tranca, I.; van Santen R.A.; Hensen E.J.M.; Pidko, E.A. Scaling Relations for Acidity and Reactivity of Zeolites. *J. Phys. Chem. C,* **2017,** 121, 42, 23520-30.

[29] Janda, A.; Vlaisavljevich, B.; Lin, L-C.; Smit, B.; Bell ,A.T. Effects of Zeolite Structural Confinement on Adsorption Thermodynamics and Reaction Kinetics for Monomolecular Cracking and Dehydrogenation of n-Butane. *J. Amer. Chem. Soc*., **2016**, 138, 14, 4739-56.

[30] Demuth, T.; Hafner, J.; Benco, L.; Toulhoat, H. Structural and Acidic Properties of Mordenite. An ab Initio Density-Functional Study. *J. Phys. Chem. B,* **2000**,104, 19, 4593-607.

[31] Bucko, T.; Benco, L.; Demuth, T.; Hafner, J. Ab initio density functional investigation of the (001) surface of mordenite. *J. Chem. Phys*., **2002,** 117, 15, 7295-305.

[32] Wilson, E.B. The Normal Modes and Frequencies of Vibration of the Regular Plane Hexagon Model of the Benzene Molecule. *Phys. Rev.*, **1934,** 45, 10, 706-14.

[33] Klots, T.D. Raman vapor spectrum and vibrational assignment for pyridine1Contribution number 370 from the Bartlesville Thermodynamics Group.1. *Spectrochim. Acta A*, 1998, 54, 10, 1481-98.

[34] Spinner, E. Vibration-spectral band assignments for the pyridinium ion: pyridine deuteriochloride and 1-methylpyridinium chloride. *J. Chem. Soc*., **1963,** 0, 3870-3.

[35] Suwaiyan A, Zwarich R. Vibrational spectra of indole. *Spectrochim. Acta A,* **1986,** 42, 9, 1017-20.

[36] Stein, S.E. "Infrared Spectra" in NIST Chemistry WebBook, NIST Mass Spec Data Center, Eds. P.J. Linstrom and W.G. Mallard, National Institute of Standards and Technology, Gaithersburg MD, 20899, doi:10.18434/T4D303, (obtained 5th december 2017).

[37] Majoube, M.; Vergoten, G. Vibrational spectra of indole and assignments on the basis of ab initio force fields. *J. Raman Spectrosc.,* **1992,** 23, 8, 431-44.

[38] Callis, P.R.; Vivian, J.T.; Slater, L.S. Ab initio calculations of vibronic spectra for indole. *Chem. Phys. Lett.,* **1995,** 244, 1, 53-8.

[39] Bickel, G.A.; Demmer, D.R.; Outhouse, E.A.; Wallace, S.C. The S1–S0 transition of indole and N-deuterated indole: Spectroscopy and picosecond dynamics in the excited state. *J. Chem. Phys*., **1989,** 91, 10, 6013-9.

[40] Bučko, T.; Hafner, J.; Benco, L. Adsorption and vibrational spectroscopy of ammonia at mordenite: Ab initio study. *J. Chem. Phys.,* **2004,** 120,21, 10263-77.

[41] Larrubia, M.A.; Gutièrrez-Alejandre, Ad.; Ramìrez, J.; Busca, G. A FT-IR study of the adsorption of indole, carbazole, benzothiophene, dibenzothiophene and 4,6-dibenzothiophene over solid adsorbents and catalysts. *Appl. Catal. A,* **2002,** 224, 1, 167-78.

[42] Hannah, R.W. Groups Containing N⌋O Bonds, or Si, P, S, or Halogen Atoms. Course Notes on the Interpretation of Infrared and Raman Spectra. John Wiley & Sons, Inc.; **2004,** p. 217-46.

[43] Laredo, G.C.; Leyva, S.; Alvarez, R.; Mares, M.T.; Castillo, J.; Cano, J.L. Nitrogen compounds characterization in atmospheric gas oil and light cycle oil from a blend of Mexican crudes. *Fuel*, **2002,** 81, 10, 1341-50.

[44] Hinman, R.L.; Whipple, E.B. The Protonation of Indoles: Position of Protonation. *J. Amer. Chem. Soc.*, **1962,** 84, 13, 2534-9.

General Conclusions

Heavy crude oil production is on raise, and its processing is crucial in modern refineries. These crudes contain larger amounts of heterocompounds which must be removed before hydroprocessing for preventing the poisoning and catalyst deactivation. Thus, the implementation of a hydrotreating unit for accomplish this goal before the hydrocracking stage is vital. However, the removal of the nitrogen-containing species dictates the efficiency of hydrocracking. In this sense, understanding the inhibitory effect of small amounts of nitrogen-containig molecules (<20 ppm of total N) on the catalytic performance is key for the upgrading of heavy oil fractions.

In the first part of this thesis, the physicochemical description of the nitrogen-containing compounds within a Vacuum Gas Oil was studied with the Fourier Transform Ion Cyclotron Resonance Mass Spectrometry. The analysis of these results hinted that the weakly basic nitrogen-containing compounds are the most refractory to the hydrotreating nitrogenated molecules. Information about the inhibitory effect of weakly basic nitrogen-containing compounds is meager. In the second part, the effect of these weakly basic nitrogenates was explored on the hydrocracking reaction of phenanthrene in a conventional Ni-MoS_2/Y-Zeolite_Alumina catalyst, by adding a mixture of carbazole and tetrahydrocarbazole in different proportions at a total concentration of 5 ppm of total N. The inhibitory effect exerted by the presence of these nitrogenates on conversion was evident. Furthermore, an increase in the proportion of tetrahydrocarbazole inhibited more the selectivity to hydrocracking products.

The study of the phenanthrene reaction allowed to identify a route which preferentially occurs on Brønsted acid sites. That is the cracking of partially hydrogenated external rings to produce naphthalenes and tetralins. Thus, the effect of different levels of smalls concentrations of weakly

basic nitrogen-containing compounds on the conversion and selectivity towards the aforementioned route, was assessed by implementing a statistical analysis. Results obtained from this methodology shown a significant inhibition on conversion but specially on selectivity, at concentrations of 1 ppm of total N, in which normally is difficult to distinguish such effects. Therefore, the blockage of Brønsted acid sites by weakly basic nitrogen-containing compounds was suggested. Interestingly, the two-factors combined effects between the studied variables, LHSV, temperature and concentration of weakly basic nitrogen-containing compounds, is an indication of underlying effects of the operational variables on the mass transfer of the weakly basic nitrogen-containing compounds to the Brønsted acid sites of the catalyst.

The implementation of theoretical calculations based on the density functional theory for studying a feasible mechanism for the isomerization of tetrahydrophenanthrene, which belongs to the cracking route of partially hydrogenated external rings. Results from this study allowed to stablish a catalytic mechanism which involves the formation of a π-complex as the first step to proceed with the consecutive postulated steps. Thus, the π-adsorption of other polynuclear aromatic hydrocarbons and nitrogenated compounds were studied for correlating the inhibitory effect exerted by these compounds on the cracking mechanism of partially hydrogenated external rings. Results evidenced that, regardless of the basicity, all the nitrogenated molecules studied exhibited higher adsorption energies than the computed for the polynuclear aromatic hydrocarbons. Even more, the formation of ion-pair complexes was observed in all the nitrogenated compounds, which suggest a strong adsorption of these compounds on Brønsted acid sites.

The theoretical evidence of the formation of ion-pair complexes of weakly basic nitrogen-containing compounds on Brønsted acid sites could explain the inhibitory effects observed even at small amounts of nitrogen content. However, the existence of theses chemisorbed species should be inspected with analytical techniques in order to support these findings.

Last part of these work is an experimental-theoretical coupled methodology for studying the adsorption of nitrogen-containing molecules in liquid phase *in situ* on a UYS zeolite, followed with ATR-IR spectroscopy. The pyridine adsorption in liquid phase was performed for validating the implemented methodology. The presence of a signal in the low-frequency region theoretically attributed to indole adsorbed on a Brønsted acid site was observed. These could be an evidence of the formation of ion-pair complexes of weakly basic nitrogenates of these characteristics on Brønsted acid sites of zeolites.

References

Agudelo, J.L., Hensen, E.J.M., Giraldo, S.A., Hoyos. (2015). L.J. Influence of steam-calcination and acid leaching treatment on the VGO hydrocracking performance of faujasite zeolite. *Fuel Process. Technol.*, 133, 89-96.

Aitani AM. (2001). Catalysts in petroleum refining and petrochemicals. *Oil Gas European Magazine* 27, 1, 42-3.

Akmaz, S., Caglayan, P.A. (2015). Effect of Catalyst, Temperature, and Hydrogen Pressure on Slurry Hydrocracking Reactions of Naphthalene. *Chem. Eng. Technol.* 38, (5), 917-30.

Al-Hajji A, A., Muller H, Koseoglu O, R. (2008). Caractérisation par spectrométrie de masse par resonance cyclotronique ionique à transformée de Fourier des azotés et soufrés dans les charges d'alimentation d'hydrocraquage. *Oil Gas Sci. Technol. – Rev. IFP* 63, (1), 115-28.

Ali, M.A., Tatsumi, T., Masuda, T. (2002). Development of heavy oil hydrocracking catalysts using amorphous silica-alumina and zeolites as catalyst supports. *Appl. Catal. A*, 233, (1–2), 77-90.

Allan, D.E. (1970). The Dehydrogenation and Isomerization of Cyclohexane Over a Platinum Alumina Mordenite Catalyst. Chemical Engineering doctoral dissertation. Louisiana State University and Agricultural & Mechanical College, 356 p.

Alwahabi, S.M., Froment, G.F. (2004). Single Event Kinetic Modeling of the Methanol-to-Olefins Process on SAPO-34. *Ind. Eng. Chem. Res*., 43, 17, 5098-111.

Ancheyta, J., Sánchez, S., Rodríguez, M.A. (2005). Kinetic modeling of hydrocracking of heavy oil fractions: A review. *Catal. Today*, 109, (1–4), 76-92.

Andanson, J-M., Baiker, A. (2010). Exploring catalytic solid/liquid interfaces by in situ attenuated total reflection infrared spectroscopy. *Chem. Soc. Rev.*, 39, 12, 4571-84.

Aprà, E., Fortunelli, A. (2003). Density-Functional Calculations on Platinum Nanoclusters: Pt13, Pt38, and Pt55. *J Phys Chem. A*, 107, (16), 2934-42.

Auerbach, S.M., Henson, N.J., Cheetham, A.K., Metiu, H.I. (1995). Transport Theory for Cationic Zeolites: Diffusion of Benzene in Na-Y. *J. Phys. Chem.*, 99, 26, 10600-8.

Ayasse, A.R., Nagaishi, H., Chan, E.W., Gray, M.R. (1997). Lumped kinetics of hydrocracking of bitumen. *Fuel*, 76, (11), 1025-33.

Bachrach, M., Marks, T.J., Notestein, J.M. (2016). Understanding the Hydrodenitrogenation of Heteroaromatics on a Molecular Level. *ACS Catal.*, 6, (3), 1455-76.

Baerlocher, C., McCusker, L.B. (2017). Database of Zeolite Structures, Available from: http://www.iza-structure.org/databases/. 2017].

Baldovino-Medrano, VG., Centeno, A., Giraldo, S.A. (2010). Evaluating the functionalities of NiMo/γ-Al2O3B2O3 catalysts in naphthalene hydrodearomatization and dibenzothiophene hydrodesfulfurization. *CT&F*, 4, 91-9.

Ballinger, T.H., Yates, J.T. (1991). IR spectroscopic detection of Lewis acid sites on alumina using adsorbed carbon monoxide. Correlation with aluminum-hydroxyl group removal. *Langmuir*, 7, 12, 3041-5.

Baltanas, M.A., Van Raemdonck, K.K., Froment, G.F., Mohedas, S.R. (1981) Fundamental kinetic modeling of hydroisomerization and hydrocracking on noble metal-loaded faujasites. *Ind. Eng. Chem. Res.* 28, 7, 899-910.

Barbosa, F.A., Santos, A.C.B.d., Silva, M.I.P.d., Stumbo, A.M. (2004). Resistance to poisoning by nitrogen compounds of NiMo/Al-MCM-41 hydrocracking catalysts, *Catal. Today*, 98, 109-113.

Barzetti T, Selli E, Moscotti D, Forni L. (1996). Pyridine and ammonia as probes for FTIR analysis of solid acid catalysts. Journal of the Chemical Society, *Faraday Trans*, 92, (8), 1401-7.

Belaya, L.A, Doronin, V.P., Sorokina, T.P., Gulyaeva, T.I. (2009). Thermal stability of zeolites Y and ZSM-5 in matrices of various compositions. *Russ. J. Appl. Chem.,* 82, (2), 236-42.

Benazzi, E., Leite, L., Marchal-George, N., Toulhoat, H., Raybaud, P. (2003). New insights into parameters controlling the selectivity in hydrocracking reactions, *J. Catal*, 217, 376-387.

Bickel, G.A., Demmer, D.R., Outhouse, E.A., Wallace, S.C. (1989). The S1–S0 transition of indole and N-deuterated indole: Spectroscopy and picosecond dynamics in the excited state. *J. Chem. Phys.*, 91, 10, 6013-9.

Bird, R.B., Stewart, W.E., Lightfoot, E.N. (2006) Transport phenomena, 2nd Edition. Wiley, American Institute of Chemical Engineers, New York.

Breysse, M., Berhault, G., Kasztelan, S., Lacroix, M., Maugé, F., Perot, G. (2001). New aspects of catalytic functions on sulfide catalysts. *Catal. Today*, 66, 1, 15-22.

Bucko, T., Benco, L., Demuth, T., Hafner, J. (2002). Ab initio density functional investigation of the (001) surface of mordenite. *J. Chem. Phys.*, 117, 15, 7295-305.

Bučko, T., Hafner, J., Benco, L. (2004). Adsorption and vibrational spectroscopy of ammonia at mordenite: Ab initio study. *J. Chem. Phys*., 120,21, 10263-77.

Callis, P.R., Vivian, J.T., Slater, L.S. (1995). Ab initio calculations of vibronic spectra for indole. *Chem. Phys. Lett*., 244, 1, 53-8.

Castellà-Ventura, M., Akacem, Y., Kassab, E. (2008). Vibrational Analysis of Pyridine Adsorption on the Brønsted Acid Sites of Zeolites Based on Density Functional Cluster Calculations. *J. Phys. Chem. C*, 112, 48, 19045-54.

Celis-Cornejo C.M., Mantilla, M.M.G., Baldovino-Medrano V.G., Ramírez-Caballero G.E. (2016). A quantum chemical study for exploring the inhibitory effect of nitrogen containing species on the adsorption of polynuclear aromatic hydrocarbons over a Brønsted acid site. *J. Phys. Conf. Ser*, 743, (1), 012010.

Celis-Cornejo, C.M., Gómez-Ballesteros, J.L, Giraldo S.A. (2013). Factors influencing the charge distribution on PdxPty bimetallic nanoparticles, *Revista ION*, 26, (2), 65-72.

Celis-Cornejo, C.M., Perez-Martínez, D.J., Orrego-Ruiz, J.A., Baldovino-Medrano, V.G. (2017). Identification of Refractory Weakly Basic Nitrogenates in a Hydrotreated Vacuum Gas Oil and Their Effect Over a Ni-MoS2/Y-Zeolite␣Alumina Catalyst Aimed for Two-stage Hydrocracking. *Energy Fuels,* (Submitted).

Chen, M., Wayne Goodman, (2007) D. Chapter 5 Oxide-supported metal clusters. In: Woodruff DP, editor The Chemical Physics of Solid Surfaces. *Elsevier*, 201-69.

Cho, Y., Kim, Y.H., Kim, S. (2011) Planar Limit-Assisted Structural Interpretation of Saturates /Aromatics /Resins /Asphaltenes Fractionated Crude Oil Compounds Observed by Fourier Transform Ion Cyclotron Resonance Mass Spectrometry. *Anal. Chem*, 83, (15), 6068-73.

Choi, H.W., Dines, M.B. (1985). Selective removal of nitrogen compounds from shale oil. *Fuel*, 64, (1), 4-8.

Coonradt, H.L., Garwood, W.E. (1964). Mechanism of Hydrocracking. Reactions of Paraffins and Olefins. *Ind. Eng. Chem. Process Des. Dev.*, 3, (1), 38-45.

Corma, A., Wojciechowski, B.W. (1982). Some ideas on cracking catalyst design. *Can. J. Chem. Eng.*, 60, 1, 11-6.

Daudin, A., Lamic, A.F., Pérot, G., Brunet, S., Raybaud, P., Bouchy, C. (2008). Microkinetic interpretation of HDS/HYDO selectivity of the transformation of a model FCC gasoline over transition metal sulfides. *Catal. Today*, 130, (1), 221-30.

Davantès, A., Costa, D., Sallman, B., Rakshit, S., Lefèvre, G. (2017). Surface Polymerization of Mo(VI) and W(VI) Anions on Hematite Revealed by in Situ Infrared Spectroscopy and DFT+U Theoretical Study. *J. Phys. Chem. C*, 121, 1, 324-32.

Davis, M.E., Davis, R.J. (2003). Fundamentals of Chemical Reaction Engineering. McGraw-Hill.

Demuth, T., Benco, L., Hafner, J., Toulhoat, H., Hutschka, F. (2001). Ab initio investigation of the adsorption of benzene in mordenite. *J. Chem. Phys.*, 114, 8, 3703-12.

Demuth, T., Hafner, J., Benco, L., Toulhoat, H. (2000). Structural and Acidic Properties of Mordenite. An ab Initio Density-Functional Study. *J. Phys. Chem. B*, 104, 19, 4593-607.

Derouane, E.G., Védrine, J.C., Pinto, R.R., Borges, P.M., Costa, L., Lemos, M. (2013). The Acidity of Zeolites: Concepts, Measurements and Relation to Catalysis: A Review on Experimental and Theoretical Methods for the Study of Zeolite Acidity. *Catal. Rev.*, 55, 4, 454-515.

Dong, D., Jeong, S., Massoth, F.E. (1997). Effect of nitrogen compounds on deactivation of hydrotreating catalysts by coke, *Catal. Today*, 37, 267-275.

Dufresne, P., Quesada, A., Mignard, S. (1989). Influence of Nitrogen Feed Content On The Performances of A Zeolite Hydrocracking Catalyst, in: Studies in Surface Science and Catalysis, Elsevier, 301-315.

Elizalde, I., Rodríguez, M.A., Ancheyta, J. (2009). Application of continuous kinetic lumping modeling to moderate hydrocracking of heavy oil. *Appl Catal. A*, 365, (2), 237-42.

Elizalde, I., Rodríguez, M.A., Ancheyta, J. (2010). Modeling the effect of pressure and temperature on the hydrocracking of heavy crude oil by the continuous kinetic lumping approach. *Appl. Catal. A*, 382, (2), 205-12.

Faye, P., Payen, E., Bougeard, D. (1998) Density Functional Approach of a γ-Alumina Supported MoS2Hydrotreating Catalyst. *J. Catal.*, 179, (2), 560-4.

Ferdous, D., Dalai, A.K., Adjaye, J. (2003). Comparison of Hydrodenitrogenation of Model Basic and Nonbasic Nitrogen Species in a Trickle Bed Reactor Using Commercial NiMo/Al2O3 Catalyst. *Energy Fuels*, 17, (1), 164-71.

Ferrando, R., Jellinek, J., Johnston, R.L. (2008). ChemInform Abstract: Nanoalloys: From Theory to Applications of Alloy Clusters and Nanoparticles. *ChemInform*, 39, (24), 845–910.

Ferwerda, R., van der Maas, J.H., van Duijneveldt, F.B. (1996). Pyridine adsorption onto metal oxides: an ab initio study of model systems. *J. Mol. Catal. A*, 104, 3, 319-28.

Fogler, H.S. (2016). Elements of Chemical Reaction Engineering, 5th Edition. Prentice Hall.

Francis J., Guillon, E., Bats, N., Pichon, C., Corma, A., Simon, L.J. (2011). Design of improved hydrocracking catalysts by increasing the proximity between acid and metallic sites. *Appl. Catal. A*, 409–410, 140-7.

Frye, C.G. (1962). Equilibria in the Hydrogenation of Polycyclic Aromatics, *J. Chem. Eng. Data*, 7, 592-595.

Fu, C.M., Schaffer AM. (1985). Effect of nitrogen compounds on cracking catalysts. *Ind. Eng. Chem. Prod. Res. Dev*, 24, (1), 68-75.

Fukuyama, H., Terai, S. (2007). Kinetic Study on the Hydrocracking Reaction of Vacuum Residue Using a Lumping Model. *Petrol. Sci. Technol.*, 25, (1-2), 277-87.

Furimsky E, Massoth FE. (1999). Deactivation of hydroprocessing catalysts. *Catal. Today*, 52, 4, 381-495.

Furimsky E. (1998). Selection of catalysts and reactors for hydroprocessing. *Appl. Catal. A*, 171, (2), 177-206.

Gafurov, M.R., Mukhambetov, I.N., Yavkin, B.V., Mamin, G.V., Lamberov, A.A., Orlinskii, S.B. (2015). Quantitative Analysis of Lewis Acid Centers of γ-Alumina by Using EPR of the Adsorbed Anthraquinone as a Probe Molecule: Comparison with the Pyridine, Carbon Monoxide IR, and TPD of Ammonia, *J. Phys. Chem. C*, 119, 27410-27415.

Gallo, P. Del, Pham-Huu, C., York, A.P.E., Ledoux, M.J. (1996). Comparison of the Effects of Nitrogen Poisoning on Molybdenum Oxycarbide and Pt/β-Zeolite Catalysts in the Isomerization of n-Heptane, *Ind. Eng. Chem. Res.*, 35, 3302-3310.

García-Martínez, J.C., González Uribe, H.A., González-Brambila, M.M., Colín-Luna, J.A., Escobedo-García, Y.E., López-Gaona, A. (2017). Selective adsorption of nitrogen

compounds using silica-based mesoporous materials as a pretreatment for deep hydrodesulfurization. *Catal. Today*., 305, 40-48.

García-Serrano, L.A., Flores-Sandoval, C.A., Zaragoza, I.P. (2003). Theoretical study of the adsorption of isobutane over H-mordenite zeolite by ab initio and DFT methods. *J. Mol. Catal. A*, 200, (1–2), 205-12.

Gómez-Vargas, L.E., Baldovino-Medrano, V.G., Pérez-Martínez, D.J. (2017). Influence of solids in slurry hydrocracking for upgrading of heavy crude oils. *Int. Symp. Adv. Hydroprocessing Oil Fractions. ISAHOF*. México, 135–136.

Gounder, R., Iglesia, E. (2011). Catalytic hydrogenation of alkenes on acidic zeolites: Mechanistic connections to monomolecular alkane dehydrogenation reactions. *J. Catal.*, 277, (1), 36-45.

Gounder, R., Iglesia, E. (2010). Effects of Partial Confinement on the Specificity of Monomolecular Alkane Reactions for Acid Sites in Side Pockets of Mordenite. Angewandte Chemie International Edition, 49, 4, 808-11.

Gounder, R., Iglesia, E. (2012). The Roles of Entropy and Enthalpy in Stabilizing Ion-Pairs at Transition States in Zeolite Acid Catalysis. *Acc. Chem. Res*., 45, 2, 229-38.

Grimme, S., Antony, J., Ehrlich, S., Krieg, H. (2010). A consistent and accurate ab initio parametrization of density functional dispersion correction (DFT-D) for the 94 elements H-Pu. *J. Chem. Phys.*, 132, 15, 154104.

Grimme, S., Ehrlich, S., Goerigk, L. (2011). Effect of the damping function in dispersion corrected density functional theory. *J. Comp. Chem.*, 32, 7, 1456-65.

Gruia A. (2006). Distillate hydrocracking. In: Jones DSJS, Pujadó PR, editors. Handbook of Petroleum Processing. Dordrecht: Springer Netherlands, 287-320.

Hafner, J., Benco, L., Bučko, T. (2006). Acid-based Catalysis in Zeolites Investigated by Density-Functional Methods. *Top. Catal*., 37, 1, 41-54.

Hannah, R.W. (2004). Groups Containing N⌋O Bonds, or Si, P, S, or Halogen Atoms. Course Notes on the Interpretation of Infrared and Raman Spectra. John Wiley & Sons, Inc., p. 217-46.

Healy, M.H., Wieserman, L.F., Arnett, E.M., Wefers, K. (1989). Infrared spectroscopy and microcalorimetric investigations of .delta.-.theta. and .kappa. aluminas using basic probe molecules: acetonitrile, pyridine, 2,6-lutidine, and n-butylamine. *Langmuir*, 5, 1, 114-23.

Herrera, J.M, Reyes, J., Roquero, P., Klimova, T. (2005). New hydrotreating NiMo catalysts supported on MCM-41 modified with phosphorus. *Microporous Mesoporous Mater*. 83, (1–3), 283-91.

Hinman, R.L. Whipple EB. (1962). The Protonation of Indoles: Position of Protonation. *J. Amer. Chem. Soc.* 84, (13), 2534-9.

Hinman, R.L., Lang, J. (1964). The Protonation of Indoles. Basicity Studies. The Dependence of Acidity Functions on Indicator Structure, *J. Amer. Chem. Soc.*, 86, (18), 3796-3806.

Hinman, R.L., Whipple, E.B. (1962). The Protonation of Indoles: Position of Protonation, *J. Amer. Chem. Soc*, 84, 2534-2539.

Hossain, M.M. (2012). Co–Pd/γ-Al2O3 catalyst for heavy oil upgrading: Desorption kinetics, reducibility and catalytic activity. *Can. J. Chem. Eng.*, 90, (4), 946-955.

Hsu C.S. (2006). Hydrotreating and hydrocracking: Fundamentals. Practical advances in *Petroleum processing. Springer*, 866.

Hsu, C.S., Hendrickson, C.L., Rodgers, R.P., McKenna, A.M., Marshall, A.G. (2011). Petroleomics: advanced molecular probe for petroleum heavy ends. *J. Mass Spectrom.*, 46, (4), 337-43.

Janda, A., Vlaisavljevich, B., Lin, L-C., Smit, B., Bell, A.T. (2016). Effects of Zeolite Structural Confinement on Adsorption Thermodynamics and Reaction Kinetics for Monomolecular Cracking and Dehydrogenation of n-Butane. *J. Amer. Chem. Soc.*, 138, 14, 4739-56.

Jeon, S.G., Na, J-G., Ko, C.H., Yi, K.B., Rho, N.S., Park, S.B. (2011). Preparation and Application of an Oil-Soluble CoMo Bimetallic Catalyst for the Hydrocracking of Oil Sands Bitumen. *Energy Fuels*, 25, (10), 4256-60.

Jia M, Lechert H, Förster H. I.R. (1992). studies on the acidity of dealuminated Y zeolite with different probe molecules. *Zeolites*, 12, 1, 32-6.

Jirátová, K., Janáček, L., Schneider, P. (1983). Influence Of Aluminium Hydroxide Peptization On Physical Properties Of Alumina Extrudates. *Stud. Surf. Sci. Catal*, 16, 653-63.

Jokuty, P.L., Gray, M.R. (1991). Resistant nitrogen compounds in hydrotreated gas oil from Athabasca bitumen, *Energy Fuels*, 5, 791-795.

Jongpatiwut, S., Li, Z., Resasco, D.E., Alvarez, W.E., Sughrue, E.L., Dodwell, G.W. (2004). Competitive hydrogenation of poly-aromatic hydrocarbons on sulfur-resistant bimetallic Pt-Pd catalysts, *Appl. Catal. A.*, 262, 241-253.

Kekäläinen, T., Pakarinen, J.M.H., Wickström, K., Vainiotalo, P. (2009). Compositional Study of Polar Species in Untreated and Hydrotreated Gas Oil Samples by Electrospray Ionization Fourier Transform Ion Cyclotron Resonance Mass Spectrometry (ESI FTICR−MS), *Energy Fuels*, 23, 6055-6061.

Kim, D., Gautam, M., Gera, D. (2002). Parametric studies on the formation of diesel particulate matter via nucleation and coagulation modes. *J. Aerosol Sci.*, 33, (12), 1609-21.

Kim, H.J., Lee, C.H., Shul, Y.G., Min, W.S. (2011). Adsorption Characteristics of Nitrogen Compounds on Silica Surface. *Adsorpt. Sci. Technol*., World Scientific, p. 584-8.

Klots, T.D. (1998). Raman vapor spectrum and vibrational assignment for pyridine1Contribution number 370 from the Bartlesville Thermodynamics Group.1. *Spectrochim. Acta A*, 54, 10, 1481-98.

Kobayashi, M., Togawa, S., Ishida, K. (2007). Effects of Small Amounts of Nitrogen Compounds in Feedstock on Performance of Hydrocracking Catalyst, *J. Jpn. Petrol. Ins.*, 50, 44-52.

Korre, S.C., Klein, M.T., Quann R.J. (1997). Hydrocracking of Polynuclear Aromatic Hydrocarbons. Development of Rate Laws through Inhibition Studies. *Ind. Eng. Chem. Res*, 36, (6), 2041-50.

Kouzu, M., Kuriki, Y., Uchida, K., Sakanishi, K., Sugimoto, Y., Saito, I. (2005). Catalytic Hydrocracking of Petroleum Residue over Carbon-Supported Nickel−Molybdenum Sulfides. *Energy Fuels*, 19, (3), 725-30.

Kresse, G., Marsman, M., Furthmüller, J. (2016). VASP the GUIDE. Computational Materials Physics. Available from: http://cms.mpi.univie.ac.at/vasp/vasp/vasp.html.

Kubelkova, L., Kotrla, J., Florian, J. (1995). H-Bonding and Interaction Energy of Acetonitrile Neutral and Pyridine Ion-Pair Surface Complexes in Zeolites of Various Acidity: FTIR and ab Initio Study. *J. Phys. Chem.*, 99, 25, 10285-93.

Kumar, H., Froment, G.F. (2006). A Generalized Mechanistic Kinetic Model for the Hydroisomerization and Hydrocracking of Long-Chain Paraffins. *Ind. Eng. Chem. Res*, 46, (12), 4075-90.

Kumar, H., Froment, G.F. (2007). Mechanistic Kinetic Modeling of the Hydrocracking of Complex Feedstocks, such as Vacuum Gas Oils. *Ind. Eng. Chem. Res*, 46, (18), 5881-97.

Kutner, M.H., Nachtsheim, C, Neter, J., Li, W. (2004). Applied linear statistical models. 5th Edition, McGraw-Hill/Irwin, 1396 p.

Lababidi, H.M.S, AlHumaidan, F.S. (2011). Modeling the Hydrocracking Kinetics of Atmospheric Residue in Hydrotreating Processes by the Continuous Lumping Approach. *Energy Fuels*, 25, (5), 1939-49.

Laredo G.C., De los Reyes, J.A., Luis Cano, J., Jesús Castillo, J. (2001). Inhibition effects of nitrogen compounds on the hydrodesulfurization of dibenzothiophene, *Appl. Catal. A*, 207, 103-112.

Laredo, G.C, Leyva, S., Alvarez, R., Mares, M.T., Castillo, J., Cano, J.L. (2002). Nitrogen compounds characterization in atmospheric gas oil and light cycle oil from a blend of Mexican crudes. *Fuel*, 81, (10), 1341-50.

Laredo, G.C., Altamirano, E.n., De los Reyes, J.A. (2003). Inhibition effects of nitrogen compounds on the hydrodesulfurization of dibenzothiophene: Part 2, *Appl. Catal. A.*, 243, 207-214.

Larrubia, M.A., Gutièrrez-Alejandre, Ad., Ramìrez, J., Busca, G. (2002). A FT-IR study of the adsorption of indole, carbazole, benzothiophene, dibenzothiophene and 4,6-dibenzothiophene over solid adsorbents and catalysts. *Appl. Catal. A*, 224, 1, 167-78.

Laxminarasimhan, C.S., Verma, R.P., Ramachandran, P.A. (1996). Continuous lumping model for simulation of hydrocracking. *AIChE J.*, 42, (9), 2645-53.

Le Page JF. (1987). Applied Heterogeneous Catalysis. IFP, *Technip*, Paris.

Leite, L., Benazzi, E., Marchal-George, N. (2001). Hydrocracking of phenanthrene over bifunctional Pt catalysts, *Catal. Today*, 65, 241-247.

Lemberton, J-L, Guisnet, M. (1984). Phenanthrene hydroconversion as a potential test reaction for the hydrogenating and cracking properties of coal hydroliquefaction catalysts. *Appl. Catal.*, 13, (1), 181-92.

León, A-Y., Parra, M-J. (2010). Determination of molecular weight of vacuum residue and their sara fractions. *CT&F*, 4, 101-12.

Lercher, J.A., Gründling, C., Eder-Mirth, G. (1996). Infrared studies of the surface acidity of oxides and zeolites using adsorbed probe molecules. *Catal. Today*, 27, 3, 353-76.

Leyva, C., Ancheyta, J., Travert, A., Maugé, F., Mariey, L., Ramírez, J. (2012). Activity and surface properties of NiMo/SiO2–Al2O3 catalysts for hydroprocessing of heavy oils. *Appl. Catal., A*, 425–426, 1-12.

Li, X., Zhu, J., Wu, B., Mao, X. (2012). Characterization of Acidic Compounds in Vacuum Gas Oils and Their Dewaxed Oils by Fourier Transform-Ion Cyclotron Resonance Mass Spectrometry, *Energy Fuels*, 26, 5646-5654.

Li, Z-k., Gao, J-S., Wang, G., Shi, Q., Xu, C-M. (2011). Influence of Nonbasic Nitrogen Compounds and Condensed Aromatics on Coker Gas Oil Catalytic Cracking and Their Characterization. *Ind. Eng. Chem. Res.*, 50, (15), 9415-24.

Liu, C., Tranca, I., van Santen R.A., Hensen E.J.M., Pidko, E.A. (2017). Scaling Relations for Acidity and Reactivity of Zeolites. *J. Phys. Chem. C*, 121, 42, 23520-30.

Liu, D., Fu, Y., Deng, W., Shi, Q., Ma, K., Hou, T. (2011). FT-ICR MS Analysis of Nitrogen-Containing Compounds in the Products of Liaohe Atmospheric Residue Hydrocracking. *Energy Fuels*, 26, (1), 624-8.

Liu, D., Kong, X., Li, M., Que, G. (2009). Study on a Water-Soluble Catalyst for Slurry-Phase Hydrocracking of an Atmospheric Residue. *Energy Fuels*, 23, (2), 958-61.

Liu, D., Li, M., Deng, W., Que, G. (2010). Reactivity and Composition of Dispersed Ni Catalyst for Slurry-Phase Residue Hydrocracking. *Energy Fuels*, 24, (3), 1958-62.

Liu, Y., Gao, L., Wen, L., Zong, B. (2009). Recent Advances in Heavy Oil Hydroprocessing Technologies. *Recent Pat. Chem. Eng*., 2, (1), 22-36.

Majoube, M., Vergoten, G. (1992). Vibrational spectra of indole and assignments on the basis of ab initio force fields. *J. Raman Spectrosc*., 23, 8, 431-44.

Martínez, J., Ancheyta, J. (2012). Kinetic model for hydrocracking of heavy oil in a CSTR involving short term catalyst deactivation. *Fuel*, 100, 193-9.

McKay, J.F., Weber, J.H., Latham, D.R. (1976). Characterization of nitrogen bases in high-boiling petroleum distillates. *Anal. Chem*, 48, (6), 891-8.

Medina, N.S., Roa, J.S. (2017). Efecto de inhibición del carbazol sobre el hidrocraqueo de fenantreno, in: Escuela de Ingeniería Química, Universidad Industrial de Santander, Bucarmanga, Colombia.

Meulen, P.Avd., Mann, R.F. (1931). The vapor pressure of pyridine. *J. Amer. Chem. Soc.*, 53, 2, 451-3.

Michel, V., Dorothée, L., Christophe, G. (2012). Use of competitive kinetics for the understanding of deep hydrodesulfurization and sulfide catalysts behavior. *Appl Catal. B*, 128, 3-9.

Milas, I., Chaer Nascimento M.A. (2006). A density functional study on the effect of the zeolite cavity on its catalytic activity: The dehydrogenation and cracking reactions of isobutane over HZSM-5 and HY zeolites. *Chem. Phys. Lett.*, 418, 4–6, 368-72.

Milas, I., Chaer Nascimento, M.A. (2003). The dehydrogenation and cracking reactions of isobutane over the ZSM-5 zeolite. *Chem. Phys. Lett.*, 373, (3–4), 379-84.

Mohanty, S., Kunzru, D., Saraf, D.N. (1990). Hydrocracking: a review. *Fuel*, 69, 12, 1467-73.

Montgomery, D. C., Runger, G. C. (2013). Applied Statistics and Probability for Engineers, 6th Edition, Wiley, 836 p.

Mora-Vergara I.D., Hernández Moscoso L., Gaigneaux E.M., Giraldo S.A., Baldovino-Medrano V.G. (2017). Hydrodeoxygenation of guaiacol using NiMo and CoMo catalysts supported on alumina modified with potassium. *Catal. Today*, (In Press).

Morales-Valencia, E.M., Baldovino-Medrano, V.G., Giraldo, S.A. (2015). Reactivity of olefins and inhibition effect on the hydrodesulfurization of a model FCC naphtha. *Fuel*, 153, (Supplement C):294-302.

Morales-Valencia, E.M., Castillo-Araiza, C.O., Giraldo, S.A., Baldovino-Medrano, V.G. (2018). Kinetic assessment of the simultaneous hydrodesulfurization of dibenzothiophene and the hydrogenation of diverse polyaromatic structures. *ACS Catal.*, 8 (5), pp 3926–3942.

Morterra, C., Chiorino, A., Ghiotti, G., Garrone, E. (1979). Surface acidity of [small eta]-alumina. Part 1.-Pyridine chemisorption at room temperature, *J. Chem. Soc., Faraday Trans*, 75, 271-288

Motaghi, M., Ulrich, B. (2011). Subramanian Slurry-phase hydrocracking—possible solution to refining margins. *Hydrocarbon Process*, 90, 37-43.

Mudunkotuwa, I.A., Minshid, A.A., Grassian, V.H. (2014). ATR-FTIR spectroscopy as a tool to probe surface adsorption on nanoparticles at the liquid-solid interface in environmentally and biologically relevant media. *Analyst*, 139, 5, 870-81.

Nagai, M., Sato, T., Aiba, A. (1986). Poisoning effect of nitrogen compounds on dibenzothiophene hydrodesulfurization on g-NiMoAl2O3 catalysts and relation to gas-phase basicity. *J. Catal.*, 97, (1), 52-8.

Naoki, T., Toshiharu, T. (2003). Preparation, Characterization, and Properties of Bimetallic Nanoparticles. Catalysis and Electrocatalysis at Nanoparticle Surfaces. CRC Press.

Nie, X., Janik, M.J., Guo, X., Song, C. (2012). A computational investigation of ring-shift isomerization of sym-octahydrophenanthrene to sym-octahydroanthracene catalyzed by acidic zeolites. *PCCP*, 14, 48, 16644-53.

Nurkowski, D., Klippenstein Stephen, J., Georgievskii, Y., Verdicchio, M., Jasper Ahren, W., Akroyd, J. (2015). Ab initio Variational Transition State Theory and Master Equation Study of the Reaction (OH)3SiOCH2 + CH3 ⇌ (OH)3SiOC2H5. Z. *Phys. Chem.*, 229:691.

Orita, H., Uchida, K., Itoh, N. (2003). Ab initio density functional study of the structural and electronic properties of an MoS2 catalyst model: a real size Mo27S54 cluster. *J. Mol. Catal. A*, 195, (1–2), 173-80.

Osipov, L.N., Agafonov, A.V., Khavkin, V.A., Rogov, S.P. (1965). Effect of nitrogen compounds on the hydrocracking of heavy distillates. *Chem. Tech. Fuels Oils*, 1, (8), 581-585.

Owen, K., Coley, T., Weaver, C.S. (1995). Automotive Fuels Reference Book.

Paier, J., Hirschl, R., Marsman, M., Kresse, G. (2005). The Perdew–Burke–Ernzerhof exchange-correlation functional applied to the G2-1 test set using a plane-wave basis set. *J. Chem. Phys.*, 122, (23), 234102.

Panella, B., Vargas, A., Ferri, D., Baiker, A. (2009). Chemical Availability and Reactivity of Functional Groups grafted to Magnetic Nanoparticles monitored In situ by ATR-IR Spectroscopy. *Chem. Mater.*, 21, 18, 4316-22.

Pawelec, B., Castaño, P., Arandes, J.M., Bilbao, J., Thomas, S., Peña, M.A. (2007). Factors influencing the thioresistance of nickel catalysts in aromatics hydrogenation. *Appl. Catal. A*, 317, (1), 20-33.

Perego, C., Peratello, S. (1999). Experimental methods in catalytic kinetics. *Catal. Today*, 52, 133-145.

Prins R. (2001). Catalytic hydrodenitrogenation. Advances in Catalysis. Academic Press, p. 399-464.

Quinn, G.P., Keough, M.J. (2002). Experimental design and data analysis for biologists. Cambridge University Press, Cambridge, UK, 527 p.

Rana, M.S., Sámano, V., Ancheyta, J., Diaz, J.A.I. (2007). A review of recent advances on process technologies for upgrading of heavy oils and residua. *Fuel*, 86, (9), 1216-31.

Ren, W., Chen, H., Yang, C., Shan, H. (2010). Molecular size characterization of heavy oil fractions in vacuum and solution by molecular dynamic simulation. *Front. Chem. Eng. China*, 4, 3, 250-6.

Restrepo-Garcia, J.R., Baldovino-Medrano, V.G., Giraldo, S.A. (2016). Improving the selectivity in hydrocracking of phenanthrene over mesoporous Al-SBA-15 based Fe–W catalysts by enhancing mesoporosity and acidity, *Appl. Catal. A. General*, 510, 98-109.

Revellin, N., Dulot, H., López-García, C., Baco, F., Jose, J. (2005). Specific Nitrogen Boiling Point Profiles of Vacuum Gasoils. *Energy Fuels*, 19, (6), 2438-44.

Rezaei, H., Liu, X., Ardakani, S.J., Smith, K.J., Bricker, M. (2010). A study of Cold Lake Vacuum Residue hydroconversion in batch and semi-batch reactors using unsupported MoS2 catalysts. *Catal. Today*, 150, (3–4), 244-54.

Rivera, D., Harris, J.M. (2001). In Situ Studies of Pyridine Adsorption to Bare and Cyano-Derivatized Silica Sol−Gel Films Using Attenuated-Total-Internal-Reflection Fourier-Transform Infrared Spectroscopy. *Langmuir*, 17, 18, 5527-36.

Rodgers, R.P., Schaub, T.M., Marshall, A.G. (2005). Petroleomics: MS Returns to Its Roots. *Anal. Chem.*, 77, (1), 20 A-7 A.

Rosnow, R. L., Rosenthal, R. (1991). If You're Looking at the Cell Means, You're Not Looking at Only the Interaction (Unless All Main Effects Are Zero), *Psychol. Bull.*, 110, 574–576.

Rozanska, X., Santen, R.Av. (2004). Chapter 6 - Reaction mechanisms in protonic zeolites. Computer Modelling of Microporous Materials. London: Academic Press, p. 165-200.

Rozanska, X., van Santen R.A., Hutschka, F., Hafner, J. (2001). A Periodic DFT Study of Intramolecular Isomerization Reactions of Toluene and Xylenes Catalyzed by Acidic Mordenite. *J. Amer. Chem. Soc.*, 123, 31, 7655-67.

Ryczkowski, J. (2001). IR spectroscopy in catalysis. *Catal. Today*, 68, 4, 263-381.

SA Rincon Ortiz, J Rodriguez Pereira, VG Baldovino-Medrano. (2017). An investigation on the cracking of dibenzothiophene over Pd-Pt/aluminosilicate. 13th EuropaCat. Florence, Italy.

Saavedra Trujillo, N.F., Jiménez Inocencio, F.Y. (2014). Necesidades de Innovación y Tecnología para la industria de petróleo y gas en Colombia. *Revista de Ingeniería*, 40, 50-6.

Sadighi, S., Ahmad, A., Irandoukht, A. (2010). Kinetic Study on a Commercial Amorphous Hydrocracking Catalyst by Weighted Lumping Strategy. *Int. J. Chem. Reac. Eng.*, 8(1)

Satterfield., C.N. (1970). Mass transfer in heterogeneous catalysis, Cambridge, Mass.

Sau, M., Basak, K., Manna, U., Santra, M., Verma, R.P. (2005). Effects of organic nitrogen compounds on hydrotreating and hydrocracking reactions, *Catal. Today*, 109, 112-119.

Sayan, Ş., Paul, J. (2002). Hydrogenation of naphthalene and methylnaphthalene: modeling and spectroscopy. *J. Mol. Catal. A: Chem*, 185, (1), 211-22.

Scherzer, J.A., Gruia, A.J. (1996). Hydrocracking Science and Technology. New York.

Simon-Masseron, A., Marques, J.P., Lopes, J.M., Ribeiro, F.R., Gener, I., Guisnet, M. (2007). Influence of the Si/Al ratio and crystal size on the acidity and activity of HBEA zeolites. *Appl. Catal. A*, 316, 1, 75-82.

Song, T., Zhang, Z., Chen J, Ring Z, Yang H, Zheng Y. (2006). Effect of Aromatics on Deep Hydrodesulfurization of Dibenzothiophene and 4,6-Dimethyldibenzothiophene over NiMo/Al2O3 Catalyst. *Energy Fuels*, 20, (6), 2344-9.

Souverijns, W., Martens, J.A., Froment, G.F., Jacobs, P.A. (1998). Hydrocracking of Isoheptadecanes on Pt/H–ZSM-22: An Example of Pore Mouth Catalysis. *J. Catal.*, 174, 2, 177-84.

Speight, J.G. (2013). Chapter 1 - Refining Heavy Oil and Extra-heavy Oil. In: Heavy and Extra-heavy Oil Upgrading Technologies. Boston: Gulf Professional Publishing, p. 1-13.

Speight, J.G. (2013). Chapter 5 - Hydrocracking, in: Heavy and Extra-heavy Oil Upgrading Technologies, Gulf Professional Publishing, Boston, pp. 95-128.

Speight, J.G. (2013). Chapter 7 - Heavy Feedstock Refining—The Future. In: Heavy and Extra-heavy Oil Upgrading Technologies. Boston: Gulf Professional Publishing, p. 149-62.

Speight, J.G. (2004). New approaches to hydroprocessing. *Catal. Today*, 98, (1–2), 55-60.

Spinner, E. (1963). Vibration-spectral band assignments for the pyridinium ion: pyridine deuteriochloride and 1-methylpyridinium chloride. *J. Chem. Soc.*, 0, 3870-3.

Stein, S.E. (2017). "Infrared Spectra" in NIST Chemistry WebBook, NIST Mass Spec Data Center, Eds. P.J. Linstrom and W.G. Mallard, National Institute of Standards and Technology, Gaithersburg MD, 20899, doi:10.18434/T4D303.

Stratiev, D.S., Shishkova, I.K., Nikolaychuk, E., Sharafutdinov, I.M., Vely, A., Mitkova, M. (2016). Relationship of the aromatic structural types in vacuum gas oil to empirical correlations based on bulk properties. *Petrol. Sci. Technol.*, 34, (9), 860-5.

Suwaiyan A, Zwarich R. (1986). Vibrational spectra of indole. Spectrochim. Acta A, 42, 9, 1017-20.

Svoboda, G.D., Vynckier, E., Debrabandere, B., Froment, G.F. (1995). Single-Event Rate Parameters for Paraffin Hydrocracking on a Pt/US-Y Zeolite. *Ind. Eng. Chem. Res*, 34, (11), 3793-800.

Tang, W., Sanville, E., Henkelman, G. (2009). A grid-based Bader analysis algorithm without lattice bias. *J. Phys. Condens. Matter*, 21, 8, 084204.

Thibault-Starzyk, F., Maugé, F. (2012). Infrared Spectroscopy. Characterization of Solid Materials and Heterogeneous Catalysts. Wiley-VCH Verlag GmbH & Co. KGaA, p. 1-48.

Thybaut, J.W., Marin, G.B. (2016). Chapter Two - Multiscale Aspects in Hydrocracking: From Reaction Mechanism Over Catalysts to Kinetics and Industrial Application, in: Advances in Catalysis, Academic Press, pp. 109-238.

Travert, A,, Dujardin, C., Maugé, F., Veilly, E., Cristol, S., Paul, J.F.(2006). CO Adsorption on CoMo and NiMo Sulfide Catalysts: A Combined IR and DFT Study. *J. Phys. Chem. B*, 2006, 110, 3, 1261-70.

Tuxen, A., Kibsgaard, J., Gøbel, H., Lægsgaard, E., Topsøe, H., Lauritsen, J.V. (2010). Size Threshold in the Dibenzothiophene Adsorption on MoS2 Nanoclusters. *ACS Nano*, 4,(8), 4677-82.

Vimont, A., Thibault-Starzyk, F., Daturi, M. (2010). Analysing and understanding the active site by IR spectroscopy. *Chem. Soc. Rev*., 39, 12, 4928-50.

W.H.O. (2000). Air Quality Guidelines for Europe. Second ed.

Wagenmakers, E.-J., Krypotos, A.-M., Criss, A.H., Iverson, G. (2012). On the interpretation of removable interactions: A survey of the field 33 years after Loftus, Mem. Cognition, 40, 145-160.

Webb PA, (1997). Orr C. Analytical Methods in Fine Particle Technology. Micromeritics.

Wei, Q., Wen, S., Tao, X., Zhang, T., Zhou, Y., Chung, K. , Xu, C. (2015). Hydrodenitrogenation of basic and non-basic nitrogen-containing compounds in coker gas oil, *Fuel Process.Technol.,* 129, 76-84.

Weitkamp J. (2012). Catalytic Hydrocracking—Mechanisms and Versatility of the Process. *ChemCatChem*, 4, 3, 292-306.

Wilm, M. (2011). Principles of Electrospray Ionization. *Mol. Cell. Proteomics*, 10, (7), M111.009407.

Wilson, E.B. (1934). The Normal Modes and Frequencies of Vibration of the Regular Plane Hexagon Model of the Benzene Molecule. *Phys. Rev.*, 45, 10, 706-14.

Wiwel, P., Hinnemann, B., Hidalgo-Vivas, A. , Zeuthen, P., Petersen, B.O., Duus, J.Ø. (2010). Characterization and Identification of the most Refractory Nitrogen Compounds in Hydroprocessed Vacuum Gas Oil. *Ind. Eng. Chem. Res.*, 49, 3184-3193.

Wu, C.F.J., Hamada, M.S. (2009). Experiments: Planning, Analysis, and Optimization, 2nd Edition.

Yagil, G. (1967). The proton dissociation constant of pyrrole, indole and related compounds. *Tetrahedron*, 23, (6), 2855-61.

Yang, M. (2014). Statistical Analysis of Unreplicated Factorial Designs Using Contrasts. M.Sc. Theses, Electronic Theses & Dissertations, in, Georgia Southern University, Statesboro, Georgia.

Yao, Q., Li, S.Q., Xu, H.W., Zhuo, J.K., Song, Q. (2009). Studies on formation and control of combustion particulate matter in China: A review. *Energy,* 34, (9), 1296-309.

Zakharov, I.I., Voroshina, O.V., Startsev, A.N. (2006). The molecular and electronic structure of the Mo12S24 macromolecule as a model of the active component of a hydrodesulfurization catalyst. *Russ. J. Phys. Chem.*, 80, (7), 1083-7.

Zhang, K., Yu, J., Gao, S., Li, C., Xu, G. (2017). Understanding Shale Oil Hydrotreatment with Composition Analysis Using Positive-Ion Mode Atmospheric Pressure Photoionization Fourier Transform Ion Cyclotron Resonance Mass Spectrometry. *Energy Fuels*, 31, (2), 1362-9.

Zhang, S., Liu, D., Deng, W., Que, G. (2007). A Review of Slurry-Phase Hydrocracking Heavy Oil Technology. *Energy Fuels*, 21, (6), 3057-62.

Publications and Technological Products

List of Publications

Published

- C.M. Celis-Cornejo, M.M.G. Mantilla, V.G. Baldovino-Medrano, G.E. Ramírez-Caballero. A quantum chemical study for exploring the inhibitory effect of nitrogen containing species on the adsorption of polynuclear aromatic hydrocarbons over a Bronsted acid site, *J. Phys. Conf. Ser*., 743 (2016) 012010.

Submitted

- C.M. Celis-Cornejo, D.J. Perez-Martínez, J.A. Orrego-Ruiz, V.G. Baldovino-Medrano. Identification of Refractory Weakly Basic Nitrogenates in a Hydrotreated Vacuum Gas Oil and Their Effect Over a Ni-MoS2/Y-Zeolite␣Alumina Catalyst Aimed for Two-stage Hydrocracking, (Submitted) *Energy Fuels*, (2017).

Under Review

- C.M. Celis-Cornejo, N.S. Medina, J.S. Roa, D.J. Perez-Martínez, V.G. Baldovino-Medrano. Inhibition effects by small amounts of weakly basic nitrogen-containing compounds over a Ni-MoS2/Y-zeolite␣alumina catalyst for two-stage hydrocracking processes., To be published, (2017).
- C.M. Celis-Cornejo, D.J. Perez-Martinez, J.F. Paul, V.G. Baldovino-Medrano. First-principles assessment of polynuclear aromatic hydrocarbons reaction mechanism over a Brønsted acid site and their inhibition by nitrogenated compounds, To be published, (2017).
- C.M. Celis-Cornejo, I. Khalil, J.F. Paul, F. Maugé, D.J. Pérez-Martínez, V.G. Baldovino-Medrano. Development of a liquid-solid ATR-IR in situ operando methodology for studying inhibitory effects of nitrogenated molecules in the liquid phase, To be published, (2017).

Symposia and Congresses

- C.M. Celis-Cornejo, M.M.G. Mantilla, V.G. Baldovino-Medrano, G.E. Ramírez-Caballero. Estudio Computacional del Efecto de Compuestos OrganoNitrogenados Durante el Hidrocraqueo de Compuestos Poliaromáticos Sobre Zeolitas. IX Simposio Colombiano de Catálisis, Cali, Colombia, 2015.
- C.M. Celis-Cornejo, M.M.G. Mantilla, V.G. Baldovino-Medrano, G.E. Ramírez-Caballero. A quantum chemical study for exploring the inhibitory effect of nitrogen

containing species on the adsorption of polynuclear aromatic hydrocarbons over a Bronsted acid site. 2nd Workshop on Processing Physic-Chemistry Advanced, Bucaramanga, Colombia, 2016.

- C.M. Celis-Cornejo, D.J. Perez-Martínez, J.A. Orrego-Ruiz, V.G. Baldovino-Medrano. C aracterización por ESI-FT-ICR-MS de compuestos nitrogenados refractarios presentes en un gasóleo de vacío colombiano hidrotratado. Congreso Iberoamericano de Catálisis, Motevideo, Uriguay, 2016.
- C.M. Celis-Cornejo, M.M. Garnica-Mantilla, P. Balbuena, V.G. Baldovino-Medrano. G.E. Ramírez-Caballero. Ab initio mechanistic and thermochemical study of the adsorption of phenanthrene over a hydrocracking catalyst. Computational chemistry for pollutant mitigation, IFPEN Energies Nouvelles, Rueil Malmaison, Paris, Francia, 2017.
- C.M. Celis-Cornejo, D.J. Perez-Martínez, V.G. Baldovino-Medrano. Evaluación del efecto inhibitorio de compuestos nitrogenados parcialmente hidrogenados sobre un catalizador de hidrocraqueo. X Simposio Colombiano de Catálisis, Tunja, Colombia, 2017.

Coadvised Works

- M.M.G. Mantilla, C.M. Celis-Cornejo, G.E. Ramírez-Caballero**.** Estudio computacional del efecto de compuestos organo nitrogenados durante el hidrocraqueo de compuestos poliaromáticos sobre zeolitas, in: Escuela de Ingeniería Química, Universidad Industrial de Santander, Bucarmanga, Colombia, **2016.**
- N.S. Medina, J.S. Roa, Efecto de inhibición del carbazol sobre el hidrocraqueo de fenantreno, in: Escuela de Ingeniería Química, Universidad Industrial de Santander, Bucarmanga, Colombia, **2017.**

Technological Products

- Carlos M. Celis-Cornejo, David J. Pérez-Martínez, Sonia A. Giraldo. Design, execution and start-up of a semi-pilot plant for reactivity tests and catalytic tests, CATATEST II, within the framework of the collaborative project between ECOPETROL-UIS. Piedecuesta, Colombia, **2014.**

ANNEX A: CHAPTER 1

Figure A1. Conversion vs time on stream for phenanthrene hydrocracking over a Ni-MoS_2/Y-zeolite␣alumina catalyst. Reaction conditions: 653 K, 6.9 MPa, LHSV=1.3 h^{-1}, and (500 NL hydrogen)/(l L feed) ratio. Carbazole to Tetrahydrocarbazole ratio is defined as $X_{WBN}=n_{Carb}/(n_{Carb}+n_{THCarb})$, where n_{Carb} and n_{THCarb} are respectively the Carbazole and Tetrahydrocarbazole moles. It is also shown the control reaction in absence of nitrogenates. The order of reactions does not imply the execution order, as experiments were randomly executed.

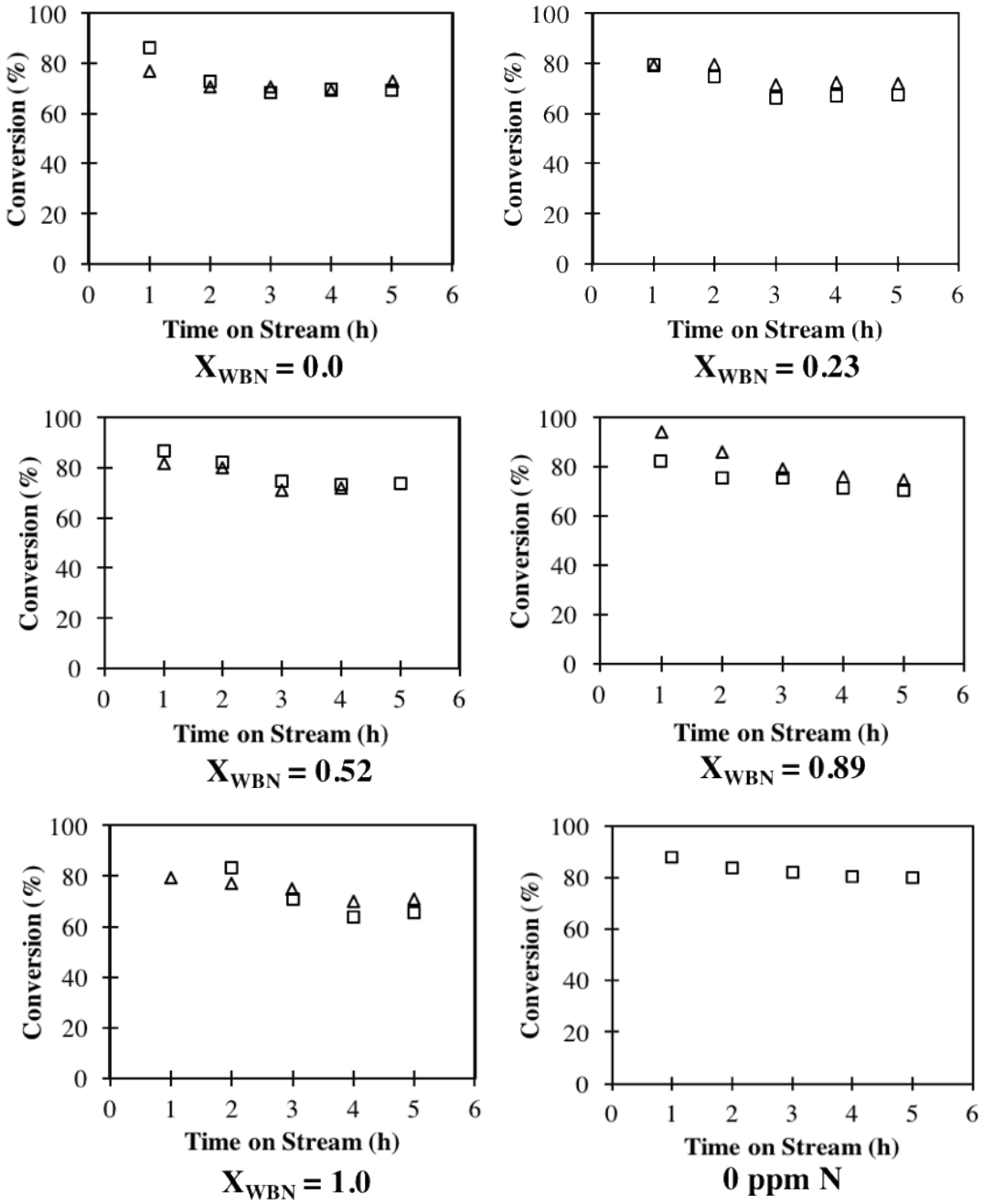

Figure A2. Results from the test proposed by Le Page [32] for ruling out external diffusion effects. Conversion vs contact time (1/LHSV), (**Δ**) 0.5 g of catalyst, (**X**) 0.1 g of catalyst and (**O**) repetition for 0.1 g of catalyst. Tests were performed for phenanthrene hydrocracking at 653 K, 6.9 MPa, (500 NL hydrogen)/(l L feed) ratio and 0 ppm of N.

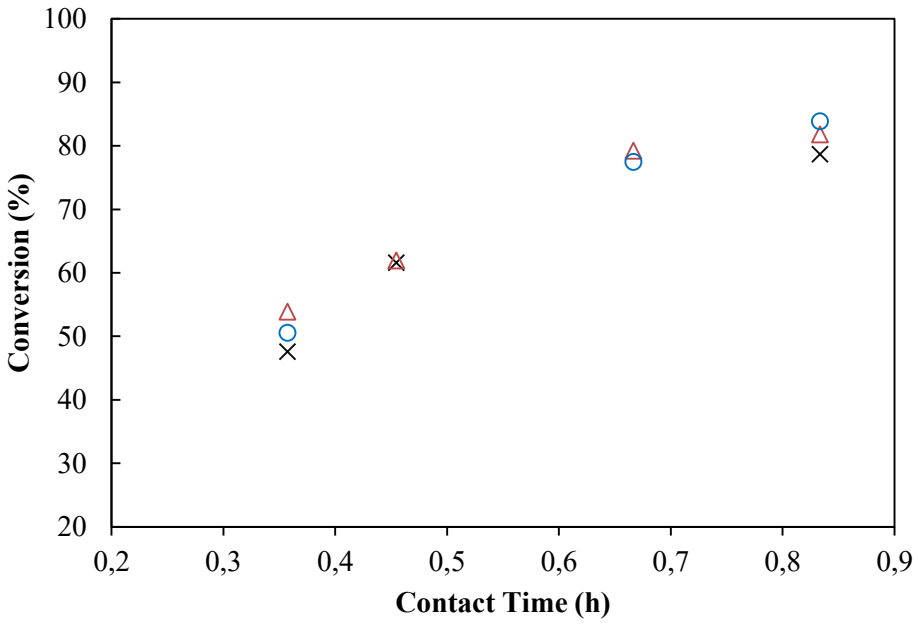

Figure A3. Chromatogram of a liquid sample taken during the hydrocracking of phenanthrene over a Ni-MoS_2/Y-zeolite␣alumina catalyst. Components assignation made for the most abundant species from parent GC-MS characterization. Sample taken after reaching the steady state in the catalytic test. Reaction conditions: T=653 K, P=6.9 MPa, and LHSV=1.3 h^{-1}. Solvent: Cyclohexane, GC internal standard: Hexadecane, MCP: Methylcyclopentane, BTX: monoaromatic fraction.

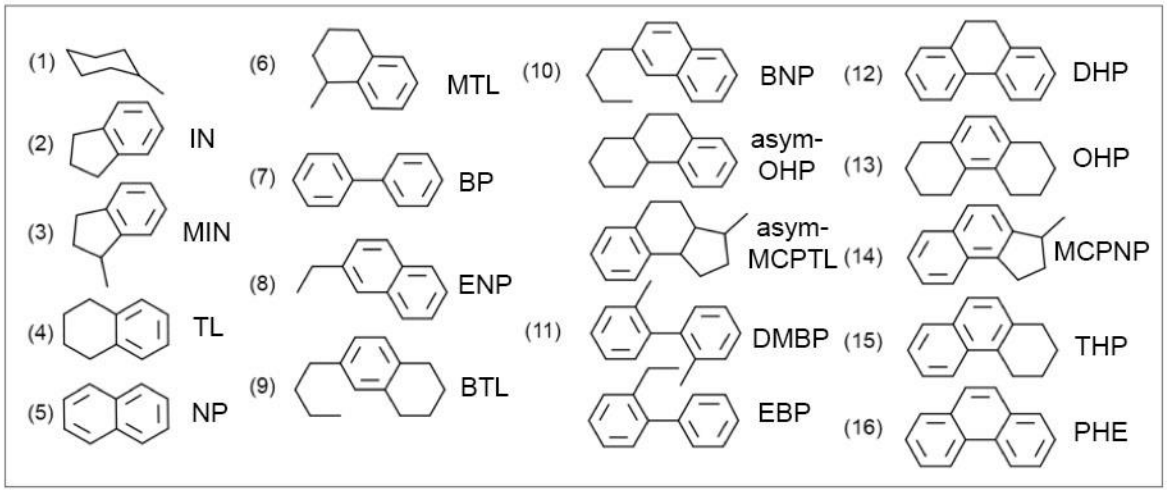

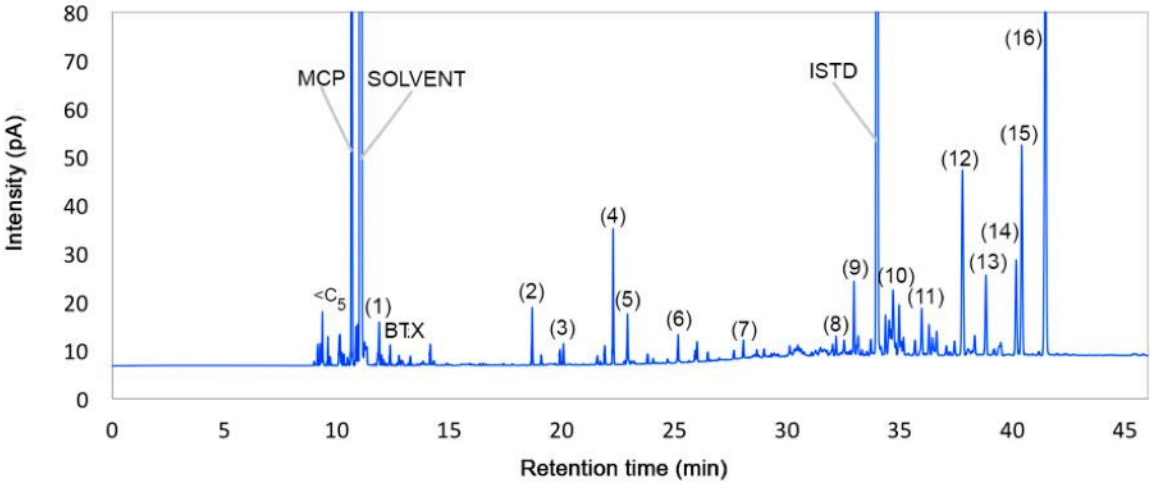

Acronym	Compound name	Acronym	Compound name
IN	Indane	asym-OHP	1,2,3,4,4a,9,10,10a-Octahydrophenanthrene
MIN	Methyl indane	asym-MCPTL	iso-Methylcyclopenta[a]tetralin
TL	Tetralin	DMBP	Dymethyl biphenyl
NP	Naphthalene	EBP	2-Ethyl biphenyl
MTL	Methyl tetralin	DHP	9,10-Dihydrophenanthrene
BP	Biphenyl	OHP	1,2,3,4,5,6,7,8-Octahydrophenanthrene
ENP	Ethyl naphthalene	MCPNP	Methylcyclopenta[a]naphthalene
BTL	6N-Butyl tetralin	THP	1,2,3,4-Tetrahydrophenanthrene
BNP	Butyl naphthalene	PHE	Phenanthrene

Figure A4. Chromatogram of a liquid sample taken during the hydrocracking of phenanthrene over a Ni-MoS_2/□-Al_2O_3 catalyst. Sample taken after reaching the steady state in the catalytic test. Reaction conditions: T=653 K, P=6.9 MPa, and LHSV=1.3 h^{-1}. Internal standard: hexadecane.

i	Compound name	i	Compound name
1	Methylcyclopentane	8	1,2,3,4,4a,9,10,10a-Octahydrophenanthrene
2	Cyclohexane	9	2-Ethyl biphenyl
3	Methylcyclohexane	10	9,10-Dihydrophenanthrene
4	Tetralin (1,2,3,4-tetrahydronaphthalene)	11	1,2,3,4,5,6,7,8-Octahydrophenanthrene
5	Biphenyl	12	1,2,3,4-Tetrahydrophenanthrene
6	Methyl tetralin	13	Phenanthrene
7	2-Butylnaphthalene		

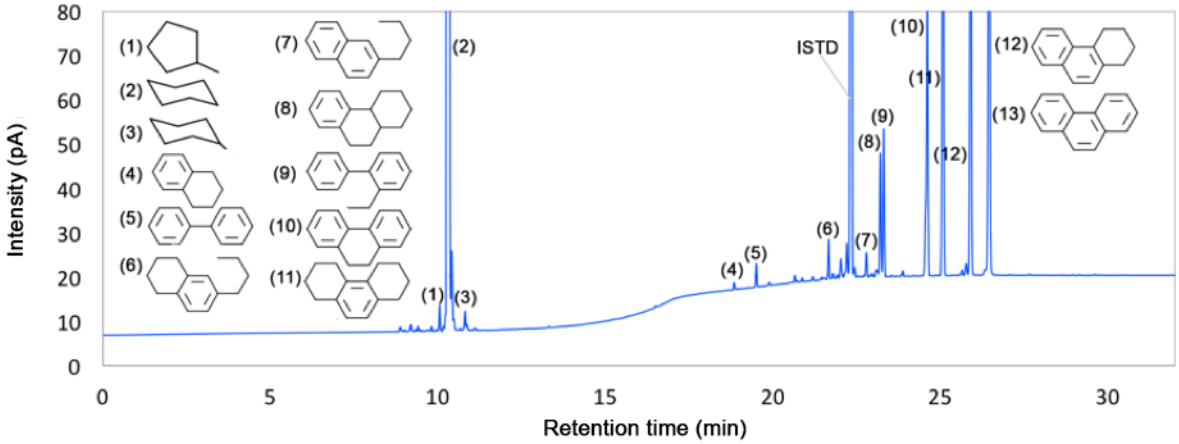

Figure A5. Normality, constant variance, and independence tests for the conversion data: (a) Residuals vs normal probability, (b) Residuals vs Predicted Value, (c) Residuals vs Execution order of the experiments.

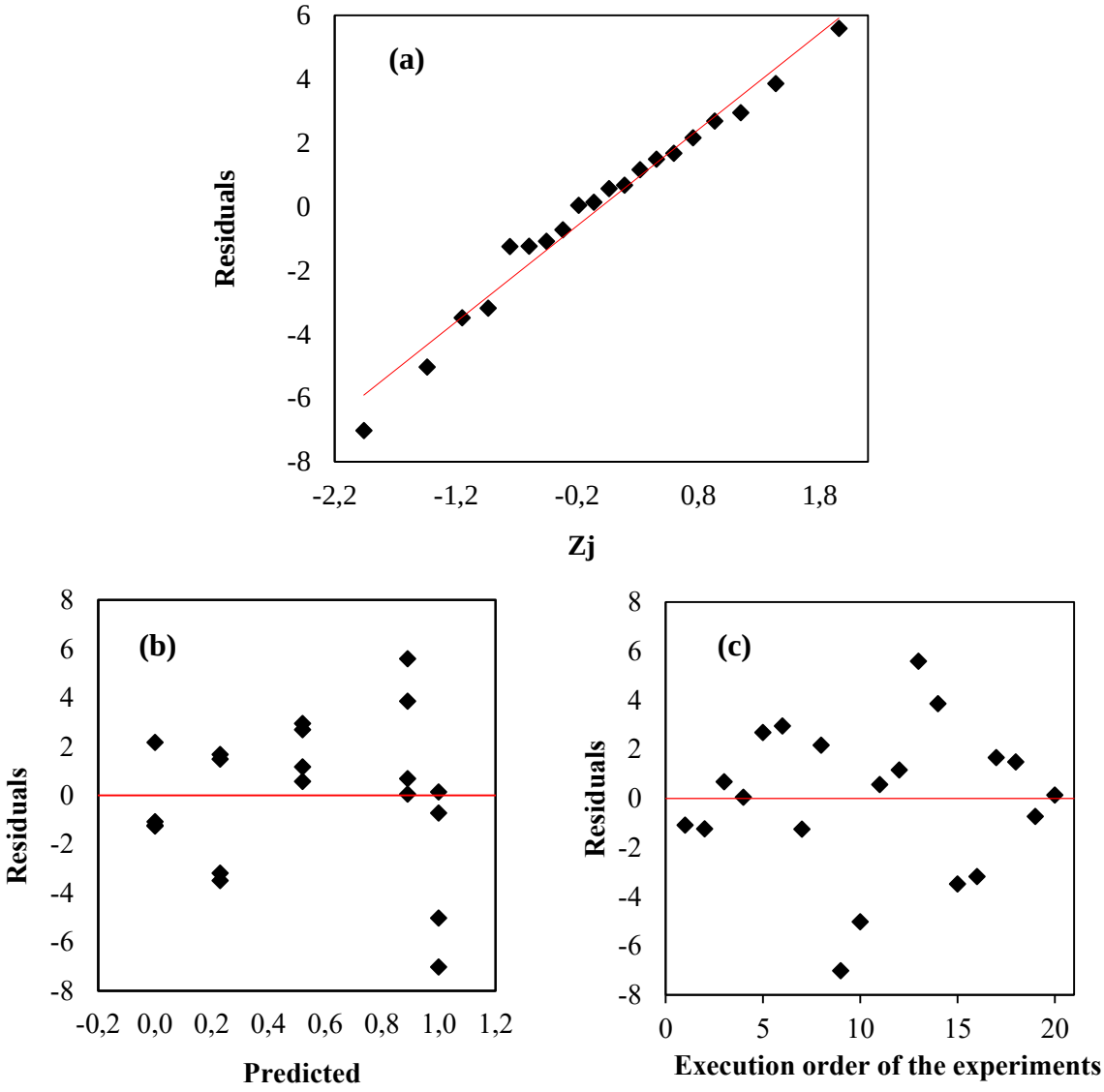

Figure A6. Normality, constant variance and independence tests for the selectivity S^{INT} data: (a) Residuals vs normal probability, (b) Residuals vs Predicted Value, (c) Residuals vs Execution order of the experiments.

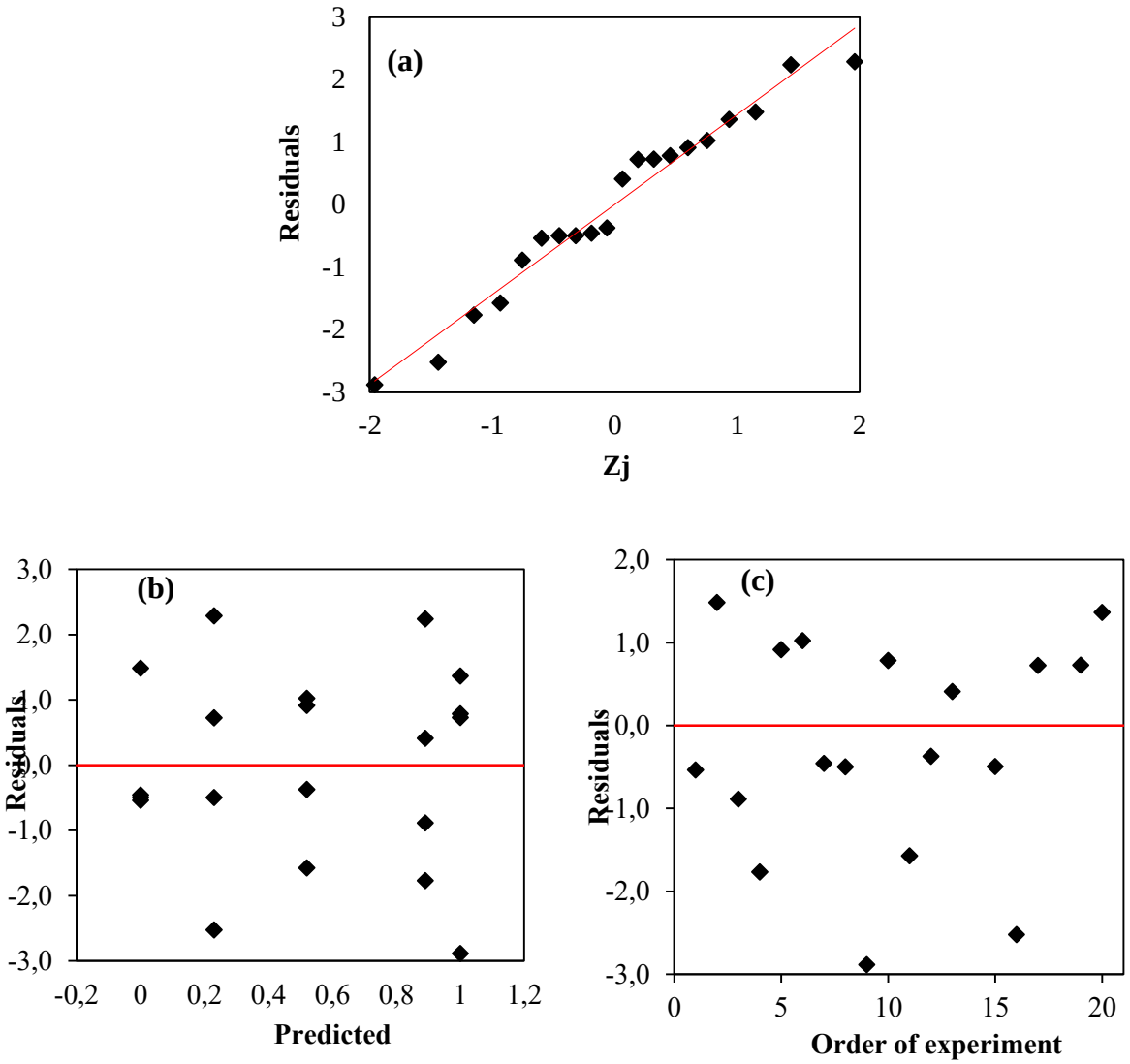

Figure A7. Normality, constant variance and independence tests for the selectivity S^{EXT} data: (a) Residuals vs normal probability, (b) Residuals vs Predicted Value, (c) Residuals vs Execution order of the experiments.

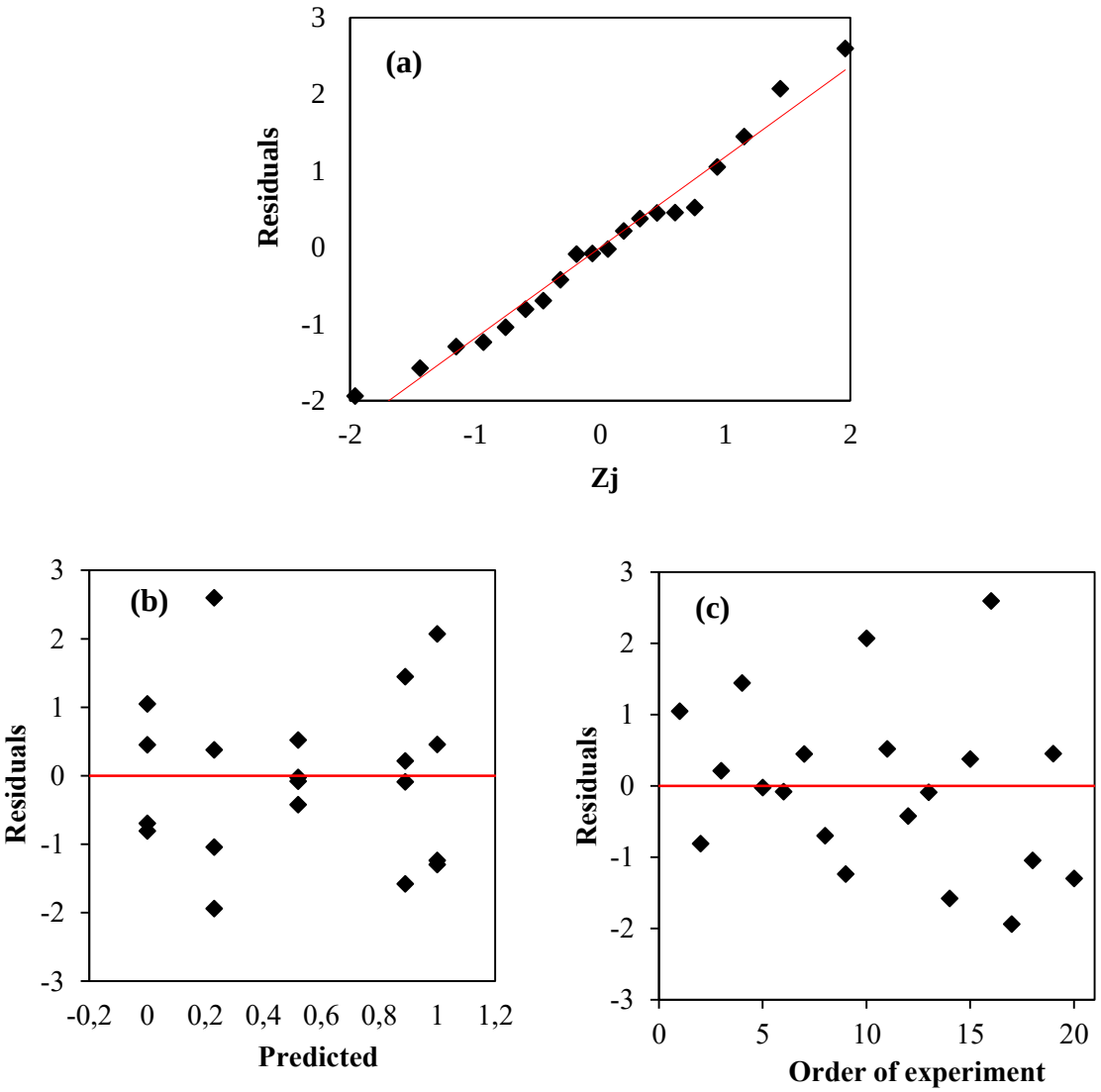

Figure A8. Normality, constant variance and independence tests for the selectivity S^{MIX} data: (a) Residuals vs normal probability, (b) Residuals vs Predicted Value, (c) Residuals vs Execution order of the experiments.

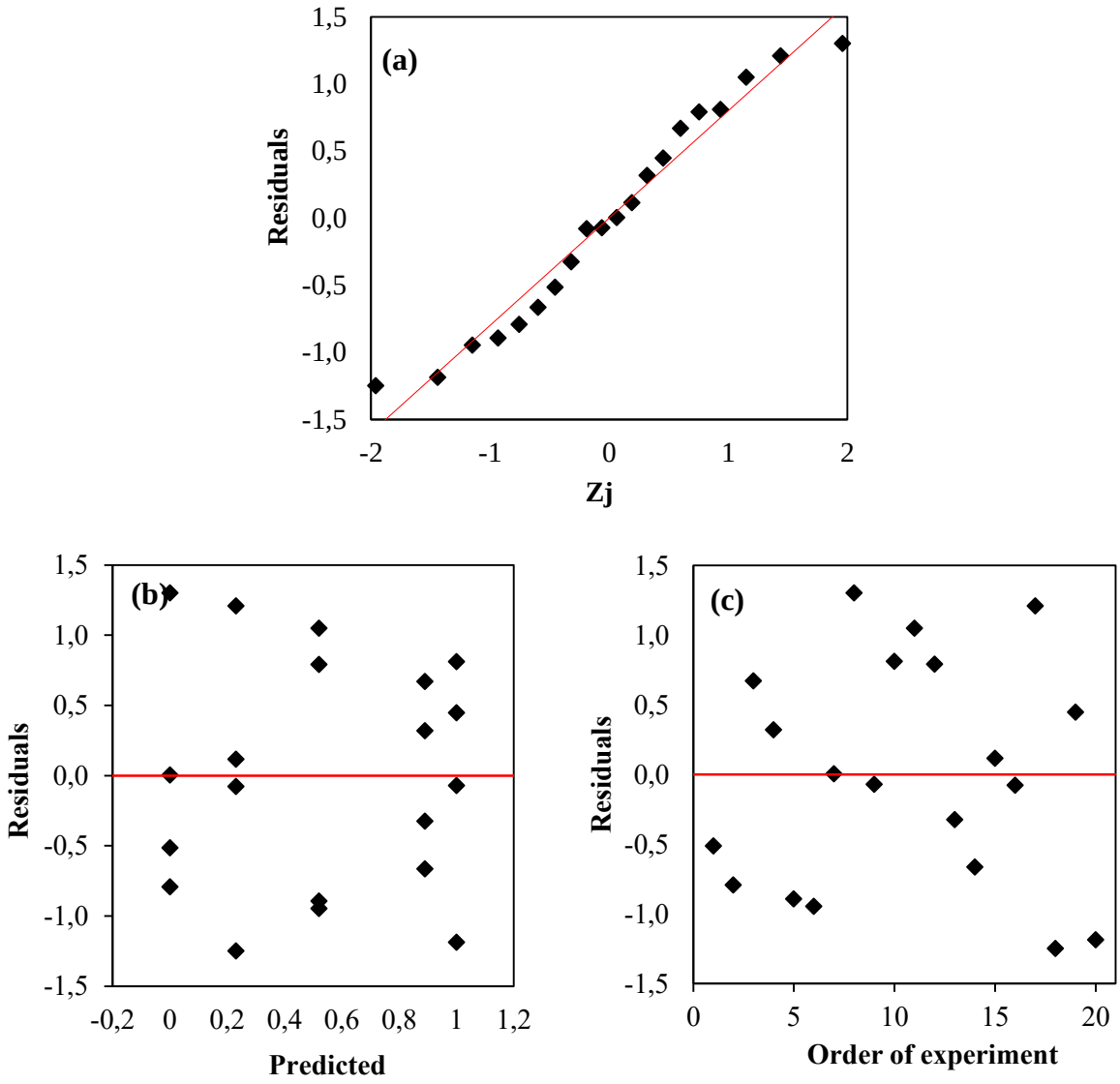

Table A1.
List of compounds identified as '*Others*' in Table 2 and their corresponding equivalent percentage in the carbon mass balance.

Compound name	Average Equivalent % in carbon mass balance
Methylcyclohexane	0.0183
Toluene	0.0084
Dimethylcyclohexane	0.0069
Ethylcyclohexane	0.0033
Butylbenzene	0.0043
Ethyl tetrahydronaphthalene	0.0042
Ethyl naphthalene	0.0059
Cyclopentyl propylbenzene	0.0069
Ethylidene bisbenzene	0.0129
Tetrahydroanthracene	0.0123
Octahydroantrhacene	0.0057
Non-asigned in HYD region	0.0160
Non-asigned in HCK region	0.2182
Total	0.3233

Table A2.
Steady state conversion data for phenanthrene hydrocracking over a Ni-MoS_2/Y-zeolite␣alumina catalyst. Reaction conditions: 653 K, 6.9 MPa, LHSV=1.3 h^{-1}, and (500 NL hydrogen)/(l L feed) ratio. The estimation of the confidence intervals was made considering unknown standard deviations, with n = 20, and $\alpha = 0.05$: $\bar{X} + t_{\alpha/2\,,n-1} * S_y/\sqrt{n} \geq \mu \geq \bar{X} - t_{\alpha/2\,,n-1} * S_y/\sqrt{n}$. *$X_{WBN}$ = $n_{Carb}/(n_{Carb}+n_{THCarb})$, where n_{Carb} and n_{THCarb} are carbazole and tetrahydrocarbazole moles, respectively.

	Phenanthrene Conversion (%C_PHE)				
Reaction (R):	**1**	**2**	**3**	**4**	**5**
X_{WBN}:	0.0	0.0	0.23	0.23	0.52
Time on Stream = 4h	69.5	69.3	67.1	72.3	73.3
Time on Stream = 5h	69.4	72.8	67.4	72.1	73.5
Reaction (R):	**6**	**7**	**8**	**9**	**10**
X_{WBN}:	0.52	0.89	0.89	1.0	1.0
Time on Stream = 4h	71.2 (3h)	71.3	76.2	63.6	69.9
Time on Stream = 5h	71.8 (4h)	70.6	74.5	65.6	70.7

Table A3.
Steady state selectivity data for phenanthrene hydrocracking over a Ni-MoS_2/Y-zeolite␣alumina catalyst as a function of X_{WBN}^*. Reaction conditions: 653 K, 6.9 MPa, LHSV=1.3 h^{-1}, and (500 NL hydrogen)/(l L feed) ratio. The values are normalized, as only the most abundant species for each route were considered. *$X_{WBN} = n_{Carb}/(n_{Carb}+n_{THCarb})$, where n_{Carb} and n_{THCarb} are carbazole and tetrahydrocarbazole moles, respectively.

		Selectivities (%)				
Sampling	X_{WBN}→	**0.0**	**0.23**	**0.52**	**0.89**	**1.0**
Time on Stream = 4h	**S^{INT}**	37.7	33.5	32.6	30.2	29.8
		37.8	34.7	30.1 (3h)	31.5	30.4
Time on Stream = 5 h		39.8	31.4	32.7	29.4	26.2
		37.8	36.2	31.3 (4h)	33.4	29.8
Time on Stream = 4h	**S^{EXT}**	55.5	60.4	61.0	62.3	63.2
		54.9	58.0	61.5 (3h)	62.0	63.2
Time on Stream = 5 h		53.6	62.6	60.9	63.5	66.5
		53.8	58.9	60.6 (4h)	60.5	64.9
Time on Stream = 4h	**S^{MIX}**	6.8	6.2	6.4	7.4	6.4
		7.3	7.3	8.4 (3h)	6.4	6.9
Time on Stream = 5 h		6.5	6.0	6.4	7.1	7.3
		8.6	4.8	8.1 (4h)	6.1	5.3

Table A4.
Analysis of variance (ANOVA) for the data of the defined selectivities as presented in Table A1.3.

ANOVA S^{INT}

Source of variation	*SS*	*DF*	*MS*	*F*	*p-value*	*F crit*
Between groups	197.91	4	49.48	18.44	$1.17x10^{-5}$	3.055
Within groups	40.25	15	2.68			
Total	238.16	19				

ANOVA S^{EXT}

Source of variation	*SS*	*DF*	*MS*	*F*	*p-value*	*F crit*
Between groups	221.61	4	55.40	30.82	$4.47x10^{-7}$	3.055
Within groups	26.96	15	1.797			
Total	248.57	19				

ANOVA S^{MIX}

Source of variation	*SS*	*DF*	*MS*	*F*	*p-value*	*F crit*
Between groups	4.44	4	1.11	1.34	0.3	3.055
Within groups	12.42	15	0.83			
Total	16.87	19				

S.V.: Source of Variation, SS: Sum of Squares, DF: Degrees of Freedom, MS: Mean Square.

ANNEX B: CHAPTER 2

Statistical Analyisis of Unreplicated 3^3 Factorial Experimental Design

The statistic model used in this work was based on the Tukey's extended model, proposed by M. Yang [34] for 3^3 factorial design.

$$Y_{ijk} = \mu_0 + (\tau_T)_i + (\tau_{[CBZ]})_j + (\tau_{LHSV})_k + (\tau_T * \tau_{[CBZ]})_{i,j} + (\tau_T * \tau_{LHSV})_{i,k} + (\tau_{[CBZ]} * \tau_{LHSV})_{j,k} + (\tau_T * \tau_{[CBZ]} * \tau_{LHSV})_{i,j,k} + \varepsilon_{ijk}$$

Where, μ_0 is the population mean; $(\tau_T)_i$ is the effect of the i-th temperature level; $(\tau_{WBN})_j$ is the effect of the j-th level of weakly basic nitrogen-containing compounds concentration; $(\tau_{LHSV})_k$ is the effect of the k-th level of the special velocity; $(\tau_{T-WBN})_{i,j}$, $(\tau_{T-LHSV})_{i,k}$, $(\tau_{WBN-LHSV})_{j,k}$ and $(\tau_{T-WBN-LHSV})_{i,j,k}$ are the effects of double and triple interactions, respectively, and ε_{ijk} is the experimental error.

Individual effects and interactions are supposed to satisfy the following definitions:

$$\sum_{i=1}^{a} (\tau_T)_i = 0; \sum_{j=1}^{b} (\tau_{LHSV})_j = 0; \sum_{k=1}^{c} (\tau_{[CBZ]})_k = 0;$$

$$\sum_{j=1}^{b} (\tau_{T,[CBZ]})_{i,j} = 0 \; for \; i = 1, \dots, a; \sum_{i=1}^{a} (\tau_{T,[CBZ]})_{i,j} = 0 \; for \; j = 1, \dots, b;$$

$$\sum_{k=1}^{c} (\tau_{T,LHSV})_{i,k} = 0 \; for \; i = 1, \dots, a; \sum_{i=1}^{a} (\tau_{T,LHSV})_{i,k} = 0 \; for \; k = 1, \dots, c;$$

$$\sum_{k=1}^{c} (\tau_{[CBZ],LHSV})_{j,k} = 0 \; for \; j = 1, \dots, b; \sum_{j=1}^{b} (\tau_{[CBZ],LHSV})_{j,k} = 0 \; for \; k = 1, \dots, c;$$

$$\sum_{k=1}^{c} (\tau_{T,[CBZ],LHSV})_{i,j,k} = 0 \; for \; i = 1, \dots, a, \quad j = 1, \dots, b;$$

$$\sum_{j=1}^{b} (\tau_{T,[CBZ],LHSV})_{i,j,k} = 0 \; for \; i = 1, \dots, a, \quad k = 1, \dots, c;$$

$$\sum_{k=1}^{c} (\tau_{T,[CBZ],LHSV})_{i,j,k} = 0 \; for \; j = 1, \dots, b, \quad k = 1, \dots, c.$$

Development of the 3^3 Tukey's extended model

The interactions and individual effects are defined as bellow:

$$(\tau_{T,[CBZ]})_{i,j} = \lambda_{T,[CBZ]}\,(\tau_T)i\,(\tau_{[CBZ]})j\,;\;\; (\tau_{T,LHSV})ik = \lambda_{T,LHSV}\,(\tau_T)i\,(\tau_{LHSV})k$$

$$\left(\tau_{[CBZ],LHSV}\right)_{i,j} = \lambda_{[CBZ],LHSV}\left(\tau_{[CBZ]}\right)j(\tau_{LHSV})k\,;$$

$$\left(\tau_{T,[CBZ],LHSV}\right)ik = \lambda_{T,[CBZ],LHSV}\,(\tau_T)i\left(\tau_{[CBZ]}\right)j(\tau_{LHSV}).$$

$$(\tau_T) = \bar{Y}_{i..} - \bar{Y}_{...};$$

$$\left(\tau_{[CBZ]}\right) = \bar{Y}_{.j.} - \bar{Y}_{...};$$

$$(\tau_{LHSV}) = \bar{Y}_{..k} - \bar{Y}_{...};$$

$$\hat{\lambda}_{T,[CBZ]} = \frac{\sum_{i=1}^{a}\sum_{j=1}^{b}\sum_{K=1}^{c}(\bar{Y}_{i..} - \bar{Y}_{...})(\bar{Y}_{.j.} - \bar{Y}_{...})Y_{ijk}}{c\sum_{i=1}^{a}\sum_{j=1}^{b}(\bar{Y}_{i..} - \bar{Y}_{...})^2\,(\bar{Y}_{.j.} - \bar{Y}_{...})^2};$$

$$\hat{\lambda}_{T,LHSV} = \frac{\sum_{i=1}^{a}\sum_{j=1}^{b}\sum_{K=1}^{c}(\bar{Y}_{i..} - \bar{Y}_{...})(\bar{Y}_{..k} - \bar{Y}_{...})Y_{ijk}}{b\sum_{i=1}^{a}\sum_{k=1}^{c}(\bar{Y}_{i..} - \bar{Y}_{...})^2\,(\bar{Y}_{..k} - \bar{Y}_{...})^2};$$

$$\hat{\lambda}_{[CBZ],LHSV} = \frac{\sum_{i=1}^{a}\sum_{j=1}^{b}\sum_{K=1}^{c}\left(\bar{Y}_{.j.} - \bar{Y}_{...}\right)(\bar{Y}_{..k} - \bar{Y}_{...})Y_{ijk}}{a\sum_{j=1}^{b}\sum_{k=1}^{c}(\bar{Y}_{.j.} - \bar{Y}_{...})^2\,(\bar{Y}_{..k} - \bar{Y}_{...})^2};$$

$$\hat{\lambda}_{T,[CBZ],LHSV} = \frac{\sum_{i=1}^{a}\sum_{j=1}^{b}\sum_{K=1}^{c}(\bar{Y}_{i..} - \bar{Y}_{...})\left(\bar{Y}_{.j.} - \bar{Y}_{...}\right)(\bar{Y}_{..k} - \bar{Y}_{...})Y_{ijk}}{\sum_{i=1}^{a}\sum_{j=1}^{b}\sum_{K=1}^{c}(\bar{Y}_{i..} - \bar{Y}_{...})^2\,(\bar{Y}_{.j.} - \bar{Y}_{...})^2(\bar{Y}_{..k} - \bar{Y}_{...})^2}.$$

The expression for Y_{ijk} is:

$$\begin{aligned} Y_{ijk} = \bar{Y}_{...} &+ (\bar{Y}_{i..} - \bar{Y}_{...}) + \left(\bar{Y}_{.j.} - \bar{Y}_{...}\right) + (\bar{Y}_{..k} - \bar{Y}_{...}) - \hat{\lambda}_{T,[CBZ]}(\bar{Y}_{i..} - \bar{Y}_{...})\left(\bar{Y}_{.j.} - \bar{Y}_{...}\right) \\ &- \hat{\lambda}_{T,LHSV}(\bar{Y}_{i..} - \bar{Y}_{...})(\bar{Y}_{..k} - \bar{Y}_{...}) - \hat{\lambda}_{[CBZ],LHSV}\left(\bar{Y}_{.j.} - \bar{Y}_{...}\right) + (\bar{Y}_{..k} - \bar{Y}_{...}) \\ &- \hat{\lambda}_{T,[CBZ],LHSV}(\bar{Y}_{i..} - \bar{Y}_{...}) + \left(\bar{Y}_{.j.} - \bar{Y}_{...}\right) + (\bar{Y}_{..k} - \bar{Y}_{...}) + \hat{\varepsilon}_{ijk} \end{aligned}$$

With:

$$\hat{\varepsilon}_{ijk} = Y_{ijk} - \bar{Y}_{...} + (\bar{Y}_{i..} - \bar{Y}_{...}) + \left(\bar{Y}_{.j.} - \bar{Y}_{...}\right) + (\bar{Y}_{..k} - \bar{Y}_{...}) - \hat{\lambda}_{T,[CBZ]}(\bar{Y}_{i..} - \bar{Y}_{...})\left(\bar{Y}_{.j.} - \bar{Y}_{...}\right) - \hat{\lambda}_{T,LHSV}(\bar{Y}_{i..} - \bar{Y}_{...})(\bar{Y}_{..k} - \bar{Y}_{...}) - \hat{\lambda}_{[CBZ],LHSV}\left(\bar{Y}_{.j.} - \bar{Y}_{...}\right) + (\bar{Y}_{..k} - \bar{Y}_{...}) - \hat{\lambda}_{T,[CBZ],LHSV}(\bar{Y}_{i..} - \bar{Y}_{...}) + \left(\bar{Y}_{.j.} - \bar{Y}_{...}\right) + (\bar{Y}_{..k} - \bar{Y}_{...})$$

The total sum of squares SST splits on:

$$SSA = bc\sum_{i=1}^{a}(\bar{Y}_{i..} - \bar{Y}_{...})^2 \ con\ df_{SSA} = 1;$$

$$SSB = ac\sum_{j=1}^{b}\left(\bar{Y}_{.j.} - \bar{Y}_{...}\right)^2 \ con\ df_{SSB} = 1;$$

$$SSC = ab\sum_{k=1}^{c}(\bar{Y}_{..k} - \bar{Y}_{...})^2 \ con\ df_{SSC} = 1;$$

$$SSAB^* = c\sum_{i=1}^{a}\sum_{j=1}^{b}\hat{\lambda}^2_{T,[CBZ]}\,(\bar{Y}_{i..} - \bar{Y}_{...})^2\left(\bar{Y}_{.j.} - \bar{Y}_{...}\right)^2;$$

$$SSAC^* = b\sum_{i=1}^{a}\sum_{k=1}^{c}\hat{\lambda}^2_{T,LHSV}\,(\bar{Y}_{i..} - \bar{Y}_{...})^2(\bar{Y}_{..k} - \bar{Y}_{...})^2;$$

$$SSBC^* = a\sum_{j=1}^{b}\sum_{k=1}^{c}\hat{\lambda}^2_{[CBZ],LHSV}\left(\bar{Y}_{.j.} - \bar{Y}_{...}\right)^2(\bar{Y}_{..k} - \bar{Y}_{...})^2$$

$$SSABC^* = \sum_{i=1}^{a}\sum_{j=1}^{b}\sum_{k=1}^{c}\hat{\lambda}^2_{T,[CBZ],LHSV}\,(\bar{Y}_{i..} - \bar{Y}_{...})^2\left(\bar{Y}_{.j.} - \bar{Y}_{...}\right)^2(\bar{Y}_{..k} - \bar{Y}_{...})^2;$$

Sum of squares residuals:

$$SSE^* = SST - SSA - SSB - SSC - SSAB^* - SSAC^* - SSBC^* - SSABC^*$$

Where,

$$df_{SSAB^*} = df_{SSAC^*} = df_{SSBC^*} = df_{SSABC^*} = 1,$$

$$df_{SSE} = abc - a - c - 2, and$$

$$SST = \sum_{i=1}^{a} \sum_{j=1}^{b} \sum_{k=1}^{c} (Y_{ijk} - \bar{Y}_{...})^2.$$

$$MSAB^* = \frac{SSAB^*}{1}, MSAC^* = \frac{SSAC^*}{1}, MSBC^* \frac{SSBC^*}{1},$$

$$MSABC^* = \frac{SSABC^*}{1}, MSE^* = \frac{SSE^*}{ab - a - b - c - 2}.$$

Figure B1. Catatest semi-pilot plants set ups employed in the reactivity tests allowing to establish the reproducibility of the results.

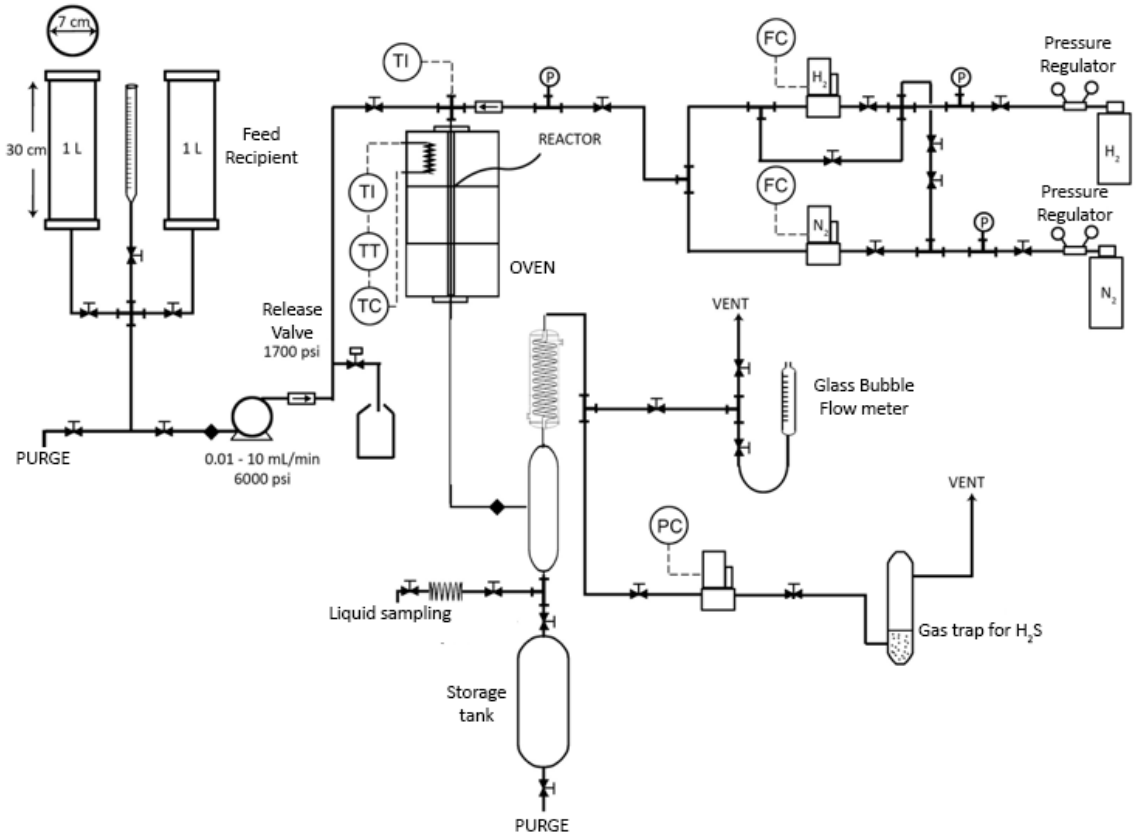

Figure B2. Calibration curves for the GC standards calibrated and their corresponding response factors. Information below corresponds to the list of non-calibrated hydrocracking products whose response factor was taken from that specific calibration curve, hexadecane (99%, Sigma-Aldrich) was used as GC Standard. Peak Area Ratio = (Area of the calibrated compound)/(Area of the GC Standard), Weight Ratio = (wt.% of the calibrated compound)/(wt.% of the GC Standard). The Response Factor (RF) is the slope of the calibration curve defined as: RF= (Peak Area Ratio)/(Weight Ratio).

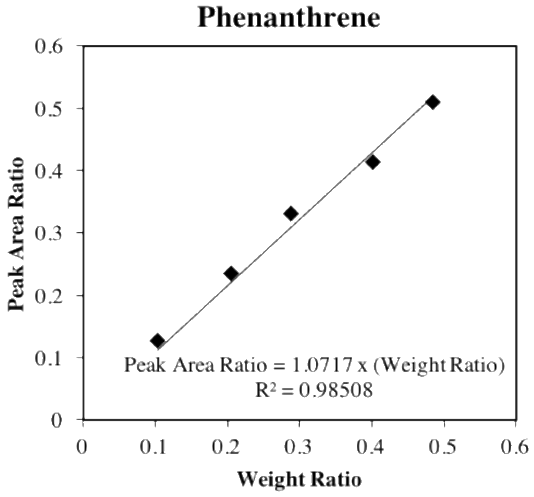

Phenanthrene

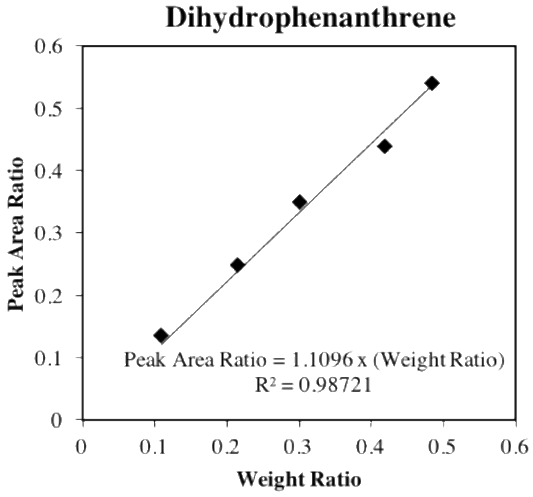

Octahydrophenanthrene, Tetrahydrophenanthrene, asym-Octahydrophenanthrene, Methylcyclopenta Naphthalene, Methylcyclopenta tetralin, iso-Methylcyclopenta tetralin.

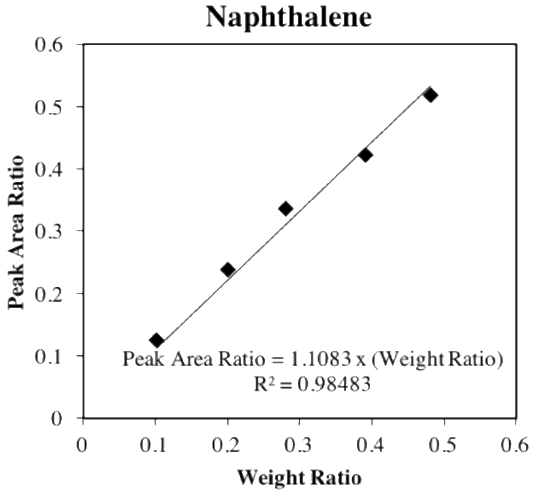

Butyl Naphthalene, Ethyl Naphthalene, Methyl Naphthalene, Naphthalene

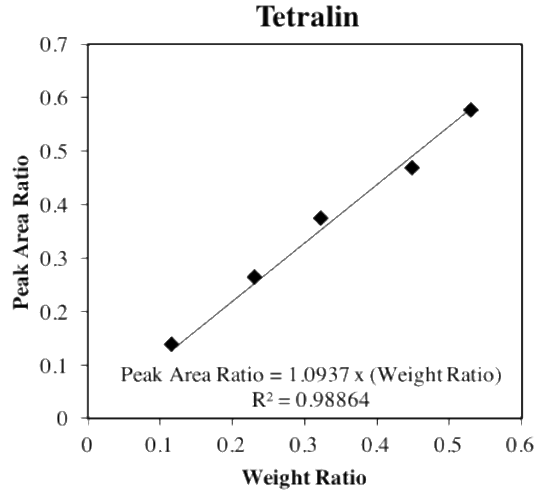

Butyl Tetralin, iso-Butyl Tetralin, Ethyl Tetralin, Methyl Tetralin, Tetralin, Methyl Indane, Indane, Butyl Benzene, Non-assigned hydrocracking products

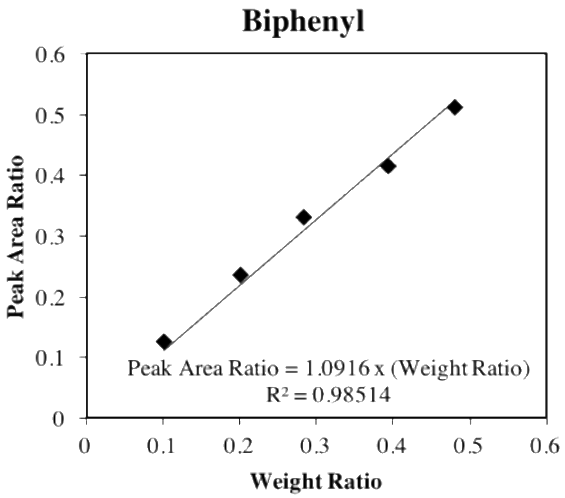

Ethyl Biphenyl, Dimethyl Biphenyl, Biphenyl, Cyclohexylbenzene.

Figure B3. Conversion vs time on stream for phenanthrene hydrocracking over a Ni-MoS_2/Y-zeolite␣alumina catalyst, for the first set of experiments in presence of carbazole. Reaction conditions: 6.9 MPa and (500 NL hydrogen)/(l L feed) ratio. WBN: relative concetration of carbazole. The order of reactions does not imply the execution order, as experiments were randomly executed.

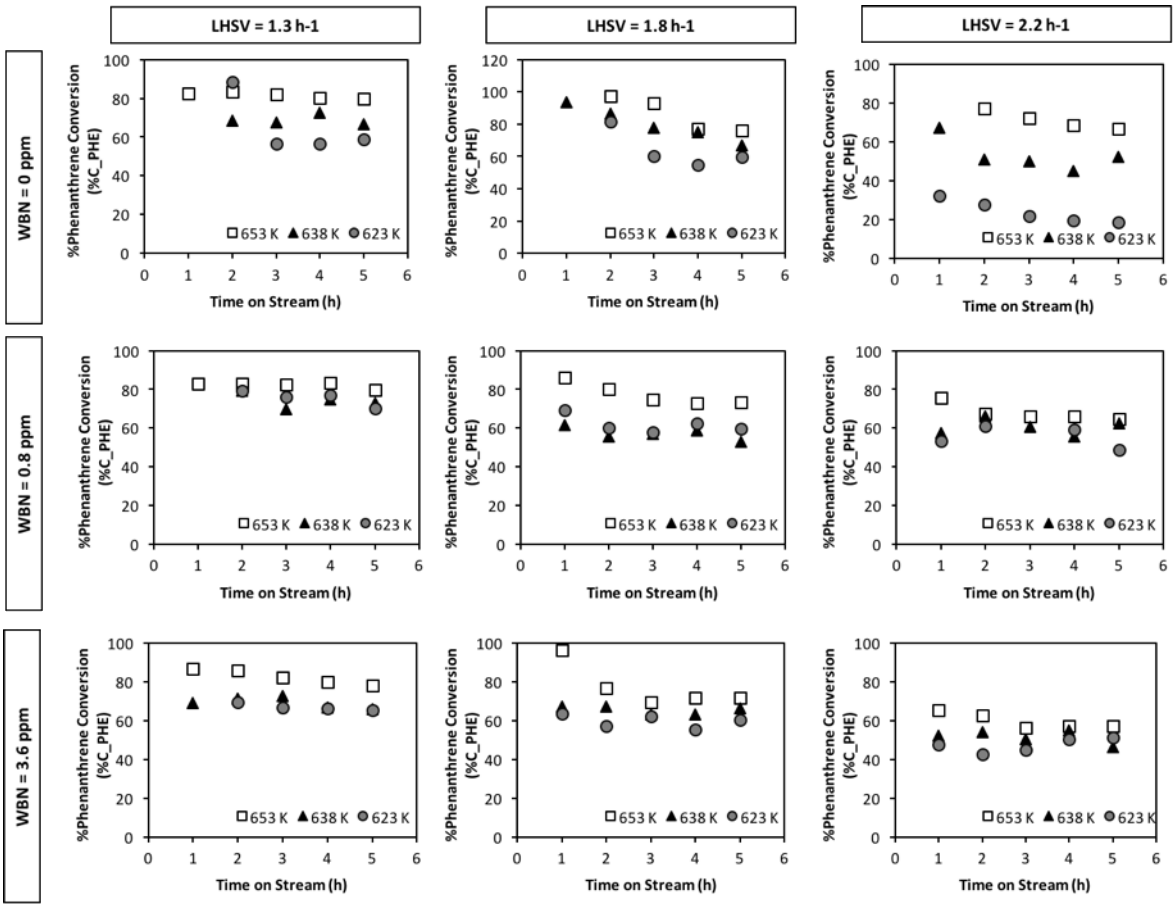

Figure B4. Conversion vs time on stream for phenanthrene hydrocracking over a Ni-MoS_2/Y-zeolite␣alumina catalyst, for the second set of experiments in presence of the mixture of carbazole and tetrahydrocarbazole in 1:1 ratio. Reaction conditions: 6.9 MPa and (500 NL hydrogen)/(l L feed) ratio. WBN: relative concetration of weakly basic nitrogen-containing compounds. The order of reactions does not imply the execution order, as experiments were randomly executed.

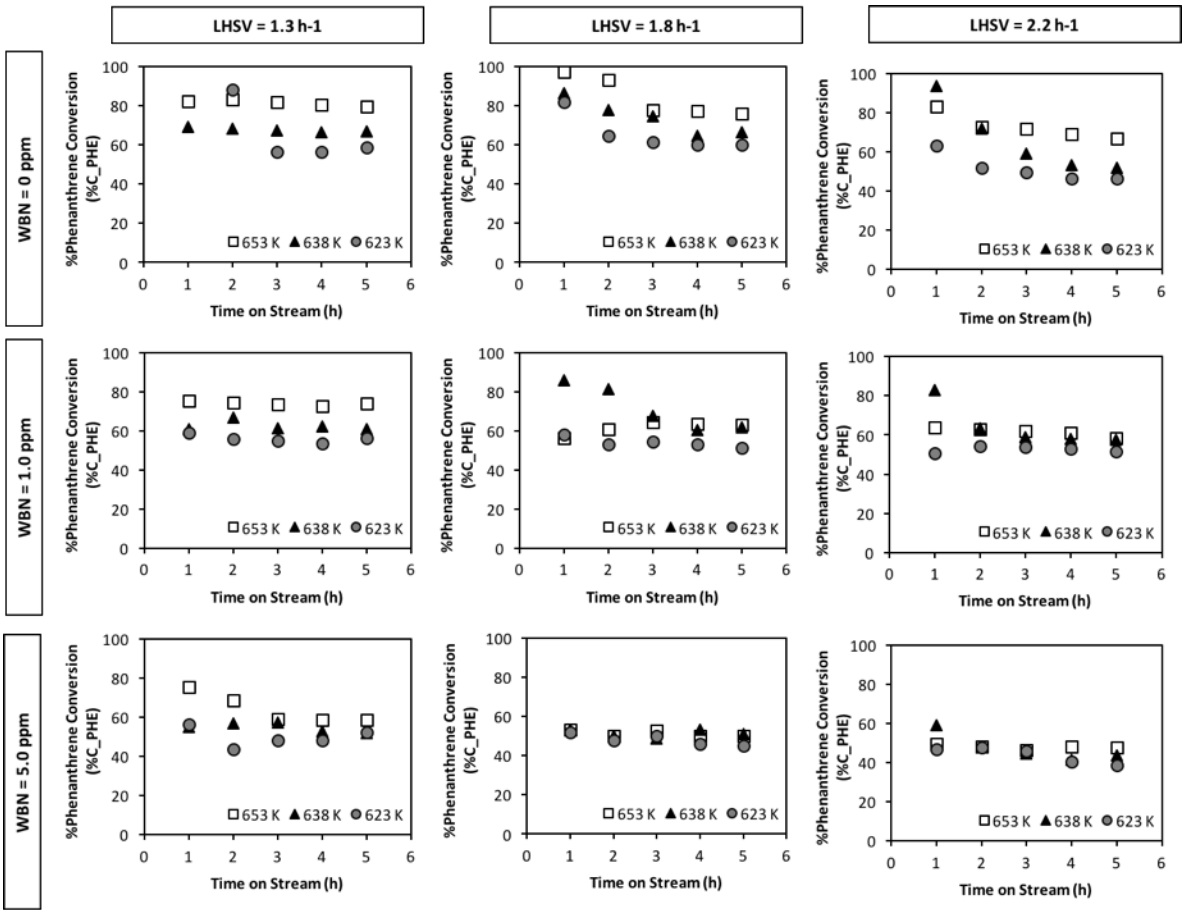

Figure B5. Conversion vs time on stream for phenanthrene hydrocracking over a Ni-MoS_2/Y-zeolite␣alumina catalyst, for the reactions under a severe basic atmosphere in presence of the mixture of carbazole and tetrahydrocarbazole in 1:1 ratio. Reaction conditions: 6.9 MPa and (500 NL hydrogen)/(l L feed) ratio. WBN: relative concetration of weakly basic nitrogen-containing compounds.

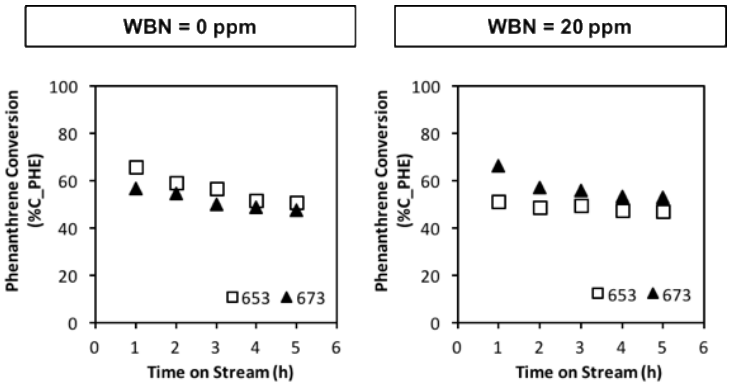

Figure B6. Normality and independence tests for conversion data, for the first set of experiments in presence of carbazole. (a) Residuals vs normal probability and (b) Residuals vs Execution order of the experiments.

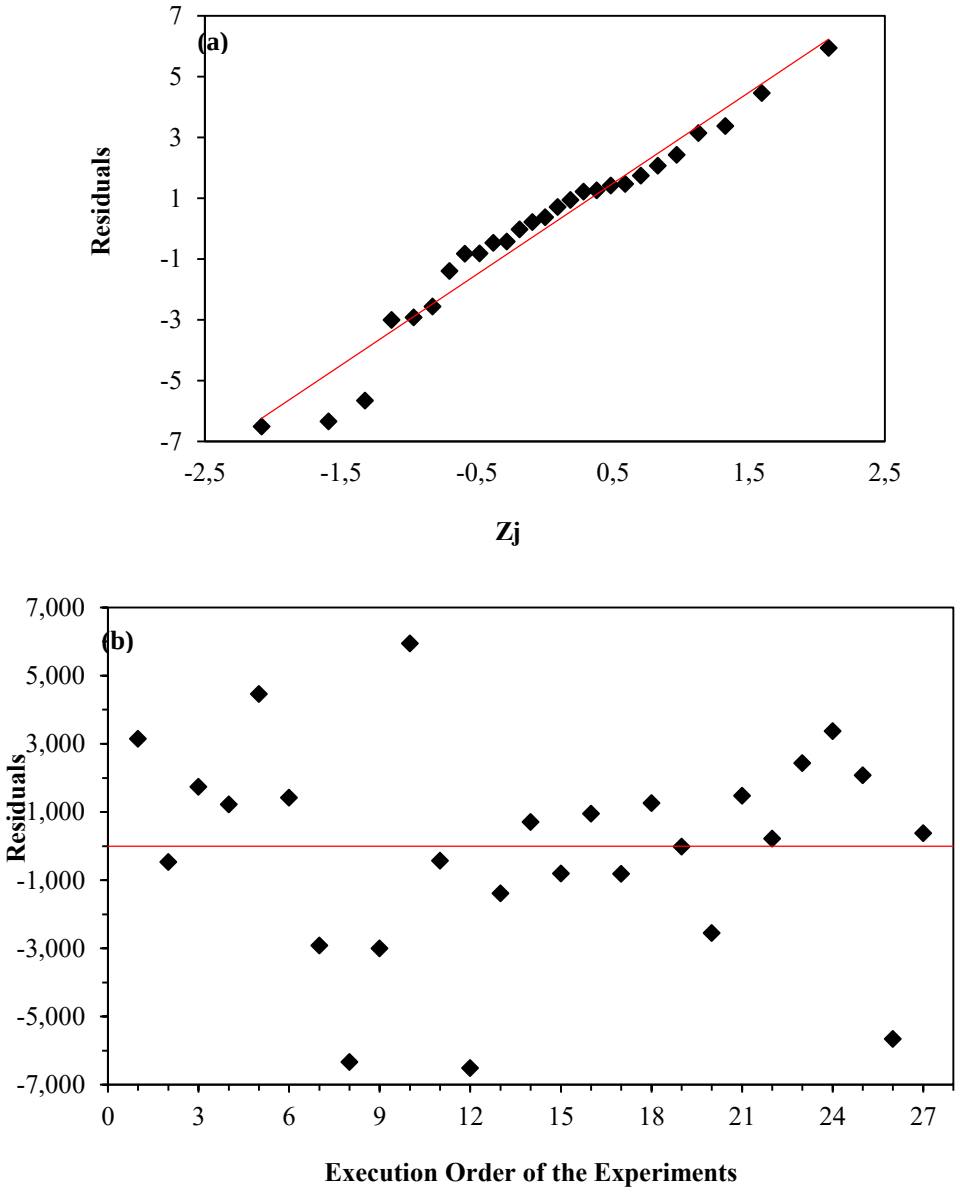

Figure B7. Normality and independence tests for the data of selectivity towards hydrocracking products, for the first set of experiments in presence of carbazole. (a) Residuals vs normal probability and (b) Residuals vs Execution order of the experiments.

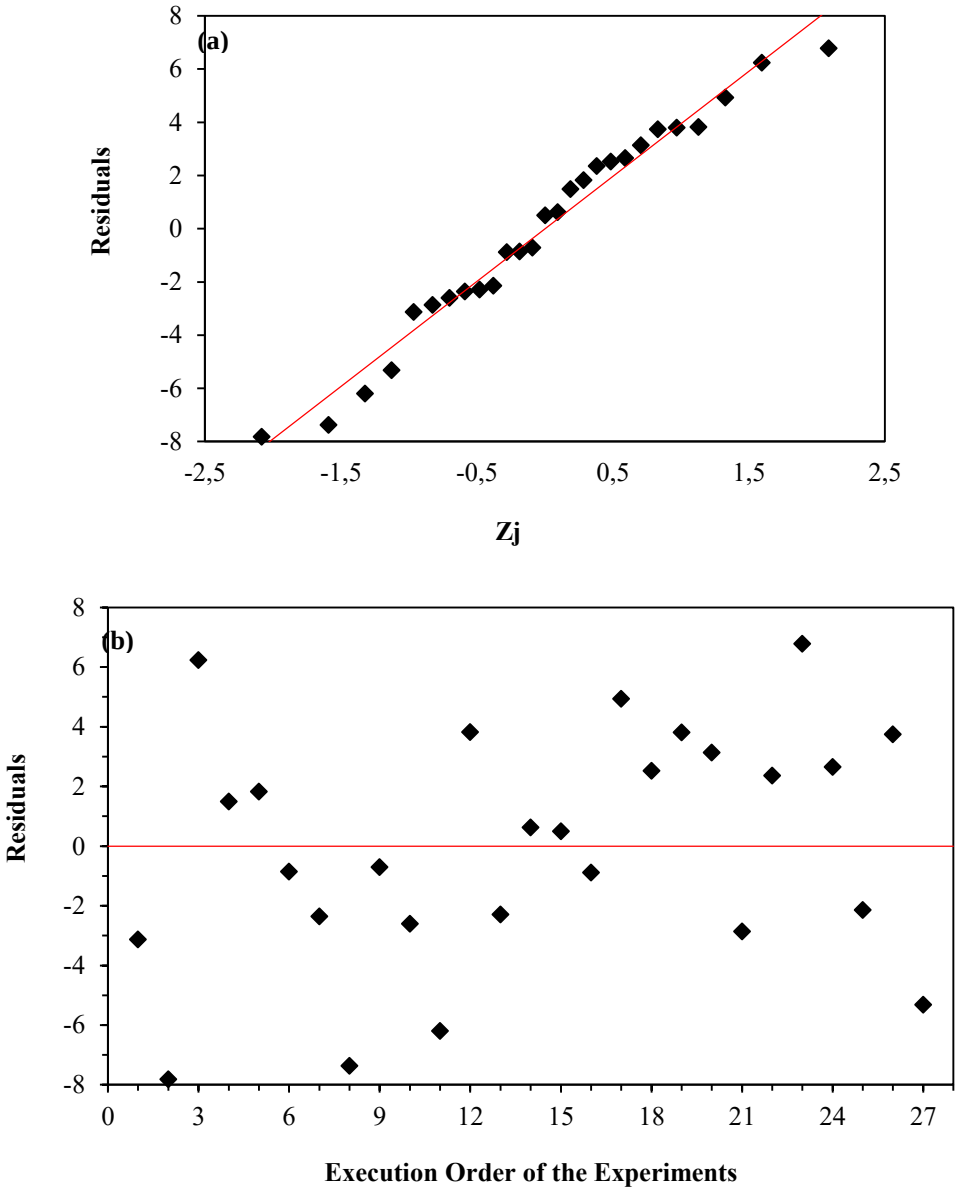

Figure B8. Normality and independence tests for the conversion data, for the second set of experiments in presence of the mixture of carbazole and tetrahydrocarbazole in 1:1 ratio. (a) Residuals vs normal probability and (b) Residuals vs Execution order of the experiments.

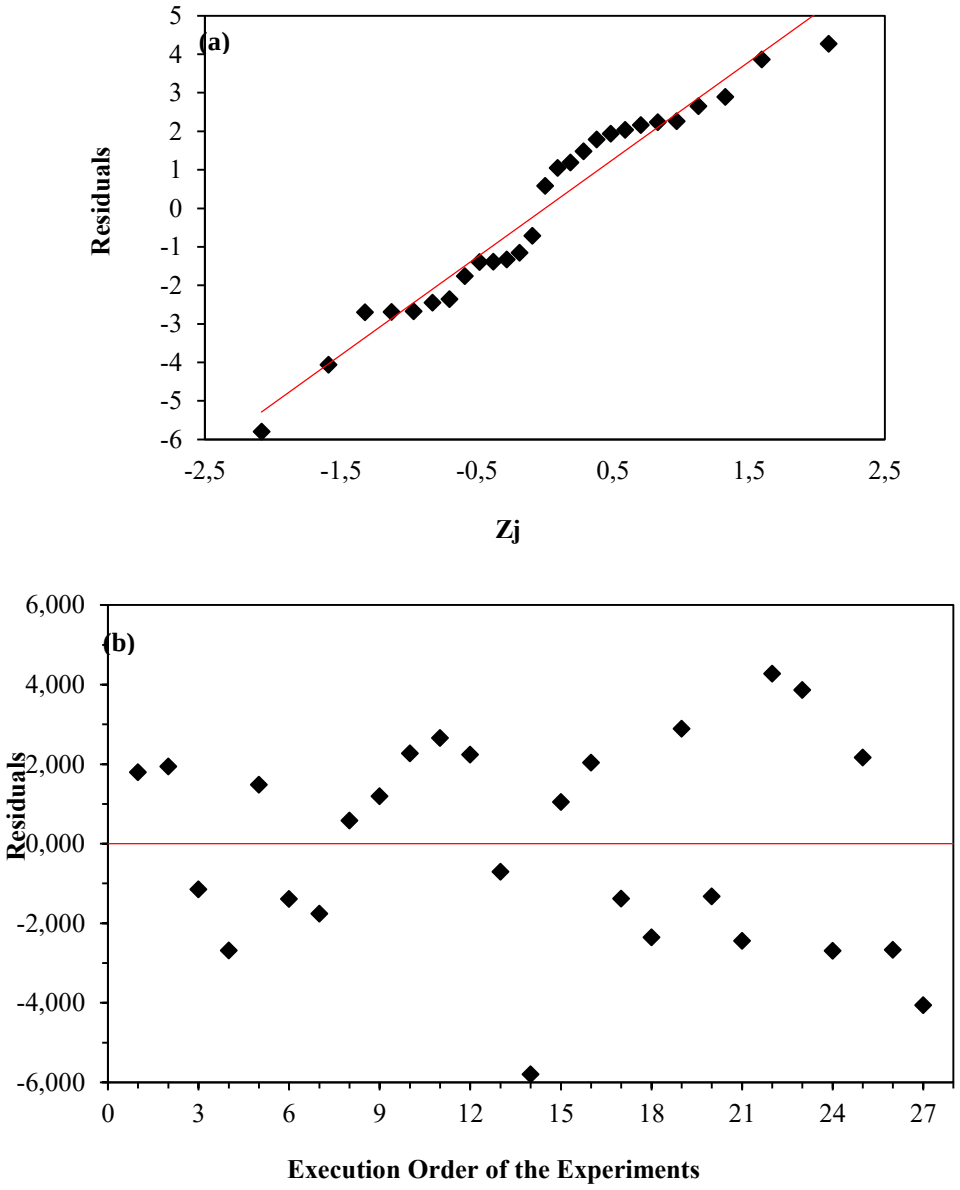

Figure B9. Normality and independence tests for the data of selectivity towards hydrocracking products, for the second set of experiments in presence of the mixture of carbazole and tetrahydrocarbazole in 1:1 ratio. (a) Residuals vs normal probability and (b) Residuals vs Execution order of the experiments.

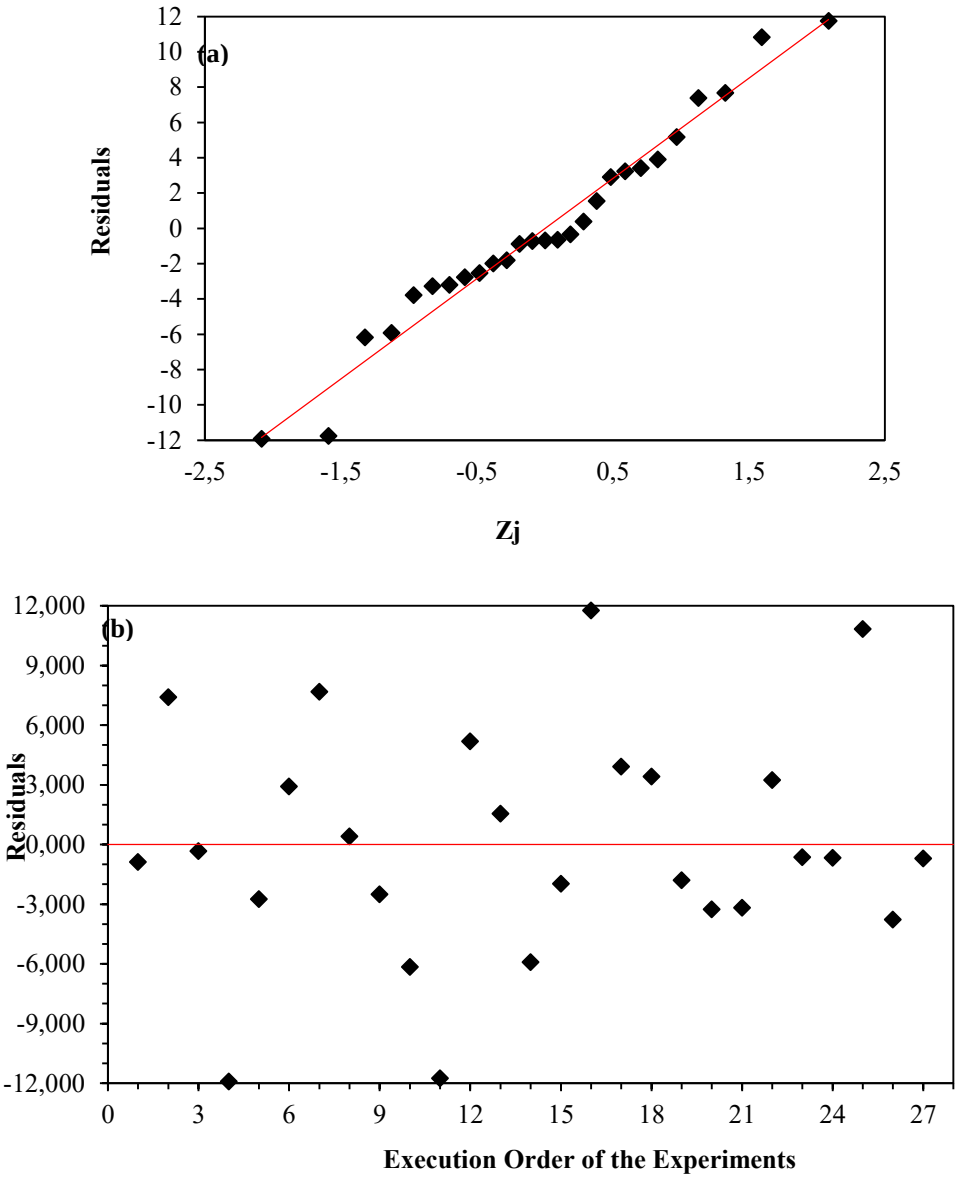

Figure B10. Normality and independence tests for the data of selectivity towards the cracking products derived from the ring opening and dealkylation of partially hydrogenated external rings, S^{EXT}, for the second set of experiments in presence of the mixture of carbazole and tetrahydrocarbazole in 1:1 ratio. (a) Residuals vs normal probability and (b) Residuals vs Execution order of the experiments.

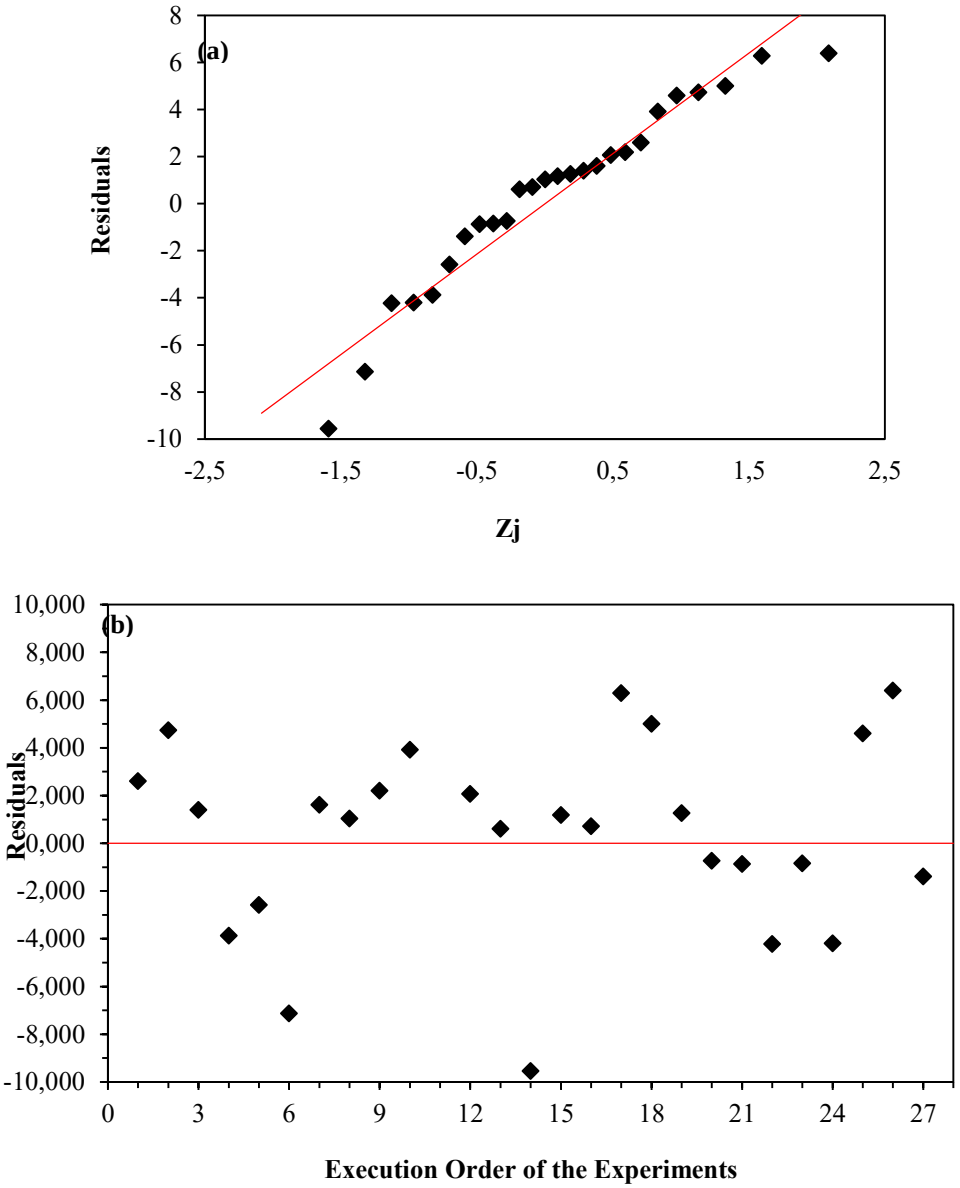

Figure B11. Normality and independence tests for the data of selectivity towards the cracking products derived from the ring opening of a partially hydrogenated internal ring, S^{INT}, for the second set of experiments in presence of the mixture of carbazole and tetrahydrocarbazole in 1:1 ratio. (a) Residuals vs normal probability and (b) Residuals vs Execution order of the experiments.

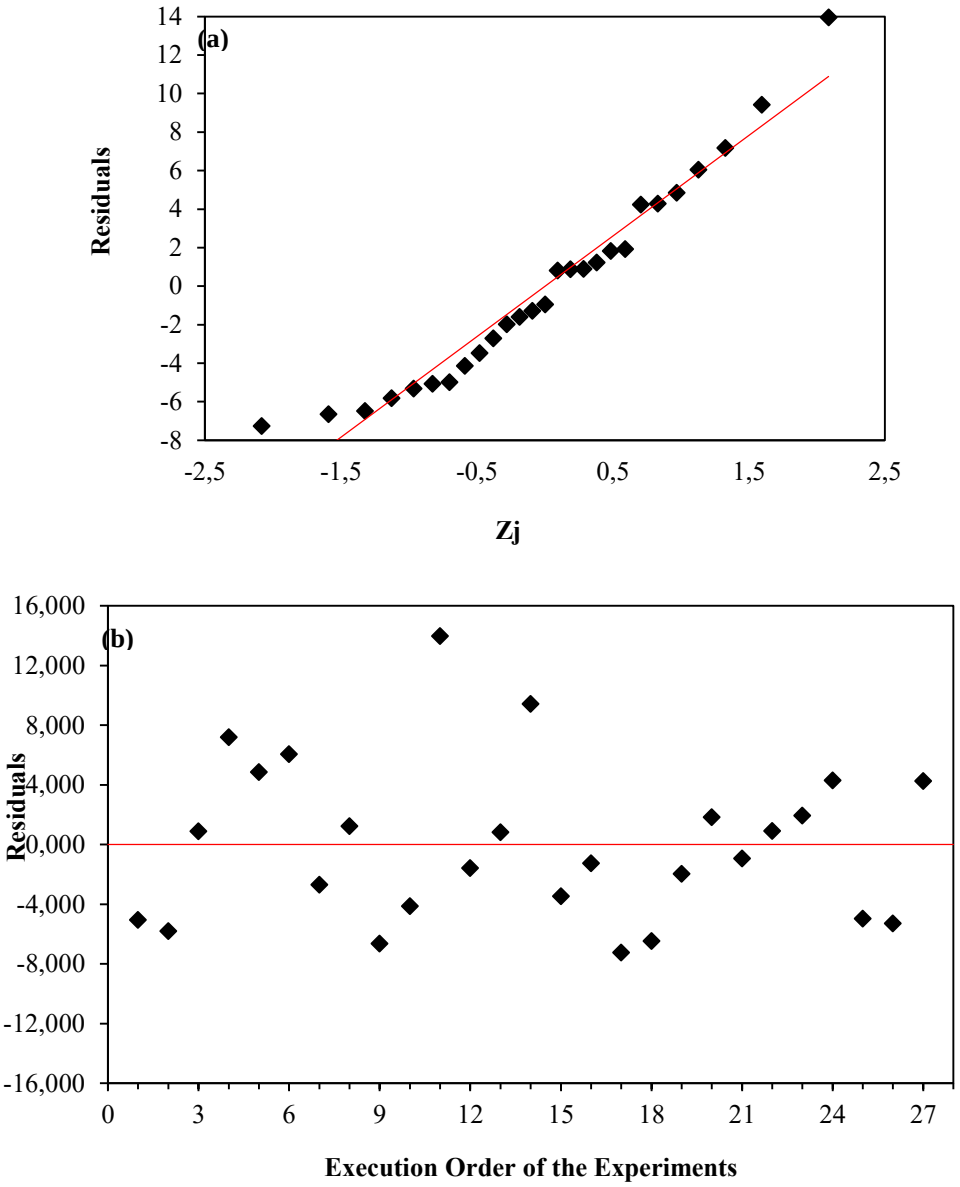

Figure B12. Normality and independence tests for the data of selectivity towards the cracking products derived from the ring opening and dealkylation of a simultaneously hydrogenated internal and external ring, S^{MIX}, for the second set of experiments in presence of the mixture of carbazole and tetrahydrocarbazole in 1:1 ratio. (a) Residuals vs normal probability and (b) Residuals vs Execution order of the experiments.

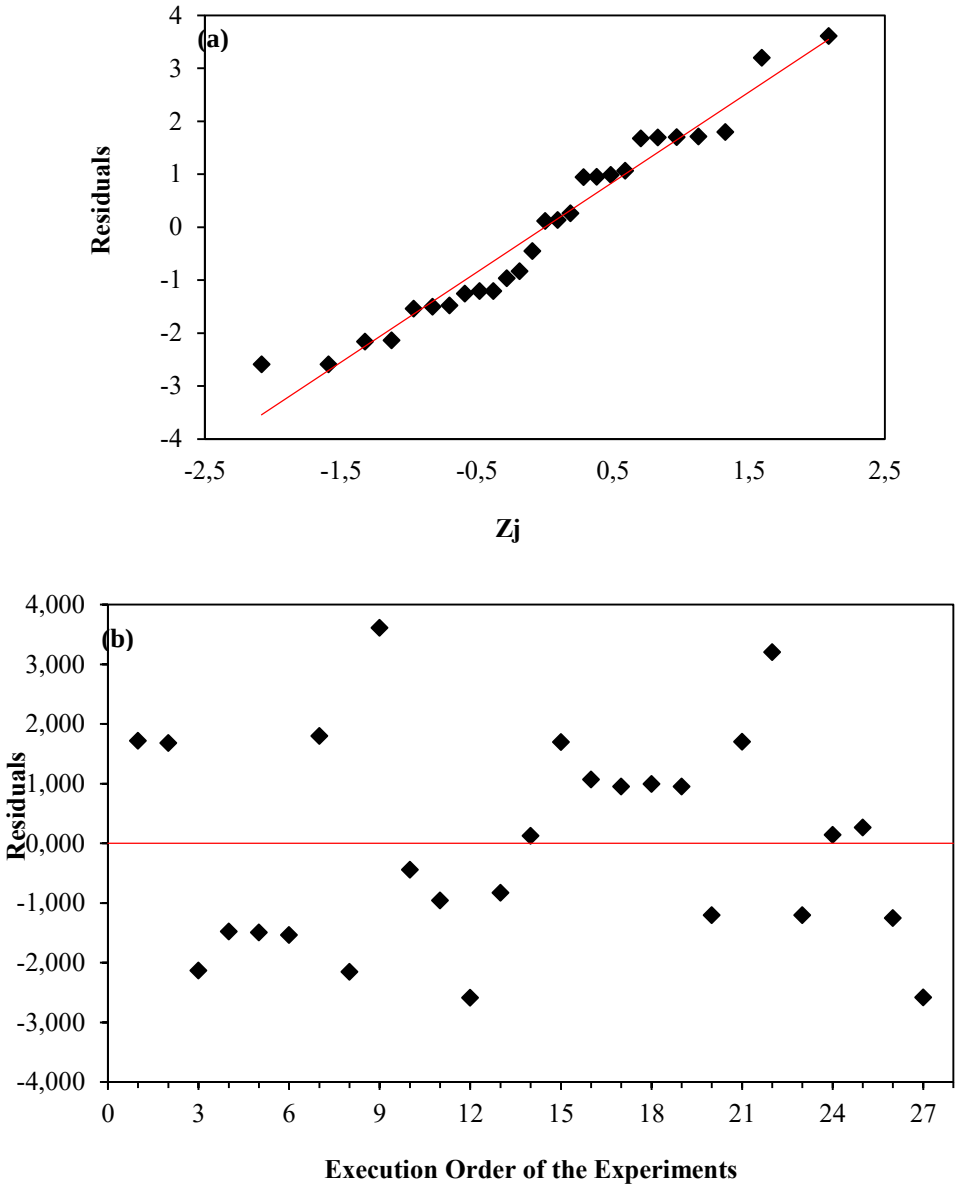

Table B1.
Results of phenanthrene conversion in % at different levels of temperature, space velocity (LHSV) and relative concentration of carbazole ([WBN]); all carried out at 6.9 MPa and (500 NL hydrogen)/(l L feed) ratio.

	Relative concentration of weakly basic nitrogenate, [WBN], (ppm)								
	0			0.8			3.6		
	Liquid hourly space velocity , LHSV, (h^{-1})								
T (K)	**1.3**	**1.8**	**2.2**	**1.3**	**1.8**	**2.2**	**1.3**	**1.8**	**2.2**
623	58.8	60.0	52.0	70.3	59.6	48.8	65.7	60.5	51.5
638	66.8	66.6	52.2	72.9	58.8	62.2	69.2	65.5	54.9
653	79.8	76.2	67.0	79.7	73.2	64.8	78.3	71.6	57.4

Table B2.

Results of phenanthrene selectivity towards the hydrocracking products in % at different levels of temperature, space velocity (LHSV) and relative concentration of carbazole ([WBN]); all carried out at 6.9 MPa and (500 NL hydrogen)/(l L feed) ratio.

	Relative concentration of weakly basic nitrogenate, [WBN], (ppm)								
	0			0.8			3.6		
	Liquid hourly space velocity , LHSV, (h^{-1})								
T (K)	**1.3**	**1.8**	**2.2**	**1.3**	**1.8**	**2.2**	**1.3**	**1.8**	**2.2**
623	22.4	10.1	18.3	20.4	13.9	9.0	13.2	16.1	6.7
638	32.8	23.4	23.2	18.2	22.8	17.9	18.0	22.1	8.5
653	59.7	49.5	47.9	52.1	43.5	28.4	41.1	39.4	12.1

Table B3.
Results of phenanthrene conversion in % at different levels of temperature, space velocity (LHSV) and relative concentration of weakly basic nitrogen-containing compounds ([WBN]); all carried out at 6.9 MPa and (500 NL hydrogen)/(l L feed) ratio.

	Relative concentration of weakly basic nitrogen-containing compounds, [WBN], (ppm)								
	0			1.0			5.0		
	Liquid hourly space velocity , LHSV, (h^{-1})								
T (K)	**1.3**	**1.8**	**2.2**	**1.3**	**1.8**	**2.2**	**1.3**	**1.8**	**2.2**
623	58.8	60.0	52.0	56.4	51.3	51.5	52.4	45.3	38.6
638	66.8	66.6	52.2	61.0	61.8	57.5	52.0	50.9	43.6
653	79.8	76.2	66.9	74.0	63.3	58.3	58.6	50.4	47.9

Table B4.
Results of phenanthrene selectivity towards the hydrocracking products in % at different levels of temperature, space velocity (LHSV) and relative concentration of weakly basic nitrogen-containing compounds ([WBN]); all carried out at 6.9 MPa and (500 NL hydrogen)/(l L feed) ratio.

	Relative concentration of weakly basic nitrogen-containing compounds, [WBN], (ppm)								
	0			**1.0**			**5.0**		
	Liquid hourly space velocity , LHSV, (h^{-1})								
T (K)	**1.3**	**1.8**	**2.2**	**1.3**	**1.8**	**2.2**	**1.3**	**1.8**	**2.2**
623	22.4	10.1	18.3	12.6	15.0	16.5	9.3	7.7	10.9
638	32.8	23.4	23.2	22.6	37.3	29.3	11.5	9.7	12.5
653	59.7	49.5	47.9	43.0	40.5	42.5	30.0	15.4	26.8

Table B5.

Selectivity towards the three postulated routes in %, as defined in Scheme 1, at different levels of temperature, space velocity (LHSV) and relative concentration of weakly basic nitrogen-containing compounds ([WBN]). All carried out at 6.9 MPa and (500 NL hydrogen)/(l L feed) ratio.

	Relative concentration of weakly basic nitrogen-containing compounds, [WBN], (ppm)								
	0			**1.0**			**5.0**		
	Liquid hourly space velocity , LHSV, (h^{-1})								
T (K)	**1.3**	**1.8**	**2.2**	**1.3**	**1.8**	**2.2**	**1.3**	**1.8**	**2.2**
Selectivity % towards the hydrocracking products derived from hydrogenated external rings, S^{EXT}									
623	68.8	53.6	65.0	57.6	64.7	57.5	39.8	27.9	36.7
638	72.7	70.3	56.9	61.6	67.1	58.3	47.4	43.4	47.0
653	70.2	71.5	70.1	68.7	66.1	63.2	61.4	54.9	60.9
Selectivity % towards the hydrocracking products derived from a hydrogenated internal ring, S^{INT}									
623	26.0	46.4	29.0	42.4	35.3	42.5	72.1	72.1	63.3
638	20.8	23.9	37.5	32.8	28.8	34.7	56.6	56.6	53.0
653	22.5	22.2	24.6	25.2	31.5	31.5	45.1	45.1	31.3
Selectivity % towards the hydrocracking products derived from simultaneous hydrogenated rings, S^{MIX}									
623	5.2	0.0	6.0	0.0	0.0	0.0	0.0	0.0	0.0
638	6.5	5.7	5.6	5.5	4.1	7.0	0.0	0.0	0.0
653	7.3	6.2	5.3	6.1	2.5	5.3	5.8	0.0	7.8

ANNEX C: CHAPTER 3

Figure C1. Adsorption of carbazole into the pore bulk system of the mordenite, considering the duplicated unit cell in z-axis. (a) Top view (b) lateral view.

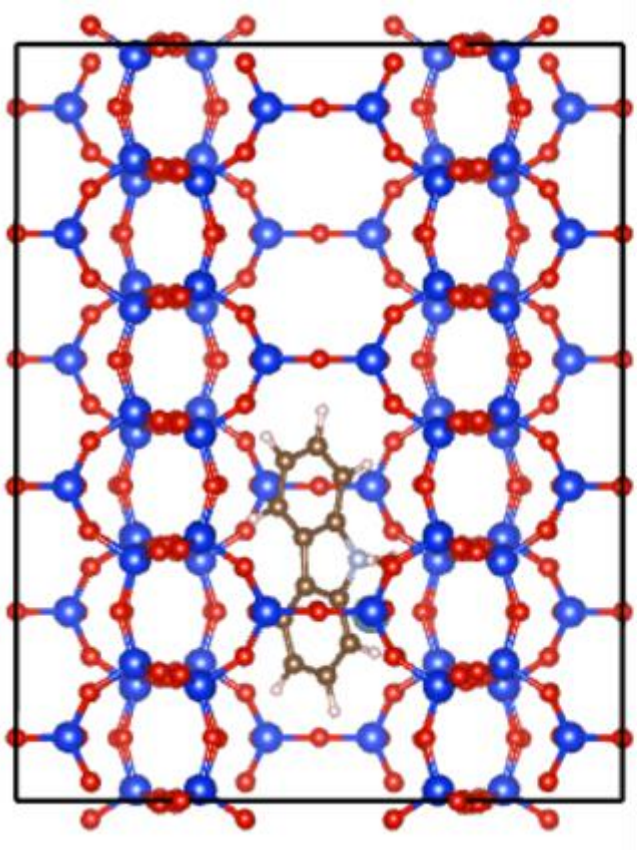

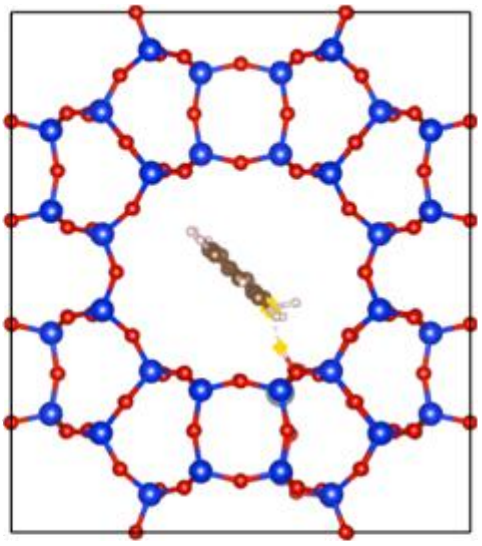

$\Delta H_{ads} = E_{Mor+Carb} - (E_{Mordenite} + E_{Carbazole})$

	Pore mouth	Inside the pore
$E_{Mordenite}$ [eV]	-1376.81	-3445.69
$E_{Carbazole}$ [eV]	-150.38	-150.38
$E_{Mor+Carb}$ [eV]	-1528.54	-3597.50
ΔH_{ads} [eV]	-1.35	-1.44
ΔH_{ads} [kJ·mol^{-1}]	-129.6	-137.81

Figure C2. Structural arrangement for the optimized intermediates and transition states.

1. Adsorbed reactive

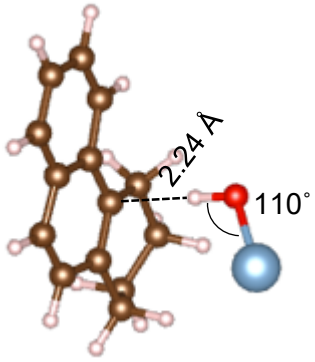

1,2,3,4-Tetrahydro phenanthrene

TS1. Protonation

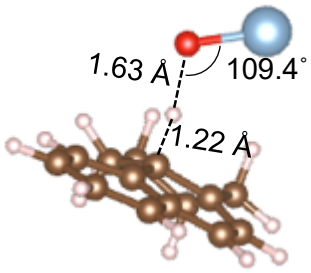

2. Protonated intermediate

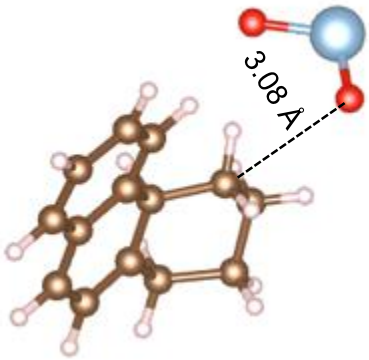

TS2. Ring opening

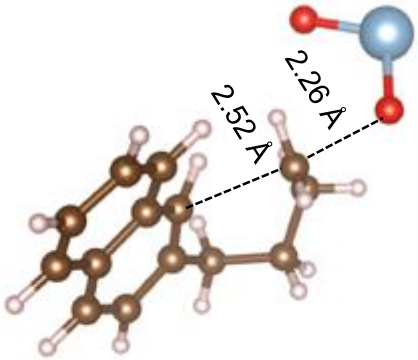

3. Alkoxide intermediate

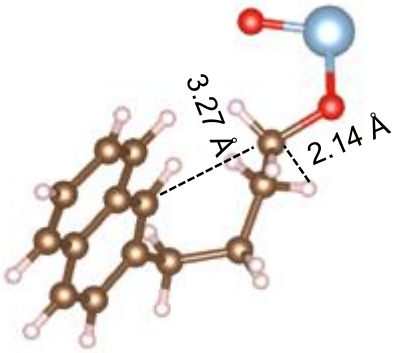

TS3. Hydride shift

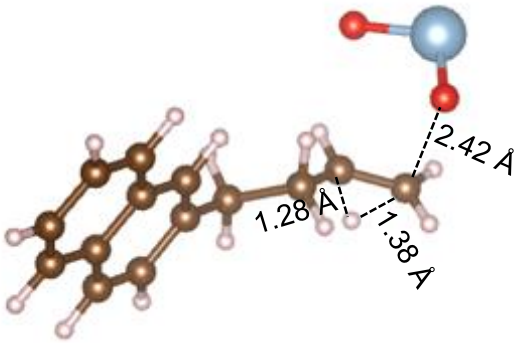

4. Carbocation formation

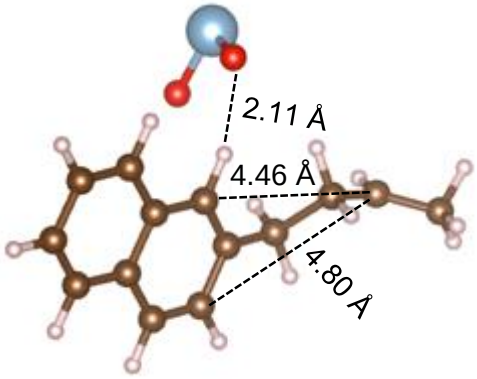

TS4. Cyclization

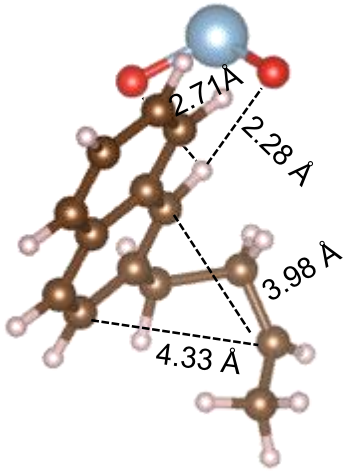

5. Cycled intermediate

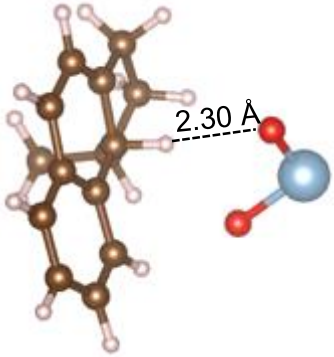

TS5. Deprotonation

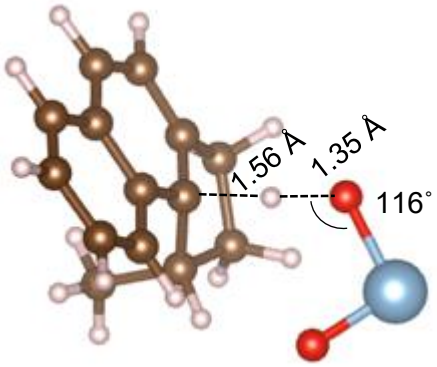

6. Adsorbed product

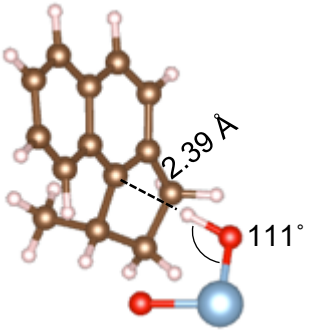

Methylcyclopenta naphthalene

Figure C3. Dehydrogenation on the zeolite, first step to the formation of an unsaturated ring following the Haag-Dessau mechanism.

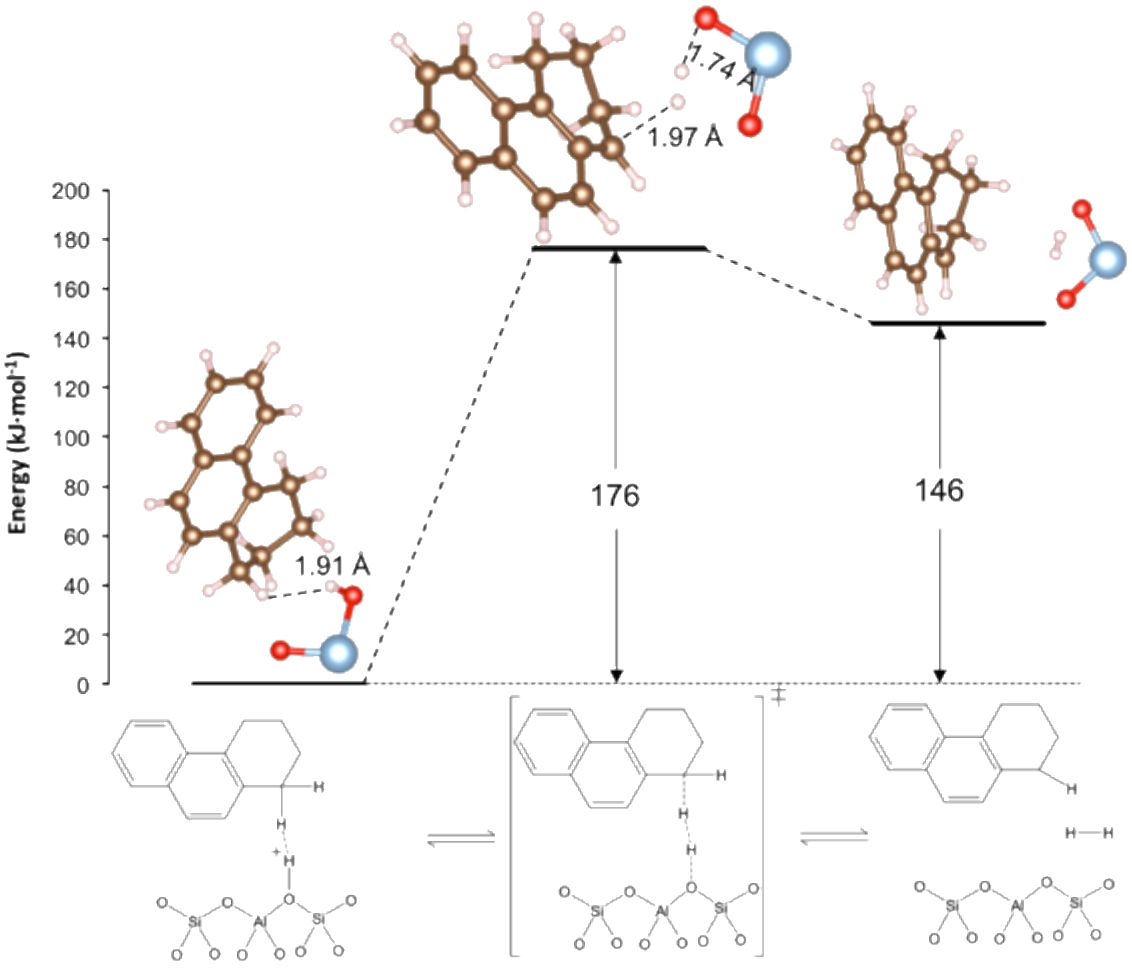

Figure C4. Optimized adsorbed complexes of the polynuclear aromatic hydrocarbons and the nitrogenated compounds on the Brønsted acid site.

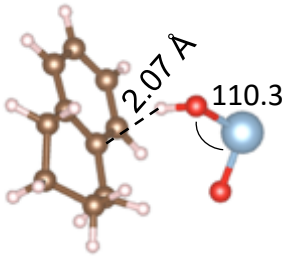

1,2,3,4-Tetrahydro naphthalene

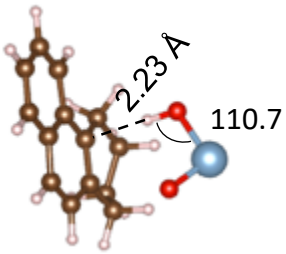

1,2,3,4-Tetrahydro phenanthrene

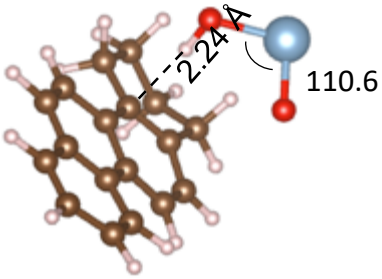

1,2,3,4-Tetrahydro chrysene

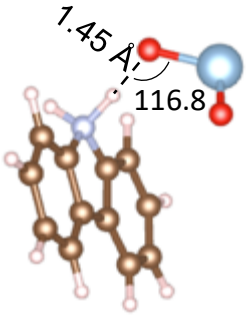

Carbazole

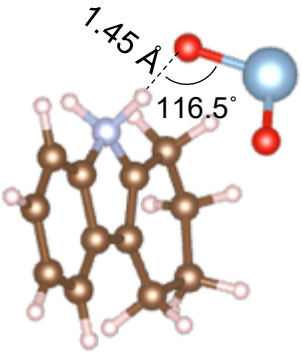

1,2,3,4-Tetrahydro carbazole

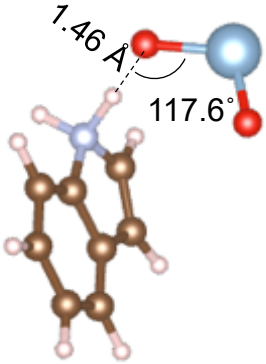

Indole

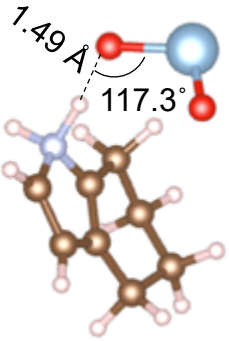

1,2,3,4-Tetrahydro indole

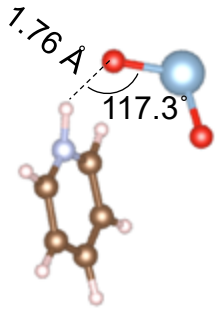

Pyridine

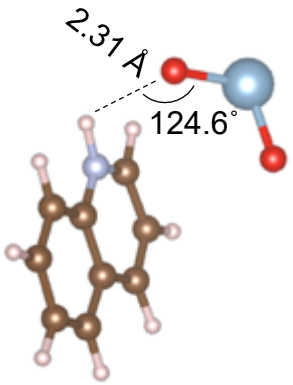

Quinoline

Figure C5. Optimized adsorbed complexes of the nitrogenated compounds on the silanol terminal groups.

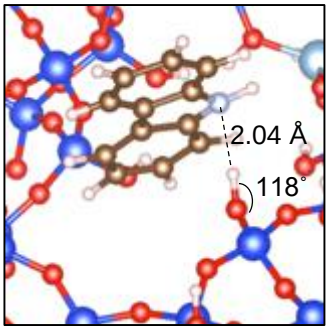

Carbazole

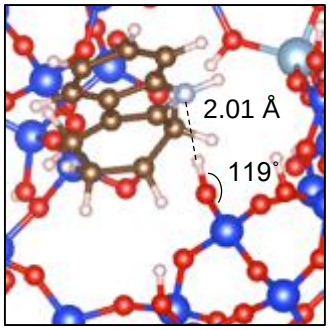

1,2,3,4-Tetrahydro carbazole

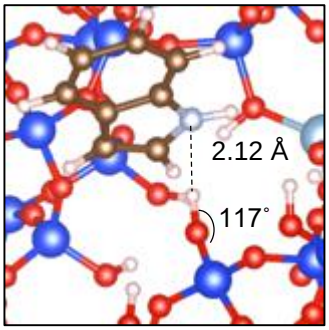

Indole

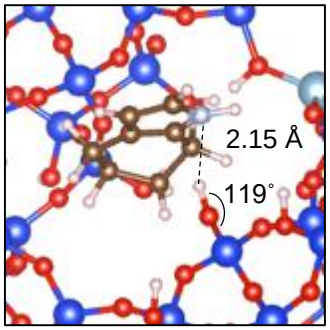

1,2,3,4-Tetrahydro indole

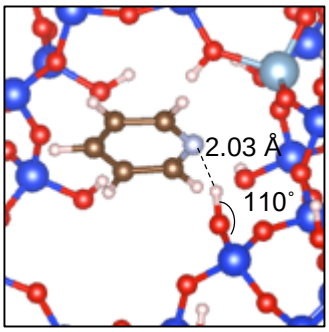

Pyridine

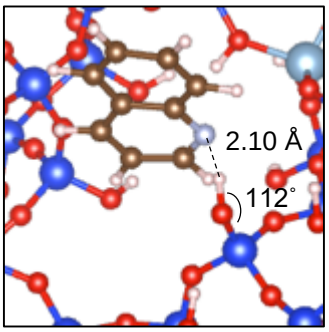

Quinoline

Table C1.

Enthalpies calculated for each step of the mechanism proposed for the isomerization of tetrahydrophenanthrene into mthylcyclopentanaphthalene.

Step	**Name**		**ΔH (kJ·mol^{-1})**
1	Protonation		12.9
2	Ring Opening		50.3
3	Hydride Shift		42.9
4	Cyclization		-90.2
5	Deprotonation		-14.9
		ΔH_{RXN}	8.6

ANNEX D: CHAPTER 4

IR *in situ* analysis

A USY zeolite (CBV760, zeolyst) was grounded and pressed at 1 Ton for preparing a thin wafer of Ø=1.6 cm and approximately 5 mg·cm^{-2} for putting them in the sample holder of the IR *in situ* cell for performing the Pyridine adsorption. The solid wafer was first treated at 673 K using a heating rate of 1.5 K/min starting from 300 K, all this under high vacuum (P >10^{-4} Pa) during 6 h. After the treatment, 133 Pa of pyridine was released for carrying out the equilibrium adsorption at room temperature (RT). Afterwards, evacuation at RT was performed at ~13 Pa and 10^{-4} Pa, followed by desorption at 373, 423, 523 and 623 K. Figure S3 shows the typical IR spectra for a very dealuminated Y Zeolite. As it could be appreciated, this material has strong acidity. After desorption at 623 K, some remaining bands support this fact. The band located at 1455 cm^{-1} is attributed to the ν_{19b} vibration mode of adsorbed pyridine species in Lewis sites. Also the peaks at 1489 cm^{-1} and 1545 cm^{-1} are contributions of the ν_{19a} and ν_{19b} vibration modes of pyridine adsorbed in Brønsted and Lewis sites and pyridinium adsorbed species, respectively.

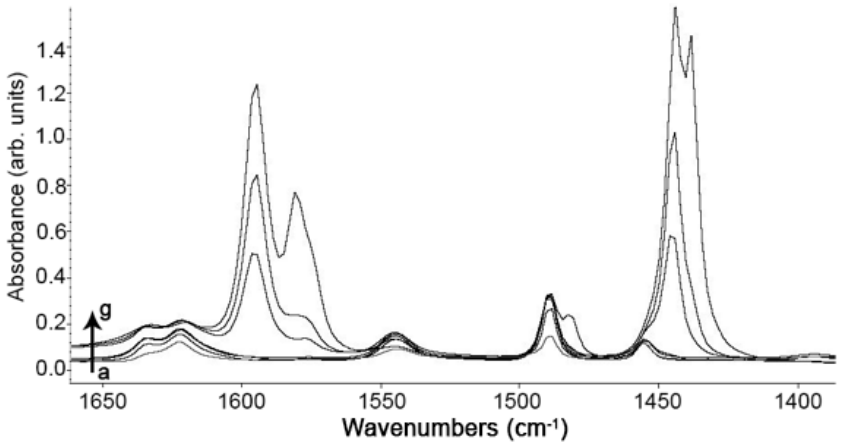

Figure D1. IR difference spectra for pyridine adsorption in the HY zeolite CBV760, a-e: evacuation at 623, 523, 423, 373 K and RT, f: evacuation at RT at 13 Pa, g: equilibrium adsorption at 133 Pa of pyridine vapor pressure.

Figure D2. Optimized mordenite surface, lattice and dimensions of the box.

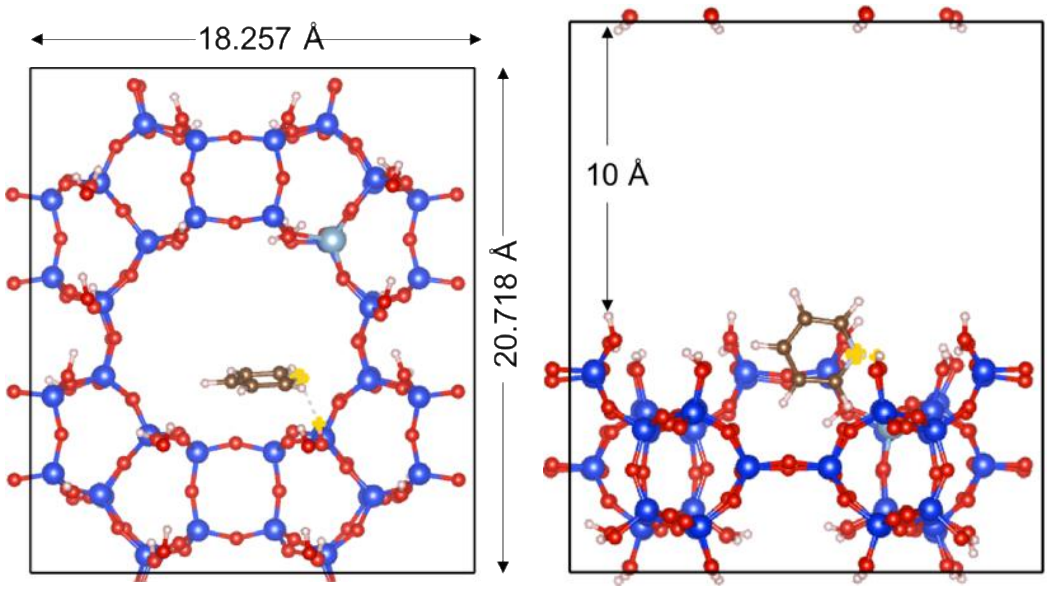

Figure D3. Optimized adsorbed complexes of the nitrogenated compounds on a silanol and a Brønsted acid site.

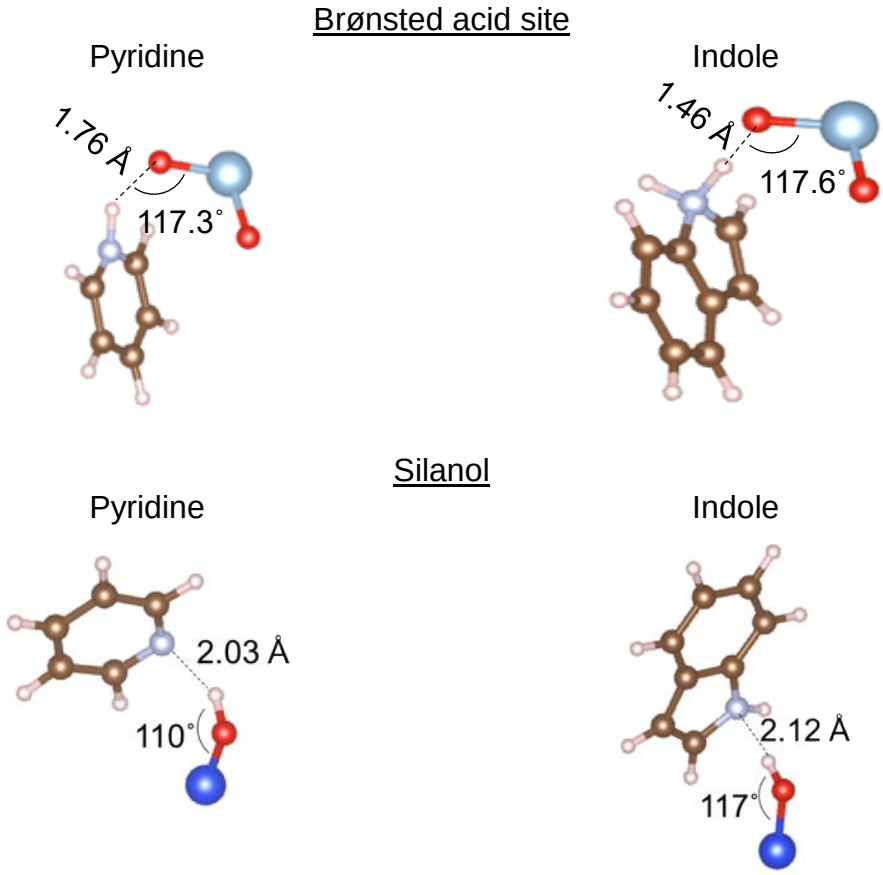

Figure D4. ATR-IR difference spectra of the indole adsorption on the USY zeolite, obtained by subtracting the spectrum of solid saturated with pure n-hexane, at different coverages from (a) initial time to (d) saturation in flow, in the region between 1200 and 1600 cm^{-1}.

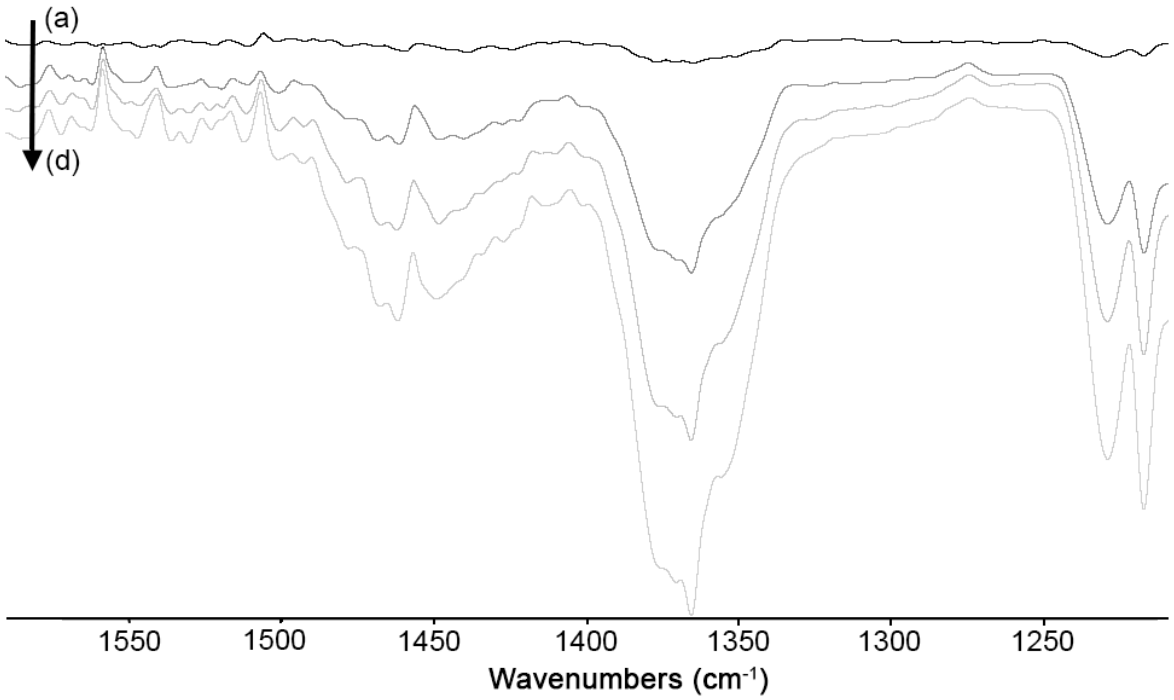

Figure D5. ATR-IR difference spectra obtained by subtracting the pure n-haxane solution in flow, before the deposition of the solid film, from the indole solution at the same flow, in the region between 700 and 900 cm^{-1}.